Novel electrocatalysts for sustainable ammonia production at ambient conditions

Younes Abghoui

Faculty of Physical Sciences
School of Engineering and Natural Sciences
University of Iceland
2017

NOVEL ELECTROCATALYSTS FOR SUSTAINABLE AMMONIA PRODUCTION AT AMBIENT CONDITIONS

Younes Abghoui

180 ECTS thesis submitted in partial fulfillment of a
Doctor Philosophiae degree in Chemistry

Ph.D. Supervisor:

Prof. Egill Skúlason

Ph.D. committee:

Prof. Egill Skúlason
Dr. Kristján Leósson
Dr. Sveinn Ólafsson

Opponents:

Dr. Justin Hargreaves
University of Glasgow, Scotland

Dr. Poul Georg Moses
Haldor Topsøe, Denmark

Faculty of Physical Sciences
School of Engineering and Natural Sciences
University of Iceland
Reykjavík, March 2017

Novel electrocatalysts for sustainable ammonia production at ambient conditions

Dissertation submitted in partial fulfillment of a *Doctor Philosophiae* degree in Chemistry

Faculty of Physical Sciences
School of Engineering and Natural Sciences
University of Iceland
Hjarðarhagi 2-6
107 Reykjavík
Iceland

Telephone: +354 525 4700

Bibliographic information:
Younes Abghoui, "Novel electrocatalysts for sustainable ammonia production at ambient conditions", Ph.D. dissertation, Faculty of Physical Sciences, University of Iceland, 2017.

ISBN 978-9935-9344-2-0

Printing:
Háskólaprent ehf., Fálkagötu 2, 107 Reykjavík

Reykjavík, Iceland, March 2017

To my kind and devoted parents and talented brother for their endless love, support and encouragement. This Ph.D thesis is lovingly dedicated to my stunning and encouraging wife, Aysun, without whom life with all its beauties would have been ugly and meaningless.

"My brain is only a receiver, in the Universe there is a core from which we obtain knowledge, strength and inspiration. I have not penetrated into the secrets of this core, but I know that it exists."

Nikola Tesla

Acknowledgments

This dissertation is submitted in candidacy for the Ph.D. degree in Chemistry, a work that was mainly accomplished at University of Iceland. The work presented herein was carried out from November 2012 to November 2016. During this time, I was also a research intern at Center for Individual Nanoparticle Functionality (CINF) and Surface Physics & Catalysis (SurfCat) at the Technical University of Denmark, DTU, from September 2015 to September 2016 where I gained the opportunity to conduct experimental CO/CO_2 electroreduction reactions to hydrocarbons and fuels.

"It will remain a myth if a dissertation is considered as the soul-wrenching creation solely of its author's time, toil and tenacity. "

It is with immense gratitude that I acknowledge my true source of inspiration in all aspects of research, my friend and my esteemed supervisor Prof. Egill Skúlason who has the attitude and the substance of a genius. I would have not been here writing this thesis if he, in the first place, had not picked me up amongst more than 300 applications he received for this PhD position. Without his unwavering support and encouragement, I would not have been granted the chance of taking delight in this marvelous adventure. I would also like to express my appreciation to him for helping me to spend my stay at DTU so that I can quench a bit of my thirst for doing electrochemical experiments in one of the best laboratories in Europe, if not the world.

It gives me great pleasure in acknowledging the willingness of Dr. Justin Hargreaves and Dr. Poul Georg Moses to attend my defence as my esteemed opponents. I hope you become well satisfied after this event and hearing my work.

I have been fortunate to be granted the privilege to work under supervision of Prof. Ib Chorkendorff, Director of The Villum Center for the Science of

Sustainable Fuels and Chemicals, and Prof. Ifan Stephens, the Leader of the Electrocatalysis Group at CINF and SurfCat in DTU. During this research internship, I learned a lot about experimental CO/CO_2 electroreduction to high-value-added products. My special thanks go to Erlend Bertheussen with whom I started doing my very first electrochemical experiments from initial preparation to electrolysis and product analyses. I also thank Kim Degn Jensen for all his helps with the XPS equipment from sample loading to conducting XPS measurements and data analyses. Jacqueline McAnulty is also acknowledged for teaching me to use the inductively coupled plasma mass spectrometry machine for the ICP measurements. I am very grateful for the chance to work in this highly competent and friendly research environment. Also, I would like to thank all the nice CINFers and SurfCaters who were my colleagues and turned into my friends. I thank Ehsan and Jenni for their warm hospitality and companionship, too.

I feel very lucky for having had the opportunity to work in a highly cooperative environment in VRIII at the University of Iceland. In my daily work, I have been blessed with a friendly and cheerful group of fellow researchers and students who were lending a sympathetic ear and putting my toils in perspective. It has been a pleasure working with my colleagues, all the former and present members of Prof. Hannes Jónsson's, Prof. Egill Skúlason's, Dr. Sveinn Ólafsson's, and Prof. Viðar Guðmundsson's groups in VRIII. I thank Nzar for all the enjoyable moments and delicious dinners we had together during his stay in Iceland. Javed has throughout my project been a nice companion in the office and I have always appreciated the useful and useless discussions about everything and nothing with him. I would also like to thank Manuel for all his help and supports during my life in Iceland. He never pulled away when I needed him. I would also like to thank Asmus, Cody, Manuel, Ebrahim, Villi, and Ragnar for proof-reading my thesis. Any errors that remain in this thesis are attributable to my negligence or stubbornness, though.

Many thanks also go to our collaborators from Innovation Center Iceland: Dr. Kristján Leósson and Dr. Helga Dögg Flosadóttir for all the meetings, discussions, initial and final ammonia experiments both in downstairs VRIII and in Innovation Center Iceland. Dr. Friðrik Magnus and Tryggvi Kristmar Tryggvason are also acknowledged for our nice collaboration on the area of catalyst synthesis.

It goes without saying that this thesis would have remained an impossible dream had it not been for my beloved family and my gorgeous wife, Aysun, not only for inculcating in me the dedication and discipline to do whatever

I undertake well, but also for being the constant source of support – emotional, morale, and of course financial. You have been always the pillar of my success and my guiding light. Thanks for not ceasing to have faith and confidence in me. I would like to show you my heart-felt appreciations for simultaneously brandishing a sword to quell the demons of my insecurities, and a wand to bring joy to my life in so many different ways to ensure that the road to my goal was not as bumpy as it could have been. How can I reciprocate just little of all precious qualities you have induced in me? So now, for many times I didn't say it before, I proudly shout loudly:

THANK YOU SO MUCH!

LOVE YOU SO MUCH!

Abstract

Commercial design of a sustainable route for on-site production of ammonia represents a potential economic and environmental breakthrough. In an analogous process to the naturally occurring enzymatic mechanism, synthesis of ammonia could be achieved in an electrochemical cell where electricity would be used to reduce atmospheric nitrogen and water into ammonia at ambient conditions. Despite significant progress made in this regard, at present there exists no (electro-) catalyst that can produce ammonia efficiently from air and water at room temperature and ambient pressure due to slow kinetics and low Faradaic efficiencies. A rapid and facile reduction of nitrogen to achieve sustainable and energy-efficient production of ammonia is critical to its use as a hydrogen storage medium, chemical feedstock, and especially for manufacturing inorganic fertilizer. For a decentralization of catalytic ammonia production, small-scale N_2 reduction devices are required that are equipped with the most stable, selective, and active (electro-) catalysts that operate at low temperature and ambient pressure.

In this thesis we report the computational design of potential new and cost-efficient electrocatalysts with transition metal nitrides, which enable electrochemical reduction of molecular nitrogen to ammonia in aqueous media at ambient conditions with only a low applied bias. The electronic structure calculations at the density functional theory level are used to appraise the performance of this new class of material for electrochemical ammonia production. The predominant reaction mechanism making this feasible is found to be the Mars-van Krevelen mechanism instead of the conventional associative or dissociative mechanisms. The most promising electrocatalysts are RuN, VN, CrN, ZrN, and NbN, which are identified among a range of transition metal nitride surfaces through a comprehensive density functional theory based analysis. All five nitrides are found to be more active toward nitrogen reduction than toward the competing hydrogen evolution reaction, in contrast to pure metal catalysts which largely evolve hydrogen. Furthermore, their stability against poisoning and possible decomposition

under operating conditions is also studied. Particular single-crystal surfaces are needed for highly-efficient ammonia formation, as polycrystalline surfaces may result in decomposition of the whole catalyst. We suggest that this is a promising step toward the development of a method for synthesizing ammonia cheaply, to prepare high-value-added nitrogenous compounds directly from air, water, and electricity at ambient conditions. An additional benefit to the present analysis is that the scheme used in this work may be applicable to other aqueous phase catalytic reactions, where a Mars-van Krevelen mechanism is operative and product selectivity and activity are key catalytic criteria.

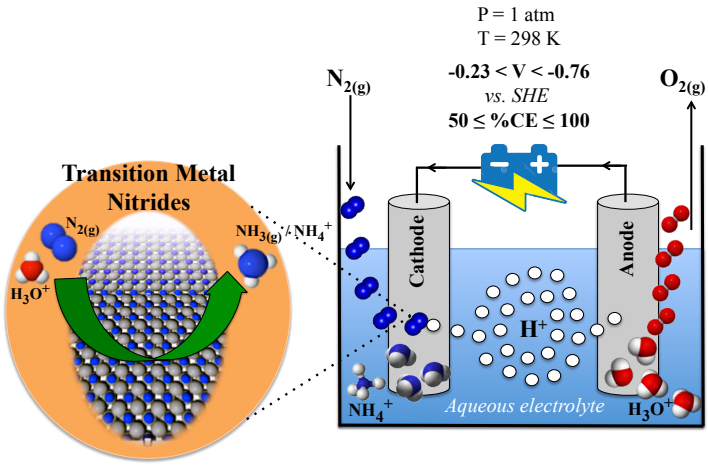

Figure 1: *This cartoon illustrates an overview of this thesis regarding the approach and outcome. The predicted onset potentials for electrochemical ammonia formation are mentioned as well as the current efficiency anticipated to achieve.*

Útdráttur

Hönnun á sjálfbærri leið til að framleiða ammóníak gæti leitt til efnahagslegrar og umhverfislegrar byltingar. Með svipuðu ferli og á sér stað í ensímum í bakteríum í jarðvegi væri hægt að framleiða ammóníak með rafefnafræðilegum aðferðum þar sem rafmagn eða sólarorka væri notað til að afoxa nitur úr andrúmsloftinu í vatnslausn og mynda ammóníak við náttúrulegar aðstæður. Í dag hefur ekki enn verið hægt að útbúa slíkt kerfi vegna hægs hvarfhraða og lágrar nýtni. Þrátt fyrir að mikil framför í átt að þessu takmarki hefur átt sér stað síðustu ár og áratugi þá er í dag enginn efnahvati til sem hvatar þetta efnahvarf rafefnafræðilega í ammóníak á nýtanlegan hátt frá lofti og vatni við herbergishita og venjulegan loftþrýsting. Hröð og sértæk afoxun niturs fyrir sjálfbæra og orkulega hagkvæma framleiðslu á ammóníaki er lykillinn til að hægt sé að nýta þetta ferli fyrir vetnisgeymslu, sem milliskref í efnaiðnað, eða til framleiðslu á ólífrænum áburði sem væri hugsanlega mesta notagildi á slíkri aðferð. Á þennan hátt væri hægt að hafa dreifða áburðarframleiðslu á smáum skala þar sem N_2 væri afoxað í litlum hvarfklefum sem væru með rafefnahvata sem væri stöðugur, sértækur og virkur fyrir ammóníaksmyndun við umhverfisaðstæður.

Í þessari doktorsritgerð er kynnt til sögunnar reikniefnafræðileg hönnun á mögulegum nýjum og hagkvæmum rafefnahvötum, málmnítríð, sem gætu framkvæmt rafefnafræðilega afoxun á nitursameindinni í ammóníak í vatnslausn við herbergisaðstæður og við lága rafspennu. Skammtafræðilegir reikningar með þéttnifellaaðferðinni (e. density functional theory, DFT) eru notaðir til að rannsaka þessa nýju tegund efnahvata fyrir rafefnafræðilega ammóníaksmyndun. Orkulægsti hvarfgangurinn fyrir þetta ferli er hinn svokallaði Mars-van Krevelen hvarfgangur í stað hefðbundna hvarfganga á borð við sameindahvarfgangs eða sundrunarhvarfgangs. Áhugaverðustu rafefnahvatarnir reyndust vera RuN, VN, CrN, ZrN og NbN samkvæmt skammtafræðilegu reikningunum þar sem mikill fjöldi af mismunandi málm nítríðum voru skoðuð ítarlega. Öll fimm nítríðin eru spáð vera virk og sértæk fyrir afoxun niturs í stað þess að mynda vetnisgas sem er samkeppnis-

hvarf, en hvatar úr hreinum málmum mynda frekar vetnisgas í stað ammóníaks. Þessi fimm áhugaverðustu málmnítríð ættu einnig að vera stöðug með tilliti til að þau skemmast ekki í raflausninni né eyðast eða sundrast við þær rafefnafræðilegu aðstæður sem þau þurfa að geta þolað. Sérstök einkristölluð yfirborð gæti þurft að nota til að ná fram hárri nýtni á ammóníaksmyndun þar sem margkristölluð yfirborð gætu leitt til að efnahvatinn eyðist upp í ferlinu. Þessi þróunarvinna gæti reynst mikilvægt skref í átt að aðferð sem getur framleitt ammóníak á ódýran hátt frá nitri andrúmsloftsins, vatni og rafmagni við venjulegur umhverfisaðstæður. Aukalegur ávinningur af aðferðafræðinni sem hér hefur verið þróuð er að hægt verður að nota svipaða aðferð til að rannsaka önnur efnahvötuð hvörf í vatnslausnum þar sem Mars-van Krevelen hvarfgangurinn er mögulegur og þar sem sértækni á myndun ákveðinna myndefna og virkni efnahvatanna eru lykilskilyrði.

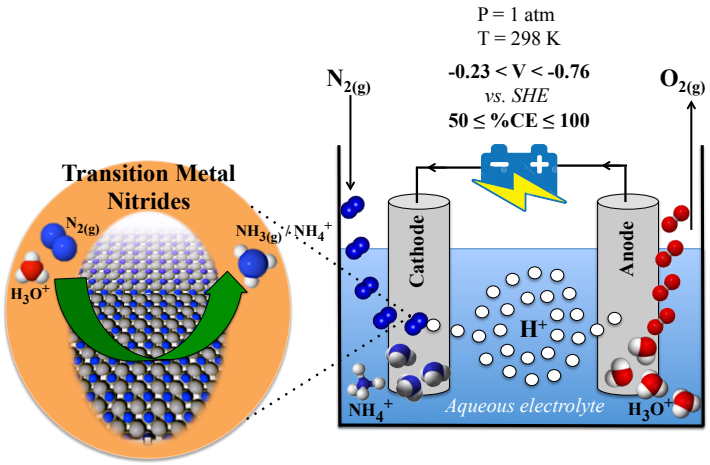

Mynd 2: *Þessi skýringarmynd sýnir yfirlit yfir efni ritgerðarinnar hvað varðar aðferðir og niðurstöður. Sýnd eru spennugildi fyrir rafefnafræðilega ammóníaksmyndun sem spáð er fyrir um auk rafstraumsnýtni.*

List of Publications

Publications included in the thesis

1. **Enabling Electrochemical Reduction of Nitrogen to Ammonia at Ambient Conditions Through Rational Catalyst Design**
   Younes Abghoui, Anna L. Garden, Valtýr F. Hlynsson, Snædís Björgvinsdóttir, Hrefna Ólafsdóttir and Egill Skúlason
   Physical Chemistry Chemical Physics ***17****, 4909-4918 (2015).*

2. **Electroreduction of N_2 to Ammonia at Ambient Conditions on Mononitrides of Zr, Nb, Cr, and V: A DFT Guide for Experiments**
   Younes Abghoui, Anna L. Garden, Jakob G. Howalt, Tejs Vegge and Egill Skúlason
   ACS Catalysis ***6****, 635-646 (2016).*

3. **Electrochemical Synthesis of Ammonia via Mars-van Krevelen Mechanism on the (111) Facets of Group III–VII Transition Metal Mononitrides**
   Younes Abghoui and Egill Skúlason
   Catalysis Today, in press (2016).

4. **Onset Potentials for Different Reaction Mechanisms of Nitrogen Activation to Ammonia on Transition Metal Nitride Electro-catalysts**
   Younes Abghoui and Egill Skúlason
   Catalysis Today, in press (2016).

5. **Computational Predictions of Catalytic Activity of Zincblende (110) Surfaces of Metal Nitrides for Electrochemical Ammonia Synthesis**
   Younes Abghoui and Egill Skúlason
   J. Phys. Chem. C, in press (2017).

6. **On the Possibility of Catalysing the Hydrogen Evolution Reaction with Transition Metal Nitrides as Cathode Material**

Younes Abghoui and Egill Skúlason
submitted to J. Mat. Chem. A, March , (2017).

7. **Applications of Nitrides as Electrocatalysts**
Anna L. Garden, Younes Abghoui, and Egill Skúlason
Book chapter submitted to Royal Society of Chemistry Book Series entitled Novel Catalytic Materials, edited by Justin Hargreaves, Andrew McFarlane and Said Laassiri , February (2017).

8. **Transition Metal Nitride Catalysts for Electrochemical Reduction of Nitrogen to Ammonia at Ambient Conditions**
Younes Abghoui and Egill Skúlason
*Procedia Computer Science **51**, 1897–1906 (2015).*

9. **Nitrogen Activation to Ammonia via a Mars-van Krevelen Mechanism on Nitride Electro-Catalysts**
Younes Abghoui and Egill Skúlason
*American Institute of Chemical Engineers **(AIChE)**, ISBN: 978-0-8169-1094-6 (2015).*

10. **Transition Metal Nitrides As Promising Electro-Catalysts for Either Reduction of Nitrogen to Ammonia or Hydrogen Evolution Reaction**
Younes Abghoui and Egill Skúlason
*American Institute of Chemical Engineers **(AIChE)**, ISBN: 978-0-8169-1094-6 (2015).*

Publications not included in the thesis

1. **Quantification of Liquid Products From the Electroreduction of CO_2 and CO Using Static Headspace-Gas Chromatography and Nuclear Magnetic Resonance Spectroscopy**
Erlend Bertheussen, Younes Abghoui, Zarko P. Jovanov, Ana-Sofia Varela, Ifan E. L. Stephens, Ib Chorkendorff
Catalysis Today, in press (2017).

2. **Computational Screening of Rutile Oxides for Electrochemical Ammonia Formation**
Árni B. Höskuldsson, Younes Abghoui, Anna B. Gunnarsdóttir and Egill Skúlason
to be submitted in March (2017).

3. **Transition Metal Sulfides for Electrochemical Ammonia Production**
   Younes Abghoui, Sigtryggur B. Sigtryggsson and Egill Skúlason
   manuscript in preparation

4. **Suitability of the (111) and (110) Surfaces of Early Transition Metal Nitrides for Hydrogen Evolution Reaction**
   Younes Abghoui and Egill Skúlason
   manuscript in preparation

Contents

Abbreviations

AEM **A**lkaline **E**xchange **M**embrane

PEM **P**olymer **E**lectrolyte **M**embrane

SSAS **S**olid **S**tate **A**mmonia **S**ynthesis

TMN **T**ransition **M**etal **N**itride

FE **F**aradaic **E**fficiency

KAAP **K**ellogg **A**dvanced **A**mmonia **P**rocess

RS **R**ocksalt

ZB **Z**incblende

DFT **D**ensity **F**unctional **T**heory

CHE **C**omputational **H**ydrogen **E**lectrode

HER **H**ydrogen **E**volution **R**eaction

Gj **G**iga **j**oule

ΔE_H **Chemisorption energy per hydrogen atom**

pH **P**otential **h**ydrogen (Capacity of Hydrogen)

SHE **S**tandard **H**ydrogen **E**lectrode

RHE **R**eversible **H**ydrogen **E**lectrode

M **M**olar

U **Applied potential**

ML **M**ono-**L**ayer

NER **N**itrogen **E**lectroreduction **R**eaction

MvK **M**ars **v**an **K**revelen mechanism

MEP **M**inimum **E**nergy **P**ath

FED **F**ree **E**nergy **D**iagram

PDS **P**otential **D**etermining **S**tep

RDS **R**ate **D**etermining **S**tep

IS **I**nitial **S**tate

TS **T**ransition **S**tate

FS **F**inal **S**tate

PES **P**otential **E**nergy **S**urface

NEB **N**udged **E**lastic **B**and

CI-NEB **C**limbing **I**mage **N**udged **E**lastic **B**and

NMA **N**ormal **M**ode **A**nalysis

ZPE **Z**ero **P**oint **E**nergy

HF **H**artree-**F**ock

HK **H**ohenberg-**K**ohn

KS **K**ohn-**S**ham

LDA **L**ocal **D**ensity **A**pproximation

GGA **G**eneralized **G**radient **A**pproximation

PAW **P**rojector-**A**ugmented-**W**ave method

PBE **P**erdew-**B**urke-**E**ernzerhof

RPBE **R**evised **P**erdew-**B**urke-**E**ernzerhof

BLYP **B**ecke-**L**ee-**Y**ang-**P**arr (Becke and Lee for the exchange part, Yang and Parr for the correlation part)

Ψ **Wave Function**

$\hat{H}$ **Hamiltonian Operator**

E_{xc} **Exchange Correlation Energy**

μ **Chemical Potential**

ΔG **Free Energy**

E_a **Activation Energy**

E_d **Dissociation Energy**

k **Arrhenius Rate Constant**

i **Current Density**

1 Introduction

The concept of chemical synthesis of ammonia directly from its elements materialized in 1913 [1] with the inauguration of the first industrial plant for production of the artificial nitrogen-based fertilizer. This turned out to be one of the most substantial scientific realizations of the 20th century transpired by Fritz Haber's inventive talent (Nobel Prize winner in 1919) and Carl Bosch's engineering skills (Nobel Prize winner in 1931), which susbtantially contributed to the ''Green Revolution and Industrialized Agriculture'' [2–4]. In all pre-industrial agriculture, nitrogen was the most commonly yield-limiting nutrient [4], and only the Haber-Bosch synthesis of ammonia broke this barrier. The ability to turn the nitrogen in air into fertilizer has enabled feeding billions more people than our planet could otherwise support. Without ammonia, thus deprived of inorganic fertilizer, almost half the world's population would be at risk of starvation [3]. Human survival has thus been depending a great deal on the Haber-Bosch process, which is the most pivotal industrial installation for catalytic cleavage of N_2 and hydrogenating nitrogen to ammonia heterogeneously over promoted transition metal-based catalysts [2].

From the beginning of industrialization, and in line with the world's population growth, global energy consumption and energy demand have also been projected to increase. Although such demand has been met from rapid consumption of fossil energy resources, this approach has led to the accumulation of CO_2 emissions in the atmosphere. Obviously, efficient and secure energy is the main enabler for welfare and economic development of any society. Modern lifestyles demand a steady and reliable supply of energy, which has roots in our mobility, prosperity and daily comfort, but we should not take this energy security for granted. As energy-related activities have significant environmental impacts, it is crucial to provide an

energy system which covers the needs of the economies and preserves the environment. Aside from hydrogen - the cleanest fuel and a green energy carrier - ammonia provides the only carbon-free chemical energy storage/carrier solution, offering advantages in terms of energy capacity and distribution infrastructure without causing end-user CO_2 emissions (unlike methane and methanol). Thus ammonia, with its high hydrogen density, could be an interesting companion to hydrogen for energy storage and energy carrier purposes [5].

Ammonia is a precious commodity in the supply chain of both food and energy, and therefore plays an important role in the development of human life. This has triggered numerous interests in developing alternative routes in pursuit of a more decentralized and environmentally friendly approach for ammonia synthesis. This thesis explores an alternative synthesis of ammonia from heterogeneous reactions of its reactants on the surface of transition metal nitride catalysts at ambient conditions where protons could come from a proton-donor-containing solution while the electrons would be driven to the electrode surface by an applied electric potential.

1.1 Growing energy demand

In the pre-industrial age, the required energy of societies was dependent on plants when biomass was the only energy carrier. The consumption of plants did not change the environment because the CO_2 liberated by the humans and animals was reabsorbed by the plants during photosynthesis. Since the beginnings of industrialization in the early 1800s, energy requirements have been rapidly increasing and different sources of energy have been utilised to meet this vital increasing demand as represented in Figure 1.1. The amount of energy provided by biomass remained almost constant, but new sources (like fossil fuels, natural gas and renewable energies) appeared helpful in providing the required energy of the world. Consequently, the world energy consumption started to increase from 5×10^{12} kWh/yr in 1860 and reached 1.58×10^{14} kWh/yr as today, and the amount of CO_2 and other greenhouse gases (GHG) increased in parallel.

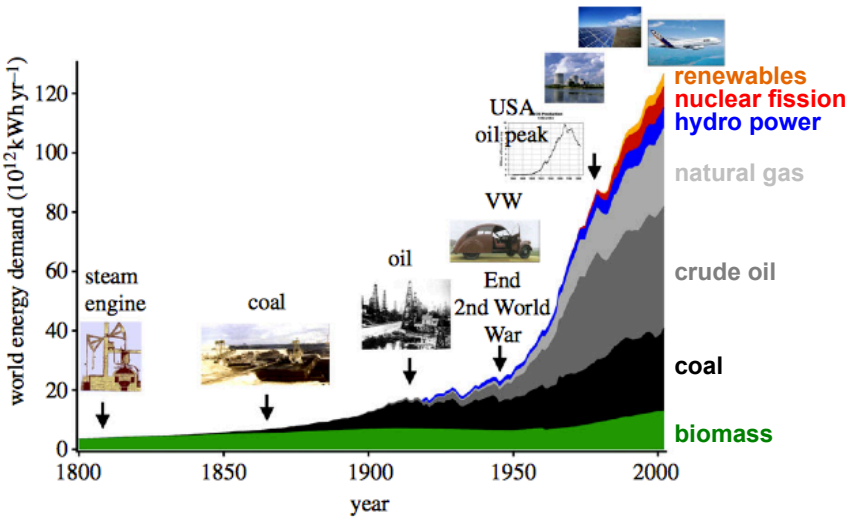

Figure 1.1: *Energy demand according to the energy carriers over the last 200 years. The figure is adapted from [6].*

1.2 Ammonia and its importance in human lives

Ammonia (NH_3) is a compound of nitrogen and hydrogen. It contributes significantly to the nutritional needs of terrestrial organisms by serving as a precursor to food and fertilizer. Ammonia, either directly or indirectly, is also a building block for the synthesis of many pharmaceutical products and is used in many commercial cleaning products. Ammonia is one of the most highly produced chemicals worldwide because it is a source of active nitrogen for fertilizer, a clean energy carrier, and a potential transportation fuel due to its high energy density and the potential lack of CO_2 emissions [5, 7]. The total worldwide ammonia production is over 200 million tonnes a year, 80% of which is used in production of fertilizer [8]. Two percent of the total world energy supply is consumed for annual extraction of 120 millions of tonnes of N_2 from air to produce ammonia for fertilizer [9]. The estimated market for ammonia in 2019 is around 102 billion dollars [9]. For comparison, Figure 1.2 shows the top-ten most produced organic and inorganic chemicals in the U.S [10]. Since nitrogen usually limits the yield of intensive agriculture, the major application of ammonia is its use as synthetic fertilizer [11]. Of the total production of NH_3 in the U.S., around 80 wt% was used as fertilizer in forms of NH_3 or NH_3-derived chemicals

such as urea, ammonium sulfate or nitrate, etc., and the remainder was used for the synthesis of plastics and explosives.

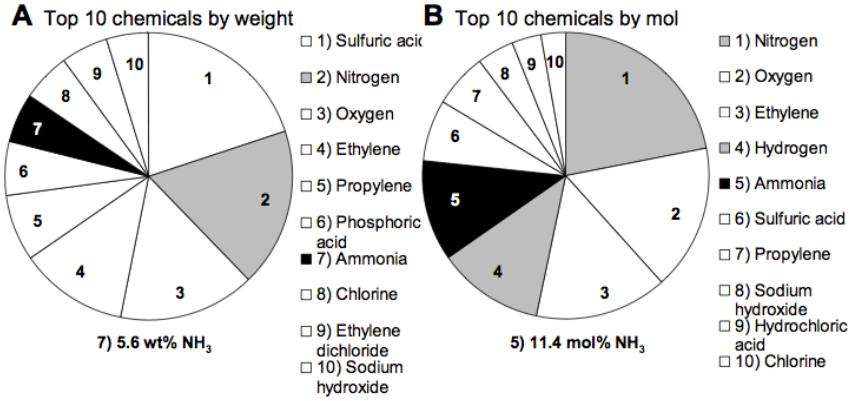

Figure 1.2: *Total production of organic and inorganic chemicals (in the U.S.), A) in wt% of 1.87 $\times$ 10^8 tonnes/total year, B) in mol% of 5.41 $\times$ 10^{12} mol/year. Data are taken in tonnes per year for all chemicals but in cubic meter per year for N_2, O_2 and H_2. The figure is reprinted from [10].*

Nitrogen is of decisive importance. This element is needed for DNA and RNA, the molecules that store and transfer genetic information. Nitrogen is also required to make proteins, receptors, and structural components of all plant and animal cells. Humans, like other animals, cannot synthesize these molecules using the abundant nitrogen found in the air. This is because molecular nitrogen is chemically inert and stable, and does not transform easily into a reactive form that plants, animals, and ultimately human beings can take up. However, microorganisms existing in nature use an enzyme called nitrogenase to produce ammonia from solvated protons, electrons, and atmospheric nitrogen. In contrast to the artificial Haber-Bosch process, nitrogenase can synthesize ammonia at room temperature and atmospheric pressure. In the enzyme, the active site is a $MoFe_7S_9N$ cluster catalyzing the electrochemical reaction: $N_2 + 8(H^+ + e^-) \rightarrow 2NH_3 + H_2$. Therefore, the nitrogen compounds necessary for the creatures have to be acquired from food production of which depends upon agriculture and thus ammonia as a source of nitrogen-based fertilizer. Therefore, intensive agriculture and food production relies on the industrial production of nitrogen-based fertilizer providing enough amounts of nitrogen to the soil, plants, and other creatures.

After the Green Revolution and Industrilized Agriculture commenced by the Haber-Bosch invention, and with increase in consumption of nitrogen-based fertilizer, the world's population has risen exponentially over the last century. Figure 1.3A illustrates clear correlation between the growth in world's population and the upward trend in average nitrogen fertilizer input. Hence, ammonia has been receiving tremendous attention as fertilizer where 85% of produced ammonia is used as ammonium sulfate, ammonium nitrate, and ammonium phosphate.

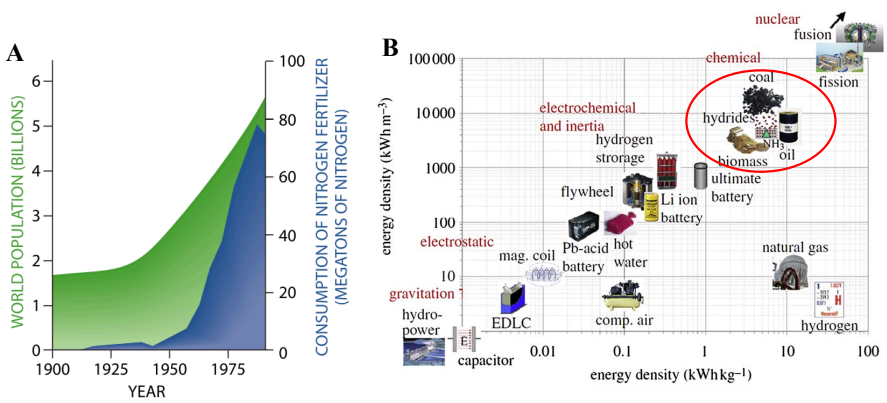

Figure 1.3: *Sudden growth in the global consumption of nitrogen fertilizer during the 20th century has been matched by a parallel increase in world's population (A), the figure is reprinted from [2]. Volumetric versus gravimetric energy density of the most important energy carriers, there are only two options with an energy density similar to that of fossil fuels: hydrides and ammonia (B), the figure is reprinted from [6].*

So far, hydrogen is known to be the cleanest source of energy. However, the low volumetric energy density of hydrogen, in both compressed gas and liquid forms, makes its storage a challenge for most applications. This is not only a limitation in the area of onboard storage, but it is also problematic in the delivery and distribution of hydrogen. Hydrogen low energy density is perhaps one of the greatest barriers to the implementation of hydrogen fuel cell vehicles. On the other hand, liquid anhydrous ammonia could be a more suitable medium for the storage of hydrogen onboard vehicles or for use as a distribution medium. When considering both the volumetric and gravimetric energy density of ammonia, it is of similar energy density as oil and coal with orders of magnitude higher volumetric energy density compared to hydrogen (demonstrated in Figure 1.3B). Therefore, in addition

to the key role of ammonia in agriculture and the food cycle, it can also be a potential energy storage and energy carrier material. Ammonia can be decomposed (cracked) over a catalyst to produce the desired fuel, hydrogen (H_2), along with nitrogen (N_2) that is a non-toxic and non-greenhouse gas. All in all, ammonia has been receiving much attention as a green fuel and hydrogen source for mobile and remote applications [12, 13], as a potential indirect hydrogen storage, and hydrogen carrier material [5, 14].

1.3 Heterogeneous catalysis and reaction mechanisms for nitrogen reduction to ammonia

Catalysis is categorized into three different subdisciplines: homogeneous, heterogeneous, and bio catalysis. This thesis chiefly focuses on electrocatalysis which has many analogues to conventional heterogeneous catalysis. Both conventional heterogeneous catalysis and electrocatalysis involve adsorption, desorption and bond making/breaking steps. Thus, many of the principles that govern reactivity of heterogeneous catalysis also remain the same. Therefore, we narrow down the discussion toward heterogeneous catalysis here. A heterogeneous catalytic reaction involves adsorption of reactants from a gas/liquid phase onto a solid surface, surface reaction of adsorbed species, and desorption of products into the gas/liquid phase (Figure 1.4A). A catalyst offers an alternative mechanism or path for the chemical reaction. Such a mechanism is more complex but energetically much more favorable due to a lowering in the activation energy. As a result, the reaction can proceed at faster rates or the same rate can be achieved with less energy input. The catalyst does not alter the thermodynamics and overall energy change of the reaction. This enables the desired process to occur under industrially feasible conditions of pressure and temperature. A catalyst can accelerate a chemical reaction by forming bonds with the reacting molecules and allowing them to react to a product, which detaches from the catalyst, and leaves it intact so that it can be available for the next reaction. The route by which a heterogeneous catalyst works is shown in Figure 1.4B. Due to interactions between the electrons of the reactants and the atoms on the surface of the catalyst, a chemical reaction takes place and the reactants are adsorbed on the surface of the catalyst (chemical bond formation or chemisorption). The reactants then react on the surface of the catalyst but are still bound to the surface. Eventually, the products of the reaction are desorbed from the surface and free up the catalytic surface area for further reactions.

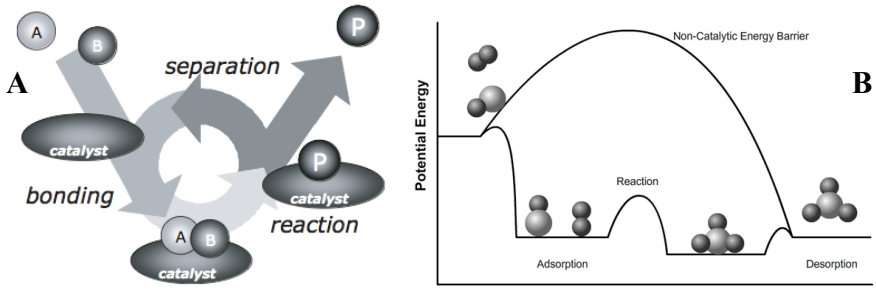

Figure 1.4: *(A) Every catalytic reaction is a sequence of elementary steps, in which reactant molecules bind to the catalyst, where they react, after which the product detaches from the catalyst, liberating it for the next cycle. (B) Potential energy diagram of a heterogeneous catalytic reaction, with gaseous reactants and products and a solid catalyst. Note that the uncatalyzed reaction has to overcome a substantial energy barrier, whereas the barriers in the catalytic route are much lower. The figure is adapted from [15].*

According to the Sabatier principle [16], a good catalyst is a material that bind moderately well to the desired reactants and products so that the interactions between a catalyst and the reactants become "just right". If the interaction is too strong, either reactants or products block the catalyst surface, causing little or no reaction to proceed and the catalyst surface is called poisoned. On the other hand, if the interaction is too weak then reactants will not bind to the surface and no reaction takes place, so more energy will be needed for its adsorption. Hence, the ideal catalyst should be the one with moderate binding free energies of the adsorbates with a compromise between these two extremes. This concept has been demonstrated for many reactions and an example is shown in Figure 1.5 with catalysts for electrochemical hydrogen evolution. In this example the energy of hydrogen adsorption is used as descriptor and the activity has a clear optimum.

Nitrogen reduction to ammonia on a catalytic surface can proceed by two broad classes of mechanism as shown in Figure 1.6: the associative and dissociative mechanisms. In the associative mechanism, the two nitrogen atoms in N_2 remain bound to each other as the molecule is hydrogenated on the surface after being adsorbed. During hydrogenation, the nitrogen atom adsorbed on the surface might initially remain intact while the outermost nitrogen atom is reduced to NH_3. After formation of the first NH_3, the other N atom is hydrogenated on the surface for formation of the sec-

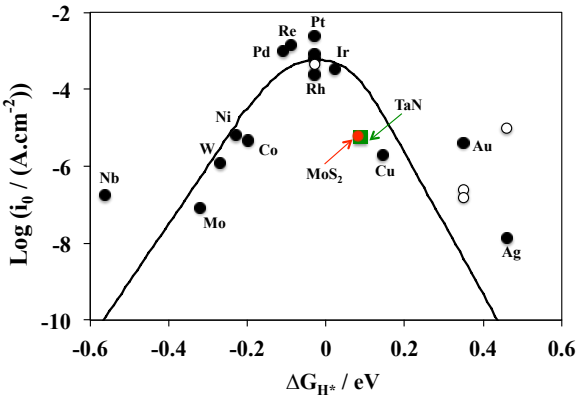

Figure 1.5: *A volcano plot of the HER for various pure metals, MoS_2, and the most promising transition metal nitride surface explored by this thesis, TaN. The $\triangle G_{H*}$ value for TaN is calculated for 2/8 ML H coverage at 1 bar of H_2 and 298 K. Experimental data are adapted from reference [17] where the circular data points are the measured exchange current density (open data points for (111) facets but filled data points for polycrystalline) plotted versus the calculated free energy of H adsorption. The metals on the left side of the volcano have high H coverage (1 ML) and the metals on the right side low H coverage (0.25 ML). The experimental data for MoS_2 is taken from reference [18]. According to Sabatier principle, those on the left leg bind H strongly and those on the right bind it weakly. The optimum binding energy is around zero where optimum rate is observed on top of the volcano.*

ond NH_3. Alternatively, both N atoms might get hydrogenated in parallel and form $2NH_3$. In the dissociative mechanism, however, the N-N bond is first dissociated before hydrogenation, leaving individual N-adatoms on the surface that are then hydrogenated and converted into NH_3 independently. Current evidence suggests that the Haber-Bosch process operates through a dissociative mechanism.

Generally, as a particle (molecule or atom) approaches the surface of a catalyst, it feels the weak van der Waals interaction. If the particle loses energy due to interaction with the surface and gets trapped in the weak attractive potential, it become physisorbed on the surface (no shared electrons between the surface and the approaching particle yet). If the particle can rearrange its electronic configuration by interacting with the sp and d electrons of the catalyst, it may become chemisorbed (share of electron and chemical bond formation). Depending on how far the particle is from the surface, and on how strong the chemisorption bond is, the molecule may have to

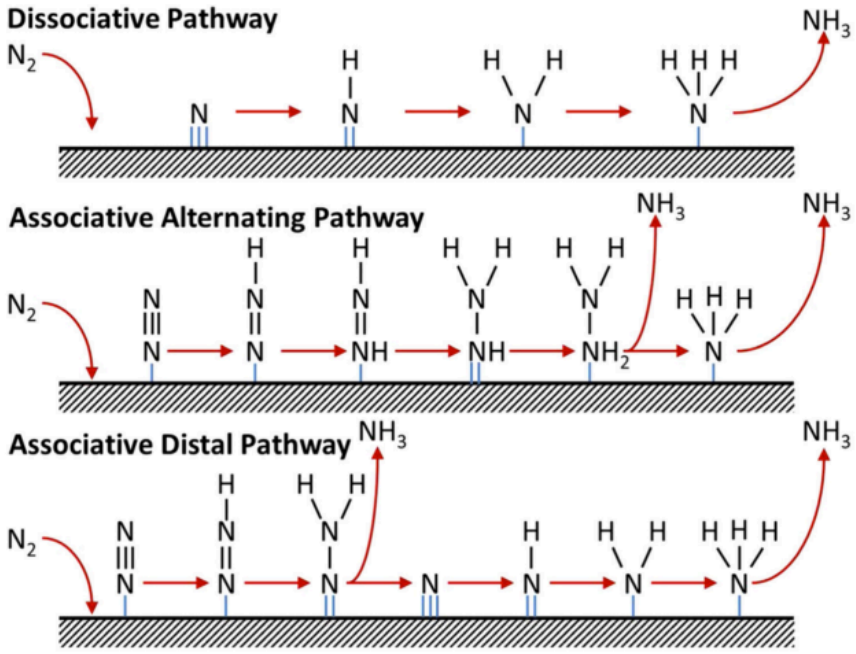

Figure 1.6: *General mechanisms for nitrogen reduction to ammonia on heterogeneous catalysts. The figure is adapted from [19].*

overcome an energy barrier, as indicated in Figure 1.7A. Usually, the barrier between physisorption and chemisorption is small [15], but it depends on the system under investigation. Since the chemisorption energy is also dependent on the orientation of the particle relative to the surface, the actual potential is more complicated than the simple one-dimensional representation in the Figure 1.7. Now assume that the chemisorbed particle is a molecule. If it gets closer to the surface, it will feel a strong repulsion and the energy rises. But if this molecule can respond to this change by changing its electron structure in the interaction with the surface, it may dissociate into two chemisorbed atoms. The potential depends on the orientation of the molecule with respect to the atoms in the surface. The barriers between the physisorption, associative and dissociative chemisorption are activation energies for the reaction from gas phase molecule to dissociated atoms and all subsequent reactions.

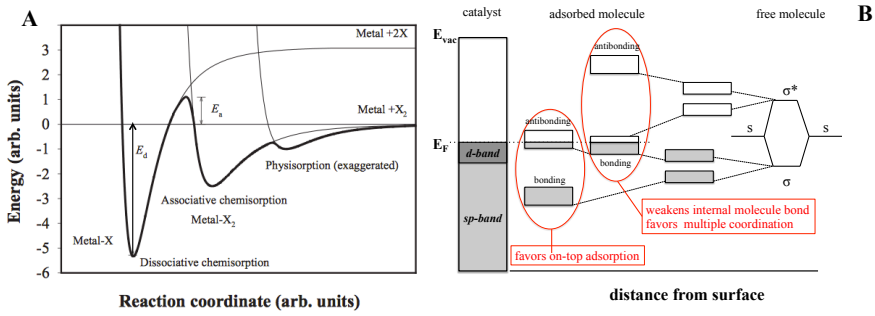

Figure 1.7: *Simplified schematic A) potential energy diagram along the reaction coordinate of a molecule X_2 approaching a catalyst surface. First the molecule feels the weak van der Waals interaction, leading to physisorption. Then associative chemisorption occurs, in which the molecule interacts chemically with the surface. If the molecule overcomes the barrier E_a, it may dissociate into two chemisorbed atoms. The energy required for desorbing these atoms again to the molecular form is E_d. B) A molecule with a bonding σ and antibonding orbitals σ* interacts with both the sp band and the narrow d band of the transition metal catalyst. The former leads to the lowering and broadening of the bands, while the latter results in splitting into bonding and antibonding orbitals. Note that if electrons fill the antibonding orbital of the molecule then the internal bonding in the molecule becomes weaker, which may lead to dissociation of the molecule. Figures are adapted from [15].*

1.4 Current industrial ammonia synthesis

For the last century, ammonia has been synthesized primarily via the energy- and capital-intensive Haber–Bosch process, an artificial nitrogen fixation process in which gaseous nitrogen and hydrogen are passed over a transition metal-based catalyst (Fe or Ru) at high pressure (150–350 atm, different from plant to plant) and high temperature (350–500 °C, different from plant to plant) to form NH_3 (Figure 1.8) according to: [2, 20]

$$N_2(g) + 3H_2(g) \rightleftharpoons 2NH_3(g) \tag{1.1}$$

where $\triangle$H = -92 kJ/mole, equivalent to -0.95 eV (-0.476 eV for 1 mole of NH_3).

The reaction is reversible and the production of ammonia is exothermic. In order to produce the maximum possible amount of ammonia in the equi-

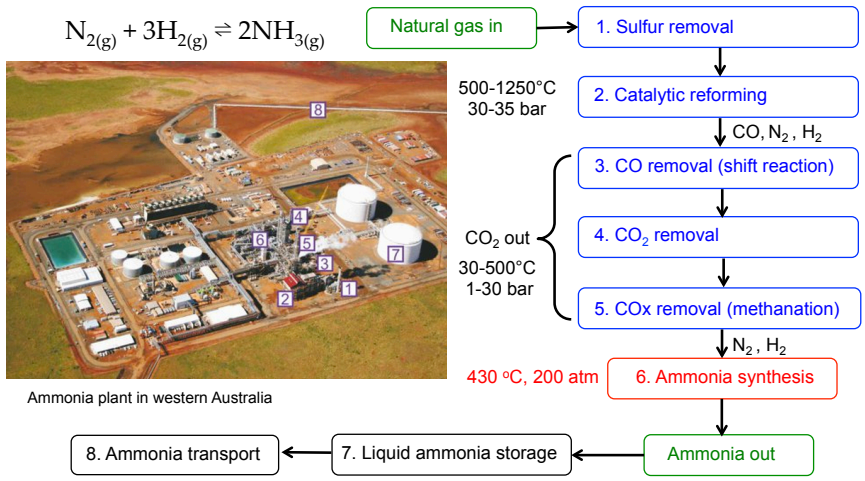

Figure 1.8: *Industrial ammonia synthesis plant and an overview of the steps before storage and transportation of the product.*

librium mixture, the position of the equilibrium needs to shift as far as possible to the right. Since this is an exothermic reaction, lowering the temperature will be favorable according to Le Chatelier's principle; however, lowering the temperature will slow down the reaction. Also, the time for the reactants to reach equilibrium and be in contact with the surface of the catalyst will increase. Therefore, it should be a compromise in temperature for producing a reasonably high proportion of the product in the equilibrium mixture in a very short time (to provide an adequate reaction rate). This compromise temperature in modern plants is around 350 °C. This high temperature definitely shifts the equilibrium towards the reactants, resulting in an undesirable decrease in the conversion of the reactants to the product as no catalyst may produce more ammonia than the equilibrium amount. The high pressures are chosen to alleviate this problem, since that shifts the equilibrium in favor of the products. High pressure also facilitates collision of the molecules of the reactants via getting them closer together and increasing the chance of hitting and sticking to the surface of the catalyst.

In the Haber-Bosch process, nitrogen is obtained from air, while hydrogen is taken mostly from steam reforming of natural gas in Europe (42 plants spread over 17 countries), but also from coal in China, and from a mix of natural gas and naphtha in India [21]. Following one hundred years of im-

provement, catalytic synthesis of ammonia has made remarkable progress. After the discovery of an iron catalyst for ammonia production in 1905, cobalt-containing iron catalysts became an important development for the iron catalyst patented by the British company Imperial Chemical Industries (ICI). The amount of cobalt gradually decreased and CeO_2 was added instead to the iron catalyst to increase the activity. In the 1970s, Ozaki's research group reported high activity for ammonia synthesis when they used Ru as an active component, potassium as a metal promoter, and carbon as a catalyst carrier [22–25]. In 1992, a new ammonia synthesis process called KAAP (Kellogg Advanced Ammonia Process) was developed that was loading ruthenium carbonyl compounds on graphite carbon carriers to make Ru/C catalysts, yielding around 20 times greater catalytic activity at milder operating conditions than that of traditional ammonia catalysts [26].

Despite the high activity of Ru/C catalysts, methanation of carbon carrier material under ammonia synthesis conditions led to shortening of the catalyst's life and added another weakness in addition to scarcity and high expense of Ru. The latest improvement in the study of ammonia synthesis catalysts is the discovery of the cobalt-molybdenum nitride (Co_3Mo_3N) catalyst [27–31]. Along with improvements in the catalyst itself, advancements in technology and engineering have also played an important role in the development of ammonia synthesis. For example, daily ammonia production has increased from the initial 5 tonnes to the current 3000 tonnes in modern plants, the reaction pressure has dropped to around 150 atm from the original 986 atm, and the energy consumption has decreased to 28-30 GJ/tonne from the initial 78-80 GJ/tonne [32, 33]. But ammonia production still consumes 2% of the total energy supply in the world and releases around 2.2 tonnes of CO_2 per tonne of ammonia [33]. Steam reforming with natural gas consumes approximately 84% of the total energy required for industrial ammonia synthesis via the Haber-Bosch process. Still, over 90% of this energy is provided by fossil fuels which leads to increased production of various greenhouse gases. The harsh operating conditions and sophisticated industrial setup of the Haber-Bosch process are all prohibitive to decentralization of environmentally-friendly ammonia synthesis. This complicates ammonia production in regions with relatively undeveloped infrastructure such as developing countries. Besides, the reliance of this process on natural gases for supplying its necessary hydrogen feedstock not only promotes severe CO_2 emission to the environment but also makes the production of ammonia, and ultimately food, susceptible to natural gas price fluctuations and political conflicts in the oil-rich regions. Most importantly, a sustainable process needs to be developed for ammonia production to maintain food supply since at some point natural gas will be depleted. Therefore,

development of a new process for green and decentralized ammonia synthesis in much milder operating conditions is desired. This thesis attempts to lead us in that direction.

1.5 Fossil-free ammonia synthesis via electrocatalysis

Electrocatalysis is the catalysis of reactions in which at least one elementary step is a charge transfer, or electrochemical reaction. Electrocatalysis is an important process in nature with many enzymes functioning as electrocatalysts. For example, the enzyme nitrogenase catalyses the electrochemical formation of NH_3 from molecular N_2 and solvated electrons and protons [34]. Similarly, hydrogenases catalyse the reduction and oxidation of molecular hydrogen, which forms the basis of metabolism for many microbial communities [35]. Electrocatalysis is finding increasing utility in industrial applications, most notably for catalysis in the renewable energy industry. The use of electricity as an energy source means that renewable sources such as solar, wind and hydropower may be used, thus decreasing the global reliance on supply-limited and CO_2-emitting fuels.

Electrocatalytic ammonia synthesis is a particularly attractive fossil-free alternative method due to the potential of utilizing renewable energy sources and generating new possibilities towards low-temperature and low-pressure ammonia synthesis with a low carbon footprint [19, 36–38]. In this approach, instead of a separate H_2(g) production process, the protons could come from a proton-donor-containing solution while the electrons would be driven to the electrode surface by an applied electric potential (Figure 1.9).

1.6 Major experimental endeavours

Over the last few decades, numerous efforts have been made towards man-made ammonia synthesis using photocatalytic [39] and electrochemical [40–45] methods. However, for many of these, it was difficult to regenerate the active nitrogen-fixing complex and only low current efficiencies of 0.1–8% at ambient conditions were obtained. To gain higher yields of ammonia, electrochemistry with the use of solid-state electrolytes [46–49], ionic liquids or molten salts [50–53], and polymer electrolyte membranes (PEMs) [54–56] have been employed. The first two categories are usually used in high-temperature ammonia synthesis (100 °C $<$ T $<$ 700 °C), but the last one is utilized in low-temperature conditions (T $<$ 100 °C). The reactor-cell design employed in most high-temperature ammonia synthesis is similar to the one depicted in Figure 1.10A, while most low-temperature ammo-

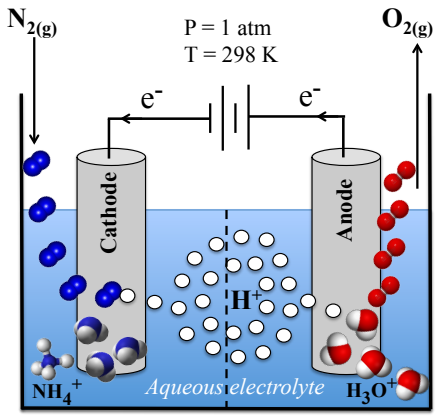

Figure 1.9: *Simple schematic representation of an electrochemical cell comprised of both the cathodic and anodic compartments separated with a membrane. The reference electrode is not shown in this cartoon.*

nia synthesis with Nafion membrane is carried out in cells similar to the one showed in Figure 1.10B. The possible electrolytes in the majority of high-temperature ammonia synthesis reactions are perovskite, composite materials with fluorite or pyrochlore structures, and molten salts.

In the high temperature solid-state ammonia synthesis (SSAS) category, high conversion of cathodic supplied nitrogen to ammonia is usually obtained. Two common types of electrolytes used in SSAS is shown in Figure 1.11. Pd or Pd-Ag showed the best performance as cathode material for high yield ammonia formation [57–61]. The best electrolytes in which Pd and Pd-Ag yielded the highest FE% are usually barium cerates, lanthanum-doped cerium oxide, lanthanum gallate and lanthanum zirconate electrolytes. The most efficient SSAS systems reported so far are 1) barium-cesium based SSAS with 70% FE [58], 2) lanthanum-serandium based SSAS with 70-73% FE [59, 60], 3) scandium-cesium based SSAS with 78% FE [57], 4) lanthanum-calcium based SSAS with 80% FE [61]. Composite electrolytes consist of a mixture of a solid oxide with a second phase which changes the overall electrical, thermal, or mechanical properties of the material. This extra phase is often a eutectic mixture of alkali metal salts such as carbonates, halides, sulphates, or hydroxides [37]. The presence of the molten phase enhances the ionic conductivity and reduces the operating temperature of the electrolyte. The eutectic mixture is a mixture of two or more components that usually do not interact to form a new chemical compound. They in-

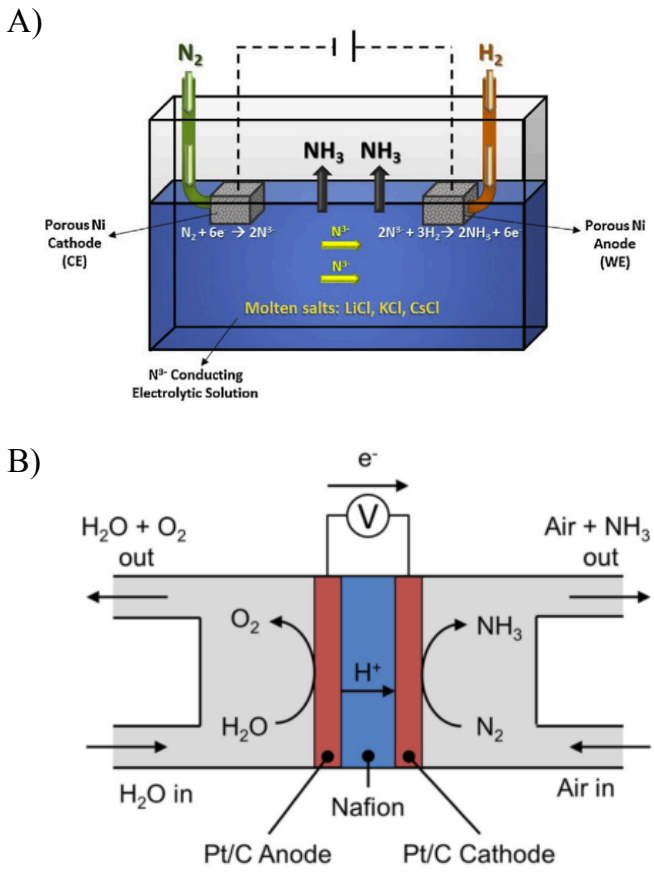

Figure 1.10: *A) Apparatus used by Murakami et al. [50]. The electrolyte was a N^{3-} conducting molten salt mixture (57.5 LiCl, 13.3 KCl, 29.2 CsCl mol%) and nitrogen was reduced on a porous Ni cathode. B) The back-to-back membrane-electrolyte-assembly cell for ammonia synthesis reported by Lan et al.. [56].*

hibit the crystallization process of one another at certain ratios resulting in a system having a lower melting point than either of the components. The most recent investigations in $LiAlO_2$-$(Li/Na/K)_2CO_3$ composite electrolyte indicate two different cathode catalysts, Fe_3Mo_3N [62] and Co_3Mo_3N [63], with relatively good performance under pure nitrogen and wet hydrogen on the side of the anode. The cobalt-molybdenum nitride showed better performance at 450 °C where a maximum rate of 3.27 $\times$ 10^{-10} mol s^{-1} cm^{-2} was obtained under applied potential of 0.8 V vs the counter electrode.

However, the FE% was only around 3%. Very recently, Qing *et al.* reported anodic ammonia formation rate of around 2.0 $\times 10^{-10}$ mol s^{-1} cm^{-2} at +1.2 V and 220 °C [49]. They synthesized ammonia directly from N_2 and steam using a composite electrolyte based on $CsH_5(PO_4)_2/SiO_2$ and Pt/C-loaded carbon paper as both cathode and anode, but the FE was only around 2%. Such low efficiency in all the cases mentioned here can be attributed to the rapid hydrogen evolution reaction (HER) at high temperature values.

Ionic liquids or molten salts were found capable of promoting ammonia formation from low efficiencies to sometimes up to 80% but requiring relatively high temperatures [50–53]. Licht *et al.* utilized a suspension of iron-oxide nanoparticles in the electrolyte (molten hydroxide, (NaOH–KOH)) for ammonia synthesis from air and steam between two Ni electrodes [53]. The rate of ammonia generated by this system was 2.4 $\times$ 10^{-9} mol s^{-1} cm^{-2}, which reached the FE of 35% under 1.23 V at ambient pressure. Despite an appreciable rate and FE, relatively high temperatures of around 200 °C were used. The highest rate of 3.33 $\times$ 10^{-9} mol s^{-1} cm^{-2} was observed when porous nickel electrodes were immersed in a eutectic mixture (of 57.5 LiCl, 13.3 KCl, 29.2 CsCl mol%) in the experiment by Murakami *et al.* [50]. The FE% obtained was 72% at 400 °C and 0.7 V vs the Li^+/Li electrode. In the electrolyte 0.5 mol% Li_3N was dissolved as the source of nitride ions (N^{3-}). In this setup, the supplied nitrogen to the cathode is reduced to N^{3-} and traveled to the anode through the electrolyte and reacted with hydrogen to produce ammonia ($N^{3-} + 3/2H_2 \rightarrow NH_3 + 3e^-$). Although low-pressure ammonia synthesis had been achieved, the aforementioned studies yet suffer from the necessity of relatively high temperatures, which leads to increased risk of product decomposition. The use of complex and expensive electrolytes is another downside that hinders decentralization of ammonia production and commercialization of these methods.

There are also studies that investigated low-temperature ammonia synthesis at ambient pressure with the use of polymer electrolyte membranes (PEMs) where the ammonia production can be separated from hydrogen feed gas and thus higher ammonia formation yields is achieved [55, 64]. The highest rate of ammonia formation reported in this fashion is 1.13 $\times$ 10^{-8} mol s^{-1} cm^{-2} with a current efficiency of around 90% obtained at 80 °C where $SmFe_{0.7}Cu_{0.3}$-xNi_xO_3 (x = 0-0.3) was used as the cathode and wet hydrogen as a feed gas [54]. Replacing the H_2 feed gas with water, Kordali *et al.* synthesized ammonia electro-catalytically from N_2 and H_2O at room temperature using a Ru cathode in a solid polymer electrolyte cell [65]. Only a low rate of ammonia formation (3.4 $\times$ 10^{-12} mol s^{-1} cm^{-2}) with a low efficiency of around 0.28% was achieved at a relatively high potential (-1.3

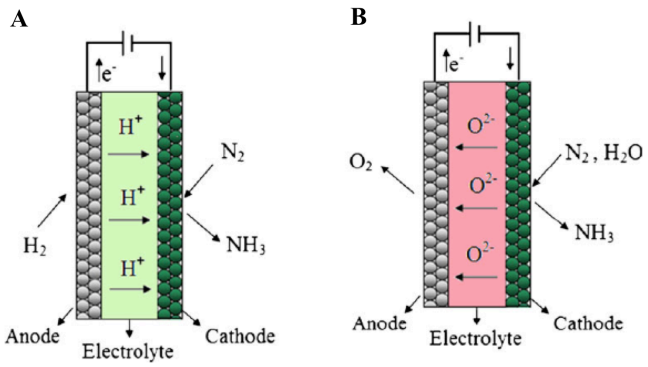

Figure 1.11: *Schematic illustration of the solid-state ammonia synthesis (SSAS) process; A) proton-conducting electrolyte and B) oxide-ion electrolyte. The figure is adapted from [36].*

V vs. SHE) mainly due to the competing HER at the cathode. Using air and water as feed gases, the highest rate of ammonia synthesis reported thus far is 1.14×10^{-9} mol s^{-1} cm^{-2}, achieved using a mixed NH_4^+/H^+ Nafion membrane [56]. However, again a low efficiency of around 1% is observed at a relatively high overpotential of -1.6 V.

Although the progress towards practical electrolytic ammonia synthesis acheived so far is promising, there are yet two major concerns. One is the issue of high temperatures observed in most of the works mentioned above, which reduce the chance of decentralization of ammonia production by truncating its practicality for consumer use. The other is the acidic environment in which material instability arises. These issues severely limit our options amongst catalytic materials and potentially eliminate many highly active and selective catalysts from consideration. Although there is no doubt about high stability, long lifetime, and fast ion transport properties of PEMs in other electrochemical applications, ammonia as a weak base is expected to react with acidic membranes and reduce proton conductivity and lifetime of the membrane [56]. In addition, acidic electrolytes can cause higher rate of HER and thus less selectivity of the catalysts towards nirogen reduction. The alternative option is to favor alkaline chemistry instead, which not only reduces the membrane reactivity with ammonia, enables low-cost materials of construction, and allows the utilization of a wider array of low-cost and active catalysts, but it also hampers the occurance of the HER and assists selectivity towards nitrogen reduction. For these reasons, alkaline exchange membranes (AEMs) are an attractive alternative to PEMs

for electrochemical ammonia synthesis [64].

A very recent example of the feasibility of an alkaline membrane electrolyzer as an ammonia generator is the work of Renner *et al.* by which catalytic efficiency was investigated for Fe, FeNi and Ni nanoparticles over Pt black and the equivalent energy consumption rate of these materials were compared to that of the Haber-Bosch process [64]. Although the ammonia production rate was only around 1.3 - 3.8 $\times 10^{-12}$ mol s^{-1} cm^{-2} at 1.2 V, with efficiency of 41% at 50 °C, FeNi high surface area particles were found to be stable and highly active for electrochemical ammonia syntheis. The energy consumption rate of this process was estimated to be 14 - 520 kwh/kg of ammonia, compared to 13.2 kwh/kg of ammonia in the current industrial process [64].

What is obvious here is that while solid-state electrolytes, PEMs, or AEMs offer promise as an electrochemical route to ammonia synthesis, they are still in the early stage of development when compared with production rates nearing that of commercial viability (4.3 – 8.7 $\times 10^{-7}$ mol s^{-1} cm^{-2}) [37]. The above examples clearly indicate that (electro-) catalytic ammonia synthesis is a particularly feasible method due to the potential of utilizing renewable energy sources and mild operating conditions. But finding (electro-) catalysts that are selective enough towards nitrogen electroreduction reaction (NER) and have a low overpotential is challenging.

1.7 Recent theoretical insights

With advancements in the field of computation and modelling, theoretical investigations have provided deeper insight into catalysis, [66–79] the importance of various active sites [80–82], the influence of phase and morphology [83], and different mechanisms of reactions [84–88]. The use of computations can thus facilitate rational catalyst design, by enabling whole classes of material to be assessed for their suitability as catalysts. According to density functional theory (DFT) analysis conducted by Skúlason *et al.* [89], the simplest catalyst for electrochemical ammonia formation would be a pure transition metal catalyst. Based on these computational calculations conducted on both the flat and stepped surfaces of a range of pure transition metals, early transition metals of Sc, Y, Ti, and Zr were predicted to bind N-adatoms more strongly than H-adatoms in 1 M aqueous electrolyte (pH = 0) at room temperature. NH_3 formation was proposed to be more favorable over H_2 evolution at operating potentials of around -1.0 to -1.5 V vs. SHE. However, these early transition metals are known to readily form oxides and it remains to be seen if they can be used for experimental N_2

activation. It was also shown that the surface of later transition metals of Fe, Rh, and Ru are mainly covered with H- adatoms under operating conditions. This inhibits nitrogen reduction to ammonia due to lack of available sites for adsorption of nitrogen, which leads to a high rate of HER. These findings might also explain the reason for the generally poor rates of ammonia production compared to hydrogen evolution in much of the existing literature.

Under-coordinated sites on surfaces or on nanoparticles often dominate the whole catalytic activity for the catalyst. The role of such under-coordinated sites have also been recently investigated on metal clusters explicitly, with [86] and without a nitrogen skin [75], as well as in the presence of O, OH, and H_2O, [90] where ammonia is predicted to be produced at around -0.6 V on MoN nanoclusters. In the last couple of examples, the studied mechanisms for electrochemical ammonia synthesis was based on the conventional associative and dissociative mechanisms (Figure 1.6) where there are always issues with endothermic adsorption of N_2 molecule on the surface (in the associative mechanism) or with high activation barriers for N_2 dissociation (in the dissociative mechanism). However, there exists the possibility of another active mechanism, specifically on the surface of metal nitride materials, where a surface N atom is reduced to NH_3 leaving N-vacancies behind, after which the catalyst is regenerated with solvated nitrogen in the electrolyte. This is the Mars-van Krevelen mechanism (MvK) [91] illustrated in Figure 2.2. Indeed, recent DFT analyses indicate possibility of the MvK on ternary nitrides and participation of N-vacancies (in large concentrations of around 10^{13} cm^{-2}) playing an important role for ammonia formation on the surface of Co_3Mo_3N [82]. Ternary nitrides Fe_3Mo_3N, Co_3Mo_3N, and Ni_2Mo_3N emerged as highly active catalysts in ammonia synthesis at 400 °C and 100 bar where promotion of Co_3Mo_3N with caesium resulted even in higher activity than that of the commercial multi-promoted iron based catalyst [28–30, 92, 93]. DFT studies on cobalt molybdenum nitride show that nitrogen vacancies can contribute to weakening of the strong triple bond of N_2 molecule and thus activate it to ammonia via the MvK mechanism. There, a molybdenum triangular cluster can be a possible activation site for nitrogen along with the surface cavity where N_2 is activated by the inner tetrahedral atom of a cobalt cluster [82, 94].

1.8 Objectives of the thesis

Given the promising performance of the ternary nitrides in catalytic synthesis of ammonia and the inception of the MvK mechanism in this regard, this thesis specifically explores the stability and activity of transition

metal mononitride surfaces for electrochemical ammonia synthesis at ambient conditions using DFT calculations. This thesis investigates whether these mononitrides display unique properties due to the presence of nitrogen vacancies in the surface, which are naturally not found on pure metals. If so, this could contribute to higher activity, better selectivity, and an easier pathway towards ammonia synthesis at ambient conditions.

For catalytic nitrogen reduction to ammonia, these TMNs have a benefit over pure transition metals since nitrogen atoms are already incorporated in their structure. That means nitrogen atoms in the first surface layer of the TMNs can in principle directly participate in the reaction of ammonia formation and leave an N-vacancy on the surface. This N-vacancy then needs to be replenished by adsorbed N_2 molecule to endure the catalytic cycle, via the MvK mechanism. In many cases, N_2 adsorption to the N-vacant site(s) becomes an exergonic process on TMNs [79, 81, 95], compared to when N_2 needs to be adsorbed on pure transition metals [89, 96] or on defect-free TMNs [87] which is usually endergonic. TMNs can be good catalysts for various reactions typically catalyzed by noble metals of high cost and limited supply. Therefore, it is interesting to investigate catalytic reactions like nitrogen activation on these TMN surfaces via the MvK mechanism.

Therefore, a systematic computational screening of 100 transition metal mononitrides was carried out to search for new electrocatalysts capable of selective conversion of nitrogen to ammonia electrochemically at ambient conditions with low overpotential (preferentially less than 1V). The hope is that this thesis can endow the scientific communities and experimentalists in the field with novel and promising candidates that warrant further investigations and improvement via experiment in pursuit of their commercialization and real life applications.

2 Theory and Methodology

The ultimate goal of most quantum chemical approaches is the approximate solution of the time-independent, non-relativistic Schrödinger equation:

$$\hat{H}\psi_n = E_n\psi_n \tag{2.1}$$

where E_n is the energy of the system, and ψ_n is the many-body wavefunction associated with state n depending on three spatial coordinates of the electrons and nuclei and one spin coordinate of electron. The Hamiltonian operator for a molecular system with M nuclei and N electrons in the absence of electric fields is denoted as $\hat{H}$, and it gives a proper description of how particles in a particular system behave and interact. The molecular Hamiltonian can be expressed in atomic units as:

$$\hat{H} = -\frac{1}{2}\sum_{i=1}^{N}\nabla_i^2 - \frac{1}{2}\sum_{A=1}^{M}\frac{1}{M_A}\nabla_A^2 - \sum_{i=1}^{N}\sum_{A=1}^{M}\frac{Z_A}{r_{iA}} + \sum_{i=1}^{N}\sum_{j>i}^{N}\frac{1}{r_{ij}} + \sum_{A=1}^{M}\sum_{B>A}^{M}\frac{Z_A Z_B}{R_{AB}} \tag{2.2}$$

where the integers i and j denote the N electrons in the system and A and B the M nuclei. The first two terms in this equation represent the kinetic energy of the electrons and nuclei, respectively where the Laplacian operator,∇^2, is defined as a sum of differential operators ($\nabla^2 = \sigma^2/\sigma x^2 + \sigma^2/\sigma y^2 + \sigma^2/\sigma z^2$). The third term is the external potential or the attractive Coulombic force between a nucleus and an electron. The fourth and fifth terms represent the repulsion interaction of electrons and nuclei, respectively. These last three terms define the potential part of the Hamiltonian. By the practical assumption known as the Born-Oppenheimer approxima-

tion [97] we can assume that the nuclei are stationary due to their heavy mass with respect to the electrons on the time scale of electronic motion. Therefore, the kinetic energy term of the nuclei is rendered invariant and the nuclei-nuclei repulsive interaction becomes a constant for each set of nuclear coordinates. The Hamiltonian, now known as the electronic Hamiltonian gets reduced to:

$$\hat{H}_{electronic} = -\frac{1}{2}\sum_{i=1}^{N}\nabla_i^2 - \sum_{i=1}^{N}\sum_{A=1}^{M}\frac{Z_A}{r_{iA}} + \sum_{i=1}^{N}\sum_{j>i}^{N}\frac{1}{r_{ij}} = \hat{T}_e + V_{eN} + V_{ee} \quad (2.3)$$

The solution of the Schrödinger equation with $\hat{H}_{electronic}$ is $\psi_{electronic}$, which is the electronic wavefunction associated with the electronic energy, $E_{electronic}$. The electronic wavefunction depends upon the electron coordinates, while the nuclear coordinates do not appear in the electronic wavefunction explicitly. The total energy, E_{tot}, is thus the sum of electronic energy and the constant nuclear-nuclear repulsion term: $E_{tot} = E_{electronic} + E_{nuc}$, where E_{nuc} is the last term expressed in equation 2.2.

The last term in equation 2.3, which describes the electron-electron repulsion, is impossible to calculate analytically and is the reason why approximations are needed. Without it, an N electron wavefunction could simply be expressed as a product of N one-electron (hydrogenic) wavefunctions. In order to decouple the motion of electrons, an effective potential V_{eff} can be defined in such a way that each electron moves in an average field of all the other electrons:

$$\hat{H}_{electronic} = -\frac{1}{2}\sum_{i=1}^{N}\nabla_i^2 - \sum_{i=1}^{N}\sum_{A=1}^{M}\frac{Z_A}{r_{iA}} + \sum_{i=1}^{N}V_{eff} \quad (2.4)$$

2.1 Hartree-Fock Theory

The HF method consists of approximating the N-electron wavefunction by a single Slater determinant of N one-electron wavefunctions.The HF energy can be expressed as a sum of 1-electron and 2-electron terms:

$$E_{HF} = \sum_{i}^{N_{elec}} < i|\hat{h}|i > +1/2\sum_{i,j}^{N_{elec}}\left([ii|jj] - [ij|ji]\right) + V_{NN} \quad (2.5)$$

where the first term is a sum of values of the 1-electron integrals for each orbital , ϕ_i, in the Slater determinant wavefunction corresponding to the kinetic and external potential. This whole term is the total kinetic energy of electrons and the nuclear-electron attraction. The $[ii|jj]$ term is the Coulomb integral for electrons in orbitals i and j, and $[ij|ji]$ is the exchange integral for electrons in orbitals i and j. The evaluation of these integrals needs a lot of computer time. The last term in equation (2.5) is the nuclear-nuclear repulsion energy. This HF energy equation comes from using the exact electronic Schrödinger Hamiltonian with the approximate Slater determinant as the wavefunction. The HF energy expression is then minimized with respect to changes in the orbitals. With the use of Lagrange's method of multipliers, to make sure the orbitals remain orthonormal, we obtain the HF equations:

$$\hat{F}\phi_i = \epsilon_i \phi_i \tag{2.6}$$

where the ϵ_i eigenvalues are the transformed Lagrange multipliers, interpreted as orbital energies in the framework of Molecular Orbital Theory. The $\hat{F}$ is the Fock operator:

$$\hat{F}_i = \hat{h}_i + \sum_{j}^{N_{elec}} (\hat{J}_j - \hat{K}_j) \tag{2.7}$$

where the second term on the right is the V_{eff}, the effective potential from all the other electrons as mentioned in equation 2.4, the $\hat{J}_j$ is the Coulomb integral and $\hat{K}_j$ is the Exchange integral. Solving these eigenvalue equations (HF equations) would give us optimal orbitals, ϕ_i, for which the HF eigenvalue equations are true, and ground-state HF wavefunction and energy is then obtained. So we need to guess initial orbitals and then iteratively find better guesses for the orbitals until we find the best ones. That minimizes the HF energy expression. Thus the HF equations are solved self consistently during a variational calculation.

2.2 Density Functional Theory

Density functional theory (DFT) is an incredible success story that with acceptable accuracy and low computational cost has turned into a standard technique used in most branches of chemistry and materials science. Walter Kohn is the founding father of DFT who was awarded with the Nobel Prize in Chemistry in 1998 for his essential contributions to the theory [98, 99]. At

the time of writing this thesis, DFT is applicable to a large range of systems, e.g., atoms, molecules and solids to nuclei and quantum and classical fluids. DFT can predict a great variety of molecular properties such as: molecular structures, total free energies, vibrational frequencies, reaction paths, ionization energies, atomization energies, electric and magnetic properties, etc. DFT can deal with spin polarized systems, superconductors with electronic pairing mechanisms, multicomponent systems such as nuclei and electron hole droplets, free energy at finite temperatures, relativistic effects, time-dependent phenomena and excited states, bosons, molecular dynamics, etc. DFT endows its users with a quantum mechanical description without the complexity of the many-body Schrödinger equation. However, it is only strictly valid for determining the properties of a systems' ground state, rather than its full eigenenergy spectrum. Time-dependent DFT, however, can deal with excited states. The conceptual framework of DFT rests on fundamental theorems proved by Kohn and Hohenberg (HK) [100] and a set of equations known as the Kohn-Sham (KS) equations [99].

The Hohenberg-Kohn theorems and Kohn-Sham equations

Conventional approaches use the wavefunction ψ as the central quantity, since ψ contains the full information of a system. However, ψ is a very complicated quantity that cannot be probed experimentally and that depends on $4N$ variables, three spatial and one spin variable for each of the N electrons. It would be much simpler if we could get the energy from only knowing the electron density, $\rho(r)$ depending only on the three spatial variables. This approach would only be possible if ρ(r) contains enough information to derive the full Hamiltonian. We can partition the Hamiltonian as follows which are the same forms as in equation 2.3:

$$\hat{H}_{electronic} = \hat{T}_e(r) + V_{eN}(r;R) + V_{ee}(r) \tag{2.8}$$

where the first term is the electron kinetic energy, the second term is nuclear-electron attraction, and the last term is electron-electron repulsion. The first HK theorem states that the external potential (which is the attractive Coulombic force between a nucleus and an electron, the V_{eN} in equation 2.3 and 2.8) and hence the total energy is a unique functional of the electron density, meaning the ground-state energy of a system is a unique functional of the ground-state density, $E[\rho(r)]$. Therefore, the density contains all the information necessary to determine any quantity of interest, including the Hamiltonian, which has the most important eigenvalue of them all, the energy. We can now write the energy as:

$$E[\rho(r)] = T_e[\rho(r)] + V_{eN}[\rho(r)] + V_{ee}[\rho(r)] \tag{2.9}$$

In order to be able to express at least a part of the V_{ee} term explicitly, we split it into two parts. The first is $J[\rho(r)] = \int\int \rho(r_1)\frac{1}{r_{1,2}}\rho(r_2)dr_1dr_2$ which is a term for the classical Coulomb energy that is exactly like in HF theory but here written out in terms of density. The second part is the $E'_{xc}[\rho(r)]$ term contains the electron-repulsion part we don't know how to deal with. The second theorem of HK says that DFT can be subjected to variational treatment i.e. any trial density will yield an energy upper bound to the true ground state energy, E_0

$$E[\rho^{trial}(r)] \geqslant E_0 \tag{2.10}$$

Deriving the kinetic energy term is too difficult, as electrons are distributed nonuniformly in an atom. However, we can calculate the kinetic energy like in HF theory by introducing orbitals. Here is where KS-DFT came into play by introducing orbitals where self-consistent equations must be solved for a set of orbitals (ϕ_i) whose density, $\rho(r)$ is defined to be the same as that of the total electron density [99]. According to KS, a fictional reference system of non-interacting electrons is constructed, in such a way, that its density is the same as that of the interacting electrons. This fictional reference system is described by a Slater determinant of molecular orbitals. Thus the kinetic energy functional is now defined as:

$$T^{KS} = \sum_{n=1}^{N} n_i < \phi_i^* | \hat{T} | \phi_i > \tag{2.11}$$

and the electron density can be expressed in terms of orbitals as below:

$$\rho(r) = \sum_{n=1}^{N} n_i |\phi_i(r)|^2 \tag{2.12}$$

The KS-DFT energy functional then looks as below:

$$E[\rho(r)] = T^{KS}[\rho(r)] + V_{eK}[\rho(r)] + J[\rho(r)] + E_{xc}[\rho(r)] \tag{2.13}$$

The E_{xc} is a very complicated term that should approximate everything that we do not know how to deal with. Only if we use the exact E_{xc} term, KS-DFT will be exact. The KS equations are:

$$F^{\hat{K}S}\phi_i = \epsilon_i\phi_i \tag{2.14}$$

where analogous to the Fock operator, the KS operator is:

$$\hat{F}^{KS}[\rho(r)] = h_i[\rho(r)] + \sum_j J_{ij}[\rho(r)] + v_{xc}[\rho(r)] \tag{2.15}$$

where the last term is the functional derivative of the exchange-correlation energy: $v_{xc}[\rho(r)] = \dfrac{\delta E_{xc}[\rho(r)]}{\delta\rho(r)}$.

The KS equations are a non-linear problem and need to be solved self consistently [101, 102].

The Exchange-Correlation Energy

The simplest *xc* functional is the local density approximation (LDA) that depends only on the value of the density at each point in the system [99]. The LDA functional is derived from studies of the homogeneous electron gas model system:

$$E_{xc}^{LDA}[\rho(r)] = \int \epsilon_{xc}^{hom}[\rho(r)]\rho(r)dr \tag{2.16}$$

where ϵ_{xc}^{hom} is the exchange-correlation energy per particle of a homogeneous electron gas of charge density ρ. The exchange term has been found analytically for the homogeneous electron gas model system by Slater and Dirac (typically called the Slater-Dirac exchange functional) where density is homogeneous and characterized by ρ [103].

$$E_x^{LDA}[\rho(r)] = -\frac{3}{4}\left(\frac{3}{\pi}\right)^{1/3}\int \rho(r)^{4/3}dr \tag{2.17}$$

The exact density dependence of the correlation energy is not known, but proper values have been determined from Quantum Monte Carlo (QMC)

calculations [104]. These have then been interpolated to provide an analytic form for $E_c^{LDA}[\rho(r)]$ [105]. The following formula has been put forward by Perdew and Wang in 1992[106]:

$$E_c^{LDA}[\rho(r)] = -A \int \rho(1+\alpha_1 r_s) \times ln\left[1 + \frac{1}{A(\beta_1 r_s^{1/2} + \beta_2 r_s + \beta_3 r_2^{3/2} + \beta_4 r_s^2)}\right] dr \tag{2.18}$$

where $r_s = (3/4\pi)^{1/3}$, A, α_1, β_1, β_2, β_3 and β_4 are fitted parameters.

By combining these two terms that are simple functionals that only use the density as ingredients, we can define the LDA functional again:

$$E_{xc}^{LDA}[\rho(r)] = E_x^{LDA} + E_c^{LDA} = \int \epsilon_x^{SD}[\rho(r)] + \epsilon_c^{LDA}[\rho(r)] \tag{2.19}$$

where the first term should take care of the self-interaction error (one electron interacts with its own mean-field) and make the functional obey the Pauli exclusion principle, and the second term should take care of electron correlation. LDA owes a part of its success to a systematic cancellation of errors, as it underestimates the correlation energy but overestimates the exchange energy. LDA is a reasonable method for estimating the properties of bulk materials, since the valence electron density in such materials changes in a rather slow manner and bears a resemblance to the homogenous electron gas. When it comes to atoms and molecules, LDA often fails to predict the correct properties. Also, LDA for complex systems has been shown to predict the wrong ground states, overestimate binding energies and neglect dispersion forces. An improvement to LDA is generalized gradient approximations (GGA)[101], which rely on the gradient of the density allowing for a certain "inhomogeneity" in the density.

$$E_{xc}^{GGA}[\rho(r)] = \int \epsilon_{xc}^{LDA}[\rho(r)] F_{xc}(\rho(r), s) dr \tag{2.20}$$

where the F_{xc} function is called an enhancement factor and can be divided up into F_x and F_c . F_x makes the larger contribution to the energy and is more important. The popular PBE exchange enhancement factor is:

$$F_x^{PBE}(s) = 1 + \frac{as^2}{1+bs^2} \tag{2.21}$$

where a and b are theoretically justified constants. GGA tends to improve total energies [107], energy barriers and structural energy differences [108–110]. Common GGA functionals are PBE [111], RPBE [112], and BLYP [113]. RPBE is the functional used in this thesis, as it has been shown to improve the chemisorption energetics of atoms and molecules on transition-metal surfaces compared to PBE.

Plane-wave basis set

In DFT calculations, the unknown KS orbitals have to be expanded in set of known mathematical functions (basis set). In the calculations conducted for this thesis, which are performed using the DFT code Vienna *ab-initio* simulation package (VASP) [114–118], the orbitals are expanded using periodic plane-wave basis sets in accordance with Bloch's theorem which is optimal for periodic systems.

In this theorem, each of the eigenfunctions of the KS equations for a periodic system are characterized by a principal quantum number n, and a crystal momentum k, and can be spanned by a discrete set of plane-waves with wave vectors $K + G$, where G denotes the reciprocal lattice vectors which is defined by $G.l = 2\pi m$ for all l where l is a lattice vector of the crystal and m is an integer. Therefore:

$$\psi^m_{nk}(r) = \sum_G c^m_{(k+G)} e^{[i(k+G).r]} \tag{2.22}$$

By the use of Bloch's theorem, the problem of the infinite number of electrons has now been mapped onto the problem of expressing the wavefunction in terms of an infinite number of reciprocal space vectors within the first Brillouin zone of the periodic cell, k. This problem is dealt with by sampling the Brillouin zone at special sets of k-points. The electronic wavefunctions at each k-point can then be expressed in terms of a discrete plane-wave basis set.

The kinetic energy in the Hamiltonian is diagonal, but the plane-waves are orthogonal. Thus despite in principle an infinite number of plane-waves are needed for each k-point sampling the Brillouin zone (a particular choice of the unit cell of the reciprocal lattice), the plane-waves converge quickly and the expansion can be truncated at G_{cut}, where

$$\left(\frac{\hbar^2}{2m}\right)|k + G_{cut}|^2 \leq E_{cut} \tag{2.23}$$

In order to reduce the number of plane-waves needed, and thereby the energy cutoff, E_{cut}, we can use a pseudopotential. This is an average potential of the core electrons and the nucleus felt by the valence electrons. Pseudopotentials generally give results of good accuracy, especially so-called ultrasoft pseudopotentials [119]. The basic idea behind the pseudopotential approximation is that the core electrons of an atomic system are nearly unaffected by changes in the chemical environment, and hence it should be possible to combine the effect from the nucleus and the core electrons for an ion into an effective potential. In this way, the "frozen" core electrons are removed from the calculations of the density, and the number of one-electron KS equations is therefore reduced considerably as well as the cutoff energy. This reduction is very important, as the number of plane-waves with an energy below E_{cut} is proportional to $E_{cut}^{3/2}$. The reason for the reduction is that the high frequency part of the basis set is generally needed to describe the core electrons and the part of the valence electrons in the core region. This is because the core orbitals are very localized and because the valence orbitals oscillates in order to be orthogonal to the core orbitals. By using the pseudopotential approximation, the orthogonality requirement disappears and the need for describing the core orbitals disappears at the same time.

Three different types of psedupotential are supported by VASP. They are: norm-conserving psedupotentials, ultra-soft psedupotentials, and projected augmented wave (PAW) potentials. The latter is the one used for calculations of these thesis. All these methods are presently frozen core methods i.e. the core electrons are pre-calculated in an atomic environment and kept frozen in the course of the remaining calculations.

2.3 Normal mode analyses

Normal mode analysis (NMA) is usually a good approach to calculate the vibrational frequencies of, e.g., adsorbed species on a surface. The main assumption made here is that the vibrations of adsorbed species may be described by harmonic oscillators if the species are in a local minimum on the PES. However, in some cases we also do this analysis for the transition states (TS) or saddle point obtained with the NEB method. This may be done if the harmonic approximation is valid, or if the PES is not too flat at the TS. Since this is a TS, it has one frequency less than the ground state because it has one less degree of freedom. That is because one of the

vibrational eigenvalues will be negative, only one imaginary frequency, as it is a maximum in one direction. A linear molecule has 3N-5 normal modes but a non-linear molecule has 3N-6 modes, where N is the number of atoms in the molecule and the subtraction of 5 or 6 comes from 3 translational modes and 2 or 3 rotational modes for the linear and non-linear molecules, respectively. The six normal modes of a 4-atom non-linear molecule, such as NH_3, are as following: one N-H symmetric stretching (3330 cm^{-1}), two N-H asymmetric stretching (3428 cm^{-1}), two H-N-H scissoring (1601 cm^{-1}), and one N-H wagging (1004 cm^{-1}) as shown in Figure 2.1[120].

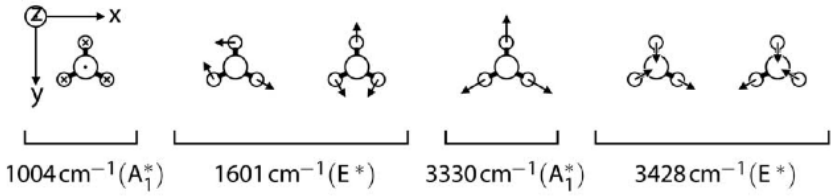

Figure 2.1: *Graphic representation of the normal modes of ammonia and their symmetry classification. N (H) atoms are shown as large (small) circles. The out-of-plane umbrella mode is depicted in such a way that atoms bearing dots (crosses) are displaced forwards (backwards). For the in-plane modes arrows (to scale for each mode) indicate atomic displacements in the paper plane. Infrared-active modes are labeled with an asterisk. Figure is reprinted from [120].*

When an atom is adsorbed on a surface it has 3 normal modes, as it is assumed that it does not diffuse on the surface (zero translational modes) and it has no rotational mode as it is only one atom bound to a fixed surface (the surface does not move). The atom vibrates in 3 directions, the x, y and z directions. The vibrational frequencies, ν, of e.g., an adsorbed atom on a surface can be calculated by:

$$\nu = \frac{1}{2\pi}\sqrt{\frac{k}{m}} \tag{2.24}$$

where m is the mass of that adsorbed atom and k is the force constant in the x direction, which can be calculated from the second derivative of the potential energy (the potential energy function is $V(x) = 1/2kx^2$:

$$k = \frac{d^2\nu}{dx^2} \tag{2.25}$$

The same is done for y and z directions. In practice, when the atom has been relaxed to its minimum on the PES, the atom is displaced slightly in each direction around the minimum and the potential energy and gradient is calculated. For each direction there are three potential energy values at three different coordinates and a parabolic function can be fitted through these points. The curvature, or the second derivative, gives the force constant and then the normal mode. These frequencies can then be divided by the speed of light to get the wave-number, in cm^{-1}.

2.4 Nudged elastic band method

Endergonic elementary processes, in principle, involve a transition between two atomic or molecular states separated by a potential barrier or a first order saddle point along the minimum energy paths (MEP). This saddle point is energetically the highest point in the MEP representing the activation energy of the process. This is also used to determine the rate at which the reaction step occurs. If the barrier is low, the thermal energy of the reactants is usually high enough to overcome the barrier and slide towards products. In this case, the reaction will be fast. But if the barrier is high, only a few reactants will have sufficient energy, and thus the reaction will be much slower. The nudged elastic band (NEB) is a method suitable for finding MEP and saddle points between known reactants and products, developed by Jónsson *et al.* [121–123]. Within the harmonic transition state theory the problem of finding the activation energy of a chemical reaction or diffusion event is reduced to finding the saddle point through which the system has to advance in order to move from the initial state to the final state. When both states are known, this saddle point is most easily read from the MEP of the event.

In NEB, a number of intermediate images are constructed along the reaction path between the known initial and final structure that are connected as a linear chain of images or replicas of the system. Each image in between the two relaxed structures are then optimized to find its lowest possible energy while maintaining equal spacing to neighboring images. This constrained optimization is done by adding an effective or ”nudging” force defined as the sum of the spring force along the band between images to make them evenly spaced, and by adding true force perpendicular to the tangent of

the band to allow images to feel the potential energy surface. The nudging force is given by:

$$F_i = F_{\parallel}^{spring} + F_{\perp}^{true} \tag{2.26}$$

where $F_{\perp}^{true}$ is the potential energy force, which is a function of the coordinates of each image i given by:

$$F_{\perp,i}^{true} = \bigtriangledown E(r_i) - \bigtriangledown E(r_i)\hat{T}_i \tag{2.27}$$

and the spring force can be expressed as:

$$F_{\parallel}^{spring} = k(\mid R_{i+1} - R_i \mid - \mid R_i - R_{i-1} \mid)\hat{T}_i \tag{2.28}$$

When the forces have been zeroed, the chain of images lies on the MEP. Better resolution of the MEP is obtained by increasing the number of images. In this thesis and for calculation of the activation energies for N_2 dissociation, replenishment of N-vacancies, and analyses of nitride decomposition, the climbing image NEB, abbreviated as CI-NEB, is used which is a small modification to the NEB method where the highest energy image is driven up to the saddle point [121]. This image does not feel the spring forces along the band. Instead, the true force at this image along the tangent is inverted. In this way, the image maximizes its energy along the band, and minimizes in all other directions. When this image converges, it will be at the exact saddle point. An example application of the CI-NEB method is shown in Figure 2.2 where the dissociative adsorption of N_2 at a VN(100) surface to form two surface N adatoms is calculated.

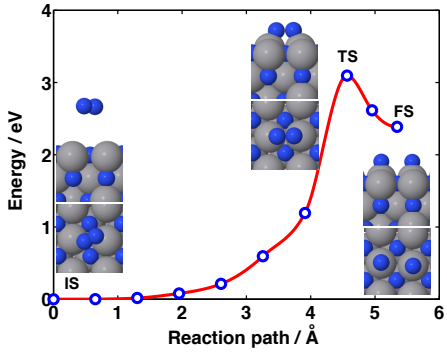

Figure 2.2: *The minimum energy path along the reaction coordinates for the dissociative adsorption of N_2 is shown with the identification of the initial, transition, and final states. Both top and side views are provided.*

2.5 Computational hydrogen electrode

In an electrochemical reaction with proton-electron transfer, the free energy change of each step is a function of the applied electrical potential. In this thesis, the effect of applying this potential is based on a simple model described by Nørskov *et al.* [66], which has henceforth been referring to as the computational hydrogen electrode (CHE) model. This model also provides an elegant way of avoiding the explicit treatment of solvated protons and excess electrons from the electrode. The reaction

$$H^+ + e^- \rightleftharpoons \frac{1}{2}H_2 \tag{2.29}$$

is at equilibrium at standard conditions (pH = 0, 1 bar H_2, 298.15 K) and therefore the electric potential is defined to be zero voltage on the standard hydrogen electrode (SHE) scale. Thus in this model, the chemical potential of a proton-electron pair, $\mu(H^+) + \mu(e^-)$, is equal to half of the chemical potential of gaseous hydrogen ($1/2\ \mu$ (H_2)) at a potential of 0 V. In this way, the chemical potential of the proton-electron pair can simply be obtained by calculating the chemical potential of gas-phase H_2. The chemical potential of the electrons can be varied as a function of the applied potential by the standard relation between chemical and electrical potential, ΔG = -eU, where e is the elementary charge and U is the applied bias. Since the SHE is defined at zero pH, the chemical potential of the solvated protons can also be varied implicitly:

$$G(pH) = -kTln[H^+] = kTln10 \times pH. \tag{2.30}$$

With this relation, the applied potential can be referenced with respect to the reversible hydrogen electrode (RHE) at a given pH. The total chemical potential of the proton-electron pair as a function of applied potential, at room temperature and pH , can be calculated as:

$$\mu(H^+) + \mu(e^-) = \frac{1}{2}\mu(H_{2(g)}) - neU - kTln10 \times pH \tag{2.31}$$

This is a simple model to include the effect of applied bias and pH. This method is generally applicable for treating reaction free energies of electrochemical systems. However, all the calculations presented in this thesis and in the attached papers are at pH = 0.

3 Computational modelling

3.1 Systems modelling

To carry out the electronic structure calculations, 25 transition metal mononitrides in four different structures, as shown in Figure 3.1, were modelled making hundred potential candidates in total. These structures are: the (100) and (111) of the NaCl-type or rocksalt (RS) and the (100) and (110) of the zincblende (ZB) structures. We modeled a five-layer nitride slab with four metal atoms and four nitrogen atoms in each layer. The bottom two layers were frozen and the uppermost layers as well as the adsorbed species were allowed to fully relax.

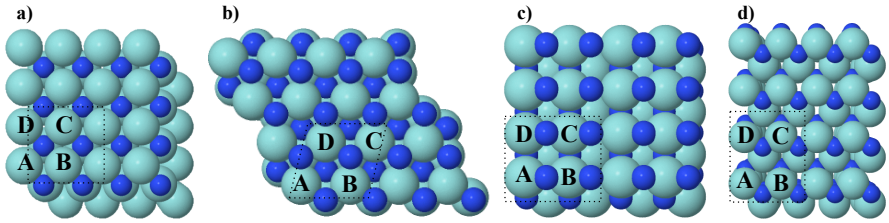

Figure 3.1: *Metal nitride unit cell and top views of the low-index surfaces used in this study: (a) rocksalt (100), (b) rocksalt (111), (c) zinc blende (100), and (d) zinc blende (110). The surface unit cells have been repeated once in the lateral directions. Metal atoms are represented by cyan spheres and nitrogen atoms by dark blue spheres.*

Boundary conditions were periodic in the x and y directions and surfaces were separated by 12Å of vacuum in the z direction. Due to the large vacuum layer used in our modelling and in order to improve calculational

convergence, the calculations were run without imposing a dipole correction perpendicular to the surface. Test calculations confirm that the effect of adding a dipole correction is small and in no cases above 35 meV. The structural optimization was considered converged when the forces on all moveable atoms were below 0.01 eV/Å in any direction. A previous study showed several of the 3d mononitrides to be either antiferromagnetic (RS VN, CrN, MnN, FeN and ZB MnN) or ferromagnetic (ZB VN, CrN) at their equilibrium lattice constants and as such are treated as spin-polarized in our calculations by turning on the corresponding tag in the INCAR file and choosing the appropriate magnetic moment [124]. The RPBE lattice constants are also taken from that study where their calculated values are 1-2% from the experimental values. All calculations were conducted with DFT using the RPBE exchange-correlation functional [112]. A plane-wave basis set with an energy cutoff of 350 eV was used to represent the valence electrons with a PAW representation [125] of the core electrons as implemented in the VASP 5.3.2 code [114–118]. Our test calculations confirm that the effect of employing higher cut-off value (500 eV) is as small as 20–45 meV on adsorption energy of the species on the surface. Therefore, 350 eV was chosen as relatively fair compromise between accuracy and speed. Iterative diagonalization of the Kohn–Sham Hamiltonian was used to determine the self-consistent electron density, with the occupation of the Kohn–Sham orbitals being smeared according to a Fermi–Dirac distribution with a smearing parameter of $k_B T = 0.1$ eV. The k-point sampling used for all the surfaces was a $4 \times 4 \times 1$ Monkhorst–Pack sampling [126]. Activation energies are calculated as the highest point along the minimum energy path (MEP) calculated using the climbing image nudged elastic band method (CI-NEB) [121, 122].

3.2 Calculating free energy pathways

The cathode reaction of the electrochemical nitrogen reduction to ammonia is considered to be:

$$N_2 + 6(H^+ + e^-) \rightleftharpoons 2NH_3 \tag{3.1}$$

The source of protons could be either water splitting or H_2 in the anode reaction. But we refer to H_2 here only as a convenient source of protons and electrons to link our absolute potential vs. standard hydrogen electrode (SHE) [66]:

$$H_2 \rightleftharpoons 2(H^+ + e^-) \tag{3.2}$$

Since we do these analyses at pH = 0, all the predicted onset potentials vs. SHE become equivalent to reversible hydrogen electrode (RHE) at zero pH. These onset potentials can be easily calculated for different pH values according to the Nernst equation when needed: $E = E^0 + (0.059 \times pH)$

With the aid of DFT, we calculate the total electronic energy of a system at absolute zero, T = 0 K. To obtain the enthalpy of the system, we need to add the zero point energy (ZPE) to the electronic energy of that configuration, which is the lowest energy that this system can have. This is usually referred to as the ground state energy, but it is noted here that this can in principle be done at any point on the potential energy surface (PES), e.g. the saddle point, not only at a local minimum of the PES. The energy associated with the ground state of the quantum harmonic oscillator is:

$$E = \frac{\hbar\omega}{2} \tag{3.3}$$

where $\hbar$ is the Planck's constant and ω is the angular frequency. To obtain the free energy of a system, we need to include the entropy contribution and add that to the enthalpy. The vibrational frequencies obtained with the normal mode analysis (NMA) are used to calculate both the ZPE of a certain configuration on the PES and also the vibrational entropy, both for ground states and TS. With the ZPE and the vibrational entropy, we can calculate the free energy change when a gas phase molecule (A_2) adsorbs (A^*) on a surface site (*):

$$\triangle G(0)_{A^*} = \triangle E_{A^*} + \triangle(ZPE) - \triangle S \tag{3.4}$$

where $\triangle$(ZPE) and $\triangle$S are the change in ZPE and entropy when the gas phase molecule is adsorbed on the surface. The frequencies of the adsorbed states are calculated via the NMA and may be used to calculate both the ZPE and the vibrational entropy of A, and we take the ZPE and the entropy of the gas phase molecules from standard molecular tables [127, 128]. These free energies are calculated for all the stable intermediates along the path to construct the free energy pathway or free energy diagram.

The $\triangle E_A{}^*$ is the binding energy (E) when a gas phase molecule is adsorbed on the surface. In case of adsorption of hydrogen, for example:

$$\triangle E_{H^*} = E_{H^*} - E_{cleanSurface} - \frac{1}{2}H_{2(g)} \tag{3.5}$$

$$\triangle G_{H^*} = \triangle E_{H^*} + [(E(ZPE)_{H^*} - \frac{1}{2}E(ZPE)_{H2(g)}) - (T(S_{H^*} - \frac{1}{2}S_{H2(g)}))] \tag{3.6}$$

The effect of an applied bias, U, is included for all electrochemical reaction steps by shifting the free energy for reactions involving n electrons by -neU:[65]

$$\triangle G(U) = \triangle G(0) - neU \tag{3.7}$$

In this thesis, a heterogeneous MvK-type mechanism is considered where a surface N atom is reduced to NH_3 and the created nitrogen vacancy (single or dimer N-vacancy) is then replenished with gaseous N_2. So hydrogenation of the surface N is carried out by adding H atoms one-by-one to it to represent a proton from the solution and an electron from the electrode surface. The reaction mechanism is shown in equations (3.8)–(3.16) and with a ball-and-stick representation in Figure 3.2.

$$^* + 6(H^+ + e^-) + N_2 \rightleftharpoons {}^*H + 5(H^+ + e^-) + N_2 \tag{3.8}$$

$$^*H + 5(H^+ + e^-) + N_2 \rightleftharpoons {}^*2H + 4(H^+ + e^-) + N_2 \tag{3.9}$$

$$^*2H + 4(H^+ + e^-) + N_2 \rightleftharpoons {}^*3H + 3(H^+ + e^-) + N_2 \tag{3.10}$$

$$^*3H + 3(H^+ + e^-) + N_2 \rightleftharpoons {}^{*-N} + NH_3 + 3(H^+ + e^-) + N_2 \tag{3.11}$$

$$^{*-N} + 3(H^+ + e^-) + N_2 \rightleftharpoons {}^*N + 3(H^+ + e^-) \tag{3.12}$$

$$^*N + 3(H^+ + e^-) \rightleftharpoons {}^*NH + 2(H^+ + e^-) \tag{3.13}$$

$$^{*}NH + 2(H^{+} + e^{-}) \rightleftharpoons {}^{*}NH_2 + (H^{+} + e^{-}) \tag{3.14}$$

$$^{*}NH_2 + (H^{+} + e^{-}) \rightleftharpoons {}^{*}NH_3 \tag{3.15}$$

$$^{*}NH_3 \rightleftharpoons {}^{*} + NH_3 \tag{3.16}$$

An asterisk,*, represents a site on the surface. A N-vacancy in the surface layer is denoted as $^{*-N}$. DFT calculations are used to calculate the minimum energy configuration of each species on the surface and to calculate adsorption energies of all intermediates according to reactions (3.8)–(3.16). A slightly different reaction mechanism, called dimer N-vacancy, is considered for the RS(100) of ScN, TiN, CrN, YN and MnN and all the ZB(110) surfaces due to the existence of a prohibitively large thermochemical barrier to replenish the N-vacancy with gaseous N_2. An example of the effect of these considerations is shown in Figure 3.3. The single N-vacancy approach studied for the RS(100) facets [95, 129] is not applicable for the RS(111) surfaces either, due to the closely packed structure of the (111) surfaces where N atoms are protruded from the surface. For these surfaces, the dimer N-vacancy approach is investigated. In this mechanism, two NH_3 molecules are formed from two surface N atoms and a dimer N-vacancy is created before regenerating the catalyst with gaseous N_2. The mechanism is given in eqns (3.17)–(3.25). In this mechanism, the free energy change to fill the N-vacancy is greatly reduced and, in most cases, N_2 adsorption is no longer the rate- determining step (RDS).

$$^{*} + 6(H^{+} + e^{-}) + N_2 \rightleftharpoons {}^{*}H + 5(H^{+} + e^{-}) + N_2 \tag{3.17}$$

$$^{*}H + 5(H^{+} + e^{-}) + N_2 \rightleftharpoons {}^{*}2H + 4(H^{+} + e^{-}) + N_2 \tag{3.18}$$

$$^{*}2H + 4(H^{+} + e^{-}) + N_2 \rightleftharpoons {}^{*}3H + 3(H^{+} + e^{-}) + N_2 \tag{3.19}$$

$$^{*}3H + 3(H^{+} + e^{-}) + N_2 \rightleftharpoons {}^{*-N} + NH_3 + 3(H^{+} + e^{-}) + N_2 \tag{3.20}$$

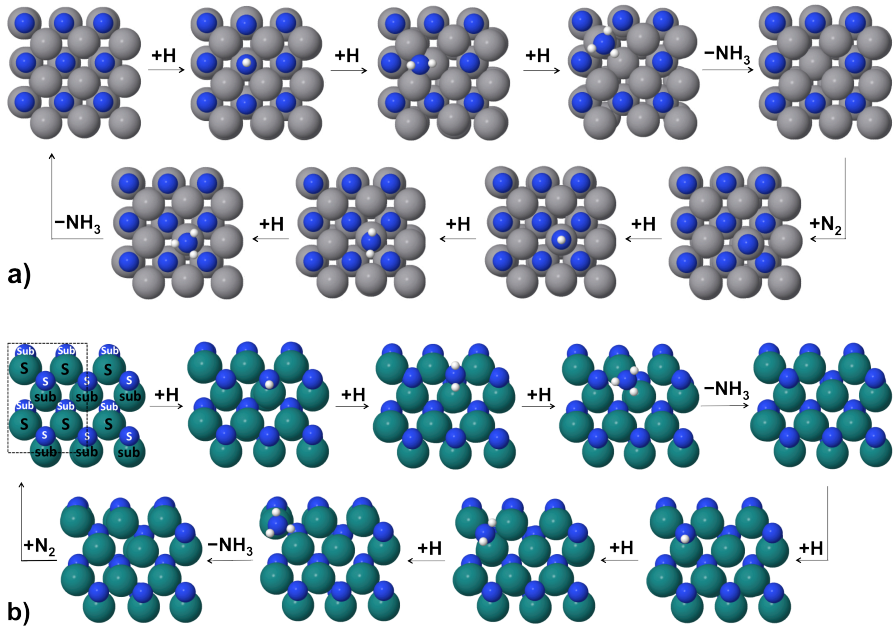

Figure 3.2: *Mars–van Krevelen mechanism for ammonia formation on the (100) facet of the RS structure (a) and the (110) facet of the ZB structure (b) of transition metal mononitrides. For better illustration, more than one supercell is depicted but for the second ammonia molecule formation, the extra adsorbates that should be visible due to periodic boundary conditions are not shown. S stands for surface atoms and sub denotes the sub-layer.*

$$^{*-N} + 3(H^+ + e^-) + N_2 \rightleftharpoons {}^{*-N} + {}^{*} H + 2(H^+ + e^-) + N_2 \tag{3.21}$$

$$^{*-N} + {}^{*} H + 2(H^+ + e^-) + N_2 \rightleftharpoons {}^{*-N} + {}^{*} 2H + (H^+ + e^-) + N_2 \tag{3.22}$$

$$^{*-N} + {}^{*} 2H + (H^+ + e^-) + N_2 \rightleftharpoons {}^{*-N} + {}^{*} 3H + N_2 \tag{3.23}$$

$$^{*-N} + {}^{*} 3H + N_2 \rightleftharpoons {}^{*-2N} + NH_3 + N_2 \tag{3.24}$$

$$*^{-2N} + N_2 \rightleftharpoons {}^{2}* \tag{3.25}$$

As a first approximation when screening for catalytic activity, the surface site in equations (3.8)–(3.16) is restricted to a single nitrogen site where each hydrogen is added to the same N atom. One NH_3 is formed after $3(H^+ + e^-)$ are transferred, and the second NH_3 is formed after $6(H^+ + e^-)$ in total. This is hereafter referred to as a "constrained" mechanism. An example of such a free energy diagram is in Figure 3.4.

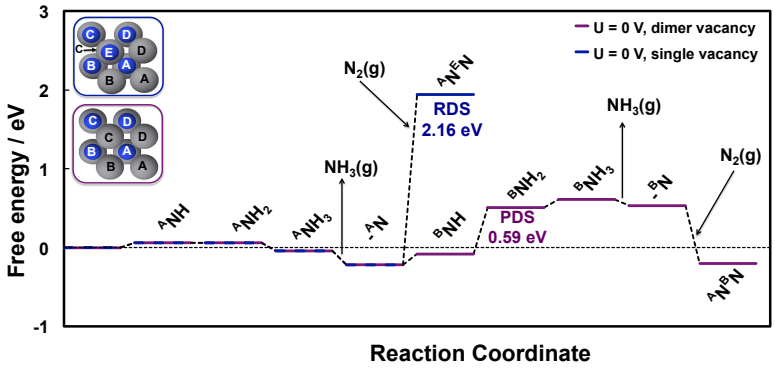

Figure 3.3: *Free energy diagram for NH_3 formation via a constrained Mars–van Krevelen mechanism on the (100) facet of RS MnN. For MnN, the potential-determining step is the fifth protonation step of surface N with $\triangle G$ = 0.59 eV. The blue line indicates the free energy of all the stable intermediates calculated at zero potential until one ammonia molecule is formed via single-vacancy approach. There is a non-electrochemical step with thermochemical barrier of 2.16 eV to fill the N-vacancy. The purple line indicates the free energy of all the intermediates when a dimer vacancy is considered at zero potential.*

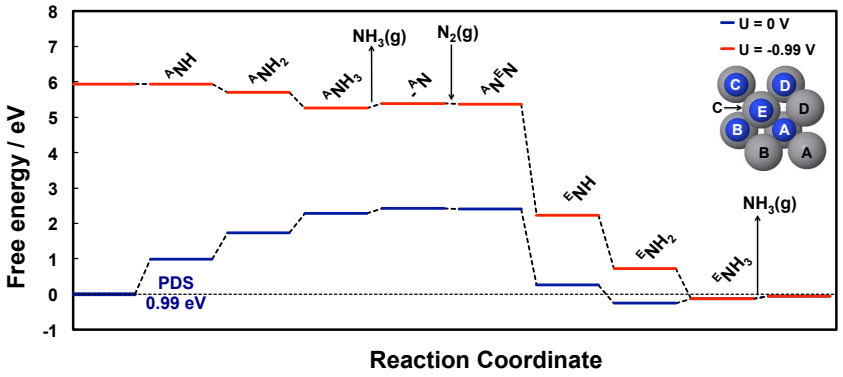

Figure 3.4: *Free energy diagram for NH_3 formation via a constrained Mars–van Krevelen mechanism on the (100) facet of RS ZrN. For ZrN, the potential-determining step is the first protonation step of surface N with $\triangle G$ = 0.99 eV. The blue line indicates the free energy of all the stable intermediates calculated at zero potential. The red line represents the free energy of all the stable intermediates at the onset potential.*

Explicit inclusion of a water layer [17] has not been considered in the present work due to the large computational effort required. It has been shown that the presence of water may help stabilize some species more than others via hydrogen bonding [130]. However, this solvation-induced stabilization of adsorbates in the NER are estimated to be below 0.1 eV [131]. From this we conclude that the onset potentials calculated in the present thesis are likely to change by a similar magnitude, and we do not include this correction in the data presented in this thesis.

3.3 Towards more realistic free energy pathways with an unconstrained mechanism

For a more detailed investigation of the catalytic activity and specially selectivity, the restriction of adsorption of H only on the surface N is lifted and all possible adsorption sites for each H are considered, including adsorption on metal atoms, other surface N atoms, bridge positions, and so on. This is accordingly referred to as an "unconstrained" mechanism. In this way, the possibility of a catalyst requiring more than six protons and electrons to form $2NH_3$ is explored and also the possibility of forming H_2, rather than NH_3. The advantage of this approach is that it allows us to

explicitly consider the possibility of hydrogen production on all these nitride candidates within our mechanistic model by removing the constraint of proton adsorption occurring only on surface nitrogen atoms. That will help us to pick the most selective candidate for experimental examinations. Figure 3.5 illustrates the free energy of the (100) facets of the RS structure of ZrN, for example. Notice how the reaction path and the PDS is changed by going from constrained (shown in Figure 3.4) to unconstrained mechanism (shown in Figure 3.5) and including the effect of coverage.

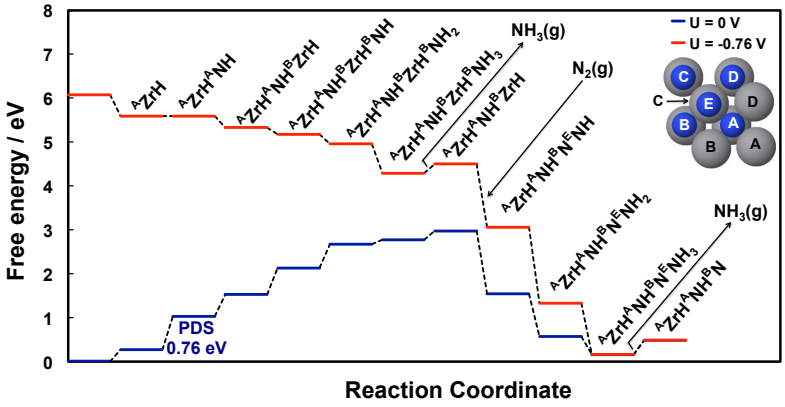

Figure 3.5: *Free energy diagram for NH_3 formation via an unconstrained Mars–van Krevelen mechanism on the (100) facet of RS ZrN. The potential-determining step is the second protonation step with $\triangle G$ = 0.76 eV. Upon replenishment of the N-vacancy, one proton that was already adsorbed on Zr metal (^{B}ZrH) migrates to the N-adatom to make NH (^{E}NH). The blue line indicates the free energy of all the stable intermediates calculated at zero potential. The red line represents the free energy of all the stable intermediates at the onset potential.*

3.4 Calculating onset potentials

The free energy of all intermediates is calculated according to equation (3.), with reference to N_2 and H_2 in the gas phase. The PDS and our measure of the catalytic activity towards NH_3 formation on each nitride is identified as the elementary reaction step with the largest increase in free energy (as shown in FEDs in Figures 3.3, 3.4, 3.5). When this elementary step can be eliminated by applying a bias, it is referred to as the onset potential, which is the bias that needs to be applied in order to shift the free energy landscape in such a way that all reactions steps become downhill in free energy.

Therefore, the onset potential is defined based on the largest difference in free energy of two adjacent steps obtained from:

$$\triangle G = -U \tag{3.26}$$

Two types of elementary steps are assumed in the modeling with regards to the effect of the onset potential in shifting the FEDs. One is an electrochemical step with proton/electron transfer, such as hydrogenation of the nitride surface. In the constructed FEDs shown earlier, the largest difference between the two adjacent electrochemical steps is termed the PDS, as it indicates the bias required making all electrochemical steps exergonic. Another type of elementary step is a non-electrochemical step without proton/electron transfer, which are replenishment of the nitride with solvated dinitrogen molecules from the electrolyte and desorption of NH_3 molecule from the surface. These types of steps cannot be tuned by applying bias and consequently determines the rate of the reaction (if those steps are endergonic on a particular TMN surfaces) and are labeled RDS. However in case desorption of ammonia becomes endergonic, the ammonia molecules formed on the surface are expected to get further protonated in acidic solutions to NH_4^+ and released into the solution, therefore facilitates this step in the reaction.

4 Results

In this chapter, we offer a summary of the results obtained with this PhD thesis. Interested readers can refer to the articles published from the contents of this thesis for more detailed description of the results. These articles are attached to the end of this thesis.

4.1 Ammonia synthesis

In this section, we provide a summary of the results obtained on nitrogen electroreduction to ammonia on the surface of transition metal nitrides. The subsections mentioned below are the most important criteria investigated in pursuit of exploring the most promising nitride candidate for experimental tests. The main competitive side reaction in ammonia production is the hydrogen evolution reaction (HER). In the next section, section 4.2, we will present results on the possibility of catalyzing the HER on the surface of these nitrides.

Structural stability

Each slab is relaxed and the total energies compared to determine the most stable facet of a given metal nitride. Most of the nitrides of the early transition metals (d^{1-5}) as well as the d^9 metals are found to be most stable in the RS crystal structure and, for all of these, the (100) facet is more stable than the (111) facet. These are ScN, TiN, VN, CrN, MnN, YN, ZrN, NbN, MoN, HfN, TaN, WN, CuN, and AgN. For most of the nitrides of the d^6, d^7 and d^8 transition metals, the ZB(110) facet is the most stable. These are FeN, CoN, NiN, RuN, RhN, PdN, OsN, and IrN. These findings agree with the generally accepted trend of early transition metal nitrides being most stable in RS structure while the later transition metal nitrides are usually

most stable in ZB [132–134]. Regarding facet stability, experimental studies show that the growth of films of ZrN, TiN, NbN, CrN, and VN results in the texture coefficient for the (100) planes of the synthesized polycrystalline films to be one of the major preferential directions [135–141]. For all considered surfaces of ReN, PtN, and AuN, significant distortion of the surface atoms is observed during relaxation and thus these nitrides are considered unstable and eliminated from further study. Although only the RS(100) and ZB(110) came out to be the most stable structures within this analysis, the stability of other facets of some of these nitrides are only slightly lower than the most stable one shown in Figure 4.1. Thus, we consider these nitrides in RS(111) and ZB(100) as well because it is possible that some nitrides in these structures/facets are also relatively stable and catalytically active.

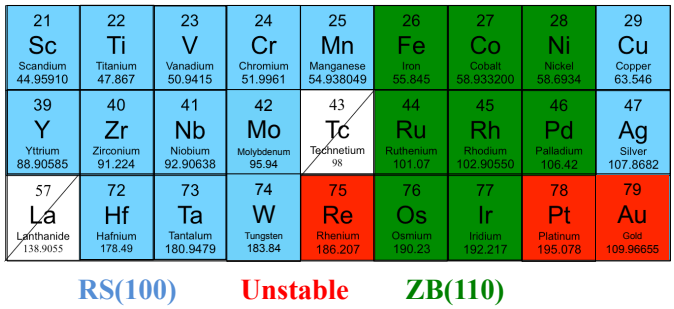

Figure 4.1: *The most stable facet of a given transition metal nitride.*

Catalytic activity

The catalytic activity of the nitrides towards electrochemical ammonia formation is calculated according to the unconstrained mechanism given in eqns (3.8)–(3.16) for most of the RS(100) nitride slabs and eqns (3.17)–(3.25) for all the RS(111) and ZB(110) nitrides slabs. At every hydrogenation step, various possible adsorption sites are inspected, including other N atoms, metal atoms, and bridging sites to evaluate the most stable adsorption site. The free energy of all intermediates is calculated according to eqn (3.4), with reference to N_2 and H_2 in the gas phase. Free energy diagrams for half of this process (formation of only one ammonia molecule) on the nitrides of V, Zr, Cr, and Nb are shown in Figure 4.2 as an example. The large free energy difference observed between the reactants (N_2 + $3H_2$) and products ($2NH_3$) is because these different metal nitride surfaces adsorb different numbers of H atoms before releasing NH_3 (in most cases, more than three proton/electron pairs are required for formation of an ammonia molecule) and not because of the energy required to form the N vacancy. The largest

free energy is shown as the PDS and the species formed at each step is also noted.

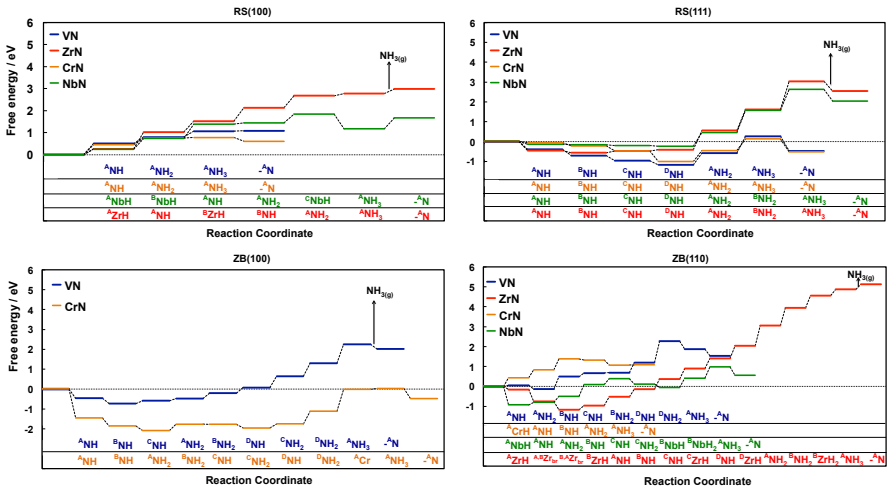

Figure 4.2: *Free energy diagrams for NH_3 formation via a Mars-van Krevelen mechanism on different facets of RS and ZB crystal structures of VN, ZrN, CrN, and NbN at zero potential. The labels below each free energy diagram show the most energetically favorable intermediates that form on the surface at each step. A, B, C, and D identify on which metal atom or surface niyrogen the H adsorbs, where those labels are specified in Figure 3.1. The terms ${}^{A,B}Zr_{br}$ and ${}^{B,A}Zr_{br}$ mentioned for the ZB(110) of ZrN indicate that H adatoms adsorb on a bridge position between two adjacent Zr atoms (${}^{A}Zr$ and ${}^{B}Zr$). The (100) facets of ZB structure of ZrN and NbN are not included here due to structural instability, and they are therefore excluded from further study. All the FEDs constructed within this thesis for formation of two ammonia molecules are available in the publications attached.*

Considering first the RS(100) nitrides, it can be seen that, for most of these nitrides, every protonation step is endergonic. However, the free energy required at each step is rather low and can be overcome with an applied bias of less than -0.80 V vs SHE. For ZrN, NbN, and VN, the release of NH_3 is also endergonic, and this cannot be overcome with an applied bias. However, in acidic conditions, the adsorbed NH_3 is likely to get further protonated to NH_4^+ and released into the solution, thereby avoiding this small increase in free energy. Thus, this step is not discussed further. A notable feature of the RS(100) nitrides is that, in general, very few H^+/e^- pairs are required to generate NH_3. For CrN and VN, each protonation

step adds to the same surface N atom, meaning that the minimum of three H^+/e^- pairs is required to form one NH_3. For the three other facets, more than the minimum H^+/e^- pairs are required due to the protons adding either to neighboring nitrogen or metal atoms in some elementary steps. This means that a higher current efficiency should be expected for formation of the first NH_3 on the RS(100) facets. However, it should be noted that this is only half of the catalytic cycle for ammonia formation on transition metal nitrides.

For the RS(111) nitrides, it is seen that the most favorable H adsorption site is always a surface N with no tendency of binding H to neighboring metal atom(s), even at high coverage. On other facets, H adsorption is usually seen on neighboring metal atom(s) at low coverage. The only exception is VN, for which metal protonation is never the lowest energy configuration on any facet, and it is always the surface N that adsorbs protons strongly. The preferential binding to the N atoms of the (111) facets can be rationalized by the texture of the facet. The N atoms protrude somewhat from the surface and are thus more exposed than the metal atoms. In general, the largest increase in free energy is greater for the (111) facets than for the (100) facets. In our previous work [95], it was found that protonation of neighboring metal atoms usually lowered the free energy of the PDS for a given nitride, by up to 0.3 eV. This might explain the observation regarding higher $\triangle G_{max}$ on (111) facets, where such proton coverage on metal atoms is missing. Another interesting point for the (111) facets is that, in all cases, all of the surface nitrogen atoms are at least singly protonated before an ammonia molecule is formed. Again, this implies a lower current efficiency.

The zincblende surfaces, in general, require more H^+/e^- pairs to form NH_3 than the analogous rocksalt surfaces; however, all surfaces are rather unique in the order of protonation. Aside from VN, where all the protons are only added to the surface nitrogen(s), some degree of metal atom protonation seems required for other nitrides before forming NH_3. The ZB(100) surfaces of CrN and VN are somewhat less active than other facets of the same nitrides toward forming one NH_3 molecule, with $\triangle G_{max}$ of around 1 eV. The ZB(100) of ZrN and NbN was found to be unstable upon geometry optimization and therefore excluded from the rest of the study. Of the ZB(110) surfaces, CrN and NbN are expected to be rather good at forming NH_3, with low values of $\triangle G_{max}$ ($\sim$0.5 eV). ZrN suffers from both a high $\triangle G_{max}$ ($\sim$1 eV) and a requirement of almost 4 times the minimum number of H^+/e^- pairs to form NH_3. A final point to note is that, for all of the nitride surfaces considered here, rather than formation of a monolayer of H on the surface that could cause recombination of hydrogen and des-

orption as H_2, NH_3 is formed. This is significant as it implies that NH_3 will be formed preferentially over the evolution of hydrogen, which was a substantial problem with pure metal surfaces [142].

The FEDs were constructed for all the nitride surfaces considered in this thesis, and can be found in the relevant publications included at the end of the thesis. Constructing these FEDs helps predict the onset potential required for nitrogen reduction to ammonia. As mentioned, these onset potentials are equivalent to the negative of the free energy change of the PDS, -$\triangle G_{PDS}$. In Figures 4.3 and 4.4, we summarize a few of the results obtained through our DFT calculations regarding the activity of all the studied nitrides. The results embedded in these two Figures are: the onset potential (or the free energy change of the PDS), the species formed prior to and right at the PDS, total number of proton-electron pairs needed for formation of $2NH_3$ molecules, and the value of the RDS (originating from replenishment of the N-vacancy). As can be seen, these nitride surfaces behave very differently in the catalytic formation of ammonia. For all the RS(100) nitrides, small onset potentials are predicted for this reaction (smaller than -1.0 V). It is also seen that usually fewer proton-electron pairs are needed for formation of ammonia on these RS(100) surfaces, while higher numbers of proton-electron pairs are predicted to be needed for formation of two ammonia molecules on other structures. That is anticipated to lower the current efficiency of ammonia formation, as the chance of HER arises due to higher H coverage on these surfaces. For VN and CrN in the RS(100), for example, high current efficiency is expected to be achieved for ammonia as all the adsorbed hydrogens are spent for reduction of nitrogen.

Amongst the nitrides presented here, there are some that easily reduce surface nitrogen to ammonia with $\triangle G_{PDS}$ of zero (exergonic reaction path) or very close to zero. These are the ZB(100) of RhN and the ZB(110) of NiN, RhN, PdN, IrN, and PtN. Nonetheless, the main issue with these materials is that replenishment of the N-vacancy is usually very slow with relatively huge $\triangle G_{RDS}$ for this step. That hinders refreshing of the catalytic cycle and thus these surfaces act more as reactants than catalysts.

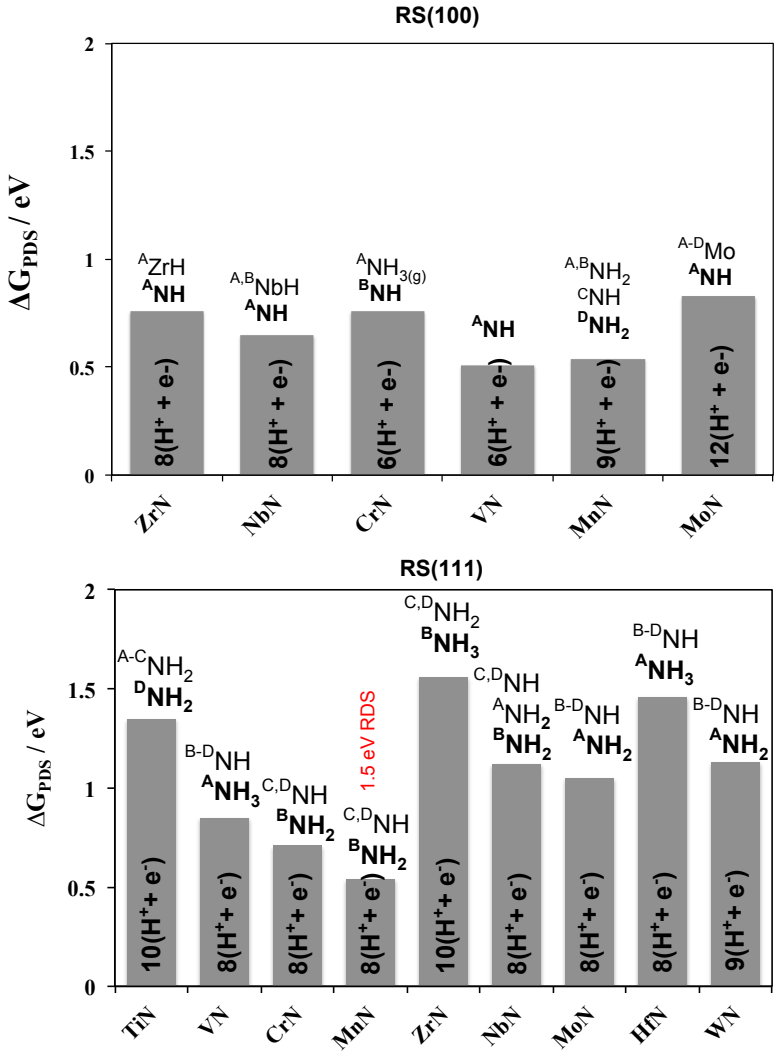

Figure 4.3: *Free energy change of the PDS ($\triangle G_{PDS}$, in eV) of nitrogen activation to ammonia on the rocksalt structures of TMN surfaces. The labels above each bar indicate the species formed prior to the PDS and the bold texts indicate the species formed right at the PDS, the notation of which is explained in Figures 3.1 and 4.2. The required number of proton-electron pairs for formation of two ammonia molecules are also included inside each bar. For MnN, the value of the RDS coming from filling the vacancy is also mentioned in red.*

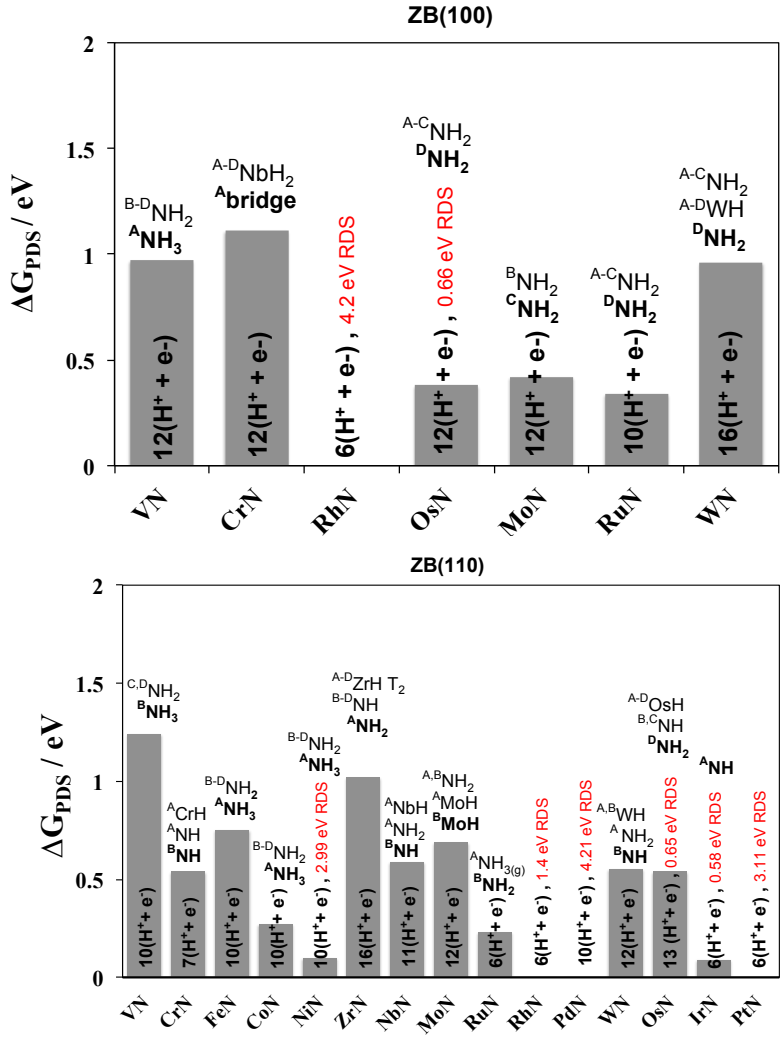

Figure 4.4: *Free energy change of the PDS ($\triangle G_{PDS}$, in eV) of nitrogen activation to ammonia on the zincblende structures of TMN surfaces. The labels above each bar indicate the species formed prior to the PDS and the bold texts indicate the species formed right at the PDS, the notation of which is explained in Figures 3.1 and 4.2. The required number of proton-electron pairs for formation of two ammonia molecules are also included inside each bar. For the (100) facets of the ZB structure of RhN and OsN, as well as the (110) facets of NiN, RhN, PdN, OsN, IrN, and PtN the value of the RDS coming from filling the vacancy is also mentioned in red.*

For the RS(111) [79] and the ZB(110) [143], a clear trend is found for the catalytic activity (or the onset potential). As can be seen from Figures 4.3 and 4.4, the activity increases from left to the right on the periodic table. Therefore, we explored if any correlation between the activity and a material dependent descriptor could be found. The onset potential predicted for ammonia formation was found to correlate well with the dissociation energy of di-nitrogen in dimer N-vacancy. This correlation is shown in Figure 4.5 where the onset potential of these materials becomes less negative as the dissociative energy of di-nitrogen on the vacant sites becomes more positive. However, as the dissociative energy becomes more endergonic it becomes harder to regenerate the N-vacancies. That means that the best material is the one that compromises both features: the onset potential and the ability to regenerate the vacant sites.

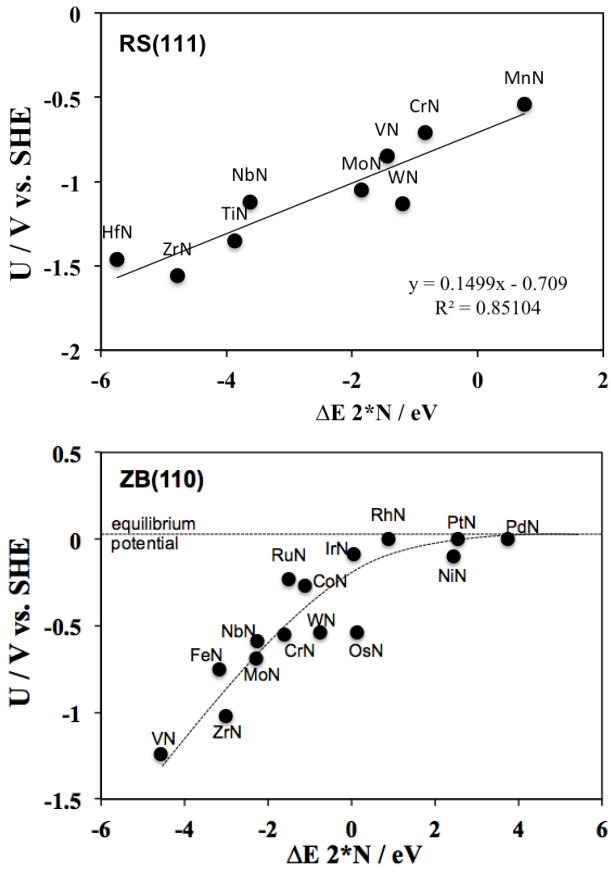

Figure 4.5: *The onset potential of ammonia formation on the RS(111) and the ZB(110) facets of TMNs as a function of the chemisorption energy of two N-adatoms in the N-vacancy.*

Stability against poisoning

In the MvK mechanism explored throughout this thesis, one important consideration is that after surface Ns have reacted and vacancies created at the surface, these vacancies must be filled with N_2 from the electrolyte for the catalytic cycle to continue. However, the vacancy might instead be filled with a H^+, O^{2-} or OH^- species from the aqueous electrolyte, any of which could block these active surface sites, prevent filling the vacancy with nitrogen, and thus poison the catalyst.

The competition between nitrogen with H^+, O^{2-} or OH^- for filling the surface vacancy is investigated by considering the free energy of filling the vacancy with any of these species relative to nitrogen $\triangle G_{(*2N-*X)}$, where X = H^+, O^{2-} or OH^-. The source of these ions is from the water molecules or hydronium ions in the electrolyte that result in formation of H^+, O^{2-} or OH^- under operating conditions. We calculate the difference in adsorption energy of these species compared to adsorbing nitrogen at the onset potential of ammonia formation. These free energies are referenced to N_2, H_2O and H_2 in the gas phase. A negative value of $\triangle G_{(*2N-*X)}$ indicates that it is thermodynamically favorable to fill the vacancy with nitrogen, rather than other three species. These values are shown in Figure 4.6 for all the nitrides investigated in this thesis, and the onset potential (V vs. RHE) of each nitride at which these values are calculated also provided in this Figure. As seen, N atoms bind more strongly than H, OH, and O atoms to the surface vacancy for most of the nitrides considered. Hence, it is likely that none of these three species will poison the surface vacancy. The weaker binding of O to N vacancy compared to H is as expected because, when the bias is tuned toward more negative values, the O species binds more weakly on the surface compared to H_2O in the gas phase:

$$H_2O + {}^* \rightarrow {}^*O + 2H^+ + 2e^- \tag{4.1}$$

Conversely, the H adsorption free energy becomes more negative when the bias is lowered:

$$H^+ + e^- \rightarrow {}^*H \tag{4.2}$$

In the RS(100) family, there is only MoN for which H and OH bind the surface vacancy more strongly than N. In the RS(111) category, this holds true for MnN and WN, while for CrN, it is only H that binds the vacancy slightly more strongly than N. For these nitrides as well: the ZB(100) of CrN, WN, OsN, and RhN plus the ZB(110) of NiN, RhN, PdN, OsN, IrN, and PtN, one of these poisoning species can block the surface vacancy. If this happens, these nitrides will have difficulty regenerating themselves by replenishing of the surface vacancy with nitrogen and consequently the catalytic cycle might cease.

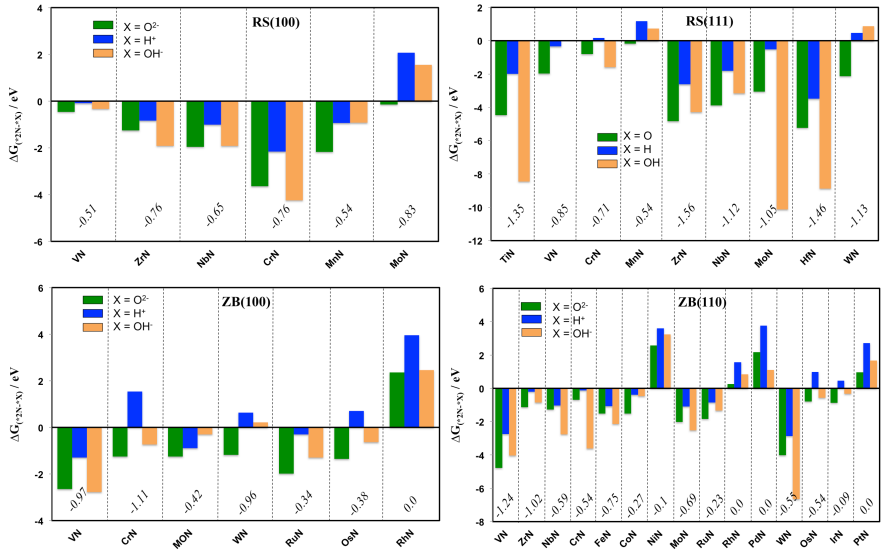

Figure 4.6: *Comparison of the free energy of adsorption of O, OH, or H (relative to 2N) to the surface vacancy of catalytically active nitrides ($\triangle G_{(*2N-*X)}$, in eV). Free energies are calculated relative to $N_2(g)$, $1/2H_2(g)$, and $H_2O_{(g)}$. All free energies are evaluated at the calculated onset potential for each nitride (onset potentials are shown vs RHE).*

Stability against decomposition

As explained earlier, in the MvK mechanism a surface nitrogen atom is reduced to form NH_3 after which the resulting vacancy is replenished by an N_2 molecule solvated in the electrolyte. For this replenishment to occur, the vacancy needs to be stable at the surface. If this is not the case, the vacancy may migrate to the bulk of the catalyst, meaning that the N-vacancy in the first surface layer is replaced with more nitrogen from the catalyst itself, rather than with N_2 from the electrolyte. This process can, in principle, continue until all the nitrogen atoms of the metal nitride have been reacted and reduced to NH_3, leaving only the pure metal. The stability of the vacancy at the surface and thus stability of the nitrides against decomposition is estimated by comparing the difference in energy of a nitride slab with a single N-vacancy in the surface layer ($E_{vac,i}$) and to that of a single N-vacancy in the first subsurface layer ($E_{vac,f}$). The minimum energy configuration of each of these slabs is found and the energy difference ($\triangle E_{vac}$ = $E_{vac,f}$ - $E_{vac,i}$) used as an estimation of the thermodynamic stability of

the vacancy at the surface of the nitride. Activation energies for vacancy migration ($E_{a,vac}$) are also calculated with CI-NEB calculations. Figure 4.7 shows the kinetics of the vacancy migration into the bulk as a function of thermodynamics for the RS(100) and ZB(110) surfaces as an example.

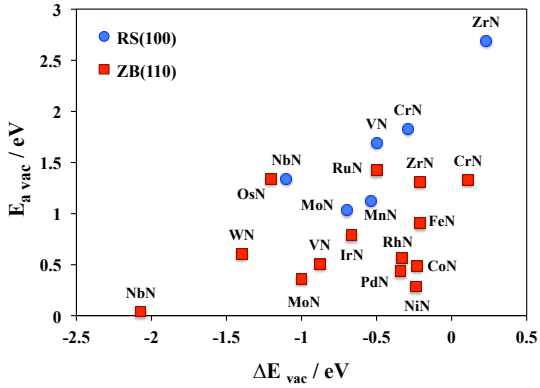

Figure 4.7: *Energy differences ($\triangle E_{vac}$) of a N vacancy at the surface layer and in the first subsurface layer of a nitride and the associated activation barrier of N vacancy migration ($E_{a,vac}$).*

As can be seen for most nitrides, it is thermodynamically favorable for the vacancy to migrate to the bulk, with $\triangle E_{vac}$ less than or close to zero. However, many of the considered nitrides in both the RS(100) and ZB(110) exhibit a high activation barrier for vacancy migration and are thus expected to demonstrate a kinetically stable N vacancy on the surface.

Regeneration of the active site on the surface

For a more detailed assessment of the stability of the nitrogen vacancy and feasibility of regeneration of the catalyst, the competition between migration of the vacancy from the surface into the bulk (decomposition) after formation of ammonia molecule and replenishment of the vacancy with nitrogen is inspected. The activation free energy (G_a) for both processes are calculated, where $G_a = E_a$ for the vacancy migration process, but $G_a = E_a + 0.6$ eV for the process of replenishing the vacancy with nitrogen. When molecular nitrogen splits and binds to the vacancy, it loses 0.6 eV of entropy at room temperature going from gas phase to the adsorbed state on the surface [128]. Therefore, even if the activation energy of vacancy replenishment is calculated to be 0.0 eV, the activation energy of migration should be higher than 0.6 eV so that replenishment can occur faster. If the vacancy is

likely to replenish faster than it migrates into the bulk, the catalyst is likely to be able to regenerate itself and endure the catalytic cycle. The free energy barriers (G_a) for each process are displayed in Figure 4.8 a-d for the most promising candidates found by this thesis as an exmaple, and the rest are accessible in the attached publications.

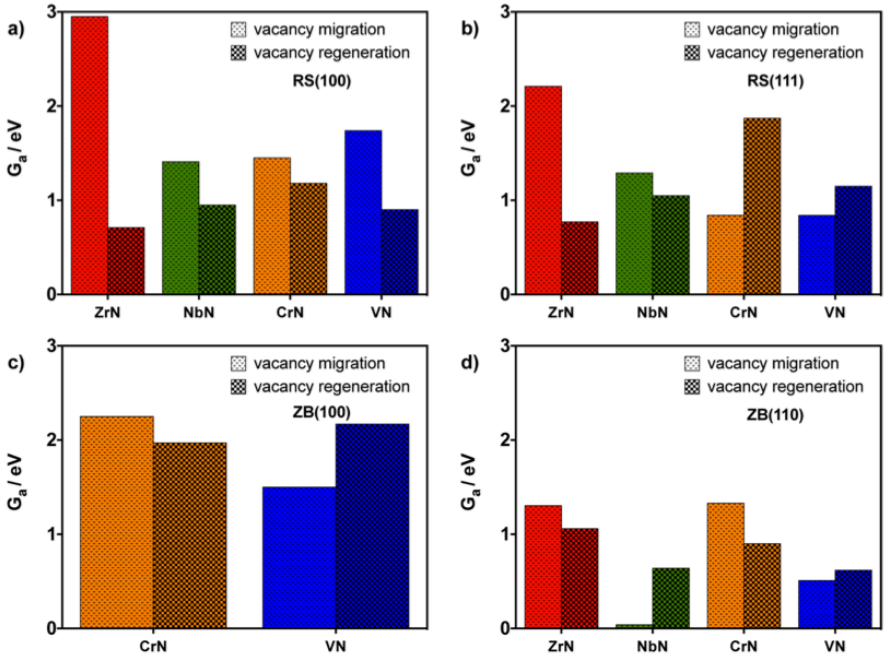

Figure 4.8: *Calculated activation free energies (G_a) of regenerating the catalyst by N_2 dissociation for replenishment of the N vacancy compared with activation free energies of vacancy migration into the bulk (migration of nitrogen atoms from the bulk toward the surface) for (a) RS(100), (b) RS(111), (c) ZB(100), and (d) ZB(110).*

As can be seen, the catalytic cycle of $2NH_3$ formation should be sustained on all facets of ZrN as regeneration of the catalyst with nitrogen (replenishment of the vacancy) always occurs faster than migration of the nitrogen content into the surface (decomposition). Therefore, a polycrystalline film of such a catalyst should not result in decomposition in an experimental setup. For NbN, both the (100) and (111) facets of the RS structure should have a stable vacancy at the surface and hence a sustainable catalytic cycle. As identified in Figure 4.7, the ZB(110) facet of NbN has a very low barrier

for vacancy migration, which is indeed lower than the barrier for vacancy replenishment. Therefore, the nitrogen content might leak out after formation of the first ammonia molecule. Furthermore, the bias required to form ammonia on this facet (-0.59 V) is lower than the bias required for ammonia formation on its other facets, thus formation of ammonia is likely to result in decomposition of the catalyst by migration of the bulk N to the surface. The only solution for using NbN as an electrocatalyst is, hence, to grow a single crystal of the RS NbN.

For the RS(100) and ZB(100/110) of CrN, vacancy migration was found to exhibit higher activation energy than vacancy replenishment. This means that regeneration of the CrN catalyst in these structures should occur much faster than its decomposition. Therefore, these facets of CrN should be able to offier sustainable catalytic cycles. But for the RS(111) of CrN, catalyst regeneration takes place much slower than decomposition, and that might result in the nitrogen content leaking out if a polycrystalline film of this catalyst is used in the experiment. This issue can be avoided if the RS(111) facet of CrN is eliminated from the experimentally synthesized CrN catalyst.

For VN, all facets except for RS(100) exhibit faster vacancy migration than replenishment of the N-vacancy and are likely to leak the nitrogen content out if ammonia is formed on these facets. However, the bias required to form NH_3 on VN RS(100) is only -0.51 V, compared with at least -0.85 V or more negative on its other facets. Hence, decomposition of a polycrystalline catalyst of VN could be prevented by applying a low bias of up to -0.8 V and forming NH_3 only on the RS(100) facets.

Promising candidates to be tested in experiments

Finally, the stable nitride candidates for which the rate and efficiency of NH_3 formation is expected to be high are collected in Figure 4.9. As can be seen, all the RS(100) surfaces require only a small bias to reduce nitrogen to ammonia. The ZB(110) of CrN is also as active. However, the RS(111) of ZrN and NbN as well as the ZB(110) of ZrN need to have more negative bias to reduce N_2 to NH_3. The ZB(110) of RuN seems promising as well with 100% current efficiency predicted at only small negative bias of -0.23 V. In addition, hydrogen production on all of these nitride candidates is explicitly considered within our mechanistic model, and accordingly, all of these candidates should suppress competitive hydrogen production, in contrast to metallic surfaces that almost exclusively evolve hydrogen gas [142].

Nitride	RS(100)	RS(111)	ZB(100)	ZB(110)
ZrN	**75% CE of NH_3 U = -0.76 V**	**60% CE of NH_3 U = -1.42 V**	Unstable	**40% CE of NH_3 U = -1.02 V**
NbN	**75% CE of NH_3 U = -0.65 V**	**75% CE of NH_3 U = -1.12 V**	Unstable	**Decomposition U = -0.59 V**
CrN	**100% CE of NH_3 U = -0.76 V**	**Decomposition U = -0.58 V**	**Non-catalytic U = -1.11 V**	**86% CE of NH_3 U = -0.54 V**
VN	**100% CE of NH_3 U = -0.51 V**	**Decomposition U = -0.85 V**	**Decomposition U = -0.97 V**	**Decomposition U = -1.06 V**
RuN	Ongoing	Ongoing	**66% CE of NH_3 U = -0.34 V**	**100% CE of NH_3 U = -0.23 V**

Figure 4.9: *Most promising facets of the nitride candidates (green background) and corresponding potential window and current efficiency for N_2 electroreduction to NH_3 via the MvK mechanism on ZrN, NbN, CrN, VN, and RuN. These data are extracted for refrences [79, 81, 87, 95, 129, 143–145].*

4.2 Hydrogen evolution reaction

In pursuit of new catalyst materials for nitrogen electroreduction reaction (NER) to ammonia, we found that amongst the mono-nitrides of most of the d-block metals, the early transition metal nitrides of Sc, Ti, Y, Hf, Mo, and Ta were most stable in the (100) facet of the NaCl-type structure and showed no catalytic activity toward NER [95, 129]. The surface of these nitrides were found to be mainly populated and covered with H up to 1 monolayer (ML) with no $*NH_3$ formation, except for MoN where $*NH_3$ was formed at -0.83 V but the catalytic cycle ended due to poisoning. Therefore, we hypothesized that they might catalyze the HER instead, which is a competing reaction to NER. In the present section, these six nitrides are investigated for electrochemical HER in acidic media. DFT calculations are used to study the thermodynamics of the cathode reaction. Free energy diagrams are constructed for the electrochemical protonation of surface to obtain onset potentials required for HER on transition metal mononitride structures. For hydrogen evolution, the Tafel mechanism is investigated here as it was found that the barrier of the Tafel reaction is the predominant and rate-limiting step on all metal electrodes and surface-independent for HER [17].

Free energy diagrams

The trends in hydrogen evolution activity over various transition metals, metal- and non-metal alloys have been investigated using DFT with the use of descriptors [146, 147]. $\triangle G_{H*}$, which is indicative of the adsorption free energy of hydrogen, has become a conventional descriptor to use when new class of materials are being screened for HER. According to this descriptor, and as explained by Sabatier principle, the best catalyst should possess free binding energies of H close to 0.0 eV. Therefore, calculating the adsorption free energy of H for different materials is expected to be a suitable approach for quick comparison of their catalytic activity towards HER. In Figure 4.10, the FEDs for hydrogen evolution over the studied nitrides are shown at zero potential (equilibrium). Their catalytic activity is also compared with the most efficient catalyst already known for this reaction, the Pt(111). For a chemical process to take place at room temperature, no reaction step can be associated with large changes in the free energy. This instantaneously eliminates Mo(110) as good catalyst, because it forms strong bonds to atomic hydrogen which implies that the hydrogen release step will be slow. The same holds true for one of the nitrides studied in this work, ScN. On the other hand, Au(111) binds weakly to atomic hydrogen and therefore it is not a good catalyst because the proton/electron transfer step is thermodynamically uphill and a relatively high overpotential is needed to surpass it to get the proton binding the surface. The same holds true for TiN studied here.

As can be seen, YN and MoN with adsorption free energy of +0.004 and -0.008 eV, respectively, seem to bind H very moderately (around 0.0 eV) and that should make them as good HER catalysts as Pt(111). They also look more promising than W-Cu catalyst with $\triangle G_{H*}$ of 0.07 eV [147] and MoS_2 edges with $\triangle G_{H*}$ = 0.08 eV [148]. HfN and TaN are also predicted to be active within this analysis with $\triangle G_{H*}$ = -0.059 and -0.092 eV, respectively. They all even look more promising when compared with Ni_2P which has a free energy of adsorption of H of 0.19 eV [149]. The binding free energies of H to the surface of ScN and TiN are -0.35 and 0.60 eV, respectively. The former binds H stronger and that makes evolution of H_2 difficult compared to Pt, whereas the latter binds H so weakly that it is difficult to add the proton on the surface without applying a more negative bias. The activity of ScN might be on par with that of Mo(111), and TiN seem to be the least active candidate from the perspective of this common descriptor. From these FEDs, it appears that some of the nitrides shown in Figure 4.10A adsorb H relatively moderately and there it could be anticipated that hydrogen evolution would be facilitated on the surface of these materials. It is a necessary

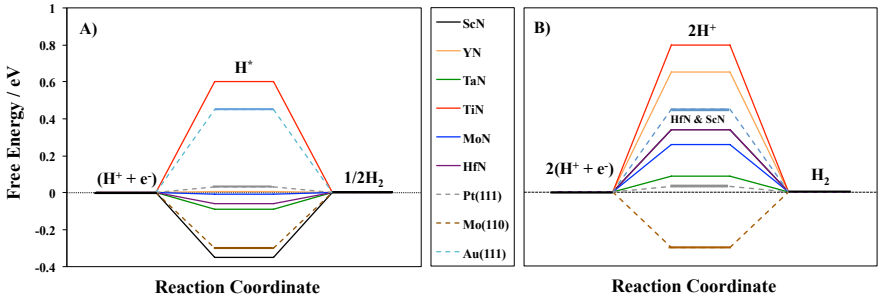

Figure 4.10: **H-descriptor based (A) and 2*Hs-descriptor based (B) free energy diagrams for the HER. In order for the H_2 to evolve, there should be at least 2*Hs on the surface to recombine via a Tafel mechanism. The *H-descriptor based FED is the conventional approach for comparison of the catalytic activity of various materials. However, as can be seen by comparing (A) and (B), the 2*H-descriptor based FED provides completely different picture and would give different predictions of the catalytic activities of these materials than the *H-descriptor would predict. The energies for the adsorbed intermediate are calculated with DFT for the coverage of 1/8 (A) and 2/8 (B) at standard conditions (pH = 0, 1 bar of H_2, U = 0, and 298 K). The values for pure metals are taken from Skúlason et al., 2010 and shown with dashed lines for comparison. For pure metals, there is an insignificant difference in the binding free energy of *H at this low coverage and therefore the values for 1/4 H coverage is used in both (A) and (B). The nitrides are shown with solid lines. The values corresponding to HfN & ScN are 0.34 eV overlaying each other in Figure B.*

but not sufficient criterion for a material to be a good catalyst that the free energy of adsorbed H is close to that of the reactant or product (i.e., $\triangle G_{H*}$ = 0).

Differential free energy of H adsorption

In the modeling, every possible adsorption site is investigated for each H addition step. DFT is used to evaluate the most stable adsorption site at each step and construct the free energy landscape until a full monolayer of hydrogen (1ML = $8H^+$) is built on the surface of the nitrides. These free energy landscapes provide more mechanistic details of the process and are shown in Figure 4.11. The transition metal nitrides of Sc, Ti, Y, Hf, and Ta investigated here reach an evenly distribution of H on the slab until 1 ML hydrogen coverage is reached (1ML = 8H*, 8 protons for 4 surface N and 4 surface metal atoms) where both metal and nitrogen atoms on the

surface are entirely protonated. Neither *NH_2 nor *NH_3 is found being an energetically favorable intermediate along the path. Therefore, no ammonia formation should be produced. The only exception is MoN that in addition to HER at lower coverage change to reduction of surface nitrogen to NH_3 at more than 6/8 H coverage on the surface corresponding to an onset potential of around -0.83 V. But below this onset potential and H coverage, no ammonia should be produced but adsorbed Hs, specially those bound the Mo metal atoms, can evolve and form H_2.

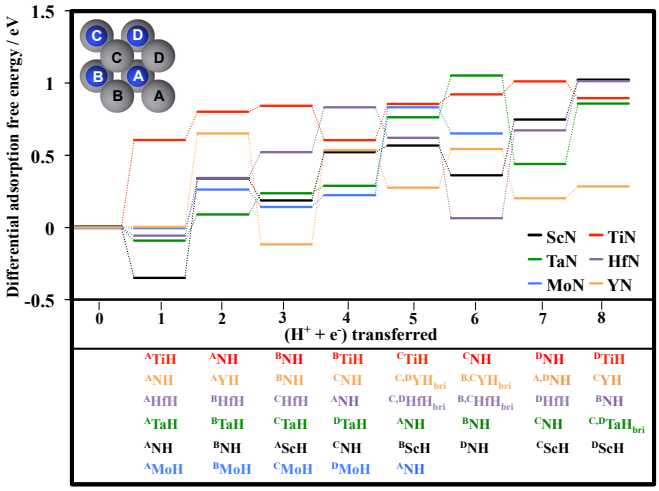

Figure 4.11: *Differential free energy of H adsorption. The labels present the most stable species formed at each hydrogenation step; *NH or *MH. The inset shows the top-view structure of the surface where the labeling from A to D indicates where the H-adatoms prefer to adsorb.*

For TaN, MoN, and HfN the protons adsorb and bind preferentially to the metal atoms rather than to the surface nitrogen atoms up to 4/8 ML for TaN and MoN and 3/8 ML for HfN. Afterwards, surface N atoms are populated each by one hydrogen (to reach 1ML). But on ScN, YN and TiN, H adsorption does not follow a specific trend regarding adsorption occurring first on metal (*MH) or on N sites (*NH). As can be seen, adsorption of the first H to the surface is very moderate for mononitrides of Y, Mo, Hf and Ta but very weak on Ti and rather strong on Sc (same as shown by figure 4.10A). When comparing the catalytic activity of these different material only based on the free energy of adsorption of first proton ($\triangle G_{H*}$ descriptor), YN seems to be the most active candidate with $\triangle G_{H*}$ around zero. But for HER to occur, either the H-adatom should react with a coming proton from elec-

trolyte via the Heyrovsky mechanism (which has been concluded to have a high activation energy [17]) or a second proton needs to be adsorbed on the surface and then recombine with the first H-adatom to evolve hydrogen via the Tafel mechanism. Therefore, using the differential H adsorption free energy of 2H* rather than 1H* is more realistic descriptor for the activity on these metal nitrides. In Figure 4.10B we use the 2H* descriptor in the FED, and as can be seen, these two descriptors give rather different trends. Considering hydrogen recombination via the Tafel mechanism, an overpotential of -0.65 V vs. RHE is needed to apply on YN in order to reach a coverage of 2/8 so that the second *H is formed and then the two *Hs can recombine to desorb H_2. Alternatively, TaN only requires a small overpotential of -87 mV to build up such coverage on the surface and evolve H_2. Therefore in reality, TaN should be by far a better candidate compared to YN. For MoN, HfN, ScN, and TiN, overpotentials of -0.26, -0.34, -0.34, and -0.8 V, respectively, are needed.

Figure 4.12 shows the hydrogen coverage on the surface as a function of the applied potential for the metal nitrides. For TiN and YN, a rather negative potential is required to reach 2/8 ML (where there is a possibility to have two Hs next to each other) but as soon as that potential is reached, the surfaces get fully covered with H adatoms. The onset potential for TiN and YN is thus large. All the other nitrides builds up the H coverage gradually as the potential becomes more negative. All these nitrides show a different trend from Pt(111). There, almost a full ML is reached at only slightly negative potential where it suddenly requires a rather negative potential to go beyond a ML.

Activation barrier of the Tafel mechanism and rate of the HER

In Figure 4.13, the activation energy (E_a/eV) is plotted as a function of hydrogen coverage until 1 ML H coverage is reached. This is compared with Pt(111) data reported by Skúlason et al. [17]. As expected, the activation barriers for HER gets lower with increasing H coverage. The activation barrier drops down gradually for all the nitrides except TiN and YN where the barriers are rather constant at any H coverage. This is due to the weak binding of H on TiN and YN where a potential of around -0.8 V and -0.65 V, respectively, are needed to get the minimum H coverage for HER.

Figure 4.14 shows the activation energy for HER on the metal nitrides studied here as a function of the electrode potential. Usually the trend is that the more negative potential applied, the higher H coverage builds on the surface. That causes the activation energy of the $2H^* \longrightarrow H_2$ reaction to drop

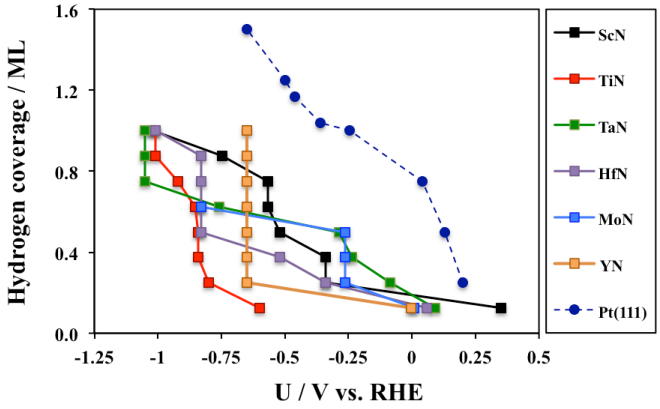

Figure 4.12: *Hydrogen coverage on the surface of the transition metal nitrides as a function of applied potential (U/V vs. RHE). 1 ML coverage corresponds to 8H* on the surface in our model system (consisting of 4 surface metal atoms and 4 surface nitrogen atoms). The values for Pt(111) are adapted from [17].*

significantly. As already mentioned, TaN needs only a small overpotential of -0.087 V to reach 2/8 coverage, which is the coverage needed for HER to start in our model system. The barrier of this Tafel reaction is calculated to be 0.84 eV, surprisingly very similar to that of Pt(111) at 0.85 eV [17]. Therefore, it is expected that TaN catalyzes HER in a relatively similar manner as Pt(111) does. Comparing the activation energies of hydrogen evolution from the surface of ScN, HfN and MoN, the Tafel reaction barrier drops significantly when coverage changes from 2/8 to 3/8. The lowest activation energy found for the Tafel reaction is for TiN (less than 0.14 eV), but a relatively high overpotential of -0.8 V is required to adsorb 2Hs on its surface before H_2 evolution starts. This makes TiN a less active candidate and can reduce its attractiveness for experimental analyses. The same holds true for YN where -0.65 V is needed to reach 2/8 ML while the activation energy of 2*Hs recombination is calculated to be rather low at 0.31 eV.

The theoretical current densities of the HER are estimated as a function of the electrode potential on the surfaces of these metal nitride catalysts and compared with that of Pt(111) in Figure 4.14B. The Tafel rate constant of HER is given by:

$$k = Aexp^{-E_a/K_BT} \tag{4.3}$$

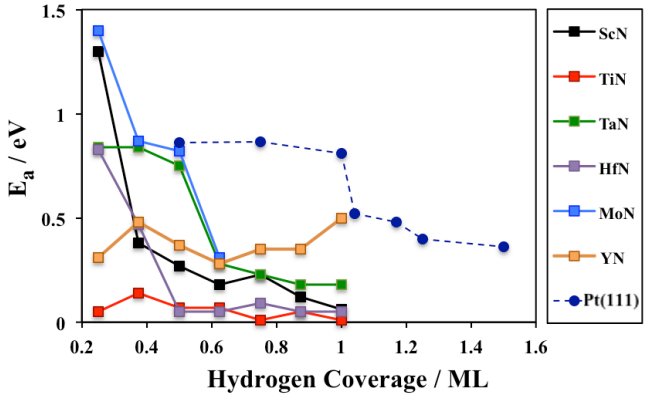

Figure 4.13: *Activation energy (E_a/eV) for the Tafel reaction in HER on several transition metal nitrides as a function of hydrogen coverage. 1ML coverage corresponds to 8H* on the surface in our model system (consisting of 4 surface metal atoms and 4 surface nitrogen atoms). The values for Pt(111) are adapted from [17].*

we assume a prefactor, A, of the order 10^{13} site^{-1} s^{-1} as an Arrhenius rate constant, which was found to agree well with the measured absolute rate for HER when used together with the calculated activation energies [17]. E_a is the activation energies of the Tafel reaction calculated by the CI-NEB method in DFT. The surface area per atom, A/N, for Pt was calculated to be 6.6×10^{-16}, and considering the lattice constant of Pt (4.02Å) we can calculate A/N for any nitrides based on its lattice constant. By applying

$$i = keN/A \tag{4.4}$$

at 298 K we can obtain the current densities.

As can be seen from Figure 4.14B, at around equilibrium potential, TaN and Pt(111) have a similar rate, and as the coverage increases the rate of HER increases gradually. Similar trends are seen for HfN, MoN, and ScN as well, where the rate of HER increases as the coverage increases. However, the trends are quite different on the surfaces of YN and TiN. First of all, as has been discussed earlier, a much more negative potential is required to start HER on YN and TiN than all the other nitrides studied here. In addition, when the onset potential is reached, the rate of the Tafel reaction is rather high and it does not change much depending on the H coverage on the surface.

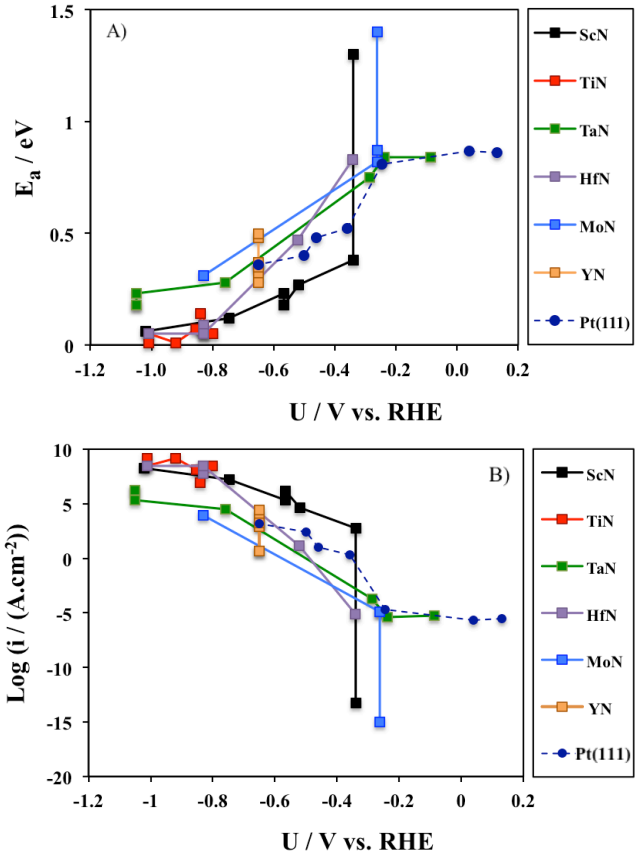

Figure 4.14: *Activation energy of Tafel reaction (E_a/eV) (A) and theoretical current densities of the Tafel reaction of the HER (B) as a function of the electrode potential, U, vs. RHE on several transition metal nitride catalysts obtained according to eqn. 4.3 and 4.4 and compared with Pt(111) adapted from [17]. Applying a potential of -0.65 V to get minimum H coverage (2/8) on YN will spontaneously result in a full H coverage as shown in Figure 4.11, and that is why all the points are lying vertically at -0.65 V for YN.*

Volcano plot

Volcano plots became common approach for comparison of the catalytic activity of different materials. Therefore, the theoretical current density of the Tafel reaction for the lowest possible coverage for HER (2/8 ML) is used to get the location of the best candidate of this study, TaN, on the experimental volcano plot made for the metals. In Figure 4.15, the theoretical current

density on the surface of TaN is obtained from the activation energy calculations when adsorbed Hs on the surface recombine and evolve H_2, and that is plotted as a function of the free energy of *H adsorbed on the surface.

The results are compared with the experimentally measured exchange current density on pure metals adapted from [17]. In the volcano, TaN is also compared with the experimental current density of MoS_2, The experimental data for MoS_2 is taken from [18]. Thus, TaN is predicted to show a relatively high rate of HER comparable to that of MoS_2 and close to Pt(111).

In conclusion, possibility of catalyzing the hydrogen evolution reaction (HER) was investigated by DFT calculations on the (100) facet of the NaCl-type structure of mononitrides of Sc, Ti, Y, Hf, Ta, and Mo at pH = 0. On the basis of the calculated differential adsorption free energy of H up to a full monolayer and activation energy of the Tafel reaction for forming H_2, we estimated the current densities of HER as a function of applied potential on all the nitrides. It was found that the most promising nitride catalyst is TaN, which should catalyze HER at potential of around -0.09 V with respect to RHE. In addition, the activation energy and rate of the Tafel reaction on TaN was found very similar to that previously reported on Pt(111) at around the equilibrium potential.

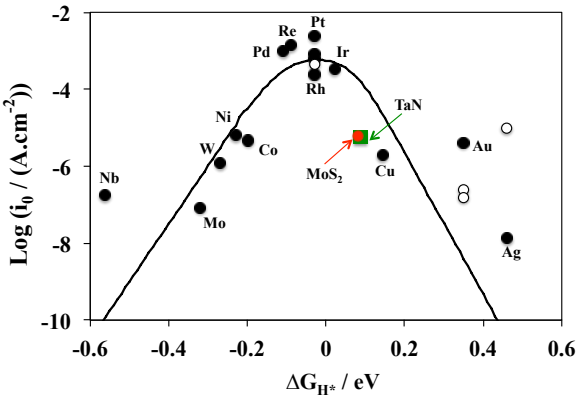

Figure 4.15: *A volcano plot of the HER for various pure metals, MoS_2, and the most promising transition metal nitride surface, TaN. The $\triangle G_{H*}$ value for TaN is calculated for 2/8 ML H coverage at 1 bar of H_2 and 298 K. Experimental data are adapted from [17] where the circular data points are the measured exchange current density (open data points for (111) facets but filled data points for polycrystalline) plotted versus the calculated free energy of H adsorption. The metals on the left side of the volcano have high H coverage (1 ML) and the metals on the right side low H coverage (0.25 ML). The experimental data for MoS_2 is taken from [18].*

5 Summary and Conclusion

With a hiking global population, increasing energy demands, and imminent climate change, major apprehensions have been raised over the security of our energy future. Evolving sustainable and fossil-free pathways to produce fuels and chemicals of international importance could play a crucial role in reducing carbon dioxide emissions while providing the feedstocks needed to make the products we use on a daily basis. One forthcoming goal is to develop electrochemical conversion processes that, by coupling to renewable energy, can convert molecules in the atmosphere (e.g., water, carbon dioxide, and nitrogen) into higher-value products (e.g., hydrogen, hydrocarbons, oxygenates, and ammonia). Electrocatalysts play a central role in these energy conversion technologies as they increase the rate, efficiency, and selectivity of the chemical transformations involved. Today's electrocatalysts, however, are not sufficient. The main challenge is to develop advanced electrocatalysts with the enhanced performance needed to enable widespread penetration of clean energy technologies.

In line with the above-mentioned goals and challenges, the overall aim of this thesis has been to investigate a new class of materials and screen for novel and promising electrocatalysts for nitrogen electroreduction to ammonia. We tried to introduce a scheme enabling electrochemical reduction of molecular nitrogen to ammonia in aqueous media at ambient conditions with only a low applied bias.

One of the most important and interesting parts of this thesis is the possibilty of ammonia formation on the surface of mononitrides via the Mars-van Krevelen mechanism. This offers a new reaction path that is thermodynamically simpler for ammonia production at ambient conditions. However, one should bear in mind that when a reaction proceeds via such mechanism,

the catalytic active site could be suseptible to poisoning or decomposition under operational conditions due to the nature of the Mars-van Krevelen chemistry. So these criteria should be scrutinized for the nitrides showing activity for the reaction.

This thesis is a detailed investigation of the transition metal mononitride electrocatalysts to gain better insight for their experimental measurements and real-life application. Four important factors have been considered in this thesis to identify promising electrocatalysts for electrochemical ammonia formation in aqueous media: (1) identification of the reaction mechanism and calculation of the N_2 dissociation barrier, (2) investigation of the catalytic activity and quantification of the potential-determining and rate-determining steps, (3) determination of kinetic or thermodynamic barriers for N vacancy diffusion into the bulk, which can consequently leak the nitrogen content out of the nitride catalysts, (4) investigation of the stability of the nitrides against poisoning in an electrochemical environment. By considering the most common crystal facets in more detail, we have been able to identify which facets of the nitrides are most active for ammonia formation as well as which facets should be avoided in order to succeed with high rates and efficiency for this reaction. The most promising nitrides are found to be the (110) of the zincblende structure of RuN as well as the (100) of the rocksalt structures of VN and CrN. These promising nitride catalysts are all stable against poisoning and decomposition in the electrochemical environment with feasible regeneration of the catalyst to ensure the continuity of the catalytic cycle of ammonia production. Additionally, none of these facets are predicted to produce hydrogen according to the explicit consideration of HER within our mechanistic model. Therefore, experimentalists are strongly encouraged to test these promising candidates in the structure and bias range proposed here for the possibility of higher-yield ammonia synthesis at ambient conditions. In addition, the (100) of the rocksalt structure of TaN was found to be promising to catalyze the hydrogen evolution reaction with experimental rates nearing MoS_2 and Pt(111). Figure 5.1 summarizes the entire thesis with regards to electrocatalytic activity of the all naturally occuring d-block elements in the periodic table.

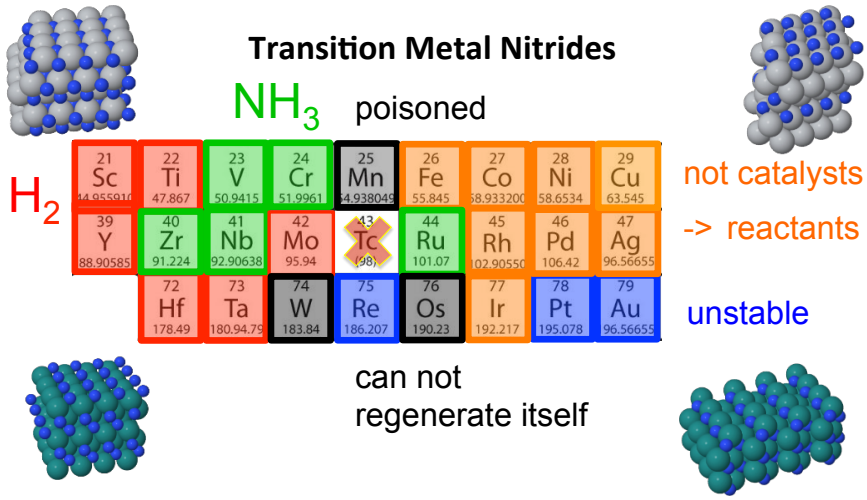

Figure 5.1: *The summary and conclusion of the results obtained throughout the screening process of transition metal mononitrides for both the NER and HER by this thesis.*

List of Figures

Bibliography

[1] **G. Ertl**. *Reactions at surfaces: From atoms to complexity (Nobel lecture)*. Angewandte Chemie International Edition, 47(19), (2008), 3524.

[2] **V. Smil**. *Global population and the nitrogen cycle*. Scientific American, 277(1), (1997), 76.

[3] **V. Smil**. *Detonator of the population explosion*. Nature, 400(6743), (1999), 415.

[4] **V. Smil**. *Nitrogen and food production: proteins for human diets*. AMBIO: A Journal of the Human Environment, 31(2), (2002), 126.

[5] **A. Klerke**, **C. H. Christensen**, **J. K. Nørskov** and **T. Vegge**. *Ammonia for hydrogen storage: challenges and opportunities*. Journal of Materials Chemistry, 18(20), (2008), 2304.

[6] **A. Züttel**, **A. Remhof**, **A. Borgschulte** and **O. Friedrichs**. *Hydrogen: the future energy carrier*. Philosophical Transactions of the Royal Society of London A: Mathematical, Physical and Engineering Sciences, 368(1923), (2010), 3329.

[7] **V. Rosca**, **M. Duca**, **M. T. de Groot** and **M. T. Koper**. *Nitrogen cycle electrocatalysis*. Chemical Reviews, 109(6), (2009), 2209.

[8] **B. Anantharaman**, **S. Hazarika**, **T. Ahmad**, **M. Nagvekar**, **S. Ariyapadi** and **R. Gualy**. *Coal gasification technology for ammonia plants*. In *Asia nitrogen & syngas 2012 conference (Oct 2012) Kuala Lumpur, Malaysia. Available at: http://www. kbr. com/Newsroom/Publications/Whitepapers/Coal-Gasification-Technology-for-Ammonia-Plants. pdf [cited 24 April 2013]*. 2012.

[9] **R. Service**. *Chemistry. New recipe produces ammonia from air, water, and sunlight.* Science (New York, NY), 345(6197), (2014), 610.

[10] **R. Michalsky**. *Thermochemical production of ammonia using sunlight, air, water and biomass*. Ph.D. thesis, Kansas State University, 2012.

[11] **V. Smil**. *Enriching the earth: Fritz Haber, Carl Bosch, and the transformation of world food production*. MIT press, 2004.

[12] **C. Zamfirescu** and **I. Dincer**. *Using ammonia as a sustainable fuel*. Journal of Power Sources, 185(1), (2008), 459.

[13] **C. Zamfirescu** and **I. Dincer**. *Ammonia as a green fuel and hydrogen source for vehicular applications*. Fuel processing technology, 90(5), (2009), 729.

[14] **R. Lan**, **J. T. Irvine** and **S. Tao**. *Ammonia and related chemicals as potential indirect hydrogen storage materials*. International Journal of Hydrogen Energy, 37(2), (2012), 1482.

[15] **I. Chorkendorff** and **J. W. Niemantsverdriet**. *Concepts of modern catalysis and kinetics*. John Wiley & Sons, 2006.

[16] **R. Parsons**. *The rate of electrolytic hydrogen evolution and the heat of adsorption of hydrogen*. Transactions of the Faraday Society, 54, (1958), 1053.

[17] **E. Skúlason**, **V. Tripkovic**, **M. E. Björketun**, **S. Gudmundsdóttir**, **G. Karlberg**, **J. Rossmeisl**, **T. Bligaard**, **H. Jónsson** and **J. K. Nørskov**. *Modeling the Electrochemical Hydrogen Oxidation and Evolution Reactions on the Basis of Density Functional Theory Calculations*. The Journal of Physical Chemistry C, 114(42), (2010), 18182.

[18] **T. F. Jaramillo**, **K. P. Jørgensen**, **J. Bonde**, **J. H. Nielsen**, **S. Horch** and **I. Chorkendorff**. *Identification of active edge sites for electrochemical H2 evolution from MoS2 nanocatalysts*. science, 317(5834), (2007), 100.

[19] **M. A. Shipman** and **M. D. Symes**. *Recent progress towards the electrosynthesis of ammonia from sustainable resources*. Catalysis Today.

[20] **D. Strongin**, **G. Somorjai** and **J. Jennings**. *Catalytic ammonia synthesis: fundamentals and practice*. Plenum Publishing Company.

[21] **D. Saygın** and **M. K. Patel**. *ChemiCal and PetroChemiCal SeCtor, Potential of best practice technology and other measures for improving energy efficiency*.

[22] **K. Urabe**, **K.-I. Aika** and **A. Ozaki**. *Activation of nitrogen by alkali metal-promoted transition metal: II. Isotopic exchange in molecular nitrogen*

over potassium-promoted ruthenium-carbon catalyst. Journal of Catalysis, 32(1), (1974), 108.

[23] **K.-I. Aika** and **A. Ozaki**. *Activation of nitrogen by alkali metal-promoted transition metal: III. On the adsorption of nitrogen over the alkali metal-promoted ruthenium catalyst*. Journal of Catalysis, 35(1), (1974), 61.

[24] **K. Urabe**, **K.-i. Aika** and **A. Ozaki**. *Activation of nitrogen by alkali metal-promoted transition metal: IV. Effect of potassium on the kinetics of isotopic equilibration of nitrogen on ruthenium catalysts*. Journal of Catalysis, 38(1-3), (1975), 430.

[25] **A. Ozaki**. *Development of alkali-promoted ruthenium as a novel catalyst for ammonia synthesis*. Accounts of Chemical Research, 14(1), (1981), 16.

[26] **A. K. Rhodes**. *New ammonia process, catalyst proven in Canadian plant*. Oil and Gas Journal, 94(47).

[27] **C. J. Jacobsen**, **S. Dahl**, **B. S. Clausen**, **S. Bahn**, **A. Logadottir** and **J. K. Nørskov**. *Catalyst design by interpolation in the periodic table: bimetallic ammonia synthesis catalysts*. Journal of the American Chemical Society, 123(34), (2001), 8404.

[28] **R. Kojima** and **K.-i. Aika**. *Cobalt molybdenum bimetallic nitride catalysts for ammonia synthesis: Part 1. Preparation and characterization*. Applied Catalysis A: General, 215(1), (2001), 149.

[29] **R. Kojima** and **K.-i. Aika**. *Cobalt molybdenum bimetallic nitride catalysts for ammonia synthesis: Part 2. Kinetic study*. Applied Catalysis A: General, 218(1), (2001), 121.

[30] **R. Kojima** and **K.-i. Aika**. *Cobalt molybdenum bimetallic nitride catalysts for ammonia synthesis: Part 3. Reactant gas treatment*. Applied Catalysis A: General, 219(1), (2001), 157.

[31] **J. Hargreaves**. *Nitrides as ammonia synthesis catalysts and as potential nitrogen transfer reagents*. Applied Petrochemical Research, 4(1), (2014), 3.

[32] **M. Appl**. *Ammonia: principles and industrial practice*. Vch Verlagsgesellschaft Mbh, 1999.

[33] **I. Rafiqul**, **C. Weber**, **B. Lehmann** and **A. Voss**. *Energy efficiency improvements in ammonia production—perspectives and uncertainties*. Energy, 30(13), (2005), 2487.

[34] **J. B. Howard** and **D. C. Rees**. *How many metals does it take to fix N2? A mechanistic overview of biological nitrogen fixation*. Proceedings of the National Academy of Sciences, 103(46), (2006), 17088.

[35] **D. W. Mulder**, **E. M. Shepard**, **J. E. Meuser**, **N. Joshi**, **P. W. King**, **M. C. Posewitz**, **J. B. Broderick** and **J. W. Peters**. *Insights into [FeFe]-hydrogenase structure, mechanism, and maturation*. Structure, 19(8), (2011), 1038.

[36] **I. A. Amar**, **R. Lan**, **C. T. Petit** and **S. Tao**. *Solid-state electrochemical synthesis of ammonia: a review*. Journal of solid state electrochemistry, 15(9), (2011), 1845.

[37] **S. Giddey**, **S. Badwal** and **A. Kulkarni**. *Review of electrochemical ammonia production technologies and materials*. International Journal of Hydrogen Energy, 38(34), (2013), 14576.

[38] **V. Kyriakou**, **I. Garagounis**, **E. Vasileiou**, **A. Vourros** and **M. Stoukides**. *Progress in the electrochemical synthesis of ammonia*. Catalysis Today.

[39] **G. Schrauzer** and **T. Guth**. *Photocatalytic reactions. 1. Photolysis of water and photoreduction of nitrogen on titanium dioxide*. Journal of the American Chemical Society, 99(22), (1977), 7189.

[40] **J. Y. Becker** and **S. Avraham**. *Nitrogen Fixation: Part II. Electrochemical Reduction of Hydrazido (-NNH2) Mo and W Complexes. Selective Formation of NH3 under Mild Conditions*. Journal of electroanalytical chemistry and interfacial electrochemistry, 280(1), (1988), 119.

[41] **J. Y. Becker** and **S. Avraham**. *Nitrogen fixation: Part III. Electrochemical reduction of hydrazido (-NNH2) Mo and W complexes. Selective formation of NH3 under mild conditions*. Journal of electroanalytical chemistry and interfacial electrochemistry, 280(1), (1990), 119.

[42] **C. J. Pickett** and **J. Talarmin**. *Electrosynthesis of ammonia*. Nature, 317(6038), (1985), 652.

[43] **A. Sclafani**, **V. Augugliaro** and **M. Schiavello**. *Dinitrogen electrochemical reduction to ammonia over Iron cathode in aqueous medium*. Journal of The Electrochemical Society, 130(3), (1983), 734.

[44] **D. V. Yandulov** and **R. R. Schrock**. *Catalytic reduction of dinitrogen to ammonia at a single molybdenum center*. Science, 301(5629), (2003), 76.

[45] **N. Furuya** and **H. Yoshiba**. *Electroreduction of nitrogen to ammonia on gas-diffusion electrodes loaded with inorganic catalyst*. Journal of Electroanalytical Chemistry and Interfacial Electrochemistry, 291(1-2), (1990), 269.

[46] **I. A. Amar**, **R. Lan**, **C. T. Petit**, **V. Arrighi** and **S. Tao**. *Electrochemical synthesis of ammonia based on a carbonate-oxide composite electrolyte*. Solid State Ionics, 182(1), (2011), 133.

[47] **I. Garagounis**, **V. Kyriakou**, **A. Skodra**, **E. Vasileiou** and **M. Stoukides**. *Electrochemical synthesis of ammonia in solid electrolyte cells*. Frontiers in Energy Research, 2, (2014), 1.

[48] **E. Vasileiou**, **V. Kyriakou**, **I. Garagounis**, **A. Vourros**, **A. Manerbino**, **W. Coors** and **M. Stoukides**. *Reaction rate enhancement during the electrocatalytic synthesis of ammonia in a BaZr0. 7Ce0. 2Y0. 1O2. 9 solid electrolyte cell*. Topics in Catalysis, 58(18-20), (2015), 1193.

[49] **G. Qing**, **R. Kikuchi**, **S. Kishira**, **A. Takagaki**, **T. Sugawara** and **S. T. Oyama**. *Ammonia Synthesis by N2 and Steam Electrolysis in Solid-State Cells at 220° C and Atmospheric Pressure*. Journal of The Electrochemical Society, 163(10), (2016), E282.

[50] **T. Murakami**, **T. Nishikiori**, **T. Nohira** and **Y. Ito**. *Electrolytic synthesis of ammonia in molten salts under atmospheric pressure*. Journal of the American Chemical Society, 125(2), (2003), 334.

[51] **T. Murakami**, **T. Nohira**, **T. Goto**, **Y. H. Ogata** and **Y. Ito**. *Electrolytic ammonia synthesis from water and nitrogen gas in molten salt under atmospheric pressure*. Electrochimica acta, 50(27), (2005), 5423.

[52] **T. Murakami**, **T. Nohira**, **Y. Araki**, **T. Goto**, **R. Hagiwara** and **Y. H. Ogata**. *Electrolytic synthesis of ammonia from water and nitrogen under atmospheric pressure using a boron-doped diamond electrode as a nonconsumable anode*. Electrochemical and solid-state letters, 10(4), (2007), E4.

[53] **S. Licht**, **B. Cui**, **B. Wang**, **F.-F. Li**, **J. Lau** and **S. Liu**. *Ammonia synthesis by N2 and steam electrolysis in molten hydroxide suspensions of nanoscale Fe2O3*. Science, 345(6197), (2014), 637.

[54] **G. Xu**, **R. Liu** and **J. Wang**. *Electrochemical synthesis of ammonia using a cell with a Nafion membrane and SmFe0. 7Cu0. 3- xNixO3 (x= 0- 0.3) cathode at atmospheric pressure and lower temperature*. Science in China Series B: Chemistry, 52(8), (2009), 1171.

[55] **Z. Zhang**, **Z. Zhong** and **L. Ruiquan**. *Cathode catalysis performance of SmBaCuMO5+ δ (M= Fe, Co, Ni) in ammonia synthesis*. Journal of Rare Earths, 28(4), (2010), 556.

[56] **R. Lan**, **J. T. Irvine** and **S. Tao**. *Synthesis of ammonia directly from air and water at ambient temperature and pressure*. Scientific reports, 3, (2013), 1145.

[57] **G. Marnellos** and **M. Stoukides**. *Ammonia synthesis at atmospheric pressure*. Science, 282(5386), (1998), 98.

[58] **C. Chen** and **G. Ma**. *Proton conduction in BaCe 1- x Gd x O 3- α at intermediate temperature and its application to synthesis of ammonia at atmospheric pressure*. Journal of Alloys and Compounds, 485(1), (2009), 69.

[59] **C. Cheng**, **W. Wenbao** and **M. Guilin**. *Proton conduction in La0. 9M0. 1Ga0. 8Mg0. 2O3-alpha at intermediate temperature and its application to synthesis of ammonia at atmospheric pressure*. Acta Chimica Sinica, 67(7), (2009), 623.

[60] **F. Zhang**, **Q. Yang**, **B. Pan**, **R. Xu**, **H. Wang** and **G. Ma**. *Proton conduction in La 0.9 Sr 0.1 Ga 0.8 Mg 0.2 O 3- α ceramic prepared via microemulsion method and its application in ammonia synthesis at atmospheric pressure*. Materials Letters, 61(19), (2007), 4144.

[61] **Y.-H. Xie**, **J.-D. Wang**, **R.-Q. Liu**, **X.-T. Su**, **Z.-P. Sun** and **Z.-J. Li**. *Preparation of La 1.9 Ca 0.1 Zr 2 O 6.95 with pyrochlore structure and its application in synthesis of ammonia at atmospheric pressure*. Solid State Ionics, 168(1), (2004), 117.

[62] **I. A. Amar**, **R. Lan**, **C. T. Petit** and **S. Tao**. *Electrochemical Synthesis of Ammonia Using Fe3Mo3N Catalyst and Carbonate-Oxide Composite Electrolyte*. Int. J. Electrochem. Sci, 10, (2015), 3757.

[63] **I. A. Amar**, **R. Lan**, **C. T. Petit** and **S. Tao**. *Electrochemical synthesis of ammonia based on Co3Mo3N catalyst and LiAlO2–(Li, Na, K) 2CO3 composite electrolyte*. Electrocatalysis, 6(3), (2015), 286.

[64] **J. N. Renner**, **L. F. Greenlee**, **K. E. Ayres** and **A. M. Herring**. *Electrochemical Synthesis of Ammonia: A Low Pressure, Low Temperature Approach*. The Electrochemical Society Interface, 24(2), (2015), 51.

[65] **V. Kordali**, **G. Kyriacou** and **C. Lambrou**. *Electrochemical synthesis of ammonia at atmospheric pressure and low temperature in a solid polymer electrolyte cell*. Chemical Communications, (17), (2000), 1673.

[66] **J. K. Nørskov**, **J. Rossmeisl**, **A. Logadottir**, **L. Lindqvist**, **J. R. Kitchin**, **T. Bligaard** and **H. Jónsson**. *Origin of the Overpotential for Oxygen Reduction at a Fuel-Cell Cathode*. The Journal of Physical Chemistry B, 108(46), (2004), 17886.

[67] **J. Greeley** and **M. Mavrikakis**. *Alloy catalysts designed from first principles*. Nature materials, 3(11), (2004), 810.

[68] **K. Honkala**, **A. Hellman**, **I. Remediakis**, **A. Logadottir**, **A. Carlsson**, **S. Dahl**, **C. H. Christensen** and **J. K. Nørskov**. *Ammonia synthesis from first-principles calculations*. Science, 307(5709), (2005), 555.

[69] **J. Hafner**, **C. Wolverton** and **G. Ceder**. *Toward computational materials design: the impact of density functional theory on materials research*. MRS bulletin, 31(09), (2006), 659.

[70] **F. Abild-Pedersen**, **J. Greeley**, **F. Studt**, **J. Rossmeisl**, **T. Munter**, **P. G. Moses**, **E. Skulason**, **T. Bligaard** and **J. K. Nørskov**. *Scaling properties of adsorption energies for hydrogen-containing molecules on transition-metal surfaces*. Physical review letters, 99(1), (2007), 016105.

[71] **F. Studt**, **F. Abild-Pedersen**, **T. Bligaard**, **R. Z. Sørensen**, **C. H. Christensen** and **J. K. Nørskov**. *Identification of non-precious metal alloy catalysts for selective hydrogenation of acetylene*. Science, 320(5881), (2008), 1320.

[72] **H.-J. Freund** and **G. Pacchioni**. *Oxide ultra-thin films on metals: new materials for the design of supported metal catalysts*. Chemical Society Reviews, 37(10), (2008), 2224.

[73] **J. Greeley**, **I. Stephens**, **A. Bondarenko**, **T. P. Johansson**, **H. A. Hansen**, **T. Jaramillo**, **J. Rossmeisl**, **I. Chorkendorff** and **J. K. Nørskov**. *Alloys of platinum and early transition metals as oxygen reduction electrocatalysts*. Nature chemistry, 1(7), (2009), 552.

[74] **J. K. Nørskov**, **T. Bligaard**, **J. Rossmeisl** and **C. H. Christensen**. *Towards the computational design of solid catalysts*. Nature chemistry, 1(1), (2009), 37.

[75] **J. G. Howalt**, **T. Bligaard**, **J. Rossmeisl** and **T. Vegge**. *DFT based study of transition metal nano-clusters for electrochemical NH 3 production*. Physical Chemistry Chemical Physics, 15(20), (2013), 7785.

[76] **V. Tripkovic**, **M. Vanin**, **M. Karamad**, **M. E. Bjo¨rketun**, **K. W. Jacobsen**, **K. S. Thygesen** and **J. Rossmeisl**. *Electrochemical CO2 and CO*

reduction on metal-functionalized porphyrin-like graphene. The Journal of Physical Chemistry C, 117(18), (2013), 9187.

[77] **A. Verdaguer-Casadevall**, **D. Deiana**, **M. Karamad**, **S. Siahrostami**, **P. Malacrida**, **T. W. Hansen**, **J. Rossmeisl**, **I. Chorkendorff** and **I. E. Stephens**. *Trends in the electrochemical synthesis of H2O2: Enhancing activity and selectivity by electrocatalytic site engineering*. Nano letters, 14(3), (2014), 1603.

[78] **D. G. Sangiovanni**, **A. B. Mei**, **L. Hultman**, **V. Chirita**, **I. Petrov** and **J. E. Greene**. *Ab Initio Molecular Dynamics Simulations of Nitrogen/VN (001) Surface Reactions: Vacancy-Catalyzed N2 Dissociative Chemisorption, N Adatom Migration, and N2 Desorption*. The Journal of Physical Chemistry C, 120(23), (2016), 12503.

[79] **Y. Abghoui** and **E. Skúlason**. *Electrochemical synthesis of ammonia via Mars-van Krevelen mechanism on the (111) facets of group III–VII transition metal mononitrides*. Catalysis Today, (2016), DOI:10.1016/j.cattod.2016.06.009.

[80] **S. Dahl**, **A. Logadottir**, **R. Egeberg**, **J. Larsen**, **I. Chorkendorff**, **E. Törnqvist** and **J. K. Nørskov**. *Role of steps in N 2 activation on Ru (0001)*. Physical Review Letters, 83(9), (1999), 1814.

[81] **Y. Abghoui**, **A. L. Garden**, **J. G. Howalt**, **T. Vegge** and **E. Skú lason**. *Electroreduction of N2 to ammonia at ambient conditions on mononitrides of Zr, Nb, Cr, and V: a DFT guide for experiments*. ACS Catalysis, 6(2), (2015), 635.

[82] **C. D. Zeinalipour-Yazdi**, **J. S. Hargreaves** and **C. R. A. Catlow**. *DFT-D3 study of molecular N2 and H2 activation on Co3Mo3N surfaces*. The Journal of Physical Chemistry C, 120(38), (2016), 21390.

[83] **D. Mckay**, **J. Hargreaves**, **J. Rico**, **J. Rivera** and **X.-L. Sun**. *The influence of phase and morphology of molybdenum nitrides on ammonia synthesis activity and reduction characteristics*. Journal of Solid State Chemistry, 181(2), (2008), 325.

[84] **S. Gudmundsdóttir**, **E. Skúlason** and **H. Jónsson**. *Reentrant Mechanism for Associative Desorption: H 2/Pt (110)-(1× 2)*. Physical review letters, 108(15), (2012), 156101.

[85] **S. Kattel**, **P. Atanassov** and **B. Kiefer**. *Catalytic activity of Co–N x/C electrocatalysts for oxygen reduction reaction: a density functional theory study*. Physical Chemistry Chemical Physics, 15(1), (2013), 148.

[86] **J. G. Howalt** and **T. Vegge**. *Electrochemical ammonia production on molybdenum nitride nanoclusters*. Physical Chemistry Chemical Physics, 15(48), (2013), 20957.

[87] **Y. Abghoui** and **E. Skúlason**. *Onset potentials for different reaction mechanisms of nitrogen activation to ammonia on transition metal nitride electrocatalysts*. Catalysis Today, (2016), DOI:10.1016/j.cattod.2016.11.047.

[88] **S. Back** and **Y. Jung**. *On the mechanism of electrochemical ammonia synthesis on the Ru catalyst*. Physical Chemistry Chemical Physics, 18(13), (2016), 9161.

[89] **E. Skulason**, **T. Bligaard**, **S. Gudmundsdóttir**, **F. Studt**, **J. Rossmeisl**, **F. Abild-Pedersen**, **T. Vegge**, **H. Jónsson** and **J. K. Nørskov**. *A theoretical evaluation of possible transition metal electro-catalysts for N 2 reduction*. Physical Chemistry Chemical Physics, 14(3), (2012), 1235.

[90] **J. G. Howalt** and **T. Vegge**. *The role of oxygen and water on molybdenum nanoclusters for electro catalytic ammonia production*. Beilstein journal of nanotechnology, 5(1), (2014), 111.

[91] **P. Mars** and **D. W. Van Krevelen**. *Oxidations carried out by means of vanadium oxide catalysts*. Chemical Engineering Science, 3, (1954), 41.

[92] **C. J. Jacobsen**. *Novel class of ammonia synthesis catalysts*. Chemical Communications, (12), (2000), 1057.

[93] **R. Kojima** and **K.-i. Aika**. *Cobalt molybdenum bimetallic nitride catalysts for ammonia synthesis*. Chemistry Letters, 29(5), (2000), 514.

[94] **C. D. Zeinalipour-Yazdi**, **J. S. Hargreaves** and **C. R. A. Catlow**. *Nitrogen Activation in a Mars–van Krevelen Mechanism for Ammonia Synthesis on Co3Mo3N*. The Journal of Physical Chemistry C, 119(51), (2015), 28368.

[95] **Y. Abghoui**, **A. L. Garden**, **V. F. Hlynsson**, **S. Björgvinsdóttir**, **H. Ólafsdóttir** and **E. Skúlason**. *Enabling electrochemical reduction of nitrogen to ammonia at ambient conditions through rational catalyst design*. Physical Chemistry Chemical Physics, 17(7), (2015), 4909.

[96] **A. Logadottir** and **J. K. Nørskov**. *Ammonia synthesis over a Ru (0001) surface studied by density functional calculations*. Journal of Catalysis, 220(2), (2003), 273.

[97] **D. A. McQuarrie**. *Quantum chemistry*. University Science Books, Sausalito, Calif, 2nd ed edition, 2008.

[98] **P. Hohenberg** and **W. Kohn**. *Inhomogeneous Electron Gas*. Phys. Rev., 136, (1964), B864.

[99] **W. Kohn** and **L. J. Sham**. *Self-Consistent Equations Including Exchange and Correlation Effects*. Phys. Rev., 140, (1965), A1133.

[100] **P. Hohenberg** and **W. Kohn**. *Density functional theory*. Phys. Rev. B, 136, (1964), 864.

[101] **K. Capelle**. *A bird's-eye view of density-functional theory*. Brazilian Journal of Physics, 36, (2006), 1318 .

[102] **K. Burke** and **Friends**. *The abc of dft*. Department of Chemistry, University of California.

[103] **P. A. Dirac**. *Note on exchange phenomena in the Thomas atom*. In *Mathematical Proceedings of the Cambridge Philosophical Society*, volume 26, pp. 376–385. Cambridge Univ Press, 1930.

[104] **D. M. Ceperley** and **B. Alder**. *Ground state of the electron gas by a stochastic method*. Physical Review Letters, 45(7), (1980), 566.

[105] **S. H. Vosko**, **L. Wilk** and **M. Nusair**. *Accurate spin-dependent electron liquid correlation energies for local spin density calculations: a critical analysis*. Canadian Journal of physics, 58(8), (1980), 1200.

[106] **J. P. Perdew** and **Y. Wang**. *Accurate and simple analytic representation of the electron-gas correlation energy*. Physical Review B, 45(23), (1992), 13244.

[107] **J. P. Perdew**, **J. A. Chevary**, **S. H. Vosko**, **K. A. Jackson**, **M. R. Pederson**, **D. J. Singh** and **C. Fiolhais**. *Erratum: Atoms, molecules, solids, and surfaces: Applications of the generalized gradient approximation for exchange and correlation*. Phys. Rev. B, 48, (1993), 4978.

[108] **B. Hammer** and **M. Scheffler**. *Local Chemical Reactivity of a Metal Alloy Surface*. Phys. Rev. Lett., 74, (1995), 3487.

[109] **D. R. Hamann**. *Generalized Gradient Theory for Silica Phase Transitions*. Phys. Rev. Lett., 76, (1996), 660.

[110] **P. Philipsen**, **G. te Velde** and **E. Baerends**. *The effect of density-gradient corrections for a molecule-surface potential energy surface. Slab calculations on Cu(100)c(2x2)-CO*. Chemical Physics Letters, 226(5–6), (1994), 583 .

[111] **J. P. Perdew**, **K. Burke** and **M. Ernzerhof**. *Generalized Gradient Approximation Made Simple*. Phys. Rev. Lett., 77, (1996), 3865.

[112] **B. Hammer**, **L. B. Hansen** and **J. K. Nørskov**. *Improved adsorption energetics within density-functional theory using revised Perdew-Burke-Ernzerhof functionals*. Phys. Rev. B, 59, (1999), 7413.

[113] **P. M. Gill**, **B. G. Johnson**, **J. A. Pople** and **M. J. Frisch**. *The performance of the Becke—Lee—Yang—Parr (B—LYP) density functional theory with various basis sets*. Chemical Physics Letters, 197(4), (1992), 499 .

[114] **G. Kresse** and **J. Hafner**. *Ab initio molecular dynamics for liquid metals*. Phys. Rev. B, 47, (1993), 558.

[115] **G. Kresse** and **J. Hafner**. *Ab initio molecular-dynamics simulation of the liquid-metal–amorphous-semiconductor transition in germanium*. Phys. Rev. B, 49, (1994), 14251.

[116] **G. Kresse** and **J. Furthmüller**. *Efficiency of ab-initio total energy calculations for metals and semiconductors using a plane-wave basis set*. Computational Materials Science, 6(1), (1996), 15 .

[117] **G. Kresse** and **J. Furthmüller**. *Efficient iterative schemes for ab initio total-energy calculations using a plane-wave basis set*. Phys. Rev. B, 54, (1996), 11169.

[118] **G. Kresse** and **D. Joubert**. *From ultrasoft pseudopotentials to the projector augmented-wave method*. Phys. Rev. B, 59, (1999), 1758.

[119] **D. Vanderbilt**. *Soft self-consistent pseudopotentials in a generalized eigenvalue formalism*. Phys. Rev. B, 41, (1990), 7892.

[120] **M. Preuss** and **F. Bechstedt**. *Vibrational spectra of ammonia, benzene, and benzene adsorbed on* Si (001) *by first principles calculations with periodic boundary conditions*. Phys. Rev. B, 73, (2006), 155413.

[121] **G. Henkelman**, **B. P. Uberuaga** and **H. Jónsson**. *A climbing image nudged elastic band method for finding saddle points and minimum energy paths*. The Journal of Chemical Physics, 113(22), (2000), 9901.

[122] **G. Henkelman** and **H. Jónsson**. *Improved tangent estimate in the nudged elastic band method for finding minimum energy paths and saddle points*. The Journal of Chemical Physics, 113(22), (2000), 9978.

[123] **H. Jónsson**, **G. Mills** and **K. W. Jacobsen**. *Nudged elastic band method for finding minimum energy paths of transitions*.

[124] **V. F. Hlynsson**, **E. Skúlason** and **A. L. Garden**. *A systematic, first-principles study of the structural preference and magnetic properties of*

mononitrides of the d-block metals. Journal of Alloys and Compounds, 603, (2014), 172 .

[125] **P. E. Blöchl**. *Projector augmented-wave method*. Phys. Rev. B, 50, (1994), 17953.

[126] **H. J. Monkhorst** and **J. D. Pack**. *Special points for Brillouin-zone integrations*. Physical review B, 13(12), (1976), 5188.

[127] **P. W. Atkins**. *Physical Chemistry*, volume 6th Edition. Oxford University Press, Oxford, 1998.

[128] **D. R. Lide**. *CRC Handbook of Chemistry and Physics, 94th Edition, 2013-2014*, volume 53. 2013.

[129] **Y. Abghoui** and **E. Skúlasson**. *Transition Metal Nitride Catalysts for Electrochemical Reduction of Nitrogen to Ammonia at Ambient Conditions*. Procedia Computer Science, 51, (2015), 1897.

[130] **V. Tripković**, **E. Skúlason**, **S. Siahrostami**, **J. K. Nørskov** and **J. Rossmeisl**. *The oxygen reduction reaction mechanism on Pt(1 1 1) from density functional theory calculations*. Electrochimica Acta, 55(27), (2010), 7975 . {EMERGING} {TRENDS} {AND} {CHALLENGES} {IN} {ELECTROCHEMISTRYSelection} of papers from the 60th Annual Meeting of the International Society of Electrochemistry 16–21 August 2009, Beijing, China.

[131] **J. H. Montoya**, **C. Tsai**, **A. Vojvodic** and **J. K. Nørskov**. *The Challenge of Electrochemical Ammonia Synthesis: A New Perspective on the Role of Nitrogen Scaling Relations*. ChemSusChem, 8(13), (2015), 2180.

[132] **B. Eck**, **R. Dronskowski**, **M. Takahashi** and **S. Kikkawa**. *Theoretical calculations on the structures, electronic and magnetic properties of binary 3d transition metal nitrides*. Journal of Materials Chemistry, 9(7), (1999), 1527.

[133] **C. Stampfl**, **W. Mannstadt**, **R. Asahi** and **A. Freeman**. *Electronic structure and physical properties of early transition metal mononitrides*. Physical Review B-Condensed Matter and Materials Physics, 63(15), (2001), 1551061.

[134] **S. Patil**, **N. Mangale**, **S. Khare** and **S. Marsillac**. *Super hard cubic phases of period VI transition metal nitrides: First principles investigation*. Thin Solid Films, 517(2), (2008), 824.

[135] **E. G. Gillan** and **R. B. Kaner**. *Rapid solid-state synthesis of refractory nitrides*. Inorganic Chemistry, 33(25), (1994), 5693.

[136] **P. Hones**, **R. Sanjines** and **F. Levy**. *Characterization of sputter-deposited chromium nitride thin films for hard coatings*. Surface and Coatings Technology, 94, (1997), 398.

[137] **H. J. Ramos** and **N. B. Valmoria**. *Thin-film deposition of ZrN using a plasma sputter-type negative ion source*. Vacuum, 73(3), (2004), 549.

[138] **D. Choi** and **P. N. Kumta**. *Chemically synthesized nanostructured VN for pseudocapacitor application*. Electrochemical and Solid-State Letters, 8(8), (2005), A418.

[139] **D. Arias**, **Y. Arango** and **A. Devia**. *Study of TiN and ZrN thin films grown by cathodic arc technique*. Applied Surface Science, 253(4), (2006), 1683.

[140] **X. Zhou**, **H. Chen**, **D. Shu**, **C. He** and **J. Nan**. *Study on the electrochemical behavior of vanadium nitride as a promising supercapacitor material*. Journal of Physics and Chemistry of Solids, 70(2), (2009), 495.

[141] **S. Shayestehaminzadeh**, **T. Tryggvason**, **F. Magnus**, **S. Olafsson** and **J. Gudmundsson**. *Ultra-thin poly-crystalline TiN films grown by HiPIMS on MgO (100)—In-situ resistance study of the initial stage of growth*. Thin Solid Films, 549, (2013), 199.

[142] **E. Skulason**, **T. Bligaard**, **S. Gudmundsdóttir**, **F. Studt**, **J. Rossmeisl**, **F. Abild-Pedersen**, **T. Vegge**, **H. Jónsson** and **J. K. Nørskov**. *A theoretical evaluation of possible transition metal electro-catalysts for N 2 reduction*. Physical Chemistry Chemical Physics, 14(3), (2012), 1235.

[143] **Y. Abghoui** and **E. Skúlason**. *Computational Predictions of Catalytic Activity of Zincblende (110) Surfaces of Metal Nitrides for Electrochemical Ammonia Synthesis*. Journal of Physical Chemistry C, (2017), DOI:10.1021/acs.jpcc.7b00196.

[144] **Y. Abghoui** and **E. Skúlason**. *Nitrogen Activation to Ammonia via a Mars-van Krevelen Mechanism on Nitride Electro-Catalysts*. AIChE, (2015), ISBN: 978-0-8169-1094- 6.

[145] **Y. Abghoui** and **E. Skúlason**. *Transition Metal Nitrides As Promising Electro-Catalysts for Either Reduction of Nitrogen to Ammonia or Hydrogen Evolution Reaction*. AIChE, (2015), ISBN: 978-0-8169-1094- 6.

[146] **J. K. Nørskov**, **T. Bligaard**, **A. Logadottir**, **J. Kitchin**, **J. G. Chen**, **S. Pandelov** and **U. Stimming**. *Trends in the exchange current for hydrogen evolution*. Journal of The Electrochemical Society, 152(3), (2005), J23.

[147] **M. E. Björketun**, **A. S. Bondarenko**, **B. L. Abrams**, **I. Chorkendorff** and **J. Rossmeisl**. *Screening of electrocatalytic materials for hydrogen evolution*. Physical Chemistry Chemical Physics, 12(35), (2010), 10536.

[148] **B. Hinnemann**, **P. G. Moses**, **J. Bonde**, **K. P. Jørgensen**, **J. H. Nielsen**, **S. Horch**, **I. Chorkendorff** and **J. K. Nørskov**. *Biomimetic hydrogen evolution: MoS2 nanoparticles as catalyst for hydrogen evolution*. Journal of the American Chemical Society, 127(15), (2005), 5308.

[149] **Z. Pu**, **Q. Liu**, **C. Tang**, **A. M. Asiri** and **X. Sun**. *Ni 2 P nanoparticle films supported on a Ti plate as an efficient hydrogen evolution cathode*. Nanoscale, 6(19), (2014), 11031.

Included Publications

Article 1

Enabling Electrochemical Reduction of Nitrogen to Ammonia at Ambient Conditions Through Rational Catalyst Design

Younes Abghoui, Anna L. Garden, Valtýr F. Hlynsson, Snædís Björgvinsdóttir, Hrefna Ólafsdóttir and Egill Skúlason

Physical Chemistry Chemical Physics ***17****, 4909-4918 (2015).*

Volume 17 | Number 7 | 21 February 2015 | Pages 4775–5492

PCCP

Physical Chemistry Chemical Physics
www.rsc.org/pccp

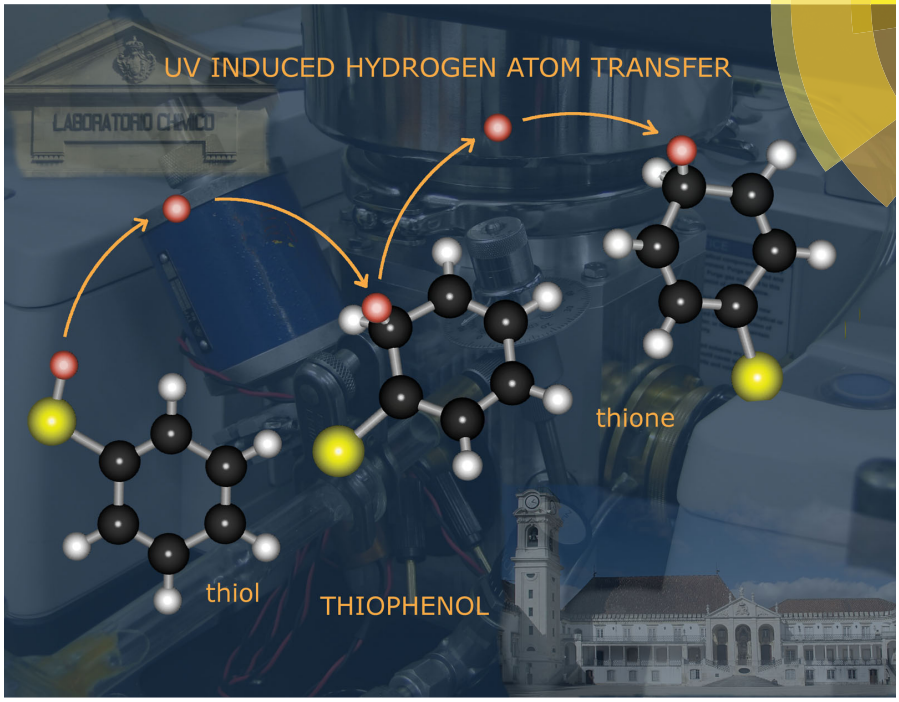

ISSN 1463-9076

PAPER
Igor Reva *et al.*
Hydrogen atom transfer reactions in thiophenol: photogeneration of two new thione isomers

PCCP

PAPER

Enabling electrochemical reduction of nitrogen to ammonia at ambient conditions through rational catalyst design†

Cite this: *Phys. Chem. Chem. Phys.*, 2015, **17**, 4909

Younes Abghoui, Anna L. Garden, Valtýr Freyr Hlynsson, Snædís Björgvinsdóttir, Hrefna Ólafsdóttir and Egill Skúlason*

Received 22nd October 2014,
Accepted 14th November 2014

DOI: 10.1039/c4cp04838e

www.rsc.org/pccp

Commercial design of a sustainable route for on-site production of ammonia represents a potential economic and environmental breakthrough. In an analogous process to the naturally occurring enzymatic mechanism, synthesis of ammonia could be achieved in an electrochemical cell, in which electricity would be used to reduce atmospheric nitrogen and water into ammonia at ambient conditions. To date, such a process has not been realized due to slow kinetics and low faradaic efficiencies. Although progress has been made in this regard, at present there exists no device that can produce ammonia efficiently from air and water at room temperature and ambient pressure. In this work, a scheme is presented in which electronic structure calculations are used to screen for catalysts that are stable, active and selective towards N_2 electro-reduction to ammonia, while at the same time suppressing the competing H_2 evolution reaction. The scheme is applied to transition metal nitride catalysts. The most promising candidates are the (100) facets of the rocksalt structures of VN and ZrN, which show promise of producing ammonia in high yield at low onset potentials.

Introduction

Ammonia (NH_3) is one of the most highly produced chemicals worldwide and is primarily used in production of fertilizer.[1,2] Ammonia is also gaining attention as an energy carrier and a potential transportation fuel due to its high energy density and lack of CO_2 emissions.[3] For the last century, ammonia has been synthesized primarily *via* the energy and capital intensive Haber–Bosch process in which gaseous nitrogen and hydrogen are passed over a Ru- or Fe-based catalyst at high pressure (150–350 atm) and high temperature (350–550 °C) to form NH_3 according to:[4,5]

$$N_{2(g)} + 3H_{2(g)} \rightleftharpoons 2NH_{3(g)} \quad (1)$$

The $H_{2(g)}$ for this process often comes from either coal or natural gas, both of which lead to increased production of various greenhouse gases. The alternative is to produce hydrogen from water splitting, which is a cleaner but very energy intensive process.

The Haber–Bosch process is in stark contrast to the function of the enzyme nitrogenase in bacteria in which ammonia is produced from solvated protons, electrons and atmospheric nitrogen at ambient conditions. The active site of the enzyme is a $MoFe_7S_9N$ cluster that catalyses the electrochemical reaction:

$$N_2 + 8H^+ + 8e^- \rightleftharpoons 2NH_3 + H_2 \quad (2)$$

The source of energy for this reaction is at least 16 adenosine triphosphate (ATP) molecules,[6,7] which are used to increase the chemical potential of the electrons and the protons. It is thus an alluring prospect that this natural process could be emulated in a man-made, commercial installation. Instead of a separate $H_{2(g)}$ production process, the protons could come from an acidic solution while the electrons would be driven to the electrode surface by an applied electric potential.

Various potential routes for ammonia synthesis at ambient conditions are currently being explored (see ref. 1, 2 and 8 for recent reviews). Numerous efforts have been made towards artificial synthesis of ammonia using photocatalytic[9] and electrochemical[10–15] methods. However, for many of these, it is difficult to regenerate the active nitrogen-fixing complex and only low current efficiencies (CE) (0.1–8% at ambient conditions) have been obtained. To gain higher yields of ammonia, solid-state proton conductors have been employed, resulting in up to 78% conversion of cathodic supplied nitrogen to ammonia.[16,17] Ionic liquids or molten salts also promote ammonia formation from low CE up to 72% at high temperatures.[18–20] While having achieved low-pressure ammonia synthesis, the abovementioned

Science Institute and Faculty of Physical Sciences, VR-III, University of Iceland, IS-107 Reykjavik, Iceland. E-mail: egillsk@hi.is

† Electronic supplementary information (ESI) available: Total energy of slabs for different facets, free energy diagrams, corrections to the free energies, decomposition potentials, scaling relations and volcano plots as well as summary table are added for Results and discussion section. See DOI: 10.1039/c4cp04838e

studies still suffer from the requirement of relatively high temperatures, which leads to increased product decomposition. Another drawback is the use of complex and expensive electrolytes that hinder commercialization. To the best of the authors' knowledge, the first observations of ammonia synthesis at milder conditions were reported with homogeneous catalysts with tungsten[21] zirconium[22] and tantalum[23] as the central atoms. However, for the sake of distributed use of ammonia, simpler methods are needed, ideally using heterogeneous catalysis, which allows for facile isolation of product.

In the past several years, numerous investigations have been conducted using various electrolytes and electrode materials to alleviate the thermodynamic requirements and optimize the ammonia formation rate using heterogeneous catalysis.[2,24–29] Much research has been focused on electrolytic cells based on solid-state electrolytes and polymer electrolyte membranes (PEM). In such setups it is easier to separate the ammonia product from hydrogen feed gas and therefore to achieve considerable formation yield of ammonia. The highest rate of ammonia formation reported with Nafion membrane is 1.13×10^{-8} mol s^{-1} cm^{-2} with a faradaic efficiency (FE) of ~90% obtained at 80 °C where $SmFe_{0.7}Cu_{0.3-x}Ni_xO_3$ (x = 0–0.3) was used as the cathode.[30] NH_4^+ was detected in dilute H_2SO_4 with pH of 3.85. This was obtained using wet H_2 as a feed gas. This is perhaps the reason for the improved formation rate of ammonia because water vapor may supply some protons[31] and thus improve conductance and consequently enhance ammonia formation. Replacing the H_2 feed gas with water, electro-catalytic ammonia synthesis from N_2 and H_2O at room temperature was obtained at Ru cathode in a solid polymer electrolyte cell and 2 M KOH.[32] Due to the competing hydrogen evolution reaction (HER) at the cathode, a low rate of ammonia formation (3.4×10^{-12} mol s^{-1} cm^{-2}) with a low FE of 0.28% was achieved at a relatively high potential (~−1.3 V *vs.* SHE). In a very recent study, a molten hydroxide (NaOH–KOH) electrolyte was reported to split water at a Ni cathode.[33] Suspension of iron-oxide nano-particles in the electrolyte was used as a catalyst for the ammonia synthesis from air and steam between two Ni electrodes. At 2 mA cm^{-2}, the rate of ammonia generated by this system was 2.4×10^{-9} mol s^{-1} cm^{-2}, which reached 35% FE under 1.23 (±0.02) V and ambient pressure. Despite an appreciable rate and FE, relatively high temperatures of around 200 °C, were used. The highest rate of ammonia synthesis that has been obtained thus far using air and water as feed gases is 1.14×10^{-9} mol s^{-1} cm^{-2}, achieved using a mixed NH_4^+/H^+ Nafion membrane.[34] However, again a low FE (1%) is observed and a high overpotential (−1.6 V) is necessary.

The above examples show that while solid state electrolytes or PEMs offer promise as an electrochemical route to ammonia formation, with production rates nearing that of commercial viability ($4.3–8.7 \times 10^{-7}$ mol s^{-1} cm^{-2}),[1] they are still in the early stage of development and little is known of their stability. Furthermore, the manufacturing cost of the complicated electrolytes means that a simpler approach is desirable for realistic commercialization.

With advancements in the field of computations and modelling, theoretical investigations have provided deeper insight into catalysis,[35–48] the importance of various active sites,[49] and different mechanism of reactions.[50,51] The use of computations can thus facilitate rational catalyst design, by enabling whole classes of material to be assessed for their suitability as catalysts. The simplest catalyst for electrochemical ammonia formation is a pure transition metal catalyst. In a recent theoretical study, electrochemical formation of ammonia on a range of flat and stepped transition metal surfaces was studied.[52] It was found that many metals require a relatively small overpotential of −0.5 to −1 V *vs.* SHE to form ammonia in 1 M aqueous electrolyte (pH = 0) at room temperature. However, the formation of $H_{2(g)}$ can be very fast and severely hinder the production of ammonia unless the surface is covered with N-adatoms, rather than H-adatoms. It was found that the majority of metals are likely covered with H-adatoms at the onset potential of ammonia formation. This is less likely for the early transition metals, however these are known to readily form oxides. Another study used a similar approach on transition metal nano-clusters[45] where molybdenum nano-clusters[53] are reported to enhance the ammonia activity compared to HER. However, the presence of water in the electrochemical environment will reduce the efficiency of catalyst by blocking its active site due to preferential adsorption of oxygen rather than nitrogen.[54]

In the present study, transition metal nitride catalysts are investigated for electrochemical formation of ammonia at ambient conditions. These materials offer the potential advantage of being able to form ammonia by way of a Mars–van Krevelen mechanism,[55] in which a surface N atom is reduced to NH_3 and the catalyst later regenerated with gaseous N_2, rather than adsorbing N_2 to the catalyst surface in the first step. Density functional theory (DFT) calculations are used to study the thermodynamics of the cathode reaction. Free energy diagrams are constructed for the electrochemical protonation of surface nitrogen or metal atoms to obtain onset potentials required for ammonia synthesis on rocksalt and zincblende transition metal mononitride structures. The effect of an external potential is included by using the computational standard hydrogen electrode[35] and the lowest onset potential required to reduce N_2 to ammonia is estimated for each nitride. Poisoning of the catalyst, surface and defect stability and decomposition of the catalyst under an applied bias are also considered.

Methodology

DFT calculations

Mononitrides of all of the naturally occurring d-block metals are considered in the present study, in both the rocksalt (RS) and zincblende (ZB) structures. Two low index facets are considered for each crystal structure, the (100) and (111) facets of the RS structure and the (100) and (110) facets of the ZB structure. Each nitride surface is modelled by 40 atoms in five layers, with each layer consisting of four metal atoms and four nitrogen atoms. The bottom two layers are fixed whereas the top layers as well as the adsorbed species are allowed to relax. Boundary conditions are periodic in the x and y directions and surfaces are separated by 12 Å of vacuum in the z direction. The structural optimization is considered converged when the forces in any direction on all moveable atoms are less than 0.01 eV $Å^{-1}$. A previous study

showed several of the 3d mononitrides to be either antiferromagnetic (RS VN, CrN, MnN, FeN and ZB MnN) or ferromagnetic (ZB VN, CrN) at their equilibrium lattice constants and as such are treated as spin-polarized.[56] The RPBE lattice constants are also taken from that study.

The calculations are conducted with density functional theory (DFT) using the RPBE exchange correlation functional.[57] A plane wave basis set with an energy cutoff of 350 eV is used to represent the valence electrons with a PAW[58] representation of the core electrons as implemented in the VASP code.[59–62] Activation energies are calculated as the highest point along the minimum energy path (MEP) calculated using the climbing image nudged elastic band method (CI-NEB).[63,64] The self-consistent electron density is determined by iterative diagonalization of the Kohn–Sham Hamiltonian, with the occupation of the Kohn–Sham states being smeared according to a Fermi–Dirac distribution with a smearing parameter of k_BT = 0.1 eV. A 4 × 4 × 1 Monkhorst–Pack k-point sampling is used for all the surfaces and maximum symmetry is applied to reduce the number of k-points in the calculations.

Electrochemical reactions and modelling

The cathode reaction of the electrochemical process is:

$$N_2 + 6(H^+ + e^-) \rightleftharpoons 2NH_3 \quad (3)$$

The source of protons is taken to be the anode reaction:[35]

$$H_2 \rightleftharpoons 2(H^+ + e^-) \quad (4)$$

In this study a heterogeneous Mars–van Krevelen-type mechanism is considered where a surface N atom is reduced to NH_3 and the created nitrogen vacancy (N-vacancy) is then replenished with gaseous N_2. Hydrogenation of the surface is carried out by adding H atoms one-by-one to the surface to represent a proton from the solution and an electron from the electrode surface. The reaction mechanism is shown in eqn (5)–(13) and with ball-and-stick representation in Fig. 1.

$$* + 6(H^+ + e^-) + N_2 \rightleftharpoons *H + 5(H^+ + e^-) + N_2 \quad (5)$$

$$*H + 5(H^+ + e^-) + N_2 \rightleftharpoons *2H + 4(H^+ + e^-) + N_2 \quad (6)$$

$$*2H + 4(H^+ + e^-) + N_2 \rightleftharpoons *3H + 3(H^+ + e^-) + N_2 \quad (7)$$

$$*3H + 3(H^+ + e^-) + N_2 \rightleftharpoons *^{-N} + NH_3 + 3(H^+ + e^-) + N_2 \quad (8)$$

$$*^{-N} + 3(H^+ + e^-) + N_2 \rightleftharpoons *N + 3(H^+ + e^-) \quad (9)$$

$$*N + 3(H^+ + e^-) \rightleftharpoons *NH + 2(H^+ + e^-) \quad (10)$$

$$*NH + 2(H^+ + e^-) \rightleftharpoons *NH_2 + (H^+ + e^-) \quad (11)$$

$$*NH_2 + (H^+ + e^-) \rightleftharpoons *NH_3 \quad (12)$$

$$*NH_3 \rightleftharpoons * + NH_3 \quad (13)$$

An asterisk represents a site on the surface. A N-vacancy in the surface layer is denoted as $*^{-N}$. DFT calculations are used to calculate the minimum energy configuration of each species on the surface and to calculate adsorption energies of all intermediates according to reactions (5)–(13). Various surface sites are considered and the optimal binding site is identified.

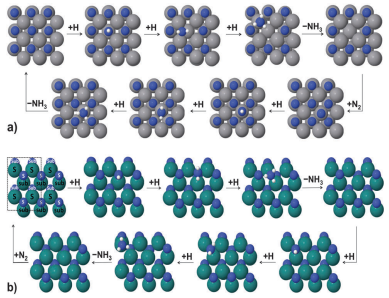

Fig. 1 Mars–van Krevelen mechanism for ammonia formation on the (100) facet of the RS structure (a) and the (110) facet of the ZB structure (b) of metal nitrides. For better illustration, more than one supercell is depicted but for the second ammonia molecule formation, the extra adsorbates that should be visible due to periodic boundary conditions are not shown. S stands for surface atoms and sub denotes the sub-layer.

A slightly different reaction mechanism is considered for the ZB surfaces and for RS ScN, TiN, CrN, YN and MnN, due to the existence of a prohibitively large thermochemical barrier to replenish the N-vacancy with gaseous N_2. In this mechanism, two NH_3 molecules are formed from two surface N atoms and a dimer N-vacancy is created before regenerating the catalyst with gaseous N_2. The mechanism is given in eqn (14)–(22). In this mechanism, the barrier to fill the N-vacancy is greatly reduced and, in most cases, N_2 adsorption is no longer the rate-determining step (RDS).

$$* + 6(H^+ + e^-) + N_2 \rightleftharpoons *H + 5(H^+ + e^-) + N_2 \quad (14)$$

$$*H + 5(H^+ + e^-) + N_2 \rightleftharpoons *2H + 4(H^+ + e^-) + N_2 \quad (15)$$

$$*2H + 4(H^+ + e^-) + N_2 \rightleftharpoons *3H + 3(H^+ + e^-) + N_2 \quad (16)$$

$$*3H + 3(H^+ + e^-) + N_2 \rightleftharpoons *^{-N} + NH_3 + 3(H^+ + e^-) + N_2 \quad (17)$$

$$*^{-N} + 3(H^+ + e^-) + N_2 \rightleftharpoons *^{-N}H + 2(H^+ + e^-) + N_2 \quad (18)$$

$$*^{-N}H + 2(H^+ + e^-) + N_2 \rightleftharpoons *^{-N}2H + (H^+ + e^-) + N_2 \quad (19)$$

$$*^{-N}2H + (H^+ + e^-) + N_2 \rightleftharpoons *^{-N}3H + N_2 \quad (20)$$

$$*^{-N}3H + N_2 \rightleftharpoons *^{-2N} + NH_3 + N_2 \quad (21)$$

$$*^{-2N} + N_2 \rightleftharpoons * \quad (22)$$

As a first approximation when screening for catalytic activity, the surface site in eqn (5)–(13) or (14)–(22) is restricted to a single nitrogen site where each hydrogen $(H^+ + e^-)$ is added to the same N atom. One NH_3 is formed after the addition of $3(H^+ + e^-)$ and the second NH_3 is formed after the addition of $6(H^+ + e^-)$ in total. This is hereafter referred to as a "constrained" mechanism. For a more detailed investigation of the catalytic activity this restriction is lifted and all possible adsorption sites for each proton are considered. This is accordingly referred

to as an ''unconstrained'' mechanism. In this way, the possibility of a catalyst requiring more than six protons and electrons to form $2NH_3$ is explored and also the possibility of forming H_2, rather than NH_3.

It is assumed that activation barriers between stable minima can be neglected during the electrochemical reactions. The free energy of each elementary step is estimated at pH = 0 according to:

$$\Delta G = \Delta E + \Delta E_{ZPE} - T\Delta S \quad (23)$$

where ΔE is the reaction energy calculated using DFT. The zero-point energy correction (ΔE_{ZPE}) and entropy difference (ΔS) are calculated within a harmonic approximation and the values of these are given in the ESI.† The effect of an applied bias, U, is included for all electrochemical reaction steps by shifting the free energy for reactions involving n electrons by $-neU$:[35]

$$\Delta G = \Delta E + \Delta E_{ZPE} - T\Delta S - neU \quad (24)$$

Explicit inclusion of a water layer[65] has not been considered in the present work due to the large computational effort required. It has been shown that the presence of water may help stabilize some species more than others *via* hydrogen bonding.[35,66] For example, *NH is expected to be stabilized slightly by hydrogen bonding, while the effect of the water layer on *N will be negligible. The effect of hydrogen-bond stabilization of the adsorbates has been estimated in a previous publication.[52] A relatively small correction for the N–H bonds was found of around 0.08 eV per H-bond. From this we conclude that the onset potentials calculated in the present study are likely to change by a similar magnitude, that is, less than 0.1 eV. Thus the correction is not done in the present study.

Results and discussion

The computational screening process begins with 104 potential transition metal nitride catalysts. To assess the potential of each candidate for making NH_3 electrochemically at ambient conditions five considerations are investigated: (i) stability of the surface, (ii) stability of a surface N-vacancy, (iii) catalytic activity, (iv) poisoning of the catalyst surface and (v) an estimate of the electric potential needed to decompose the metal nitrides into its metal form and ammonia. These will be discussed in turn herein.

Stability of facets

As a first approximation in the search for a suitable catalyst, only the most stable crystal facet of the four facets considered in this study [RS(100), RS(111), ZB(100) and ZB(110)] is explicitly investigated for ammonia formation. Each slab is relaxed and the total energies compared to determine the most stable facet of a given metal nitride (see Table S1 in ESI†). Most of the nitrides of the early transition metals (d^{1-5}) as well as the d^9 metals are found to be most stable in the RS crystal structure and, for all of these, the (100) facet is more stable than the (111) facet. These are ScN, TiN, VN, CrN, MnN, YN, ZrN, NbN, MoN, HfN, TaN, CuN, and AgN. For most of the nitrides of the d^6, d^7 and d^8 transition metals, the ZB(110) facet is the most stable. These are FeN, CoN, NiN, RuN, RhN, PdN, OsN, and IrN. These findings agree with the generally accepted trend of early transition metal nitrides being most stable in RS structure while the later transition metal nitrides are usually most stable in ZB.[67–69] Regarding facet stability, experimental studies show that the growth of films of ZrN, TiN, NbN and CrN results in the texture coefficient for the (100) planes of the synthesized polycrystalline to be one of the major preferential directions.[70–74] For all considered surfaces of WN, ReN, AuN and PtN, significant distortion of the surface atoms is observed during relaxation and thus these nitrides are considered unstable and eliminated from further study. In total, this first consideration reduces the number of potential catalysts from 104 to 21. Among the candidates eliminated at this stage, it is of course possible that some structures/facets are also relatively stable and catalytically active. For simplicity the present work is restricted to only on the most stable facets and calculations for other facets are ongoing.

Stability of the surface nitrogen vacancy

In the Mars–van Krevelen mechanism considered in the present work, a surface nitrogen atom is reduced to form NH_3 after which the resulting vacancy is replenished by a gaseous N_2 molecule. For this replenishment to occur, the N-vacancy needs to be stable at the surface. If this is not the case, the N-vacancy may migrate to the bulk of the catalyst, that is, the reacted nitrogen on the surface is replaced with more nitrogen from the catalyst itself, rather than with gaseous N_2. This process can, in principle, continue until all the nitrogen atoms of the metal nitride have reacted and formed NH_3, leaving only the pure metal.

The stability of the N-vacancy at the surface of the catalyst is estimated by comparing the difference in energy of a nitride slab with a single N-vacancy in the surface layer ($E_{vac,1}$) and to that of a single N-vacancy in the first subsurface layer ($E_{vac,2}$). The minimum energy configuration of each of these slabs is found and the energy difference ($\Delta E_{vac} = E_{vac,2} - E_{vac,1}$) used as an estimation of the thermodynamic stability of the vacancy at the surface of the nitride. Activation barriers for vacancy migration ($E_{a,vac}$) are also calculated and both ΔE_{vac} and $E_{a,vac}$ are presented in Fig. 2. It is found that, for most of the nitrides, it is thermodynamically favourable for the vacancy to migrate to the bulk, with ΔE_{vac} less than or close to zero. However, it is clear that many of the nitrides exhibit a high activation barrier for vacancy migration and are thus likely to demonstrate a stable surface vacancy. All nitrides with an activation barrier for a vacancy migration of >1 eV are retained for further screening, since a barrier of such magnitude is unlikely to be overcome at room temperature.

Catalytic activity

The catalytic activity of the nitrides towards electrochemical ammonia formation is initially calculated according to the constrained mechanism given in eqn (5)–(13) for most of the RS(100) nitride slabs and eqn (14)–(22) for all the ZB(110) nitrides and some of the RS(100) nitride slabs. The free energy of all intermediates is calculated according to eqn (23), with reference to

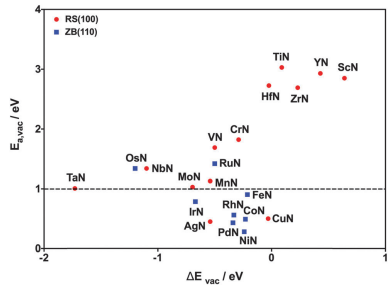

Fig. 2 Energy difference (ΔE_{vac}) of a vacancy in the surface layer and in the first subsurface layer of a nitride and the associated activation barrier of vacancy migration ($E_{a,vac}$). The dashed line at $E_{a,vac}$ = 1 eV represents the cutoff above which metal nitrides are considered sufficiently stable for further study.

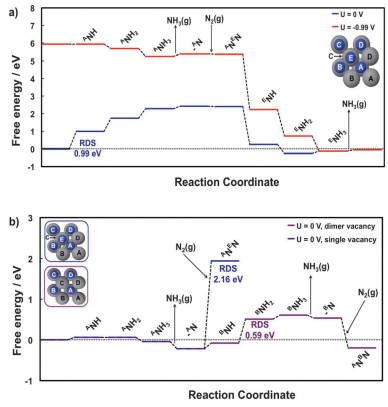

Fig. 3 Free energy diagram for NH_3 formation *via* a constrained Mars–van Krevelen mechanism on the (100) facet of RS ZrN (a) and the (100) facet of RS MnN (b). For ZrN, the rate-determining step is the first protonation step of surface N with ΔG = 0.99 eV. The blue line indicates the free energy of all the stable intermediates calculated at zero potential. The red line represents the free energy of all the stable intermediates at the onset potential. The purple line indicates the free energy of all the intermediates when a dimer vacancy is considered at zero potential.

N_2 and H_2 in the gas phase. The free energy diagram for ZrN (RS) is presented in Fig. 3a where the effect of applied bias is included. Fig. 3b shows the free energy diagram for MnN (RS), where the pathways towards NH_3 formation *via* both a single and a dimer vacancy are illustrated and compared.

The rate-determining step (RDS) and our measure of the catalytic activity towards NH_3 formation on each nitride is identified as the elementary reaction step with the largest increase in free energy. When this elementary step can be eliminated by applying a bias, it is referred to as the onset potential, which is the bias that needs to be applied in order to shift the free energy landscape in such a way that all reactions steps become downhill in free energy. From Fig. 3a it can be seen that for ZrN the RDS is the first protonation step, with ΔG_{RDS} = 0.99 eV. Thus, by applying an external bias of −0.99 V, this increase in free energy can be eliminated and all electrochemical steps will then be downhill in free energy. For those steps that do not involve electron transfer, however, there is no change in the free energy when applying an external bias. This is seen in Fig. 3a for ZrN where the release of NH_3 is slightly uphill in free energy. In reality, the adsorbed NH_3 is likely to get further protonated to NH_4^+ and released into the solution, thereby avoiding this small increase in free energy. For the other elementary step that does not involve electron transfer, namely the addition of $N_{2(g)}$, however, there is no such effect from the electrochemical environment. For all of the ZB and some of the RS nitrides, addition of $N_{2(g)}$ to fill the N-vacancy is endothermic, which corresponds to an increase in free energy that cannot be surpassed by an external applied bias. For this reason, a mechanism of forming a dimer N-vacancy instead is considered for these nitrides. The result is that the free energy landscape changes significantly in such a way that the addition of $N_{2(g)}$ becomes downhill in free energy in all cases and the RDS becomes an electrochemical step instead, which can be eliminated with the bias (see Fig. 3b).

The free energy change of the RDS of each nitride is shown in Fig. 4. Most of the nitrides exhibit relatively high activity towards ammonia formation, with the exception of ScN, YN and HfN, which have $\Delta G_{RDS} > 1.5$ eV. All of the nitrides with $\Delta G_{RDS} \leq 1.5$ eV are considered potentially active and are retained for a more detailed mechanistic study.

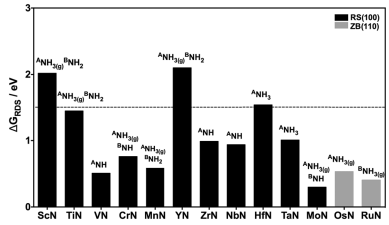

Fig. 4 Free energy change (ΔG_{RDS}, in eV) of the rate-determining step of NH_3 formation on transition metal nitride catalysts. A constrained mechanism is considered, where H addition is restricted to a single surface site and 6($H^+ + e^-$) are used to form 2NH_3. The horizontal dashed line indicates the cut-off value in the screening for an appropriate catalyst; all nitrides with $\Delta G_{RDS} \leq 1.5$ eV have the possibility of being catalytically active towards ammonia formation and are considered further in the study. The labels on each bar indicate the species formed in the rate-determining step, the notation of which is explained in Fig. 3.

An interesting point to note is that there is no clear trend in the nature of the RDS; for some nitrides the addition of the first proton is rate-limiting, while for others the addition of the third, fourth, or fifth proton is rate-limiting while for some it is the release of the ammonia molecule which is the RDS. This is in contrast to the case of electrochemical ammonia formation on pure metals, for which primarily only two different RDS exist across the whole series of pure transition metal surfaces. That results in a volcano-shaped activity curve when plotted against a common descriptor.[52] Several descriptors were investigated for possible correlation with the calculated activity. As shown in Fig. S2 in the ESI,† the binding energies of species do not scale well with a single descriptor such as the binding energy of *N. However, when *H is used as a descriptor, much better correlation is observed, with the exception of a few outliers. Similar conclusions have recently been reported where departures from the scaling laws are observed for adsorption energies of C, H and O on metal carbides.[75] With *H as the descriptor for the catalytic activity of N_2 reduction on the metal nitrides, a volcano-type plot can be obtained (see Fig. S3 in the ESI†). However, more scatter is observed for these nitrides here than for the pure metals.[52] Hence, all nitrides are calculated explicitly in this study whereas a high-throughput screening may be carried out in the near future.

For those nitrides that exhibit reasonable catalytic activity when H adsorption is constrained to a single N atom, an unconstrained mechanism is considered. In this approach, at each H addition step every possible adsorption site is investigated, including other N atoms, metal atoms and bridging sites. DFT is used to evaluate the most stable adsorption site at each step. Free energy diagrams for NH_3 formation *via* this unconstrained mechanism are shown in Fig. 5 for the (100) facet of RS structure of ZrN (a) as well as the (110) facet of ZB structure of OsN (b) and the remainder are given in the ESI.†

For VN, CrN and RuN, the mechanism is found to be identical to the constrained mechanism, where each added H adds to the same N atom, forming one NH_3, then the second, with only $6(H^+ + e^-)$ required to form $2NH_3$. For ZrN, (Fig. 5a), allowing the H to bind to any surface site results in firstly a surface Zr atom being protonated, and then an N atom. The protonation of N is the RDS in NH_3 formation, similar to the constrained mechanism. However, the presence of an H atom on the adjacent Zr atom lowers the free energy of *NH formation by 0.23 eV. A similar case is seen for NbN, where two neighbouring Nb atoms are protonated before the RDS, which is protonation of the first surface N. The free energy of the RDS is lowered by 0.29 eV due to the H coverage on the Nb. For OsN and MnN the unconstrained mechanism leads to a different RDS and a different reaction path than when a constrained mechanism is considered. For MnN, $3(*NH_2)$ and $1(*NH)$ form before the first ammonia is released and $9(H^+ + e^-)$ are needed to form $2NH_3$. In this case, no metal atoms are protonated. In contrast, for OsN, (Fig. 5b), H atoms cover all the metal atoms on the surface as well as surface N atoms and $13(H^+ + e^-)$ are needed to form $2NH_3$. For OsN addition of $N_{2(g)}$ to fill the N-vacancy is endothermic, which corresponds to an increase in free energy that cannot be surpassed by an external applied bias as no proton–electron transfer is involved at this step.

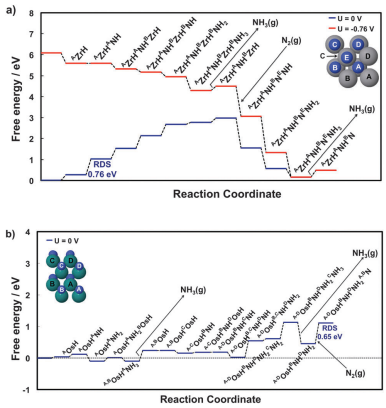

Fig. 5 Free energy diagram for NH_3 formation *via* an unconstrained Mars–van Krevelen mechanism on the (100) facet of RS ZrN (a) and the (110) facet of ZB OsN (b). For ZrN the rate-determining step is the second protonation step with ΔG = 0.76 eV. Upon replenishment of the N-vacancy, one proton that was already adsorbed on Zr metal (^{B}ZrH) migrates to the N-adatom to make NH (^{E}NH). The blue line indicates the free energy of all the stable intermediates calculated at zero potential. The red line represents the free energy of all the stable intermediates at the onset potential. For OsN the RDS is to fill the N-vacancy with ΔG = 0.65 eV. As the RDS involves no proton-electron transfer, no bias is applied and the free energy landscape of OsN is depicted only at zero potential.

An interesting trend that is observed from comparison of the constrained and unconstrained mechanisms is that for RS nitrides, a relatively low coverage of H is required to make $2NH_3$. Furthermore, additional H atoms generally add to neighbouring metal atoms, rather than other N atoms, which lowers ΔG_{RDS} by ~0.05–0.3 eV, relative to the constrained mechanism. In contrast, for ZB nitrides, a higher coverage of H is needed to form $2NH_3$. The result of this is that ΔG_{RDS} is increased by ~0.12 eV, relative to the constrained mechanism. For such cases that require more than the minimum $6(H^+ + e^-)$ to form $2NH_3$, a lower faradaic efficiency is likely to be observed. For TiN and TaN an unconstrained mechanism yields a full H coverage on the surface with no NH_3 formation. The catalytic activity of these nitrides are thus instead being considered as potential hydrogen evolution catalysts, the results of which are beyond the scope of the present study.

After exclusion of those nitrides that either do not form NH_3 (TiN and TaN) or have an onset potential of > 1.5 V (ScN, YN and HfN), eight metal nitride catalysts are considered potentially active towards NH_3 formation and presented in Fig. 6. The six RS nitrides as well as RuN ZB should make ammonia electrochemically under ambient conditions whereas ZB OsN likely requires high pressure to fill the N-vacancy in order to complete the catalytic cycle of ammonia formation.

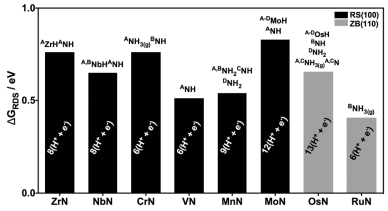

Fig. 6 Free energy change (ΔG_{RDS}, in eV) of the rate-determining step of NH_3 formation on transition metal nitride catalysts. An unconstrained mechanism is considered, where at each H addition step every possible adsorption site is investigated including other N atoms, metal atoms and bridging sites and at least 6($H^+ + e^-$) are needed to form $2NH_3$. The labels above each bar indicate the species formed in the rate-determining step, the notation of which is explained in Fig. 5. The labels in each bar indicate the number of protons and electrons required to make $2NH_3$.

Poisoning of the surface vacancy

As previously discussed, in the Mars–van Krevelen mechanism considered in this work a surface N is reacted, leaving a surface vacancy at the surface and for the catalytic cycle to complete, this vacancy must be filled with $N_{2(g)}$. However, there exists the possibility of the vacancy rather being filled with H atoms or O atoms from the aqueous electrolyte, both of which would block this surface site for completion of the catalytic cycle. In the present section the competition between N, O and H for filling the surface vacancy is investigated by considering the free energy of filling the vacancy with O or H relative to N ($\Delta G_{(*N-*X)}$, where X = O or H). These free energies are referenced to N_2, H_2O and H_2 in the gas phase and are calculated at the onset potential for each nitride. A negative value of $\Delta G_{(*N-*X)}$ indicates that it is thermodynamically favourable to fill the vacancy with N, rather than O or H. The values of $\Delta G_{(*N-*X)}$ are shown in Fig. 7 for all the catalytically active nitrides.

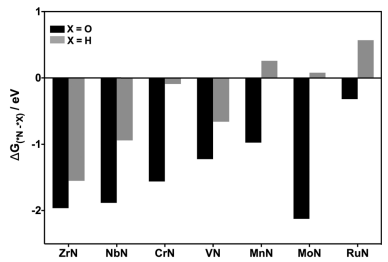

Fig. 7 Free energy of adsorption of O or H (relative to N) to the surface vacancy of catalytically active nitrides ($\Delta G_{(*N-*X)}$, in eV). Free energies are calculated relative to $N_{2(g)}$, $H_{2(g)}$ and $H_2O_{(g)}$. All free energies are evaluated at the calculated onset potential for each nitrides: ZrN, −0.76 V; NbN, −0.65 V; CrN, −0.76 V; VN, −0.51 V; MnN, −0.54 V; MoN, −0.83 V; and RuN, −0.41 V.

It can be seen that N atoms bind more strongly to the surface vacancy than O atoms by over 1 eV for most nitrides. Thus it is unlikely that the surface vacancy will be poisoned by O atoms. For poisoning by H, however, it can be seen that the surface vacancy in MnN, MoN and RuN is likely to be filled by H, rather than N. For the remaining nitrides, ZrN, NbN, CrN and VN, the vacancy is likely refilled by N and thus the catalytic cycle may continue to form the second NH_3. These results are as expected as when the bias is tuned towards more negative values, the electropositive O species bind weaker on the surface compared to H_2O in the gas phase, as they would rather form bonds with the surface when the bias is more positive:

$$H_2O + * \rightarrow *O + 2H^+ + 2e^- \quad (25)$$

Conversely, the H adsorption free energy, becomes more negative when the bias is lowered:

$$H^+ + e^- \rightarrow H* \quad (26)$$

Stability of the nitrides with respect to decomposition at the onset potential

The final criterion considered in the present study for an appropriate metal nitride catalyst for electrochemical NH_3 formation is the stability of the catalyst with respect to decomposition when an external bias is applied. The decomposition of a metal mononitride (MN) into the corresponding pure metal (M) and NH_3 can be expressed as:

$$MN_{(s)} + 3(H^+ + e^-) \rightarrow M_{(s)} + NH_{3(g)} \quad (27)$$

The overall free energy change of the reaction can be expressed in terms of free energies of formation as:

$$\Delta G_r = \Delta G_f(NH_{3(g)}) - \Delta G_f(MN_{(s)}) - 3\Delta G(H^+/e^-) \quad (28)$$

The term $3\Delta G(H^+/e^-)$ gives the contribution to the free energy by the protons and electrons. To find the applied potential at which the nitride is reduced to the metal, ΔG_r is required to be zero, or

$$3\Delta G(H^+/e^-) = \Delta G_f(NH_{3(g)}) - \Delta G_f(MN_{(s)}) \quad (29)$$

Therefore, the required potential can be expressed as:

$$U = -\Delta G(H^+/e^-)/3 \quad (30)$$

The free energy of formation of each nitride is calculated using DFT and the free energy of formation of $NH_{3(g)}$ is taken to be −0.17 eV at standard conditions.[76] The decomposition potential of all the catalytically active nitrides are given in Fig. 8. For a given nitride to be suitable for electrochemical formation of NH_3, the decomposition potential must be more negative than the onset potential for the ammonia formation.

According to Fig. 8, ZrN is the only candidate that should not decompose at the electric potential needed to form ammonia. However, it should be emphasized that this is a purely thermodynamic analysis and no kinetic effects are taken into account. As was seen earlier in Section 3.2 (Fig. 2), activation barriers for the first step of decomposition of the metal nitride into the metal and ammonia usually involves high activation barriers

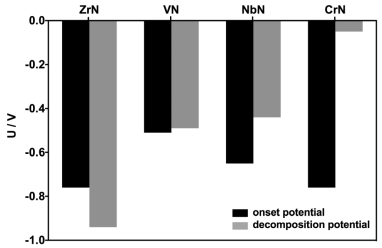

Fig. 8 Decomposition potential for stable and active metal nitrides according to eqn (27). Also included are the calculated onset potentials for electrocatalytic NH_3 formation. All values are calculated at 300 K (see Table S4 in the ESI†).

(between 1 and 3 eV), which would mean that although thermodynamically unstable, decomposition of most nitrides would be extremely slow at room temperature. For VN, the onset potential is similar as the potential required to decompose the nitride. However, the activation barrier for the N-vacancy to migrate into the bulk is around 1.7 eV and so the nitride might be maintained by replenishing the N-vacancies with $N_{2(g)}$. Given the standard error in DFT and in our models applied here, and the relatively high barrier to N-vacancy migration (1.34 eV), NbN may perhaps be used as a catalyst too. For CrN, the decomposition potential is much less negative than the onset potential and this will likely decompose before appreciable amounts of NH_3 will be formed (see Table S5 in the ESI† for summary).

The culmination of the five criteria investigated in this screening for a potential catalyst for electrochemical ammonia formation at ambient conditions yields two very promising candidates, namely ZrN and VN (both RS(100)). ZrN is particularly promising as it has been shown experimentally that RS is the most stable ground-state configuration,[77] and the (100) is always one of the preferential texture coefficients.[70,71,74,78] In contrast to pure transition metals,[52] the surface of these nitride catalysts are not likely to get covered by hydrogen at the onset potentials required for ammonia formation. As a result, faradaic losses due to the competitive HER, which is the main limiting issue with pure transition metals,[52] should not occur for these nitrides. Hence, high yield of ammonia formation is predicted in experiments. Furthermore, the catalysts require only a low applied bias for ammonia formation and are likely stable towards poisoning and decomposition.

Summary and conclusions

In this paper, an efficient scheme is proposed that utilizes first principles calculations to screen for nitrogen reduction electrocatalysts that efficiently form ammonia at ambient conditions and in aqueous electrolyte. In this work the scheme is applied to transition metal nitrides. However, it could also be utilized for any reaction where the possibility of Mars–van Krevelen mechanism is explored. The most promising nitride catalysts are the (100) facets of rocksalt VN and ZrN, which should form ammonia at −0.51 V and −0.76 V with respect to SHE, respectively. The suggested catalysts should not decompose or be poisoned by oxygen or hydrogen from the aqueous electrolyte. NbN could also be a good catalyst worthy of further investigations if kinetic barriers are sufficiently high as to avoid decomposition with an applied bias. In contrast to previous studies where relatively high onset potentials are required for ammonia formation and hydrogen evolution is a competing reaction,[52,53] the most promising RS candidates presented in this paper (VN and ZrN) only need a low applied bias to form ammonia and the competing HER is suppressed. Therefore, a significant amount of ammonia compared with hydrogen gas can be expected. Furthermore, at the onset potential, the N-vacancy is stable towards both protonation and oxidation from water and it should get easily repaired with atmospheric nitrogen injected to the system at ambient conditions. Other crystal facets and other mechanisms of ammonia formation on these nitride catalysts are currently being studied to further investigate the catalytic capability of this class of catalyst. Experimentalists are strongly encouraged to test these promising candidates for the possibility of high yield electrochemical ammonia production at ambient conditions.

Acknowledgements

The authors would like to thank Prof. Tejs Vegge, Prof. Ib Chorkendorff and Dr Jakob G. Howalt at the Technical University of Denmark (DTU), Dr Felix Studt at Stanford/SLAC and Prof. Hannes Jónsson of the University of Iceland for helpful discussions. Financial support is acknowledged from the Icelandic Research Fund, Nordic Energy Research by way of the Nordic Initiative for Solar Fuel Development, the Icelandic Student Innovation Fund, and the Research Fund of the University of Iceland. The calculations were in part carried out on the Nordic high performance computer (Gardar).

References

1 S. Giddey, S. P. S. Badwal and A. Kulkarni, *Int. J. Hydrogen Energy*, 2013, **38**, 14576–14594.
2 I. A. Amar, R. Lan, C. T. G. Petit and S. Tao, *J. Solid State Electrochem.*, 2011, **15**, 1845–1860.
3 A. Klerke, C. H. Christensen, J. K. Nørskov and T. Vegge, *J. Mater. Chem.*, 2008, **18**, 2304–2310.
4 V. Smil, *Sci. Am.*, 1997, **277**, 76–81.
5 J. R. Jennings, *Catalytic ammonia synthesis: fundamentals and practice*, Plenum, New York, 1991.
6 J. M. Berg, J. L. Tymoczko and L. Stryer, *Biochemistry*, W. H. Freeman, New York, 2002.
7 B. K. Burgess and D. J. Lowe, *Chem. Rev.*, 1996, **96**, 2983–3012.
8 I. Garagounis, V. Kyriakou, A. Skodra, E. Vasileiou and M. Stoukides, *Front. Energy Res.*, 2014, **2**, 1–10.
9 T. D. Schrauzer and N. Guth, *J. Am. Chem. Soc.*, 1977, **99**, 7189–7193.

10 J. Y. Becker, *J. Electroanal. Chem. Interfacial Electrochem.*, 1988, **250**, 385–397.
11 J. Y. Becker and S. A. Tsarfaty, *J. Electroanal. Chem. Interfacial Electrochem.*, 1990, **280**, 119–127.
12 C. Pickett and J. Talarmin, *Nature*, 1985, **317**, 652–653.
13 A. Sclafani, V. Augugliaro and M. Schiavello, *J. Electrochem. Soc.*, 1983, **130**, 734–736.
14 D. V. Yandulov and R. R. Schrock, *Science*, 2003, **301**, 76–78.
15 N. Furuya and H. Yoshiba, *J. Electroanal. Chem. Interfacial Electrochem.*, 1990, **291**, 269–272.
16 G. Marnellos and M. Stoukides, *Science*, 1998, **282**, 98–100.
17 G. Marnellos, S. Zisekas and M. Stoukides, *J. Catal.*, 2000, **193**, 80–87.
18 T. Murakami, T. Nishikiori, T. Nohira and Y. Ito, *J. Am. Chem. Soc.*, 2003, **125**, 334–335.
19 T. Murakami, T. Nohira, T. Goto, Y. H. Ogata and Y. Ito, *Electrochim. Acta*, 2005, **50**, 5423–5426.
20 T. Murakami, T. Nohira, Y. Araki, T. Goto, R. Hagiwara and Y. H. Ogata, *Electrochem. Solid-State Lett.*, 2007, **10**, E4–E6.
21 J. Catt, A. J. Pearman and R. L. Richards, *Nature*, 1975, **253**, 39–40.
22 J. Pool, E. Lobkovsky and P. Chirik, *Nature*, 2004, **427**, 527–530.
23 P. Avenier, M. Taoufik, A. Lesage, X. Solans-Monfort, A. Baudouin, A. de Mallmann, L. Veyre, J.-M. Basset, O. Eisenstein, L. Emsley and E. A. Quadrelli, *Science*, 2007, **317**, 1056–1060.
24 A. Denvir and O. Murphy, *US Pat.*, US7314544 B2, 2008.
25 M. Ouzounidou, A. Skodra, C. Kokkofitis and M. Stoukides, *Solid State Ionics*, 2007, **178**, 153–159.
26 T. M. Pappenfus, K. Lee, L. M. Thoma and C. R. Dukart, *ECS Trans.*, 2009, **16**, 89–93.
27 I. A. Amar, R. Lan, C. T. G. Petit, V. Arrighi and S. Tao, *Solid State Ionics*, 2011, **182**, 133–138.
28 B. Lin and K. Wei, *Catal. Commun.*, 2013, **41**, 110–114.
29 Z. Song, T. Cai, J. C. Hanson, J. A. Rodriguez and J. Hrbek, *J. Am. Chem. Soc.*, 2004, **126**, 8576–8584.
30 G. Xu, R. Liu and J. Wang, *Sci. China, Ser. B: Chem.*, 2009, **52**, 1171–1175.
31 Z. J. Li, J. D. Wang, R. Q. Liu and Y. H. Xie, *J. Rare Earths*, 2005, **23**, 62–67.
32 V. Kordali, G. Kyriacou and C. Lambrou, *Chem. Commun.*, 2000, 1673–1674.
33 S. Licht, B. Cui, B. Wang, F.-F. Li, J. Lau and S. Liu, *Science*, 2014, **345**, 637–640.
34 R. Lan, J. T. S. Irvine and S. Tao, *Sci. Rep.*, 2013, **3**, 1–7.
35 J. K. Nørskov, J. Rossmeisl, A. Logadottir, L. Lindqvist, J. R. Kitchin, T. Bligaard and H. Jónsson, *J. Phys. Chem. B*, 2004, **108**, 17886–17892.
36 J. Greeley and M. Mavrikakis, *Nat. Mater.*, 2004, **3**, 810–815.
37 K. Honkala, A. Hellman, I. N. Remediakis, A. Logadottir, A. Carlsson, S. Dahl, C. H. Christensen and J. K. Nørskov, *Science*, 2005, **307**, 555–558.
38 J. Hafner and C. Wolverton, *MRS Bull.*, 2006, **31**, 659–668.
39 F. Abild-Pedersen, J. Greeley, F. Studt, J. Rossmeisl, T. Munter, P. Moses, E. Skúlason, T. Bligaard and J. Nørskov, *Phys. Rev. Lett.*, 2007, **99**, 0161051.
40 F. Studt, F. Abild-Pedersen, T. Bligaard, R. Z. Sørensen, C. H. Christensen and J. K. Nørskov, *Science*, 2008, **320**, 1320–1322.
41 H.-J. Freund and G. Pacchioni, *Chem. Soc. Rev.*, 2008, **37**, 2224–2242.
42 J. Greeley, I. E. L. Stephens, A. S. Bondarenko, T. P. Johansson, H. A. Hansen, T. F. Jaramillo, J. Rossmeisl, I. Chorkendorff and J. K. Nørskov, *Nat. Chem.*, 2009, **1**, 552–556.
43 J. K. Nørskov, T. Bligaard, J. Rossmeisl and C. H. Christensen, *Nat. Chem.*, 2009, **1**, 37–46.
44 J. K. Nørskov, F. Abild-Pedersen, F. Studt and T. Bligaard, *Proc. Natl. Acad. Sci. U. S. A.*, 2011, **108**, 937–943.
45 J. G. Howalt, T. Bligaard, J. Rossmeisl and T. Vegge, *Phys. Chem. Chem. Phys.*, 2013, **15**, 7785–7795.
46 V. Tripkovic, M. Vanin, M. Karamad, M. E. Björketun, K. W. Jacobsen, K. S. Thygesen and J. Rossmeisl, *J. Phys. Chem. C*, 2013, **117**, 9187–9195.
47 A. Verdaguer-Casadevall, D. Deiana, M. Karamad, S. Siahrostami, P. Malacrida, T. W. Hansen, J. Rossmeisl, I. Chorkendorff and I. E. L. Stephens, *Nano Lett.*, 2014, **14**, 1603–1608.
48 A. A. Peterson, F. Abild-Pedersen, F. Studt, J. Rossmeisl and J. K. Nørskov, *Energy Environ. Sci.*, 2010, **3**, 1311–1315.
49 S. Dahl, A. Logadottir, R. Egeberg, J. Larsen, I. Chorkendorff, E. Törnqvist and J. Nørskov, *Phys. Rev. Lett.*, 1999, **83**, 1814–1817.
50 S. Gudmundsdóttir, E. Skúlason and H. Jónsson, *Phys. Rev. Lett.*, 2012, **108**, 156101.
51 S. Kattel, P. Atanassov and B. Kiefer, *Phys. Chem. Chem. Phys.*, 2013, **15**, 148–153.
52 E. Skúlason, T. Bligaard, S. Gudmundsdóttir, F. Studt, J. Rossmeisl, F. Abild-Pedersen, T. Vegge, H. Jónsson and J. K. Nørskov, *Phys. Chem. Chem. Phys.*, 2012, **14**, 1235–1245.
53 J. G. Howalt and T. Vegge, *Phys. Chem. Chem. Phys.*, 2013, **15**, 20957–20965.
54 J. Howalt and T. Vegge, *Beilstein J. Nanotechnol.*, 2014, **5**, 111–120.
55 P. Mars and D. W. Van Krevelen, *Eng. Sci.*, 1954, **3**, 41–45.
56 V. F. Hlynsson, E. Skúlason and A. L. Garden, *J. Alloys Compd.*, 2014, **603**, 172–179.
57 B. Hammer, L. Hansen and J. Nørskov, *Phys. Rev. B: Condens. Matter Mater. Phys.*, 1999, **59**, 7413–7421.
58 P. Blöchl, *Phys. Rev. B: Condens. Matter Mater. Phys.*, 1994, **50**, 17953–17979.
59 G. Kresse and J. Hafner, *Phys. Rev. B: Condens. Matter Mater. Phys.*, 1993, **47**, 558–561.
60 G. Kresse and J. Hafner, *Phys. Rev. B: Condens. Matter Mater. Phys.*, 1994, **49**, 14251–14269.
61 G. Kresse and J. Furthmüller, *Comput. Mater. Sci.*, 1996, **6**, 15–50.
62 G. Kresse and J. Furthmüller, *Phys. Rev. B: Condens. Matter Mater. Phys.*, 1996, **54**, 11169–11186.
63 G. Henkelman, B. P. Uberuaga and H. Jónsson, *J. Chem. Phys.*, 2000, **113**, 9901–9904.
64 G. Henkelman and H. Jónsson, *J. Chem. Phys.*, 2000, **113**, 9978–9985.

65 E. Skúlason, V. Tripkovic, M. E. Björketun, S. Gudmundsdóttir, G. Karlberg, J. Rossmeisl, T. Bligaard, H. Jónsson and J. K. Nørskov, *J. Phys. Chem. C*, 2010, **114**, 18182–18197.
66 V. Tripkovic, E. Skúlason, S. Siahrostami, J. K. Nørskov and J. Rossmeisl, *Electrochim. Acta*, 2010, **55**, 7975–7981.
67 B. Eck, R. Dronskowski, M. Takahashi and S. Kikkawa, *J. Mater. Chem.*, 1999, **9**, 1527–1537.
68 C. Stampfl, W. Mannstadt, R. Asahi and A. Freeman, *Phys. Rev. B: Condens. Matter Mater. Phys.*, 2001, **63**, 1551061.
69 S. K. R. Patil, N. S. Mangale, S. V. Khare and S. Marsillac, *Thin Solid Films*, 2008, **517**, 824–827.
70 H. J. Ramos and N. B. Valmoria, *Vacuum*, 2004, **73**, 549–554.
71 D. F. Arias, Y. C. Arango and A. Devia, *Appl. Surf. Sci.*, 2006, **253**, 1683–1690.
72 P. Hones, R. Sanjines and F. Levy, *Surf. Coat. Technol.*, 1997, **94**, 398–402.
73 S. Shayestehaminzadeh, T. K. Tryggvason, F. Magnus, S. Olafsson and J. T. Gudmundsson, *Thin Solid Films*, 2013, **549**, 199–203.
74 E. Gillan and R. Kaner, *Inorg. Chem.*, 1994, **768**, 5693–5700.
75 R. Michalsky, Y.-J. Zhang, A. J. Medford and A. A. Peterson, *J. Phys. Chem. C*, 2014, **118**, 13026–13034.
76 D. R. Lide, *CRC Handbook of Chemistry and Physic*, Florida, 78th edn, 1997.
77 L. A. Salguero, L. Mancera, J. A. Rodríguez and N. Takeuchi, *Phys. Status Solidi*, 2006, **243**, 1808–1812.
78 C. Ma, J. Huang and H. Chen, *Surf. Coat. Technol.*, 2000, **134**, 289–294.

II Article 2

Electroreduction of N_2 to Ammonia at Ambient Conditions on Mononitrides of Zr, Nb, Cr, and V: A DFT Guide for Experiments

Younes Abghoui, Anna L. Garden, Jakob G. Howalt, Tejs Vegge and Egill Skúlason

ACS Catalysis ***6****, 635-646 (2016).*

ACS Catalysis
FEBRUARY 2016 VOLUME 6 NUMBER 2 PUBS.ACS.ORG/ACSCATALYSIS

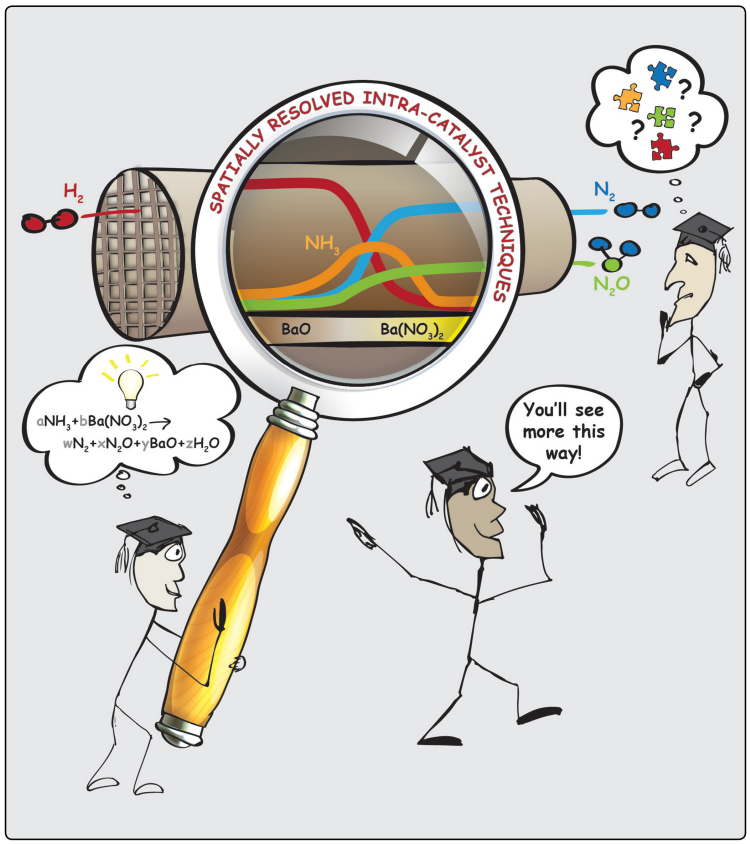

ACS Publications
Most Trusted. Most Cited. Most Read.
www.acs.org

ACS Catalysis

Research Article

pubs.acs.org/acscatalysis

Electroreduction of N_2 to Ammonia at Ambient Conditions on Mononitrides of Zr, Nb, Cr, and V: A DFT Guide for Experiments

Younes Abghoui,[†] Anna L. Garden,[‡] Jakob G. Howalt,[§] Tejs Vegge,[§] and Egill Skúlason*[,†]

[†]Science Institute and Faculty of Physical Sciences, VR-III, University of Iceland, IS-107 Reykjavik, Iceland

[‡]Department of Chemistry, University of Otago, P.O. Box 56, Dunedin 9054, New Zealand

[§]Department of Energy Conversion and Storage, Technical University of Denmark, DK-2800 Kgs. Lyngby, Denmark

Supporting Information

ABSTRACT: A rapid and facile reduction of nitrogen to achieve sustainable and energy-efficient production of ammonia is critical to its use as a hydrogen storage medium, chemical feedstock, and especially for manufacturing inorganic fertilizers. For a decentralization of catalytic ammonia production, small-scale N_2 reduction devices are required that are equipped with the most stable, selective, and active catalysts that operate at low temperature and ambient pressure. Here, we report the development of new and cost-efficient catalysts, transition metal nitrides, which enable electrochemical reduction of molecular nitrogen to ammonia in aqueous media at ambient conditions with only a low applied bias. The most promising catalysts are VN, ZrN, NbN, and CrN, which are identified among a range of transition metal nitride surfaces through a comprehensive density functional theory based analysis. All four nitrides are found to be more active toward nitrogen reduction than toward the competing hydrogen evolution reaction, in contrast to pure metal catalysts, which largely evolve hydrogen. Furthermore, their stability against poisoning and possible decomposition under operating conditions is also studied. Particular single-crystal surfaces are needed for ZrN, NbN, and CrN because polycrystalline surfaces may result in decomposition of the whole catalyst. Polycrystalline surfaces of VN may, however, be used since the rocksalt (100) facet is predicted to produce ammonia via a Mars−van Krevelen mechanism with only a −0.5 V overpotential, thereby avoiding decomposition. We suggest that this is a promising step toward the development of a method for synthesizing ammonia cheaply, to prepare high-value-added nitrogenous compounds directly from air, water, and electricity at ambient conditions. An additional benefit to the present analysis is that the method used in this work may be applicable to other aqueous phase catalytic reactions, where a Mars−van Krevelen mechanism is operative and product selectivity and activity are key catalytic criteria.

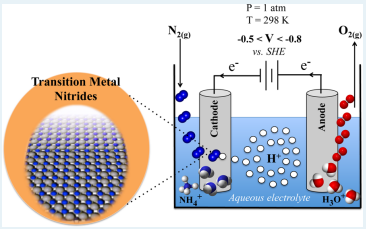

KEYWORDS: *density functional theory calculations, electrochemical synthesis of ammonia, transition metal nitride catalysts, electroreduction of nitrogen to ammonia, electrocatalysis*

INTRODUCTION

One of the most significant scientific realizations of the 20th century is the synthesis of ammonia from its gaseous elements in the Haber-Bosch process that contributes to the annual production of over 200 million tons of ammonia per year, 80% of which is used in the production of fertilizer.[1,2] The Haber-Bosch process utilizes a promoted metal catalyst and operates at high temperatures and pressures to achieve a sufficient rate and yield of ammonia. The H_2 feedstock necessary for the process is often natural gas, the production of which results in high CO_2 emissions and is itself a finite resource. In contrast to the Haber-Bosch process, the enzyme nitrogenase catalyzes the synthesis of ammonia at ambient conditions electrochemically, using solvated protons and electrons. Up to this point, an efficient, analogous man-made electrochemical method for synthesizing ammonia has not been realized industrially, largely due to the high energy input.[3−5] Therefore, development of an electrode material for stable electrochemical synthesis of ammonia from N_2, protons, and electrons (eq 1) at ambient conditions is desired.

In the Haber-Bosch process, N_2 dissociation is the rate-determining step and cleavage of the strong N−N bond is widely regarded as the main bottleneck in catalytic ammonia synthesis (where coverage effects can also be important),[6] and electrochemical approaches might circumvent it. To date, numerous investigations have been conducted using various electrolytes, electrode materials, and different electrochemical membrane reactors to alleviate the thermodynamic requirements and optimize the ammonia formation rate using a heterogeneous electrocatalytic approach.[7−19] However, produc-

Received: August 30, 2015
Revised: December 5, 2015
Published: December 9, 2015

DOI: 10.1021/acscatal.5b01918
ACS Catal. 2016, 6, 635−646

tion rates nearing those needed to become commercially viable ($4.3–8.7 \times 10^{-7}$ mol s^{-1} cm^{-2})[20] at moderate operational environments are yet to be reached. The nitrogen electroreduction reaction (NER) is difficult to catalyze to ammonia in aqueous electrolytes at ambient conditions, as the hydrogen evolution reaction (HER) is a competing reaction with usually higher current efficiency (CE).[15] The highest CE reported so far for ammonia synthesis at ambient conditions directly from air and water is less than 1%, with the formation rate of around 1.14×10^{-9} mol cm^{-2} s^{-1} at −1.6 V of applied potential,[15] whereas Licht et al. have reached a CE of 35% at 200 °C, 25 bar, and −1.2 V in a NaOH/0.5 KOH electrolyte.[21] Hence, stable catalyst materials that are able to activate N_2, capable of stabilizing N−H species moderately on the surface and noble enough to release the nitrogen from the surface in the form of NH_3 with higher efficiency toward NER rather than HER or other side products, are desired, where the supplied electrons from renewable energy sources ideally make only ammonia and not hydrogen gas. Accordingly, numerous theoretical and computational attempts have been made to search for an electrocatalyst that is active and selective toward NER.[22−27]

Under-coordinated sites on surfaces or on nanoparticles often dominate the whole catalytic activity for the catalyst. We have recently investigated the role of such under-coordinated sites on metal clusters explicitly, with[24] and without a nitrogen skin[23] as well as in the presence of O, OH, and H_2O,[25] where ammonia is produced at around −0.6 V on MoN nanoclusters. Licht et al. have also shown that nano-Fe_2O_3 can produce ammonia at 250 °C and 25 bar.[21] In this study, we are, however, specifically addressing whether nitride surfaces might display other properties than those found for metals, for example, due to the presence of nitrogen vacancies in the surface, which are naturally not found on metals.

In one of our previous studies,[27] a systematic screening of transition metal nitrides was carried out to search for new electrocatalysts capable of selective conversion of nitrogen to ammonia electrochemically at ambient conditions with low overpotential (significantly less than 1 V). Density functional theory (DFT) calculations were used to study the thermodynamics of the cathode reaction on 26 different d-block metal mononitrides in the rocksalt and zinc blende crystal structures. Only the most stable facet was studied in detail for catalytic activity, which in all cases was either the rocksalt (100) or zinc blende (110) facet. In reality, in the manufacturing of these (electro)catalysts, a multifaceted structure is more probable than a single-crystal catalyst, even for metal nitrides grown with thin film techniques.[28−32] Therefore, consideration of other crystallographic textures of these promising nitride catalysts is necessary to gain a realistic insight into the catalytic properties, selectivity, and stability of these metal nitride catalysts.

In the present paper, the most promising nitride electrocatalysts identified by our previous study are investigated in more detail. We include other possible stable low-index facets that may exist on polycrystalline surfaces of those metal nitrides. That is done to both estimate the activity of those other facets and also to investigate if those facets will get poisoned, if the surface will not regenerate or even result in a decomposition of the whole catalyst. Therefore, the catalytic activity of N_2 reduction to ammonia of various crystal facets of ZrN, NbN, CrN, and VN is calculated by considering a Mars−van Krevelen mechanism. Feasibility of nitrogen activation via this mechanism was recently reported on the surface of Co_3Mo_3N, too.[33] These transition metal nitrides offer the potential advantage of being able to form ammonia by way of a Mars−van Krevelen mechanism, in which a surface N atom is reduced to NH_3 and the catalyst later regenerated with dissolved N_2, rather than adsorbing N_2 to the catalyst surface in the first step. The possibility of N vacancy replenishment by N_2 from the solution and endurance of the catalytic cycle is studied from both a thermochemical and kinetic perspective. The possibility of poisoning the N vacancies on the surface by O, OH, and solvated protons from water is considered at the applied potential needed for NER.

METHODOLOGY

Electrochemical Reactions. A heterogeneous Mars−van Krevelen (MvK) mechanism[34] is considered where one ammonia (NH_3) molecule is formed by protonation of a surface N atom and a N vacancy is created before the catalyst is regenerated with dissolved N_2 from the electrolyte. Reducing another nitrogen at the surface then forms the second NH_3 molecule and completes the catalytic cycle. The overall cathode reaction of the electrochemical process is

$$N_{2(g)} + 6(H^+ + e^-) \rightarrow 2NH_{3(g)} \quad (1)$$

The source of protons is taken to be the anode reaction:[35]

$$H_2 \rightleftharpoons 2(H^+ + e^-) \quad (2)$$

Hydrogenation of the surface is carried out by adding H atoms one-by-one to the surface to represent a proton from the solution and an electron from the electrode surface. At every protonation step, adsorption at various possible sites is explicitly calculated, including other N atoms, metal atoms, and bridging sites to evaluate the most stable adsorption site. The reaction steps given in eqs 3−6 represent the formation of the first ammonia molecule. An asterisk denotes a surface site and "$*^{-N}$" denotes a surface N vacancy.

$$* + 6(H^+ + e^-) \rightarrow *H + 5(H^+ + e^-) \quad (3)$$

$$*H + 5(H^+ + e^-) \rightarrow *2H + 4(H^+ + e^-) \quad (4)$$

$$*2H + 4(H^+ + e^-) \rightarrow *3H + 3(H^+ + e^-) \quad (5)$$

$$*3H + 3(H^+ + e^-) \rightarrow *^{-N} + NH_{3(g)} + 3(H^+ + e^-) \quad (6)$$

Ideally, it only takes three protons and electrons to form the first ammonia molecule. However, since we allow the additional H atom to adsorb in the lowest energy position, more than three H atoms are needed in some cases if the H atoms bind rather to another N atom on the surface or to a metal atom instead. For all of the metal nitrides considered in this work, ammonia molecule is released in the end.

Two general mechanisms are considered for replenishing the N vacancy and regenerating the catalyst. The first is a dissociative mechanism in which gaseous N_2 dissociates, resulting in one N atom replenishing the N vacancy ($*N_{vac}$) and the other binding on top of a neighboring surface metal atom ($*N_{metal}$). This is depicted in eqs 7−11.

$$*^{-N} + 3(H^+ + e^-) + N_{2(g)} \rightarrow *N_{vac} + *N_{metal} + 3(H^+ + e^-) \quad (7)$$

$$*N_{metal} + 3(H^+ + e^-) \rightarrow *NH + 2(H^+ + e^-) \quad (8)$$

DOI: 10.1021/acscatal.5b01918
ACS Catal. 2016, 6, 635−646

$$*NH + 2(H^+ + e^-) \rightarrow *NH_2 + (H^+ + e^-) \quad (9)$$

$$*NH_2 + (H^+ + e^-) \rightarrow *NH_3 \quad (10)$$

$$*NH_3 \rightarrow * + NH_{3(g)} \quad (11)$$

If addition of N_2 to fill the vacancy is found to be endothermic, then an alternative approach is considered in which the vacancy remains until after formation of the second ammonia molecule, after which it and the second vacancy (denoted $*^{-2N}$) are dissociatively filled by N_2. This is referred to as the dimer vacancy variant and is depicted in eqs 12−16.

$$*^{-N} + 3(H^+ + e^-) + N_{2(g)} \rightarrow *^{-N} + *H + 2(H^+ + e^-) + N_{2(g)} \quad (12)$$

$$*^{-N} + *H + 2(H^+ + e^-) + N_{2(g)} \rightarrow *^{-N} + *2H + (H^+ + e^-) + N_{2(g)} \quad (13)$$

$$*^{-N} + *2H + (H^+ + e^-) + N_{2(g)} \rightarrow *^{-N} + *3H + N_{2(g)} \quad (14)$$

$$*^{-N} + *3H + N_{2(g)} \rightarrow *^{-2N} + NH_{3(g)} + N_{2(g)} \quad (15)$$

$$*^{-2N} + N_{2(g)} \rightarrow 2* \quad (16)$$

The second mechanism considered for replenishing the N vacancy and re-forming the catalyst is an associative mechanism. In this mechanism, gaseous N_2 binds to the vacancy (denoted $*N_{2,vac}$) and is directly protonated without dissociation until an $*NNH_3$ intermediate is formed. This is depicted in eqs 17−21. Note that $*N_{vac}$ refers to the regenerated catalyst and is equivalent to the asterisk in eqs 11 and 16.

$$*^{-N} + 3(H^+ + e^-) + N_2 \rightarrow *N_{2,vac} + 3(H^+ + e^-) \quad (17)$$

$$*N_{2,vac} + 3(H^+ + e^-) \rightarrow *NNH_{vac} + 2(H^+ + e^-) \quad (18)$$

$$*NNH_{vac} + 2(H^+ + e^-) \rightarrow *NNH_{2,vac} + (H^+ + e^-) \quad (19)$$

$$*NNH_{2,vac} + (H^+ + e^-) \rightarrow *NNH_{3,vac} \quad (20)$$

$$*NNH_{3,vac} \rightarrow *N_{vac} + NH_{3(g)} \quad (21)$$

DFT calculations are used to calculate the minimum energy configuration of each species on the surface and to calculate adsorption energies of all intermediates according to reactions depicted in eqs 3−21. Various surface sites are considered, and the optimal binding site is identified. It is assumed that activation barriers for protonation steps can be neglected during the electrochemical reactions.

The free energy of each elementary step at zero potential, $\Delta G(0)$, is estimated according to

$$\Delta G(0) = \Delta E + \Delta E_{ZPE} - T\Delta S \quad (22)$$

ΔE is the reaction energy calculated using DFT. The zero-point energy correction (ΔE_{ZPE}) and change in entropy (ΔS) are calculated for the adsorbed species using harmonic vibrational frequencies obtained from a normal-mode analysis. The values of these are given in the Supporting Information (Table S1). Gas phase values are taken from standard molecular tables.[36] By use of the computational standard hydrogen electrode[35] approach, the chemical potential for $(H^+ + e^-)$ is related to that of $1/2H_2(g)$, and the free energy difference for the reaction $*A + (H^+ + e^-) \rightarrow *AH$, under standard conditions (pH 0, pressure of 1 atm, and at 25 °C), is calculated as the free energy change for the reaction $*A + 1/2H_2 \rightarrow *AH$. The effect of an applied bias, U, is included for all electrochemical reaction steps by shifting the free energy for reactions involving n electrons by $-neU$:[35]

$$\Delta G(U) = \Delta G(0) - neU \quad (23)$$

Explicit inclusion of a water layer[37] has not been considered in the present work due to the large computational effort required. It has previously been shown that the presence of water may help stabilize some species more than others via hydrogen bonding. For example, *NH is expected to be stabilized slightly by hydrogen bonding, while the effect of the water layer on *N will be negligible. The effect of hydrogen-bond stabilization of the adsorbates has been estimated in a previous publication.[22] A relatively small correction for the N−H bonds was found to be around 0.08 eV per H bond. From this, we conclude that the onset potentials being calculated in the present study are likely to change by a similar magnitude, that is, less than 0.1 eV. Thus, the correction is not done in the present study.

Computational Details. All calculations were performed using DFT with the RPBE exchange-correlation functional.[38] The core electrons were described by a PAW representation,[39] and the valence wave functions were expanded in a basis set of plane waves with an energy cutoff of 350 eV. The electron density of the valence states was obtained by a self-consistent iterative diagonalization of the Kohn−Sham Hamiltonian, with the occupation of the Kohn−Sham states being smeared according to a Fermi−Dirac distribution with a smearing parameter of $k_BT = 0.1$ eV. Activation energies were calculated as the highest point along the minimum energy path (MEP) acquired using the climbing image nudged elastic band method (CI-NEB).[40,41] A 4 × 4 × 1 Monkhorst−Pack k-point sampling is used for all the surfaces. All calculations were performed using the Vienna ab initio simulation package (VASP).[42−45]

Mononitrides of Zr, Nb, Cr, and V were considered in both the rocksalt (RS) and zinc blende (ZB) structures in the present study, as they were previously found to be very promising for electrochemical ammonia formation.[27] Two low-index facets were considered for each crystal structure, the (100) and (111) facets of the RS structure and the (100) and (110) facets of the ZB structure, as shown in Figure 1. To model each nitride surface, 40 atoms in five layers with each layer consisting of four metal atoms and four nitrogen atoms

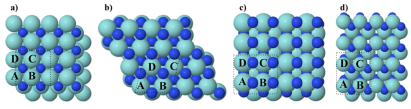

Figure 1. Metal nitride unit cell and top views of the low-index surfaces used in this study: (a) rocksalt (100), (b) rocksalt (111), (c) zinc blende (100), and (d) zinc blende (110). The surface unit cells have been repeated once in the lateral directions. Metal atoms are represented by cyan spheres and nitrogen atoms by dark blue spheres.

DOI: 10.1021/acscatal.5b01918
ACS Catal. 2016, 6, 635−646

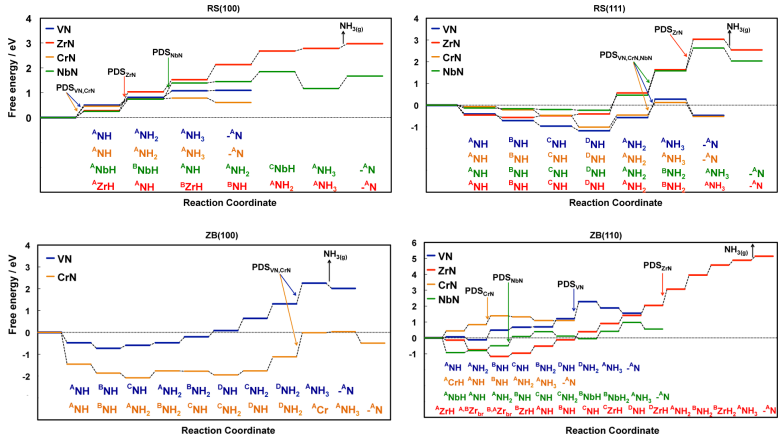

Figure 2. Free energy diagrams for NH_3 formation via a Mars−van Krevelen mechanism on different facets of RS and ZB crystal structures of VN, ZrN, CrN, and NbN at zero potential. The labels below each free energy diagram show the most energetically favorable intermediates that form on the surface at each step. A, B, C, and D identify on which metal atom/surface N the H adsorbs, where those labels are specified in Figure 1. The terms $^{A,B}Zr_{br}$ and $^{B,A}Zr_{br}$ mentioned for the ZB(110) of ZrN indicate that H adatoms adsorb on a bridge position between two adjacent Zr atoms (^{A}Zr and ^{B}Zr). The (100) facets of ZB structure of ZrN and NbN are not included here due to structural instability, and they are therefore excluded from further study. Further detailed information regarding assessment of the stability of these metal nitrides is provided in Table S2.

were used. The bottom two layers were fixed, whereas the adsorbate(s) together with the three topmost layers of the nitrides were allowed to fully relax. Boundary conditions were periodic in the *x* and *y* directions, and surfaces were separated by 12 Å of vacuum in the *z* direction. Due to the large vacuum layer and in order to improve calculational convergence, the calculations were run without imposing a dipole correction. Test calculations confirm that the effect of adding a dipole correction is small and in no cases above 35 meV. The structural optimization was considered converged when the forces in any direction on all moveable atoms were less than 0.01 eV/Å. All calculations were spin-paired with the exception of VN and CrN, as they were previously shown to have magnetic properties at their equilibrium lattice constants.[46] The magnetic moment of VN and CrN and the RPBE lattice constants were taken from ref 46, where their calculated values are 1−2% from the experimental values.

RESULTS AND DISCUSSION

The catalytic activity of ZrN, NbN, CrN, and VN in the RS(100/111) and the ZB(100/110) structures for reducing N_2 to NH_3 via a MvK mechanism is investigated. We found that this mechanism is more energetically favorable on the surface of nitrides compared to the common associative or dissociative mechanisms studied generally on surfaces. For the associative mechanism, the formation of $*N_2H$ was found to be thermodynamically unfavored on the surface of these nitrides. For the dissociative mechanism, very large kinetic barriers of more than 2.5 eV were found for splitting of dinitrogen on the surface (see Supporting Information, Figures S2 and S3). Stability of a surface nitrogen vacancy (N vacancy) with respect to both migration into the bulk and poisoning in an electrochemical environment and ease of N vacancy replenishment and therefore endurance of catalytic cycle are also investigated. Two different kinds of elementary steps are considered in the modeling. One is an electrochemical step with proton/electron transfer, such as protonation of the nitride surface. In the constructed free energy diagrams discussed below, the largest difference between two adjacent electrochemical steps is termed the potential-determining step (PDS) as it indicates the bias required to make all electrochemical steps exothermic. The other step is a non-electrochemical step without proton/electron transfer, such as replenishment of the nitride with $N_{2(g)}$. This type of step cannot be tuned by applying bias and consequently determines the rate of reaction and is labeled as such, rate-determining step (RDS).

Catalytic Activity. *Formation of the Initial NH_3 Molecule.* DFT calculations are used to investigate the reactivity of different facets of the nitride candidates toward reduction of a surface nitrogen atom to form a single ammonia molecule according to eqs 3−6. At every protonation step, various possible adsorption sites are inspected, including other N atoms, metal atoms, and bridging sites to evaluate the most stable adsorption site. The free energy of all intermediates is calculated according to eq 22, with reference to N_2 and H_2 in the gas phase. Free energy diagrams for this process on all nitrides considered are shown in Figure 2. The large free energy difference observed between the reactants (N_2 + $3H_2$) and products ($2NH_3$) is because these different metal nitride surfaces adsorb different numbers of H atoms before releasing NH_3 (in most cases, more than three proton/electron pairs are required for formation of an ammonia molecule) and not because of the energy required to form the N vacancy. The

DOI: 10.1021/acscatal.5b01918
ACS Catal. 2016, 6, 635−646

largest free energy increase and the associated proton transfer step in the mechanism of forming one ammonia molecule on different facets are collected in Table 1.

Table 1. Largest Free Energy Increase (ΔG_{max} in eV) and the Associated PDS (Electrochemical Step with the Largest Increase in Free Energy) in the Mechanism of Forming One Ammonia Molecule via a Mars−van Krevelen Mechanism on Different Facets of RS and ZB Crystal Structures of VN, ZrN, CrN, and NbN[a]

	RS(100)		RS(111)		ZB(100)		ZB(110)	
	ΔG_{max}	PDS	ΔG_{max}	PDS	ΔG_{max}	PDS	ΔG_{max}	PDS
ZrN	0.76	#2	1.42	#7	–	–	1.02	#11
NbN	0.65	#3	1.12	#6	–	–	0.59	#4
CrN	0.46	#1	0.58	#6	1.11	#9	0.54	#3
VN	0.51	#1	0.85	#6	0.97	#9	1.06	#7

[a]The # indicates which protonation step in Figure 2 determines the potential.

Considering first the RS(100) nitrides, it can be seen that, for most of these nitrides, every protonation step is endergonic. However, the free energy required at each step is rather low and can be overcome with an applied bias of less than −0.80 V vs SHE for all nitrides. For ZrN, NbN, and VN, the release of NH_3 is also endergonic, and this cannot be overcome with an applied bias. However, in acidic conditions, the adsorbed NH_3 is likely to get further protonated to NH_4^+ and released into the solution, thereby avoiding this small increase in free energy. Thus, this step is not discussed further. A notable feature of the RS(100) nitrides is that, in general, very few H^+/e^- pairs are required to generate NH_3. For CrN and VN, each protonation step adds to the same surface N atom, meaning that the minimum of three H^+/e^- pairs is required to form one NH_3. For the three other facets, more than the minimum H^+/e^- pairs are required due to the protons adding either to neighboring nitrogen or metal atoms in some elementary steps. This means that a higher current efficiency should be expected for formation of the first NH_3 on the RS(100) facets. However, it should be noted that this is only half of the catalytic cycle for ammonia formation on transition metal nitrides.

For the RS(111) nitrides, it is seen that the most favorable H adsorption site is always a surface N with no tendency of binding H to neighboring metal atom(s), even at high coverage. On other facets, H adsorption is usually seen on neighboring metal atom(s) at low coverage. The only exception is VN, for which metal protonation is never the lowest energy configuration on any facet, and it is always the surface N that adsorbs protons strongly. The preferential binding to the N atoms of the (111) facets can be rationalized by the texture of the facet. The N atoms protrude somewhat from the surface and are thus more exposed than the metal atoms. In general, the largest increase in free energy is greater for the (111) facets than for the (100) facets. In our previous work,[27] it was found that protonation of neighboring metal atoms usually lowered the free energy of the PDS for a given nitride, by up to 0.3 eV. This might explain the observation regarding higher ΔG_{max} on (111) facets, where such proton coverage on metal atoms is missing. Another interesting point for the (111) facets is that, in all cases, all of the surface nitrogen atoms are at least singly protonated before an ammonia molecule is formed. Again, this implies a lower current efficiency.

The zinc blende surfaces, in general, require more H^+/e^- pairs to form NH_3 than the analogous rocksalt surfaces; however, all surfaces are rather unique in the order of protonation. Aside from VN, where all the protons are only added to the surface nitrogen(s), some degree of metal atom

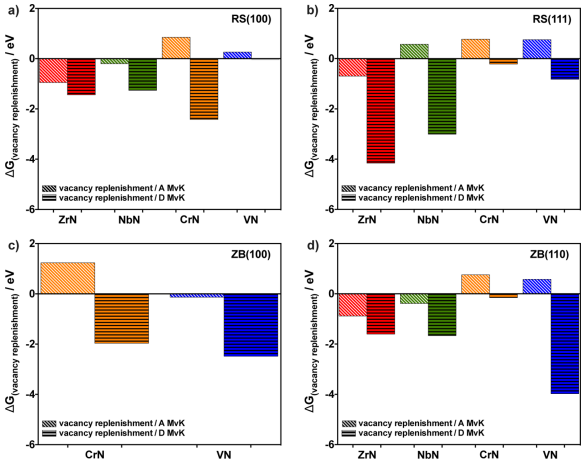

Figure 3. Free energy change for replenishing the vacancy associatively and dissociatively on (a) RS(100), (b) RS(111), (c) ZB(100), and (d) ZB(110).

DOI: 10.1021/acscatal.5b01918
ACS Catal. 2016, 6, 635−646

Table 2. Largest Increase in Free Energy of Any Elementary Step in the Formation of the Second NH_3 Molecule (ΔG_{max}, in eV) and Barrier of N_2 Dissociation ($E_{a(N\cdots N)}$, in eV)

	RS(100)			RS(111)			ZB(100)			ZB(110)		
	assoc.	dissoc.		assoc.	dissoc.		assoc.	dissoc.		assoc.	dissoc.	
	ΔG_{max}	ΔG_{max}	$E_{a(N\cdots N)}$	ΔG_{max}	ΔG_{max}	$E_{a(N\cdots N)}$	ΔG_{max}	ΔG_{max}	$E_{a(N\cdots N)}$	ΔG_{max}	ΔG_{max}	$E_{a(N\cdots N)}$
ZrN	0.76	0.76	0.11	1.42	1.56	0.18	–	–	–	1.02	1.02	0.46
NbN	0.65	0.65	0.35	1.12	1.12	0.45	–	–	–	0.59	0.59	0.04
CrN	0.85	0.76	0.58	0.77	0.71	1.27	1.24	1.11	2.09	0.76	0.54	0.30
VN	0.51	0.51	0.30	0.85	0.85	0.55	0.97	1.22	1.57	1.06	1.24	0.21

protonation seems required for other nitrides before forming NH_3. The ZB(100) surfaces of CrN and VN are somewhat less active than other facets of the same nitrides toward forming one NH_3 molecule, with ΔG_{max} of around 1 eV. The ZB(100) of ZrN and NbN was found to be unstable upon geometry optimization and therefore excluded from the rest of the study. Of the ZB(110) surfaces, CrN and NbN are expected to be rather good at forming NH_3, with low values of ΔG_{max} (~0.5 eV). ZrN suffers from both a high ΔG_{max} (~1 eV) and a requirement of almost 4 times the minimum number of H^+/e^- pairs to form NH_3. A final point to note is that, for all of the nitride surfaces considered here, rather than formation of a monolayer of H on the surface that could cause recombination of hydrogen and desorption as H_2, NH_3 is formed. This is significant as it implies that NH_3 will be formed preferentially over the evolution of hydrogen, which was a substantial problem with pure metal surfaces.[22]

Replenishment of N Vacancies and Endurance of the Catalytic Cycle. After the formation of the first NH_3 molecule as detailed above, the created N vacancy must be replenished for the catalytic cycle to persist. This is done by adsorption of solvated N_2, where one of the N atoms is used to refill the N vacancy and the other N atom is used to form a second NH_3 molecule. As identified in our previous study,[27] for a number of the nitrides, replenishing the single N vacancy on the surface requires a prohibitively large increase in free energy. This can be circumvented by first forming a second NH_3 molecule, leaving two N vacancies (a vacancy dimer) on the surface, after which gaseous N_2 is adsorbed. These mechanisms are given in eqs 7−11 and 12−16. It was found that, for some of the nitrides studied here, a single-vacancy mechanism is possible, with the exceptions of all of the RS(111) surfaces, RS(100) of CrN, ZB(100) of CrN and VN, and ZB(110) of ZrN and VN. These two mechanisms are hereafter collectively referred to as a "dissociative mechanism", as the adsorbed N_2 dissociates without protonation. An alternative mechanism is considered in which the adsorbed N_2 is protonated prior to dissociation. This is referred to as the "associative mechanism" and is detailed in eqs 17−21. In the present section, replenishment of the surface N vacancy and formation of the second NH_3 molecule is investigated for all surfaces to identify the likely mechanism operating. Energy barriers that cannot be overcome by an external bias, namely, replenishment of the vacancy and dissociation of N_2, are investigated and discussed.

The first consideration is to check whether ammonia forms via a dissociative (D, in Figure 3) or an associative (A, in Figure 3) mechanism. Free energy diagrams are shown for the overall mechanisms in the Supporting Information (see Figure S1). For simplicity, rather than discussing the whole of the free energy diagrams, only two key steps in the mechanism are discussed to identify whether a dissociative or associative mechanism is operating. The first is the elementary step in which the N vacancy is replenished and the second is the elementary step that has the largest increase in free energy. The change in free energy associated with vacancy replenishment in both the associative and dissociative mechanisms is shown in Figure 3. The largest increase in free energy for any elementary step (ΔG_{max}) as well as the barrier for N_2 dissociation [$E_{a(N\cdots N)}$] are given in Table 2.

Considering first the RS(100) surfaces, it can be seen from Figure 3a that for all nitrides it is thermodynamically preferable for the vacancy to be replenished dissociatively. Furthermore, for all nitrides, dissociative replenishment is exothermic. According to Table 2, the barrier for N_2 dissociation is relatively low for ZrN, NbN, and VN (0.11, 0.35, and 0.30 eV, respectively) and should be able to be overcome at ambient conditions. For CrN, the N_2 dissociation barrier is 0.58 eV, which means that the rate would be rather slow if the mechanism were to proceed dissociatively. However, it can be seen that for the associative mechanism an increase in free energy of 0.85 eV is required to fill the vacancy. As this is not an electrochemical step, it would restrict the rate of reaction even more than the dissociative mechanism and is likely not favored. It is concluded that all RS(100) nitride surfaces likely form the second NH_3 molecule via a dissociative mechanism.

An interesting observation arises for the RS(100) of NbN and ZrN. On these surfaces, there are H adatoms present at the point of N_2 adsorption. It is found that over the course of N_2 addition and dissociation, neighboring hydrogen atoms migrate to the outermost N adatom on the vacancy. It is likely that this weakens the N−N bond, thus facilitating dissociation, resulting in the relatively low barrier to N_2 dissociation on these nitrides.

Figure 3b shows that dissociative replenishment of the vacancy is exothermic for all RS(111) nitrides. However, on ZrN, a later protonation step becomes the elementary step with the largest increase in free energy, which is larger in the dissociative mechanism compared to the associative mechanism (see Table 2). Thus, it is concluded that formation of the second NH_3 molecule on ZrN is likely by way of the associative mechanism. For NbN, it is exothermic to replenish the vacancy dissociatively, compared with endothermic associative replenishment. Furthermore, the barrier to dissociate N_2 is relatively small, thus the dissociative mechanism is the most probable. For CrN, the dissociative mechanism is thermodynamically favored; however, a large barrier exists for N_2 dissociation. Thus, it is likely that CrN proceeds via an associative mechanism. However, it is worth noting that there is a significant increase in free energy required to replenish the vacancy associatively (0.77 eV), and thus NH_3 formation on RS(111) CrN is likely to be slow. For VN, both mechanisms exhibit a large barrier that cannot be overcome with an applied potential; for the associative mechanism, it is endothermic to fill the vacancy, and for the dissociative mechanism, a barrier of

DOI: 10.1021/acscatal.5b01918
ACS Catal. 2016, 6, 635−646

0.55 eV exists for N_2 dissociation. The dissociative mechanism is likely favored but rather slow.

For the ZB(100) surfaces, dissociative vacancy replenishment is exothermic. However, for both surfaces, large barriers of over 1.50 eV exist for N_2 dissociation. That makes dissociative ammonia formation inactive at ambient conditions. On the ZB(100) surfaces of VN, an associative path should be possible, but on ZB(100) surfaces of CrN, the associative path is likely very slow due to presence of a non-electrochemical step (filling the vacancy with N_2) with free energy change of 1.24 eV. Hence, the presence of ZB(100) facets of CrN in polycrystalline film of this catalyst will not be able to catalyze the N_2 electroreduction to ammonia.

For the ZB(110) surfaces, dissociative vacancy replenishment is exothermic in all cases and with relatively low barriers for dissociation, and most are likely to form the second NH_3 molecule dissociatively. However, the ZB(110) surfaces of ZrN and NbN are likely to have both the dissociative and the associative mechanism operating. The non-electrochemical N_2 adsorption step of the associative mechanism is endothermic on both CrN and VN on this facet and will be unlikely to have any important role in the overall activity.

Generally, for the nitrides with a N_2 dissociation barrier of ≲0.5 eV, such as RS(100) of ZrN, NbN, and VN, RS(111) of ZrN and NbN, as well as ZB(110) of ZrN, NbN, CrN, and VN, cleavage of N_2 and replenishment of the N vacancy should be achieved. The existence of these low barriers for N_2 dissociation can be attributed to two factors: the existence of N vacancy sites on these surfaces that activates the highly inert N_2 and the high affinity of these nitrides (specifically the transition metal atoms) to nitrogen acting as a driving force for dissociative adsorption of N_2.

A final result considering the N_2 dissociation barriers on the surface N vacancy of the metal nitrides studied here is that there is no apparent correlation between the thermochemical energy of dissociation (ΔE) and the kinetic barrier (E_a). This departure from the Brønsted−Evans−Polanyi (BEP) relations implies that this class of materials may be particularly promising for efficient N_2 reduction catalysis as the activity of previously identified heterogeneous N_2 reduction catalysts is limited by these BEP relations.[6,47] These data are shown in Figure 4. This indicates the need for explicit calculations of the barriers rather than inference of E_a from calculated ΔE.

The free energy change of the electrochemical step with the highest increase in free energy (ΔG_{PDS}) of each facet of the transition metal nitride catalysts is shown in Figure 5 based on the most favorable reaction mechanism as deduced above. It should be noted that this includes the whole mechanism to form $2NH_3$. Most of the facets exhibit relatively high activity toward ammonia formation. Concerning the nature of the PDS of the reaction, there is no clear trend either within a given facet or a given metal nitride, which supports our procedure of studying this as explicitly as we have done here, instead of using a much more approximate model as the scaling relation of adsorption energies.[48]

To summarize the results of the catalytic investigations, it has been found that, for most of the nitride catalysts, a relatively low applied bias is required to tune the electrochemical steps such that the reaction is spontaneous. Investigation of the kinetics of non-electrochemical steps shows that, for most nitrides, the barrier for splitting N_2 is low enough to provide significant rate at room temperature. For VN in the ZB(100) structure, the N_2 dissociation barrier is high but may be

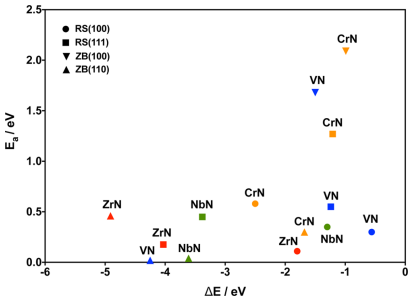

Figure 4. Activation energy barrier, E_a, and reaction energy, ΔE, for N_2 dissociation on a N vacancy of transition metal nitrides.

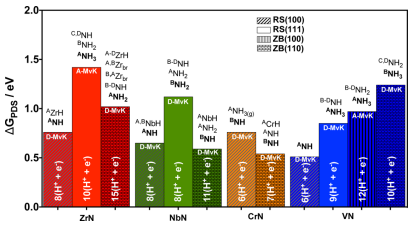

Figure 5. Comparison of the free energy change (ΔG_{PDS}, in eV) of the most endothermic electrochemical step of NH_3 formation on four different facets of ZrN, NbN, CrN and VN. A MvK mechanism is considered, where at each H addition step every possible adsorption site is investigated including other N atoms, metal atoms and bridging sites with at least 6(H^++e^-) needed to form $2NH_3$. The most favorable reaction mechanism for filling the N-vacancy, either associative (A-MvK) or dissociative (D-MvK), is specified inside the bar corresponding to each surface. The labels above each bar indicate the species formed prior to PDS and the bold text indicates the species formed right at the PDS, the notation of which is explained in Figures 2 and E1. The number inside each bar indicates the number of protons and electrons required to complete the catalytic cycle of $2NH_3$ formation. The RS(111) and ZB(100) facets of CrN are not included here since they both have a high barrier to dissociate N_2 on the N-vacancy as well as associative N_2 addition to the N-vacancy is endothermic, see Figure 3, Table 2 and Figure S1. Hence, all the facets presented in this figure have PDS which can be tuned by applying a bias of U = -ΔG_{PDS}.

circumvented by proceeding via an associative mechanism. Only two nitride surfaces, that is, RS(111) and ZB(100) facets of CrN, are found to have prohibitively high kinetic barriers for N_2 dissociation and are also endothermic for associative vacancy replenishment, neither of which can be tuned by the bias. Therefore, these facets are not shown in Figure 5. Furthermore, due to the fact that after formation of one ammonia molecule a surface vacancy remains that cannot be replenished by nitrogen on those particular facets of CrN, there exists a possibility that this may cause leaking of the nitrogen from the bulk of the catalyst, resulting in decomposition of the

DOI: 10.1021/acscatal.5b01918
ACS Catal. 2016, 6, 635−646

catalyst into pure metal and ammonia. This will be considered further in the next section.

An overall conclusion of the results in Figure 5 is that the (100) facets of RS structure of ZrN, NbN, CrN, and VN are promising NH_3 electrocatalysts as identified by our previous study,[27] and the ZB(110) facets of CrN and NbN seem to be equally as active, with onset potentials of only 0.54 and 0.59 V, respectively. It can be seen that the RS(111) facets of ZrN and NbN and the ZB(110) facets of ZrN and VN need high overpotentials for NH_3 formation, with onset potentials more negative than −1.0 V vs SHE. To increase the rate of NH_3 formation on these catalysts, the exposure of those less active facets should be minimized as much as possible. This is experimentally possible by growing single-crystal nitride catalysts, with some control over the exposed facets.[32] As mentioned in our previous study,[20] the RS(100) facets of both CrN and VN are particularly interesting not only because of onset potentials of significantly less than −1.0 V but also because the current efficiency of these catalysts might be relatively high due to the low number of H^+/e^- pairs required to form $2NH_3$.

Stability of N Vacancies on the Surfaces. As already discussed, in a Mars−van Krevelen mechanism, NH_3 is formed by way of reacting a surface N atom, leaving a N vacancy on the surface that must be replenished with gaseous N_2 for the catalytic cycle to complete. However, there exists the possibility that the N vacancy can migrate to the bulk of the nitride (i.e., N atoms from the bulk migrate to the surface) instead of being replenished with a nitrogen molecule from the solution. This can, in principle, continue until all of the nitrogen in the catalyst has reacted and formed ammonia, leaving only the pure metal, which has been suggested to be inactive or inefficient for NH_3 formation in most cases.[22] Therefore, stability of the N vacancy at the surface of the catalyst is estimated by comparing the difference in energy of a nitride slab with a N vacancy in the surface layer ($E_{vac,1}$) and to that of a N vacancy in the first subsurface layer ($E_{vac,2}$). The minimum energy configuration of each of these slabs is found and the energy difference ($\Delta E_{vac} = E_{vac,2} - E_{vac,1}$) used as an estimate of the thermodynamic stability of the vacancy at the surface of the nitride. Activation barriers for vacancy migration ($E_{a,vac}$) are also calculated, and both ΔE_{vac} and $E_{a,vac}$ are presented in Figure 6. For most nitrides, it is thermodynamically favorable for the vacancy to migrate to the bulk, with ΔE_{vac} less than or close to zero. However, many of the considered nitrides exhibit a high activation barrier for vacancy migration and are thus expected to demonstrate a kinetically stable N vacancy on the surface, where the filling of the vacancy with N_2 from the solution (presented in Figure 4) may be faster than for the N vacancy to migrate to the bulk. This will be compared explicitly below. The one clear exception is NbN in ZB(110), for which there is neither a thermodynamic nor a kinetic barrier against vacancy migration. Therefore, despite the high catalytic activity of this facet, it is unlikely to make a suitable electrocatalyst for NH_3 formation. Accordingly, the ZB(110) facet of NbN needs to be avoided when such a catalyst is synthesized and used for electrochemical ammonia formation. The second lowest barrier for vacancy migration is for the ZB(110) of VN, with an activation barrier of 0.51 eV. The VN catalyst could be reduced completely if a N vacancy is formed. However, this facet is relatively inactive toward ammonia formation since a potential of −1.24 V vs SHE is needed to form ammonia on that specific facet (see Figure 5 above). Therefore, in practice, this may not be of any concern since such a high negative bias is not needed in order to form ammonia from other facets of the VN catalyst.

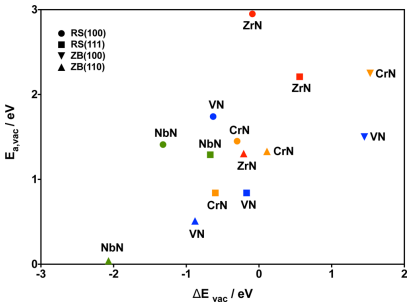

Figure 6. Energy differences (ΔE_{vac}) of a N vacancy at the surface layer and in the first subsurface layer of a nitride and the associated activation barrier of N vacancy migration ($E_{a,vac}$).

For a more detailed assessment of the stability of the N vacancy, the competition between migration of the N vacancy from the surface into the bulk (or migration of bulk nitrogen to the surface) after formation of the first ammonia molecule and regeneration of the N vacancy with N_2 is inspected. If the vacancy is likely to replenish faster than it migrates into the bulk, the catalyst is likely to be able to be regenerated and the second NH_3 molecule formed. The free energy barriers (G_a) for each process are displayed in Figure 7a−d, where for the vacancy migration process $G_a = E_a$ and for the process of replenishing the vacancy $G_a = E_a + 0.6$, where the 0.6 eV is used to account for the loss of entropy of $N_{2(g)}$.[49]

As can be seen, the catalytic cycle of $2NH_3$ formation should be sustained on all facets of ZrN as regeneration of the catalyst with nitrogen (replenishment of the vacancy) always occurs faster than migration of the nitrogen content into the surface (decomposition). Therefore, a polycrystalline film of such a catalyst should not result in decomposition in an experimental setup. For NbN, both the (100) and (111) facets of the RS structure should have a stable vacancy at the surface and hence a sustainable catalytic cycle. As identified above, the ZB(110) facet of NbN has a very low barrier for vacancy migration, which is indeed lower than the barrier for vacancy replenishment. Therefore, the nitrogen content might leak out after formation of the first ammonia molecule. Furthermore, the bias required to form ammonia on this facet (−0.59 V vs SHE) is lower than the bias required for ammonia formation on the other facets, thus formation of ammonia is likely to result in decomposition of the catalyst by migration of the bulk N to the surface. The only solution for using NbN as an electrocatalyst is, hence, to grow a single crystal of the RS NbN. As a result, the ZB NbN is not further discussed in following subsections.

The RS(111) and ZB(100) of CrN, which were eliminated due to the high barrier of N_2 dissociation and endothermic associative N_2 addition, are brought back in Figure 7 to investigate whether regeneration occurs faster than decomposition. For the RS(111), catalyst regeneration takes place much slower than decomposition, and that might result in leaking the nitrogen content of this facet out if polycrystalline film of this catalyst is used in the experiment. For the ZB(100),

DOI: 10.1021/acscatal.5b01918
ACS Catal. 2016, 6, 635−646

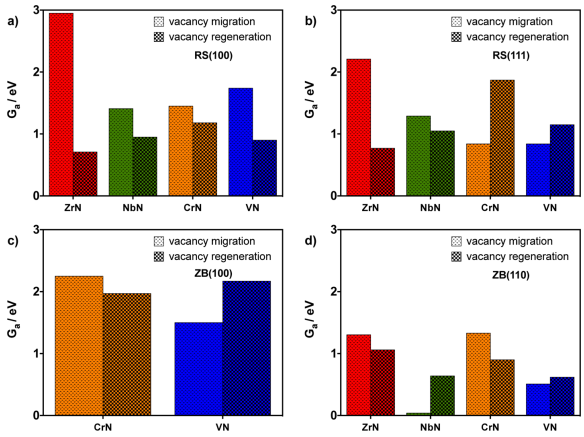

Figure 7. Calculated activation free energies (G_a) of regenerating the catalyst by N_2 dissociation for replenishment of the N vacancy compared with activation free energies of vacancy migration into the bulk (migration of nitrogen atoms from the bulk toward the surface) for (a) RS(100), (b) RS(111), (c) ZB(100), and (d) ZB(110).

the decomposition is slower than regeneration. It means that existence of this latter facet in a polycrystalline film of CrN should not cause leaking of the nitrogen content out of the catalyst. Therefore, the decomposition of CrN may only arise from the existence of the RS(111) facet and not from the other facets in a polycrystalline film of this catalyst. This issue can be avoided if the RS(111) facet of CrN is eliminated from the experimentally synthesized CrN catalyst.

For VN, all facets except for RS(100) exhibit faster vacancy migration than replenishment of the N-vacancy and are likely to leak the nitrogen content out if ammonia is formed on these facets. However, the bias required to form NH_3 on VN RS(100) is only −0.51 V vs SHE, compared with at least −0.85 V or more negative on its other facets. Hence, decomposition of a polycrystalline catalyst of VN could be prevented by applying a low bias of up to −0.5 V vs SHE and forming NH_3 only on the RS(100) facets. For this reason, only the RS(100) facet of VN will be discussed further.

Poisoning of the Surface Vacancy. In addition to being stable at the surface, the vacancy must also be filled with $N_{2(g)}$ from the reaction environment. Here, we focus on aqueous solutions, having both water and solvated protons near the solid−liquid interface. Hence, there exists the possibility that the vacancy could rather be filled with protons, O, or OH groups from the aqueous electrolyte, all of which would block this surface active site and thereby prevent completion of the catalytic cycle.[25] In the present section, the competition between N, O, OH, and H for filling the surface vacancy is investigated by considering the free energy of filling the vacancy with O, OH, or H relative to 2N ($\Delta G_{(*2N-*X)}$, where X = O, OH, or H). These free energies are referenced to N_2, H_2O, and $1/2H_2$ (or $H^+ + e^-$) and are calculated at the onset potential for ammonia formation proposed for each facet. A negative value of $\Delta G_{(*2N-*X)}$ indicates that it is thermodynamically favorable to fill the vacancy with N, rather than O, OH, or H. The values of $\Delta G_{(*2N-*X)}$ are shown in Figure 8 for all the catalytically active facets of promising nitrides.

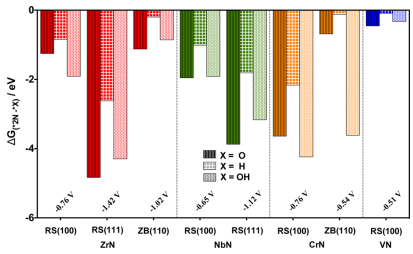

Figure 8. Comparison of the free energy of adsorption of O, OH, or H (relative to 2N) to the surface vacancy of catalytically active nitrides ($\Delta G_{(*2N-*X)}$, in eV). Free energies are calculated relative to $N_{2(g)}$, $1/2H_{2(g)}$, and $H_2O_{(g)}$. All free energies are evaluated at the calculated onset potential for each nitride (based on the most favorable reaction mechanism and shown vs SHE). The adsorption energy of two N atoms is compared with one O, one OH, or one H since the nitrogen comes from N_2 filling the vacancy where one of the N adsorbs to the vacancy and the other N adsorbs on top of the metal atom nearby. However, only one O or OH or H fills the vacancy from the surrounding water or solvated protons in water.

It can be seen that N atoms bind more strongly than H, OH, and O atoms to the surface vacancy for all facets considered. Hence, it is likely that none of these three species will poison the surface vacancy. Therefore, for all of these facets, the vacancy is likely to be refilled by nitrogen, and thus the catalytic cycle should endure to form the second NH_3. The weaker binding of O to N vacancy compared to H is as expected

DOI: 10.1021/acscatal.5b01918
ACS Catal. 2016, 6, 635−646

because, when the bias is tuned toward more negative values, the O species bind weaker on the surface compared to H_2O in the gas phase:

$$H_2O + * \rightarrow *O + 2H^+ + 2e^- \quad (24)$$

Conversely, the H adsorption free energy becomes more negative when the bias is lowered:

$$H^+ + e^- \rightarrow *H \quad (25)$$

Removal of Surface Oxygen to Water. Under sample preparation, handling, or reaction conditions, there exists a possibility of oxide formation on the surface of the catalyst. This may occur either upon transfer from the growth conditions (usually UHV) through an atmospheric environment to the electrochemical setup or upon exposure to the electrochemical media. Electrochemical removal of an oxygen atom on the surface may be expressed according to the following reactions:

$$*O + 2(H^+ + e^-) \rightarrow H_2O_{(g)} + * \quad (26)$$

$$\Delta G = G_f[H_2O_{(g)}] - G_{*O} - G_f[H_{2(g)}] \quad (27)$$

$$\Delta G = G_f[H_2O_{(g)}] - (\Delta E_{*O} + \Delta E_{ZPE*O} - T\Delta S_{*O} - neU) \quad (28)$$

$$U = -(G_f[H_2O_{(g)}] - (\Delta E_{*O} + \Delta E_{ZPE*O} - T\Delta S_{*O}))/2 \quad (29)$$

For electroreduction of oxygen adatoms to water, $2(H^+ + e^-)$ are required. In order for the reaction free energy in eq 27 to equal 0, a potential of U needs to be applied given by eq 29. The free energy of adsorbed oxygen (*O) on the surface is calculated using DFT with reference to water. The free energy of formation of $H_2O_{(g)}$ and $H_{2(g)}$ is taken to be −2.36 eV and 0, respectively, at standard conditions taken from thermochemical table values.[49] These potentials are calculated and depicted in Figure 9 for all the nitrides and compared with the

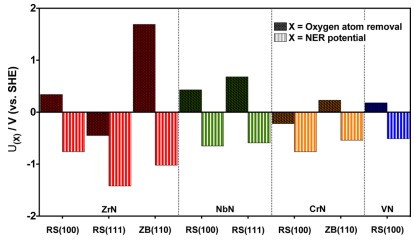

Figure 9. Required potential for removal of oxygen that might form on the surface of the nitride catalysts. The values are calculated with DFT and solved for eq 29.

corresponding potential required for NER at each facet. A positive value of U indicates that spontaneous removal of O from the surface will occur upon exposure to the electrolyte under reducing conditions. Consequently, for all nitride surfaces studied here, the oxygen adatoms should spontaneously reduce to water before a sufficiently negative potential is reached to get an appreciable rate of NER. The important point to note is that in the case where a thick oxide layer is formed on the surface due to long-time exposure of the metal nitrides to air, the oxide layer removal may be more challenging than addressed here. However, it should be possible that such an oxide layer can be practically prevented in many ways, for example, by coating the surface of the catalyst with a thin layer of a material that will later be easily removed in electrochemical setup prior to NER. However, this analysis demonstrates that there will be no tendency for O atoms to poison the surface when the surface is in contact with the aqueous electrolyte.

Candidates To Be Tested in Experiments. Finally, the stable nitride candidates for which the rate and efficiency of NH_3 formation is expected to be high are collected in Figure 10. As

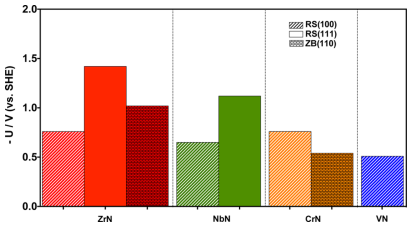

Figure 10. Comparison of the proposed bias for N_2 electroreduction to NH_3 via a MvK mechanism on stable facets of ZrN, NbN, CrN, and VN.

can be seen, all the RS(100) surfaces require only a small bias to reduce nitrogen to ammonia. The ZB(110) of CrN is also as active. However, the RS(111) of ZrN and NbN as well as the ZB(110) of ZrN needs to have more negative bias to reduce N_2 to ammonia. In addition, hydrogen production on all of these nitride candidates is explicitly considered within our mechanistic model, and accordingly, all of these candidates should suppress competitive hydrogen production, in contrast to metallic surfaces that almost exclusively evolve hydrogen gas.[22] From Figure 5, it is known how many electrons and protons (n) are needed to make $2NH_3$. The current efficiency is calculated as $6/n \times 100\%$ (6 being the minimum number of H^+/e^- pairs) and is summarized in Table 3 along with the onset potential for ammonia production. It is assumed here that the

Table 3. Most Promising Facets of the Nitride Candidates (Green Background) and Corresponding Potential Window and Current Efficiency for N_2 Electroreduction to NH_3 via a MvK Mechanism on ZrN, NbN, CrN, and VN

	RS(100)	RS(111)	ZB(100)	ZB(110)
ZrN	75% CE of NH_3 U = -0.76 V	60% CE of NH_3 U = -1.42 V	-	40% CE of NH_3 U = -1.02 V
NbN	75% CE of NH_3 U = -0.65 V	75% CE of NH_3 U = -1.12 V	-	Decomposition U = -0.59 V
CrN	100% CE of NH_3 U = -0.76 V	Decomposition U = -0.58 V	Non-catalytic U = -1.11 V	86% CE of NH_3 U = -0.54 V
VN	100% CE of NH_3 U = -0.51 V	Decomposition U = -0.85 V	Decomposition U = -0.97 V	Decomposition U = -1.06 V

DOI: 10.1021/acscatal.5b01918
ACS Catal. 2016, 6, 635−646

H adatoms that do not form NH_3 will contribute to H_2 formation from the surfaces[27] and thus offer a lower bound to the current efficiency. The current efficiency is high in most cases for these metal nitrides. Table 3 shows a summary over the transition metal nitride candidates and corresponding potential window for experimental ammonia formation.

It can be concluded that the most promising surface of these nitrides for electrochemical ammonia formation should be the RS(100). Besides, all of these four nitrides naturally crystallize in NaCl-type structure (rocksalt) under normal conditions.[50−57] These are promising nitride catalysts that show high activity and selectivity toward NER and ammonia formation at potentials around −0.5 to −0.8 V, while the equilibrium potential of ammonia formation from H_2(g) and N_2(g) is around +0.06 V.[36] The most recent experimental work at ambient conditions utilized Pt/C electrodes to synthesize ammonia from air and water at a potential of around −1.6 V with about 1% CE.[15] Moreover, the endurance of the catalytic cycle seems to be sustained and secured on the surface of these candidates. Because they are stable enough against both poisoning and decomposition in aqueous solution, replenishment of the N vacancy at ambient conditions seems feasible as the kinetic barriers of dissociation of nitrogen on the vacant site are relatively small. However, in order to achieve higher current densities in electrochemical experiments, the following facets of the nitrides should be avoided: the ZB(100) of CrN and VN as well as ZB(110) of VN, as these facets are relatively inactive (require applied potentials of more than −1.0 V vs SHE) for ammonia formation but can exist in a polycrystalline film of the catalyst.[28,31] In order to prevent decomposition of the whole catalyst, the following surfaces need to be avoided: the RS(111) of CrN and VN as well as ZB(110) of NbN, as migration of the N vacancy to the bulk of catalyst should proceed faster than replenishment of the N vacancy and regeneration of the catalyst. Growing a single crystal of other facets that are active and stable for a given nitride may eliminate the possibility of decomposition. If polycrystalline films are used, the mentioned issue may also be avoided in some cases by controlling the bias. For instance, the problem arising with the ZB(100) facet of CrN and VN may be avoided by not applying a bias more negative than −1.0 V vs SHE, whereas catalyst decomposition arising from the ZB(110) facet of NbN cannot be avoided with a control of the bias since ammonia is formed at lower bias on this facet than on other active facets of NbN. All in all, the DFT insight gained on these different nitride catalysts might guide experiments and contribute to reach more economically viable energy efficiency investments toward distributed and higher-yield ammonia formation.

CONCLUSION

This study is a detailed investigation of the promising nitride candidates from our recent work[27] to gain better insight for their experimental measurements and real-life application. The facets previously omitted due to lower stability are investigated as these metal nitrides are usually synthesized in a polycrystalline structure, and here the low-index facets of rocksalt and zinc blende structures are considered that are common for these metal nitrides.[46] Five important factors have been considered in this work to identify promising catalysts for electrochemical ammonia formation in aqueous media: (1) Identification of the reaction mechanism and calculation of the N_2 dissociation barrier. (2) Investigation of the catalytic activity and quantification of the potential-determining and rate-determining steps. (3) Determination of kinetic or thermodynamic barriers for N vacancy diffusion into the bulk, which can consequently leak the nitrogen content out of the nitride catalysts. (4) Investigation of the stability of the nitrides against poisoning in an electrochemical environment. (5) Estimation of the potential required for removal of any oxygen atoms that may adsorb onto the surface upon exposure to electrochemical environment. By considering the most common crystal facets in more details, we have been able to identify which facets of the nitrides are most active for ammonia formation as well as which facets should be avoided in order to succeed with high rates and efficiency for this reaction. These promising nitride catalysts are all stable against poisoning and decomposition in electrochemical environment with feasible regeneration of the catalyst ensuring the continuity of the catalytic cycle of ammonia production. Moreover, any primary oxygen that might form on surface should spontaneously be reduced to water at electrochemical environment prior to NER initiation. Besides, none of these facets should produce hydrogen according to the explicit consideration of HER within our mechanistic model. More interesting is the RS(100) of VN and CrN that is expected to result in ammonia formation with relatively higher current efficiency as it requires the minimum number of six proton/electron pair for formation of two ammonia molecules; that is, no H_2 gas is expected to be formed. Therefore, experimentalists are strongly encouraged to test these promising candidates in the structure and bias range proposed here for the possibility of higher-yield ammonia synthesis at ambient conditions.

ASSOCIATED CONTENT

Supporting Information

The Supporting Information is available free of charge on the ACS Publications website at DOI: 10.1021/acscatal.5b01918.

Zero-point energy and entropy contributions to the free energies. The free energy diagrams for comparison of associative and dissociative mechanisms. Energy per metal−nitrogen pair of the various metal nitride slabs. Investigation of the stability of the N vacancy against poisoning by O, OH, and proton from the electrochemical media. The first three elementary steps in the free energy diagram toward ammonia formation via an associative mechanism on the clean surface of these nitrides and the activation barrier of splitting dinitrogen on the clean surface for a dissociative mechanism (PDF)

AUTHOR INFORMATION

Corresponding Author

*E-mail: egillsk@hi.is.

Notes

The authors declare no competing financial interest.

ACKNOWLEDGMENTS

This work was supported from the Icelandic Research Fund, the Research Fund of the University of Iceland, and the Catalysis for Sustainable Energy (CASE) initiative funded by the Danish Agency for Science, Technology and Innovation. The calculations were in part carried out on the Nordic high performance computer (Gardar).

DOI: 10.1021/acscatal.5b01918
ACS Catal. 2016, 6, 635−646

REFERENCES

(1) Bharthwaj, A.; Hazarika, S.; Tufail, A.; Manoj, N.; Siva, A.; Ron, G. Coal gasification technology for ammonia plants. In *Nitrogen & Syngas Conference*, Athens, Greece, February 20−23, 2012.
(2) *Market Study: Ammonia*; Cerasena Market Intelligence Consulting available at http://www.ceresana.com/en/market-studies/agriculture/ammonia/ammonia-market-study-analysis-trends.html (accessed July 10, 2015).
(3) Thayumanavan, B.; Parvathy, K. Biochemistry of Nitrogen Fixation and Assimilation. In *Biotechnology of biofertilizers*; Kannaiyan, S., Ed.; Narosa Publishing House: New Delhi, India, 2002; pp 74−83.
(4) Burgess, B. K.; Lowe, D. J. *Chem. Rev.* **1996**, *96*, 2983−3012.
(5) Stryer, L. *Biochemistry*, 4th ed.; W.H. Freeman: New York, 1995; p 1120.
(6) Vojvodic, A.; Medford, A. J.; Studt, F.; Abild-Pedersen, F.; Khan, T. S.; Bligaard, T.; Nørskov, J. K. *Chem. Phys. Lett.* **2014**, *598*, 108−112.
(7) Kordali, V.; Kyriacou, G.; Lambrou, C. *Chem. Commun.* **2000**, *17*, 1673−1674.
(8) Marnellos, G.; Karagiannakis, G.; Zisekas, S.; Stoukides, M. *Stud. Surf. Sci. Catal.* **2000**, *130*, 413−418.
(9) Marnellos, G.; Zisekas, S.; Stoukides, M. *J. Catal.* **2000**, *193*, 80−87.
(10) Murakami, T.; Nishikiori, T.; Nohira, T.; Ito, Y. *J. Am. Chem. Soc.* **2003**, *125*, 334−335.
(11) Murakami, T.; Nohira, T.; Goto, T.; Ogata, Y. H.; Ito, Y. *Electrochim. Acta* **2005**, *50*, 5423−5426.
(12) Murakami, T.; Nohira, T.; Araki, Y.; Goto, T.; Hagiwara, R.; Ogata, Y. H. *Electrochem. Solid-State Lett.* **2007**, *10*, E4−E6.
(13) Xu, G.; Liu, R.; Wang, J. *Sci. China, Ser. B: Chem.* **2009**, *52*, 1171−1175.
(14) Michalsky, R.; Pfromm, P. H. *J. Phys. Chem. C* **2012**, *116*, 23243−23251.
(15) Lan, R.; Irvine, J. T. S.; Tao, S. *Sci. Rep.* **2013**, *3*, 1−7.
(16) Kugler, K.; Ohs, B.; Scholz, M.; Wessling, M. *Phys. Chem. Chem. Phys.* **2014**, *16*, 6129−6138.
(17) Kitano, M.; Kanbara, S.; Inoue, Y.; Kuganathan, N.; Sushko, P. V.; Yokoyama, T.; Hara, M.; Hosono, H. *Nat. Commun.* **2015**, *6*, 6731−6740.
(18) Michalsky, R.; Avram, A. M.; Peterson, B. A.; Pfromm, P. H.; Peterson, A. A. *Chem. Sci.* **2015**, *6*, 3965−3974.
(19) Vasileiou, E.; Kyriakou, V.; Garagounis, I.; Vourros, A.; Manerbino, A.; Coors, W. G.; Stoukides, M. *Top. Catal.* **2015**, *58*, 1193−1201.
(20) Giddey, S.; Badwal, S. P. S.; Kulkarni, A. *Int. J. Hydrogen Energy* **2013**, *38*, 14576−14594.
(21) Licht, S.; Cui, B.; Wang, B.; Li, F.-F.; Lau, J.; Liu, S. *Science* **2014**, *345*, 637−640.
(22) Skúlason, E.; Bligaard, T.; Gudmundsdóttir, S.; Studt, F.; Rossmeisl, J.; Abild-Pedersen, F.; Vegge, T.; Jónsson, H.; Nørskov, J. K. *Phys. Chem. Chem. Phys.* **2012**, *14*, 1235−1245.
(23) Howalt, J. G.; Bligaard, T.; Rossmeisl, J.; Vegge, T. *Phys. Chem. Chem. Phys.* **2013**, *15*, 7785−7795.
(24) Howalt, J. G.; Vegge, T. *Phys. Chem. Chem. Phys.* **2013**, *15*, 20957−20965.
(25) Howalt, J.; Vegge, T. *Beilstein J. Nanotechnol.* **2014**, *5*, 111−120.
(26) Matanović, I.; Garzon, F. H.; Henson, N. J. *Phys. Chem. Chem. Phys.* **2014**, *16*, 3014−3026.
(27) Abghoui, Y.; Garden, A. L.; Hlynsson, V. F.; Björgvinsdóttir, S.; Ólafsdóttir, H.; Skúlason, E. *Phys. Chem. Chem. Phys.* **2015**, *17*, 4909−4918.
(28) Hones, P.; Sanjines, R.; Levy, F. *Surf. Coat. Technol.* **1997**, *94*, 398−402.
(29) Gillan, E.; Kaner, R. *Inorg. Chem.* **1994**, *33*, 5693−5700.
(30) Ramos, H. J.; Valmoria, N. B. *Vacuum* **2004**, *73*, 549−554.
(31) Arias, D. F.; Arango, Y. C.; Devia, A. *Appl. Surf. Sci.* **2006**, *253*, 1683−1690.
(32) Shayestehaminzadeh, S.; Tryggvason, T. K.; Magnus, F.; Olafsson, S.; Gudmundsson, J. T. *Thin Solid Films* **2013**, *549*, 199−203.
(33) Zeinalipour-Yazdi, C. D.; Hargreaves, J. S. J.; Catlow, C. R. A. *J. Phys. Chem. C* **2015**, DOI: 10.1021/acs.jpcc.5b06811.
(34) Mars, P.; van Krevelen, D. W. *Chem. Eng. Sci.* **1954**, *3*, 41−45.
(35) Nørskov, J. K.; Rossmeisl, J.; Logadóttir, A.; Lindqvist, L.; Kitchin, J. R.; Bligaard, T.; Jónsson, H. *J. Phys. Chem. B* **2004**, *108*, 17886−17892.
(36) Atkins, W. *Physical Chemistry*, 6th ed.; Oxford University Press: Oxford, 1998; pp 485, 866−867, 925−927, and 942.
(37) Skúlason, E.; Tripkovic, V.; Björketun, M. E.; Gudmundsdóttir, S.; Karlberg, G.; Rossmeisl, J.; Bligaard, T.; Jónsson, H.; Nørskov, J. K. *J. Phys. Chem. C* **2010**, *114*, 18182−18197.
(38) Hammer, B.; Hansen, L.; Nørskov, J. *Phys. Rev. B: Condens. Matter Mater. Phys.* **1999**, *59*, 7413−7421.
(39) Blöchl, P. *Phys. Rev. B: Condens. Matter Mater. Phys.* **1994**, *50*, 17953−17979.
(40) Henkelman, G.; Uberuaga, B. P.; Jónsson, H. *J. Chem. Phys.* **2000**, *113*, 9901−9904.
(41) Henkelman, G.; Jónsson, H. *J. Chem. Phys.* **2000**, *113*, 9978−9985.
(42) Kresse, G.; Hafner, J. *Phys. Rev. B: Condens. Matter Mater. Phys.* **1993**, *47*, 558−561.
(43) Kresse, G.; Hafner, J. *Phys. Rev. B: Condens. Matter Mater. Phys.* **1994**, *49*, 14251−14269.
(44) Kresse, G.; Furthmüller, J. *Comput. Mater. Sci.* **1996**, *6*, 15−50.
(45) Kresse, G.; Furthmüller, J. *Phys. Rev. B: Condens. Matter Mater. Phys.* **1996**, *54*, 11169−11186.
(46) Hlynsson, V. F.; Skúlason, E.; Garden, A. L. *J. Alloys Compd.* **2014**, *603*, 172−179.
(47) Bligaard, T.; Nørskov, J. K.; Dahl, S.; Matthiesen, J.; Christensen, C. H.; Sehested, J. *J. Catal.* **2004**, *224*, 206−217.
(48) Abild-Pedersen, F.; Greeley, J.; Studt, F.; Rossmeisl, J.; Munter, T.; Moses, P.; Skúlason, E.; Bligaard, T.; Nørskov, J. K. *Phys. Rev. Lett.* **2007**, *99*, 016105.
(49) Lide, D. R. *CRC Handbook of Chemistry and Physic*, 78th ed.; CRC Press: Boca Raton, FL, 1997; p 2447.
(50) Rebholz, C.; Ziegele, H.; Leyland, A.; Matthews, A. *Surf. Coat. Technol.* **1999**, *115*, 222−229.
(51) He, X.-M.; Baker, N.; Kehler, B. A.; Walter, K. C.; Nastasi, M.; Nakamura, Y. *J. Vac. Sci. Technol., A* **2000**, *18*, 30−36.
(52) Olaya, J. J.; Rodil, S. E.; Muhl, S.; Sánchez, E. *Thin Solid Films* **2005**, *474*, 119−126.
(53) De Souza, E. F.; Chagas, C. A.; Ramalho, T. C.; Teixeira da Silva, V.; Aguiar, D. L. M.; Gil, R. S.; de Alencastro, R. B. *J. Phys. Chem. C* **2013**, *117*, 25659−25668.
(54) Mei, A. B.; Hellman, O.; Wireklint, N.; Schlepütz, C. M.; Sangiovanni, D. G.; Alling, B.; Rockett, A.; Hultman, L.; Petrov, I.; Greene, J. E. *Phys. Rev. B: Condens. Matter Mater. Phys.* **2015**, *91*, 054101.
(55) Wong, M. S. *J. Vac. Sci. Technol., A* **1993**, *11*, 1528−1533.
(56) Bazhanov, D. I.; Knizhnik, A. A.; Safonov, A. A.; Bagatur'yants, A. A.; Stoker, M. W.; Korkin, A. A. *J. Appl. Phys.* **2005**, *97*, 044108.
(57) Schwarz, K.; Williams, A.; Cuomo, J. *Phys. Rev. B: Condens. Matter Mater. Phys.* **1985**, *32*, 8312−8316.

DOI: 10.1021/acscatal.5b01918
ACS Catal. 2016, 6, 635−646

III Article 3

Electrochemical Synthesis of Ammonia via Mars-van Krevelen Mechanism on the (111) Facets of Group III–VII Transition Metal Mononitrides

Younes Abghoui and Egill Skúlason

Catalysis Today, in press (2016).

G Model
CATTOD-10245; No. of Pages 7
ARTICLE IN PRESS

Catalysis Today xxx (2016) xxx–xxx

Contents lists available at ScienceDirect

Catalysis Today

journal homepage: www.elsevier.com/locate/cattod

Electrochemical synthesis of ammonia via Mars-van Krevelen mechanism on the (111) facets of group III–VII transition metal mononitrides

Younes Abghoui, Egill Skúlason*

University of Iceland, Reykjavik, Iceland

ARTICLE INFO

Article history:
Received 1 April 2016
Received in revised form 31 May 2016
Accepted 2 June 2016
Available online xxx

Keywords:
Nitrogen activation
Electrochemical ammonia synthesis
DFT calculations
Transition metal nitrides
Mars-van Krevelen mechanism

ABSTRACT

Density functional theory (DFT) calculations were carried out on a new class of materials in pursuit of nitrogen activation and electrochemical ammonia formation at ambient conditions. The source of proton provided by the anode could be either water splitting or H_2. But we focused only on the cathode reaction here where nitrogen is reduced to ammonia. The Mars-van Krevelen mechanism was studied on the (111) facets of the NaCl-type structure of earlier transition metal mononitrides of Sc, Ti, V, Cr, Mn, Y, Zr, Nb, Mo, Hf, Ta, W, and Re. The catalytic activity was investigated, free energy of all intermediates was calculated along the reaction path and free energy diagrams were constructed to explore the potential-determining steps of the reaction and accordingly estimate onset potential necessary for nitrogen activation on each different metal nitrides. The possibility of catalyst poisoning in electrochemical environment was also scrutinized at the bias needed for running the reaction. In addition, hydrogen production on all these nitride candidates was explicitly considered within our mechanistic model by removing the constraint of proton adsorption occurring only on surface nitrogen atoms and accordingly most of these candidates show capability for suppressing competitive hydrogen production, in contrast to metallic surfaces that almost exclusively evolve hydrogen gas. The likelihood of catalyst decomposition and catalyst regeneration was assessed for the most interesting nitrides. It was found that the only active and stable nitride catalyst that can regenerate itself and activate nitrogen to ammonia is NbN, and others should decompose to their parental metals under operational conditions.

1. Introduction

Transition metal nitrides (TMNs) are typically metallic in character with nitrogen occupying interstitial positions in the metal atom arrangement. Due to the incorporation of nitrogen into the metal lattice, TMNs exhibit different physical and chemical properties from the parent metals endowing them with attractive electronic conductivity and catalytic activity [1]. The formation of TMNs modifies the nature of the d-band of the parent metal, resulting in a contraction of the metal d-band and increase of the lattice parameter, corresponding to the enhanced d-electron density. Such a d-band contraction would cause a greater density of states (DOS) near the Fermi level in comparison with the parent metal [2]. That results in a similar electronic structure with noble metals up to the Fermi level. Therefore, TMNs have evolved a potential candidate for the noble metal material catalyst and consequently represented better activity i.e. for electrochemical ammonia synthesis [3–5] and solar thermochemical ammonia production [6–8] when compared with pure metals [9]. For catalytic nitrogen reduction to ammonia, these TMNs have the extra benefit over pure transition metals since nitrogen atoms are already incorporated in their structure. That means nitrogen atoms in the first surface layer of the TMNs can in principle be reduced directly to ammonia and leave a N-vacancy on the surface. This N-vacancy then needs to be replenished by adsorbing N_2 molecule to endure the catalytic cycle [10]. This is known as a Mars-van Krevelen (MvK) mechanism [11]. In many cases, N_2 adsorption to the N-vacant site(s) becomes an exothermic process on TMNs [4] compared to when N_2 needs to be adsorbed on pure transition metals [9,12] or on clean TMNs [13], which is usually endothermic. Therefore, it is interesting to investigate catalytic reactions like nitrogen activation on these TMN surfaces via a MvK mechanism where its feasibility has recently been reported on different TMNs [3,4,10,14]. All these characteristics mentioned above, together with high resistance against corrosion and high

* Corresponding author.
E-mail address: egillsk@hi.is (E. Skúlason).

http://dx.doi.org/10.1016/j.cattod.2016.06.009
0920-5861/

Please cite this article in press as: Y. Abghoui, E. Skúlason, Electrochemical synthesis of ammonia via Mars-van Krevelen mechanism on the (111) facets of group III–VII transition metal mononitrides, Catal. Today (2016), http://dx.doi.org/10.1016/j.cattod.2016.06.009

G Model
CATTOD-10245; No. of Pages 7
ARTICLE IN PRESS

melting points, make TMNs a promising choice for the cathode electrode material of some electrochemical reactions like the Nitrogen Electroreduction Reaction (NER).

NER is considered an important electrochemical approach for conversion and storage of renewable energy via nitrogen activation and electrochemical ammonia formation. Ammonia is extremely attractive as an energy carrier and a transportation fuel owing to its high energy density and lack of CO_2 emissions [15]. Such renewable approach to produce ammonia is also important for decentralized and evenly distributed production of fertilizers throughout the world. If that were realized, the sophisticated infrastructures and economical-intensive operational conditions needed for the Haber-Bosch process would be surmounted. Therefore, successful NER can help develop environmentally and economically friendly methodologies for growing a new energy economy.

The simplest catalyst for electrochemical ammonia formation would be a pure transition metal catalyst. However, many of these metals require a relatively large overpotential of up to −1.5 V vs. standard hydrogen electrode (SHE) to activate nitrogen and form ammonia in 1 M aqueous electrolyte (pH = 0) at room temperature [9], where the equilibrium potential for ammonia formation is around +0.06 V. In addition to susceptibility of some of these pure metals to readily form oxides, the formation of H_2(g) is very fast on most of them and severely hinder the production of ammonia on those surfaces. Recent theoretical studies revealed the possibility of employing under-coordinated molybdenum nanoclusters, with [3] and without [16] a nitrogen skin, for nitrogen activation and electrochemical ammonia formation. There it was found that ammonia can be formed at −0.6 V vs. SHE but the N-vacant sites that are created in that process get poisoned with oxygen from the electrolyte [17]. This led us to the idea of using a computational search to find a TMN that would be active for nitrogen electroreduction to ammonia via a MvK mechanism but at the same time free of poisoning from the electrolyte [4]. There it was shown that the energy lowest surface facets of the earlier TMNs are the (100) facets of the rocksalt (RS) structures whereas the (110) facets of the zincblende (ZB) structures were energy lowest for the later TMNs when comparing the energetics of RS(100), RS(111), ZB(110) and ZB(100) facets using electronic structure calculations [4]. The most active and selective nitride surfaces that catalyze nitrogen activation to ammonia electrochemically at ambient conditions and relatively small overpotentials turned out to be the RS(100) facets [4,14]. However, the RS(111) facets of earlier TMNs are also one of the most prevalent texture orientations when characterizing the manufactured TMN surfaces [18–21] and those deserve a detailed theoretical investigation for their NER activity.

In this study, we use theoretical calculations to screen for a stable and active catalyst amongst a range of RS(111) TMN surfaces for catalyzing electrochemical nitrogen activation and producing ammonia. DFT calculations are used to study the thermodynamics of the cathode reaction. Free energy diagrams are constructed for the electrochemical protonation of surface nitrogen or metal atoms to obtain onset potentials required for ammonia synthesis on these types of mononitride structures. The effect of an external bias is included by using the computational standard hydrogen electrode [22], and the lowest onset potential required to produce ammonia is estimated for each nitride. Stability of the active sites in electrochemical environment and poisoning of the catalyst under an applied bias are also considered. The likelihood of catalyst regeneration over decomposition was also investigated for the most interesting candidates of this RS(111) materials. In addition, the competing hydrogen evolution reaction (HER) on all these nitride surfaces was explicitly investigated within our mechanistic model and the TMN with higher selectivity towards HER were eliminated from the rest of study.

2. Methodology

2.1. Computations

All calculations were conducted with density functional theory (DFT) using the RPBE exchange correlation functional [23]. A plane wave basis set with an energy cutoff of 350 eV was used to represent the valence electrons with a PAW representation [24] of the core electrons as implemented in the VASP code [25,26]. Our test calculations confirm that the effect of employing higher cutoff value (500 eV) is as small as 20–45 meV on adsorption energy of the species on the surface. Therefore, 350 eV was chosen as relatively fair compromise between accuracy and speed. Iterative diagonalization of the Kohn–Sham Hamiltonian was used to determine the self-consistent electron density, with the occupation of the Kohn–Sham states being smeared according to a Fermi–Dirac distribution with a smearing parameter of $k_BT = 0.1$ eV. The k-point sampling used for all the surfaces was a $4 \times 4 \times 1$ Monkhorst–Pack sampling.

A five-layer slab with four metal atoms and four nitrogen atoms in each layer was used to model each nitride. The bottom two layers were fixed whereas the top layers as well as the adsorbed species were allowed to fully relax. Boundary conditions were periodic in the x and y directions and surfaces were separated by 12 Å of vacuum in the z direction. The structural optimization was considered converged when the forces in any direction on all moveable atoms were below 0.01 eV Å^{-1}. The RPBE lattice constants used in this study were: ScN: 4.56 Å, TiN: 4.29 Å, VN: 4.17 Å, CrN: 4.19 Å, MnN: 4.21 Å, YN: 4.95 Å, ZrN: 4.65 Å, NbN: 4.48 Å, MoN: 4.40 Å, HfN: 4.57 Å, TaN: 4.44 Å, WN and ReN: 4.37 Å. These RPBE-calculated lattice constants are 1–2% from the experimental values.

2.2. Reaction pathways and electrochemical modeling

The cathode reaction of the electrochemical process is:

$$N_2 + 6(H^+ + e^-) \rightleftharpoons 2NH_3 \quad (1)$$

The source of protons could be either water splitting or H_2 in the anode reaction. But we refer to H_2 here only as a convenient source of protons and electrons to link our absolute potential vs. SHE [22]:

$$H_2 \rightleftharpoons 2(H^+ + e^-) \quad (2)$$

We consider a heterogeneous MvK mechanism where two surface N atoms are reduced to make $2NH_3$ and the created nitrogen vacancies (dimer N-vacancy) are then replenished with solvated N_2 from the electrolyte. The single N-vacancy approach studied for the (100) facets [4,14] is not applicable here due to the closely packed structure of the (111) surfaces where N atoms are protruded from the surface. Hydrogenation of the surface is carried out by adding H atoms one-by-one to the surface to represent a proton from the solution and an electron from the electrode. For protonation, all the possible adsorption sites on the surface are investigated and the most stable site and accordingly the most stable intermediate are taken into account for upcoming protonation steps. In this approach we therefore do not constrain the protons to adsorb to a given atom or a molecule on the surface, and therefore we call this an unconstrained MvK mechanism. The hypothetical reaction mechanism is shown in Eqs. (3)–(11):

$$* + 6(H^+ + e^-) + N_2 \rightleftharpoons *H + 5(H^+ + e^-) + N_2 \quad (3)$$

$$*H + 5(H^+ + e^-) + N_2 \rightleftharpoons *2H + 4(H^+ + e^-) + N_2 \quad (4)$$

$$*2H + 4(H^+ + e^-) + N_2 \rightleftharpoons *3H + 3(H^+ + e^-) + N_2 \quad (5)$$

Please cite this article in press as: Y. Abghoui, E. Skúlason, Electrochemical synthesis of ammonia via Mars-van Krevelen mechanism on the (111) facets of group III–VII transition metal mononitrides, Catal. Today (2016), http://dx.doi.org/10.1016/j.cattod.2016.06.009

G Model
CATTOD-10245; No. of Pages 7
ARTICLE IN PRESS
Y. Abghoui, E. Skúlason / Catalysis Today xxx (2016) xxx–xxx

$$*3H + 3(H^+ + e^-) + N_2 \rightleftharpoons *^{-N} + NH_3 + 3(H^+ + e^-) + N_2 \quad (6)$$

$$*^{-N} + NH_3 + 3(H^+ + e^-) + N_2 \rightleftharpoons *^{-N} + NH_3 + *H + 2(H^+ + e^-) + N_2 \quad (7)$$

$$*^{-N} + NH_3 + *H + 2(H^+ + e^-) + N_2 \rightleftharpoons *^{-N} + NH_3 + *2H + (H^+ + e^-) + N_2 \quad (8)$$

$$*^{-N} + NH_3 + *2H + (H^+ + e^-) + N_2 \rightleftharpoons *^{-N} + NH_3 + *3H + N_2 \quad (9)$$

$$*^{-N} + NH_3 + *3H + N_2 \rightleftharpoons *^{-2N} + 2NH_3 + N_2 \quad (10)$$

$$*^{-2N} + N_2 + 2NH_3 \rightleftharpoons * + 2NH_3 \quad (11)$$

An asterisk (*) represents a site on the surface. A nitrogen vacancy in the surface layer is denoted as $*^{-N}$ and a dimer N-vacancy as $*^{-2N}$. DFT calculations are used to calculate the minimum energy configuration of each species on the surface and adsorption energies of all intermediates according to reactions (3)–(11). Various surface sites are considered and the optimal binding site is identified. It is assumed that activation barriers between stable minima can be neglected during the electrochemical reactions. The free energy of each elementary step is estimated at pH = 0 according to:

$$\Delta G(0) = \Delta E + \Delta E_{ZPE} - T\Delta S \quad (12)$$

$\Delta G(0)$ is the free energy change of the reaction at zero potential, and ΔE is the reaction energy calculated with DFT. The zero-point energy correction (ΔE_{ZPE}) and entropy differences (ΔS) including entropy changes from the solids are calculated within a harmonic approximation and the values of these are given elsewhere [14]. The effect of an applied bias, U, is included implicitly for all electrochemical reaction steps by shifting the free energy for reactions involving n electrons by $-neU$, where $\Delta G(U)$ is the free energy change of the reaction at onset potential:

$$\Delta G(U) = \Delta G(0) - neU \quad (13)$$

3. Results and discussion

3.1. Catalytic activity

We studied the possibility of catalyzing electrochemical nitrogen activation to ammonia via a MvK mechanism as given in Eqs. (3)–(11) on the RS(111) facets of earlier TMNs, where upon protonation of the surface (with consideration of all the feasible adsorption sites for H) two nitrogen atoms were reduced to ammonia and two nitrogen vacant sites created before the catalyst gets replenished by solvated nitrogen molecules in the system. For all the nitrides studied here it was found that during surface protonation, the most energetically favorable adsorption site for protons was on surface nitrogen atoms, except for TaN where the proton adsorbs rather to a Ta atom first. In all cases (except for TaN) none of the metallic atoms on the surface bind H stronger than the surface N atoms. This means that when considering 4 nitrogen atoms and 4 metallic atoms on the surface per unit cell, the most thermodynamically favorable intermediate is *NH and not the *M (adsorption on metallic sites). Successive protonation of the surface resulted in population of all the surface nitrogen atoms (formation of 4*NH on the surface or a 4/8 monolayer (ML) coverage) without any favorable adsorption of H on metal atoms. Subsequent protonation resulted in the formation of either $1*NH_2$ (on the surface of HfN, VN, CrN, WN, and MnN), or $2*NH_2$ (on the surface of ZrN, MoN, and NbN) prior to formation of the first ammonia molecule (see Fig. 1). On the surfaces of ScN, TiN and YN, after formation of *4NH, successive protonation of the surface contributed to formation of $*4NH_2$ without formation of any $*NH_3$ intermediate. Thus, 1ML coverage on these three surfaces did not lead to any ammonia formation. For TiN addition of extra proton, the 9th proton, caused formation of $*NH_3$ species and then ammonia formation. But for ScN and YN, this addition caused recombination of surface H adatoms and evolution of H_2 instead. Therefore, ScN and YN are excluded from the rest of study, as they cannot be used to activate nitrogen to ammonia. TaN was also found different than the other nitrides in a way that the first proton binds the Ta metal ion stronger than a N ion on the surface, but thereafter the next proton binds to the surface N and forms *NH. Like ScN and YN, TaN was also found of better activity for forming H_2 rather than ammonia. ReN was found unstable upon geometry optimization and also excluded from the rest of study. The free energy of all intermediates is calculated according to Eq. (12), with reference to N_2 and H_2 in the gas phase. The free energy diagram for CrN and MnN is presented in Fig. 1 and the remaining free energy diagrams are shown in Fig. S1 of the supplementary material, where a pathway towards NH_3 formation via a dimer-vacancy MvK mechanism is illustrated and the effect of applied bias is included. The potential-determining step (PDS) and the measure of the catalytic activity towards nitrogen activation to ammonia on each of the nitrides are identified as the elementary reaction step with the largest increase in free energy (ΔG). If this elementary step is a proton-electron transfer step, it can be eliminated by applying a bias and thus shift the free energy landscape in such a way that all reactions steps become downhill in free energy.

As can be seen for CrN, the PDS is the seventh protonation step after formation of the first ammonia, with $\Delta G_{PDS} = 0.71$ eV. Thus, by applying an external bias of -0.71 V vs. SHE, this increase in free energy can be eliminated and all electrochemical steps will then be downhill in free energy. For those steps that do not involve electron transfer, however, there is no favorable change in the free energy when applying an external bias. This is seen for MnN, for example, where the fifth protonation step is the PDS by 0.54 eV, but filling the dimer-vacancy being a non-proton/electron transfer step becomes very uphill in free energy (1.36 eV) and cannot be surpassed by an external applied bias. So it becomes a RDS and temperature or pressure modification is required to speed up this step. For all the other (111) nitrides, addition of N_2(g) to fill the dimer-vacancy is exothermic occurring spontaneously under ambient conditions. The free energy change of the PDS of each nitride is shown in Fig. 2. Most of the nitrides exhibit relatively low onset potentials towards ammonia formation, with the exception of TiN, ZrN and HfN.

It was found that for most of the nitrides studied here, there were $8(H^+ + e^-)$ needed for activation of nitrogen and formation of two ammonia molecules. The only exceptions were WN, TiN, and ZrN for which 9, 10, and $10(H^+ + e^-)$ were required for formation of two ammonia molecules, respectively. Of course, only $6(H^+ + e^-)$ are needed to make $2NH_3$, and these "extra" H^+/e^- couples do not indicate that we have a loss of efficiency since they will be converted later on to ammonia. Hence the picture is as follows; we start by loading the nitride with H^+/e^- couples and we create NH and NH_2 species on the surface until ammonia is formed. According to Fig. 2, the most interesting nitrides are those with ΔG_{PDS} close to or preferentially less than 1 eV. Here, we predict that we do not have any H_2 formation which makes this much more promising and efficient than the pure metals that will convert

Please cite this article in press as: Y. Abghoui, E. Skúlason, Electrochemical synthesis of ammonia via Mars-van Krevelen mechanism on the (111) facets of group III–VII transition metal mononitrides, Catal. Today (2016), http://dx.doi.org/10.1016/j.cattod.2016.06.009

G Model
CATTOD-10245; No. of Pages 7
ARTICLE IN PRESS

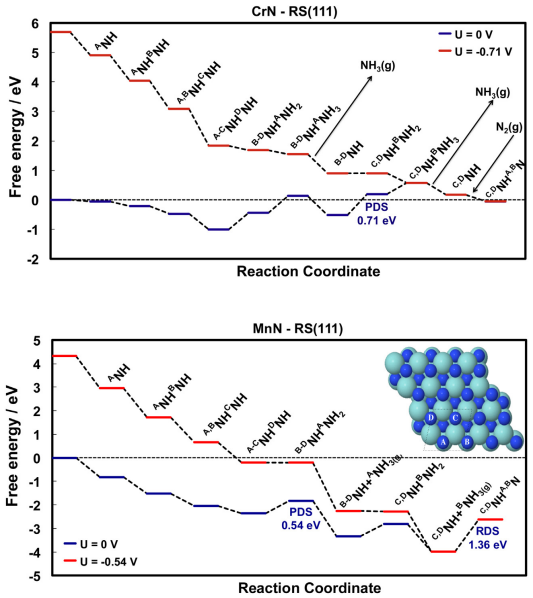

Fig. 1. Free energy diagram (FED) for nitrogen activation to ammonia via a dimer-vacancy MvK mechanism on CrN and MnN. For CrN the PDS is the seventh protonation step with ΔG_{PDS} = 0.71 eV. The blue line indicates the free energy of all the stable intermediates calculated at zero potential vs. SHE. The red line represents the free energy of all the stable intermediates at the onset potential. For MnN the PDS is the fifth protonation step while there is also a rate-determining step (RDS) to fill the dimer-vacancy with ΔG_{RDS} = 1.36 eV. As the RDS involves no proton-electron transfer, applying the bias cannot change the free energy landscape in a way surmounting the increase in free energy of this step. The top view of the RS (111) metal nitride unit cell is shown in the inset where it has been repeated once in the lateral directions. Cyan spheres represent metal atoms and dark blue spheres represent nitrogen atoms. The N atoms of the TMNs are labeled A, B, C and D and the adsorption site at each step of the FEDs are indicating which N atoms are reduced each time. The ^{A,B}N labeling of the final step indicates that a dimer-vacancy has been filled by dissociating N_2. (For interpretation of the references to color in this figure legend, the reader is referred to the web version of this article.)

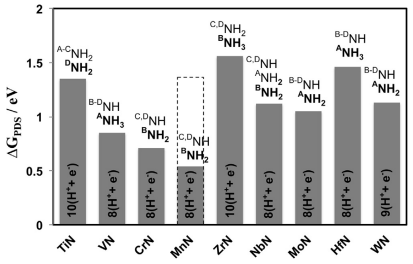

Fig. 2. Free energy change of the PDS (ΔG_{PDS}, in eV) of nitrogen activation to ammonia on the (111) facets of the RS structures of TMN surfaces. The labels above each bar indicate the species formed prior to PDS and the bold texts indicate the species formed right at the PDS, the notation of which is explained in Fig. 1. For MnN, the RDS coming from filling the vacancy is also included with a dashed-bar.

most of the electricity to H_2 [9]. The candidate having the lowest onset potential for ammonia formation according to this study seems to be MnN with ΔG_{PDS} = 0.54 eV or U = −0.54 V vs. SHE. But according to the free energy diagram illustrated in Fig. 1, filling the dimer-vacancy that is necessary for regeneration of the catalyst is 1.36 eV endothermic. This step becomes the RDS for the reaction, which cannot be tuned by applying external bias and therefore is very difficult and slow at ambient conditions. So MnN is not a good catalyst at room temperature and pressure, but it could be a very good reactant for ammonia formation [6], where both theoretical [27] and experimental [28] studies show that it is thermodynamically stable in NaCl type structure, and this stoichiometry (MnN) is more stable than other phases like Mn_4N, $Mn_2N_{0.86}$, Mn_3N_2. CrN and VN, however, seem very interesting material with relatively low onset potentials for nitrogen activation and ammonia formation. NbN, MoN and WN are predicted to have only slightly higher overpotential (slightly more negative onset potentials) and those could also be interesting candidates for this process.

Another interesting observation is the clear trend found in Fig. 2 for the catalytic activity (or the onset potential) of these nitrides. As can be seen, the activity increases from left to the right of the periodic table. Therefore, we explored if any correlation between the activity and a material dependent descriptor could be found. The onset potential predicted for ammonia formation was found to correlate well with the dissociation energy of di-nitrogen in a

Please cite this article in press as: Y. Abghoui, E. Skúlason, Electrochemical synthesis of ammonia via Mars-van Krevelen mechanism on the (111) facets of group III–VII transition metal mononitrides, Catal. Today (2016), http://dx.doi.org/10.1016/j.cattod.2016.06.009

G Model
CATTOD-10245; No. of Pages 7
ARTICLE IN PRESS
Y. Abghoui, E. Skúlason / Catalysis Today xxx (2016) xxx–xxx

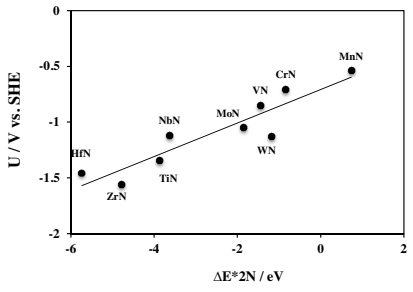

Fig. 3. The onset potential of ammonia formation on the (111) facets of the RS structure of TMNs as a function of the chemisorption energy of two N adatoms in a dimer vacancy.

dimer N-vacancy. This correlation is shown in Fig. 3 where the onset potential of these materials becomes less negative as the dissociative energy of di-nitrogen on the vacant sites becomes more positive. However as the dissociative energy becomes more endothermic, the harder it is to regenerate the N-vacancies as can be seen for the MnN in Figs. 1–3. That means that the best material is the one that compromises both features; the onset potential and the ability to regenerate the vacant sites. This is a volcano-like feature where the left leg determines the onset potential but the right leg determines the rate of regenerating the catalyst.

3.2. Poisoning of the surface vacancy

The catalytic activity of these nitrides was investigated via MvK mechanism due to the potential benefit these materials offer by the explicit incorporation of nitrogen in their surfaces. After surface Ns have reacted and surface vacancies created at the surface, these vacancies must be filled with N_2 from the electrolyte for the catalytic cycle to endure. However, the vacancy might rather get filled with a proton, O or OH species from the aqueous electrolyte, all of which could block these surface sites and avoid filling of the N-vacancies with nitrogen. Thus, the competition between N with O, H and OH for filling the surface vacancy is investigated by considering the free energy of filling the vacancy with any of these species relative to nitrogen ($\Delta G(^*2N\text{-}^*X)$), where X = O, H or OH). The source of these ions are from the water in the electrolyte that results in formation of O^{2-}, OH^- and H^+ under operating conditions. We calculate the difference in adsorption energy of these species compared to adsorbing N_2 (where two N atoms adsorb to the dimer N-vacancy) at the onset potential of ammonia formation. Therefore, these free energies are referenced to N_2, H_2O and H_2 in the gas phase. A negative value of $\Delta G(^*2N\text{-}^*X)$ indicates that it is thermodynamically favorable to fill the vacancy with nitrogen, rather than other three species. These values are shown in Fig. 4 for all the catalytically active nitrides.

It can be seen that N atoms bind more strongly to the surface vacancy compared with O for all nitrides. Thus the surface vacancies are unlikely to get poisoned by this species. N atoms also bind more strongly to the surface vacancy compared with OH species for all the nitrides except for MnN and WN. For poisoning by H, however, it can be seen that the surface vacancy in MnN and WN is likely to be filled by H, rather than N, whereas CrN is only slightly more favorable to adsorb H rather than N but that is within the uncertainty of these calculations. For the remaining nitrides, the vacancy is expected to replenish by nitrogen and consequently the catalytic cycle may continue to form NH_3.

As can be seen from this analysis of the possibility of poisoning the N-vacancies, H might block the surface vacancy on CrN. If that is the case, CrN will have difficulties to regenerate itself by replenishing of the surface vacancy with nitrogen and consequently the catalytic cycle might cease. For the other promising candidates; VN, NbN and MoN, the binding energies of O, H and OH are weaker to the surface vacancy when compared with nitrogen and thus it should replenish the surface vacancy under the applied potential in the electrochemical environment.

Overall, when considering both the activity (Fig. 2) and the possibility of poisoning (Fig. 4) the most promising candidates are CrN and VN (where MnN has been ruled out because of regeneration issue) and the second most promising candidates are NbN and MoN (where WN has been ruled out because of poisoning issue). These nitrides should reduce nitrogen to ammonia at potentials around −0.7 V to −1.1 V. The onset potential required for the reaction on CrN is only −0.71 V vs. SHE that makes it very interesting. Therefore, more detailed stability assessment of N-vacancy

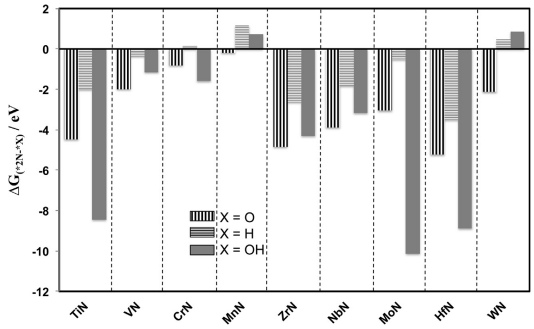

Fig. 4. Free energy of adsorption of O, H or OH relative to dissociated nitrogen on the surface vacancy of catalytically active nitrides. Free energies are calculated relative to N_2(g), H_2(g) and H_2O(g). All free energies are evaluated at the calculated onset potential for each nitrides, TiN: −1.35 V, VN: −0.85 V, CrN: −0.71 V, MnN: −0.54 V, ZrN: −1.56 V, NbN: −1.12 V, MoN: −1.05 V, HfN: −1.46 V, and WN: −1.13 V.

Please cite this article in press as: Y. Abghoui, E. Skúlason, Electrochemical synthesis of ammonia via Mars-van Krevelen mechanism on the (111) facets of group III–VII transition metal mononitrides, Catal. Today (2016), http://dx.doi.org/10.1016/j.cattod.2016.06.009

G Model
CATTOD-10245; No. of Pages 7
ARTICLE IN PRESS

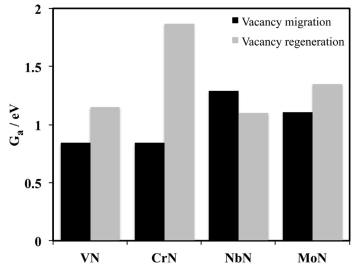

Fig. 5. Calculated activation free energies (G_a) of regenerating the catalyst by N_2 dissociation for replenishment of the N-vacancy compared with activation free energies of vacancy migration into the bulk (migration of nitrogen atoms from the bulk towards the surface).

is carried out for these four nitrides in section 3.3 where competition between catalyst decomposition and regeneration is taken into account. Despite high stability of TiN, ZrN, and HfN against poisoning, they are not that interesting with very negative onset potentials of around −1.5 V vs. SHE required for ammonia formation. Thus these last three nitrides are excluded from the stability analysis of N-vacancy in the following section.

3.3. Regenerating active sites on the surfaces

As already explained, in a MvK mechanism, ammonia is formed via reacting surface N atoms and forming N-vacancy on the surface that must be replenished for the catalytic cycle to endure. However, there exists the possibility that the N-vacancy migrates to the bulk of the nitride (i.e. N atoms from the bulk migrate to the surface) instead of being replenished with a nitrogen molecule from the solution. If that is the case, the nitride will decompose to ammonia and its parent metal and the catalytic cycle will cease. For a detailed assessment whether active sites are regenerated on the surfaces, the competition between migration of the N-vacancy from the surface into the bulk and regeneration of the N-vacancy with N_2 is studied for the most interesting nitride candidates; VN, CrN, NbN and MoN, see Fig. 5. If the vacancy is likely to replenish faster than it migrates into the bulk, the catalyst is likely to be able to regenerate and the catalytic cycle to endure. The free energy activation barriers (G_a) for both processes are calculated, where $G_a = E_a$ for the vacancy migration process, but $G_a = E_a + 0.6$ eV for the process of replenishing the vacancy (catalyst regeneration). When molecular nitrogen splits and binds to the vacancies, it looses 0.6 eV of entropy at room temperature going from gas phase to the adsorbed state on the surface. The entropy loss of molecular nitrogen is taken from Ref. [29].

Whereas VN, CrN and MoN all showed relatively good activity (Fig. 2) and low probability of being poisoned from the electrolyte (except perhaps CrN which could get poisoned from adsorption of protons, see Fig. 4), there are lower activation barriers found for migration of the N vacancy into the bulk (first step of decomposition) compared to regeneration of the N vacancy with nitrogen. That implies that the rate of decomposition should be faster than the rate of regeneration and accordingly these three nitrides should decompose to ammonia and their parent metal under operating conditions. NbN, however, seems very interesting in the sense that it should regenerate itself and thus endure the catalytic cycle of ammonia formation on its surface, since the activation barrier of migration is higher than the barrier for regenerating the N-vacancies with N_2 molecules.

4. Conclusions

A theoretical analysis of the possibility of nitrogen activation for electrochemical ammonia formation in an aqueous electrolyte at ambient conditions was investigated on the (111) facets of the rock-salt structure of ScN, TiN, VN, CrN, MnN, YN, ZrN, NbN, MoN, HfN, TaN, WN, and ReN. Except ScN, YN, and TaN that were found more selective for hydrogen evolution reaction, other (111) nitride surfaces were found more selective toward nitrogen electroreduction reaction under electrochemical environment. VN, CrN and MnN were found to have the lowest onset potential (from −0.8 V to −0.5 V vs. SHE) among all the nitrides studied here but NbN, MoN and WN have also relatively low onset potentials (around −1.1 V vs. SHE). However, MnN and WN were found susceptible to poisoning in electrochemical media, and MnN has also a very endothermic reaction step to adsorb N_2 to the N-vacancies and those cannot be regenerated. For the remaining nitrides, VN, CrN, NbN, and MoN, kinetics were taken into account in order to conclude whether the N vacancies created during the catalytic cycle will be regenerated with N_2 molecules or will be unstable and migrate into the bulk of the nitride. When calculating the free energy activation barriers of both these processes, we show that only NbN is a promising candidate that can be regenerated and endure the catalytic cycle of nitrogen activation and ammonia formation under operating conditions and the remaining candidates should decompose to ammonia and their parent metals under operating conditions.

Acknowledgements

Financial support is acknowledged from the Icelandic Research Fund and the Research Fund of the University of Iceland. The calculations were in part carried out on the Nordic high performance computer (Gardar).

Appendix A. Supplementary data

Supplementary data associated with this article can be found, in the online version, at http://dx.doi.org/10.1016/j.cattod.2016.06.009.

References

[1] L.E. Toth, Transition Metal Carbides and Nitrides, Refractory Materials, vol. 7, Academic Press, New York and London, 1971.
[2] E. Siegel, d-bandwidth contraction upon metalloid formation: a resolution of the bonding controversy in transition metal carbides, nitrides and borides, Semicond. Insul. 5 (1979) 47–60.
[3] J. Howalt, T. Vegge, Electrochemical ammonia production on molybdenum nitride nanoclusters, Phys. Chem. Chem. Phys. 15 (2013) 20957–20965.
[4] Y. Abghoui, A.L. Garden, V.F. Hlynsson, S. Björgvinsdóttir, H. Ólafsdóttir, E. Skúlason, Enabling electrochemical reduction of nitrogen to ammonia at ambient conditions through rational catalyst design, Phys. Chem. Chem. Phys. 17 (2015) 4909–4918.
[5] I. Matanović, F.H. Garzon, N.J. Henson, Electro-reduction of nitrogen on molybdenum nitride: structure, energetics, and vibrational spectra from DFT, Phys. Chem. Chem. Phys. 16 (2014) 3014–3026.
[6] R. Michalsky, P.H. Pfromm, An ionicity rationale to design solid phase metal nitride reactants for solar ammonia production, J. Phys. Chem. C 116 (2012) 23243–23251.
[7] R. Michalsky, P.H. Pfromm, A. Steinfeld, Rational design of metal nitride redox materials for solar-driven ammonia synthesis, Interface Focus 5 (2015) 20140084.
[8] R. Michalsky, A.M. Avram, B.A. Peterson, P.H. Pfromm, A.A. Peterson, Chemical looping of metal nitride catalysts: low-pressure ammonia synthesis for energy storage, Chem. Sci. 6 (2015) 3965–3974.
[9] E. Skúlason, T. Bligaard, S. Gudmundsdóttir, F. Studt, J. Rossmeisl, F. Abild-Pedersen, T. Vegge, H. Jónsson, J.K. Nørskov, A theoretical evaluation of possible transition metal electro-catalysts for N2 reduction, Phys. Chem. Chem. Phys. 14 (2012) 1235–1245.

Please cite this article in press as: Y. Abghoui, E. Skúlason, Electrochemical synthesis of ammonia via Mars-van Krevelen mechanism on the (111) facets of group III–VII transition metal mononitrides, Catal. Today (2016), http://dx.doi.org/10.1016/j.cattod.2016.06.009

G Model
CATTOD-10245; No. of Pages 7
ARTICLE IN PRESS

[10] C.D. Zeinalipour-Yazdi, J.S.J. Hargreaves, C.R.A. Catlow, Nitrogen activation in a Mars-Van Krevelen mechanism for ammonia synthesis on Co3Mo3N, J. Phys. Chem. C (2015) 1–18.
[11] P. Mars, D.W. Van Krevelen, Special supplement to chemical engineering science, Eng. Sci. 3 (1954) 41–45.
[12] Á. Logadóttir, J.K. Nørskov, Ammonia synthesis over a Ru(0001) surface studied by density functional calculations, J. Catal. 220 (2003) 273–279.
[13] Y. Abghoui, E. Skúlason, Mechanistic study of nitrogen activation to ammonia on transition metal nitride electro-catalysts, Catal. Today (2016).
[14] Y. Abghoui, A.L. Garden, J.G. Howalt, T. Vegge, E. Skúlason, Electroreduction of N2 to ammonia at ambient conditions on mononitrides of Zr, Nb, Cr, and V: a DFT guide for experiments, ACS Catal. (2015) 635–646.
[15] A. Klerke, C.H. Christensen, J.K. Nørskov, T. Vegge, Ammonia for hydrogen storage: challenges and opportunities, J. Mater. Chem. 18 (2008) 2304–2310.
[16] J.G. Howalt, T. Bligaard, J. Rossmeisl, T. Vegge, DFT based study of transition metal nano-clusters for electrochemical NH3 production, Phys. Chem. Chem. Phys. 15 (2013) 7785–7795.
[17] J. Howalt, T. Vegge, The role of oxygen and water on molybdenum nanoclusters for electro catalytic ammonia production, Beilstein J. Nanotechnol. 5 (2014) 111–120.
[18] P. Hones, R. Sanjines, F. Levy, Characterization of sputter-deposited chromium nitride thin films for hard coatings, Surf. Coat. Technol. 94 (1997) 398–402.
[19] E. Gillan, R. Kaner, Rapid solid-state synthesis of refractory nitrides, Inorg. Chem. 768 (1994) 5693–5700.
[20] H.J. Ramos, N.B. Valmoria, Thin-film deposition of ZrN using a plasma sputter-type negative ion source, Vacuum 73 (2004) 549–554.
[21] S. Shayestehaminzadeh, T.K. Tryggvason, F. Magnus, S. Olafsson, J.T. Gudmundsson, Ultra-thin poly-crystalline TiN films grown by HiPIMS on MgO(100)—in-situ resistance study of the initial stage of growth, Thin Solid Films 549 (2013) 199–203.
[22] J.K. Nørskov, J. Rossmeisl, A. Logadottir, L. Lindqvist, J.R. Kitchin, T. Bligaard, H. Joinsson, Origin of the overpotential for oxygen reduction at a fuel-cell cathode, J. Phys. Chem. B 108 (2004) 17886–17892.
[23] B. Hammer, L. Hansen, J. Nørskov, Improved adsorption energetics within density-functional theory using revised Perdew-Burke-Ernzerhof functionals, Phys. Rev. B 59 (1999) 7413–7421.
[24] P. Blöchl, Projector augmented-wave method, Phys. Rev. B 50 (1994) 17953–17979.
[25] G. Kresse, J. Hafner, Ab initio molecular dynamics for liquid metals, Phys. Rev. B 47 (1993) 558–561.
[26] G. Kresse, J. Furthmüller, Efficient iterative schemes for ab initio total-energy calculations using a plane-wave basis set, Phys. Rev. B Condens. Matter 54 (1996) 11169–11186.
[27] R. Yu, X. Chong, Y. Jiang, R. Zhou, W. Yuan, J. Feng, The stability electronic structure, elastic and metallic properties of manganese nitrides, RSC Adv. 5 (2015) 1620–1627.
[28] K. Suzuki, T. Kaneko, H. Yoshida, Y. Obi, H. Fujimori, H. Morita, Crystal structure and magnetic properties of the compound MnN, J. Alloys Compd. 306 (2000) 66–71.
[29] D.R. Lide, CRC Handbook of Chemistry and Physic, 78th ed., Florida, 1997.

Please cite this article in press as: Y. Abghoui, E. Skúlason, Electrochemical synthesis of ammonia via Mars-van Krevelen mechanism on the (111) facets of group III–VII transition metal mononitrides, Catal. Today (2016), http://dx.doi.org/10.1016/j.cattod.2016.06.009

IV Article 4

Onset Potentials for Different Reaction Mechanisms of Nitrogen Activation to Ammonia on Transition Metal Nitride Electro-catalysts

Younes Abghoui and Egill Skúlason

Catalysis Today, in press (2016).

G Model
CATTOD-10482; No. of Pages 9
ARTICLE IN PRESS

Catalysis Today xxx (2016) xxx–xxx

Contents lists available at ScienceDirect

Catalysis Today

journal homepage: www.elsevier.com/locate/cattod

Onset potentials for different reaction mechanisms of nitrogen activation to ammonia on transition metal nitride electro-catalysts

Younes Abghoui, Egill Skúlason*

University of Iceland, Reykjavik, Iceland

ARTICLE INFO

Article history:
Received 31 March 2016
Received in revised form 9 November 2016
Accepted 25 November 2016
Available online xxx

Keywords:
Nitrogen activation
Electrochemical ammonia formation
DFT calculations
Transition metal nitrides
Reaction mechanisms
Mars-van Krevelen mechanism

ABSTRACT

Recent theoretical calculations with DFT suggest that transition metal nitrides (TMNs) are promising materials to catalyze N_2 electroreduction to ammonia at ambient conditions. To realize which mechanism is more favourable, we conduct DFT calculations to explore the catalytic activity of these materials in their most stable structures via conventional associative (AM) and dissociative (DM) mechanisms, and then compare the corresponding results with that of Mars-van Krevelen (MvK) mechanism we recently reported. The dissociation of N_2 on the clean surfaces is endothermic on most of these nitrides and the activation barriers large in all cases, which is inhibitive of a DM on these materials. The onset potential predicted for ammonia formation on these TMNs is always less negative via MvK than with AM, except a few cases, where both mechanisms have similar onset potentials. In those cases, the AM is less favourable than MvK since the adsorption of N_2 molecule is endothermic. Therefore, the MvK is almost always the favourable mechanism. We used the computational hydrogen electrode method and neglected any proton-electron transfer reaction barriers in this work but including those will be necessary to make a more definitive statement, which is the subject of future work.

1. Introduction

The use of ammonia as an energy carrier and specially fertilizer has triggered numerous interests in developing alternative routes in pursuit of a more decentralized and environmentally friendly approach for ammonia synthesis. Without ammonia and thus deprived of inorganic fertilizer, almost half the worldís population would be at risk of starvation [1]. Human survival has thus been depending a great deal on the Haber–Bosch process [2], which is the most pivotal industrial installation for catalytic cleavage of N_2 and hydrogenating nitrogen to ammonia heterogeneously over promoted transition metal-based catalysts. Although Ru and Fe within the Haber-Bosch process show good activity for this catalytic conversion, the harsh operational conditions and sophisticated industrial setup of the Haber-Bosch process are all prohibitive to decentralization of ammonia synthesis. This complicates ammonia production in regions with relatively undeveloped infrastructure such as developing countries. Besides, the reliance of this process on natural gases for supplying its necessary hydrogen feedstock not only promotes severe CO_2 emission to the environment but it also makes the production of ammonia and accordingly food susceptible to natural gas price fluctuations and political conflicts in the oil-rich regions. Most importantly, a sustainable process needs to be developed for ammonia production to maintain food supply since at some point natural gas will be depleted.

A few reviews recently appeared in the literature that gather several potential routes for ammonia production [3–5]. In the last few decades, numerous efforts have been made towards manmade ammonia synthesis using photocatalytic [6] and electrochemical [7–12] methods. However, for many of these, it was difficult to regenerate the active nitrogen-fixing complex and only low current efficiencies of 0.1–8% at ambient conditions were obtained. To reach higher yields of ammonia, solid-state proton conductors have been investigated, and that contributed up to 78% conversion of cathodic supplied nitrogen to ammonia [13,14]. A recent study investigated cathodic synthesis of ammonia in a proton conducting double-chamber solid electrolyte cell where a ceramic proton conductor composed of $BaZr_{0.7}Ce_{0.2}Y_{0.1}O_{2.9}$ (BZCY72) was used as electrolyte [15]. The catalyst used as the cathode was a Ni-BZCY72 cermet and a Pt film served as the anodic electrode. The highest production rate achieved was 0.5×10^{-9} mol s^{-1} cm^{-2}, but at −2.4 V and 620 °C. Very recently, Qing and co-authors reported anodic ammonia formation rate of around 2.0×10^{-10} mol s^{-1} cm^{-2} at +1.2 V and 220 °C [16]. They synthesized ammonia directly from N_2

* Corresponding author.
E-mail address: egillsk@hi.is (E. Skúlason).

http://dx.doi.org/10.1016/j.cattod.2016.11.047
0920-5861/

Please cite this article in press as: Y. Abghoui, E. Skúlason, Onset potentials for different reaction mechanisms of nitrogen activation to ammonia on transition metal nitride electro-catalysts, Catal. Today (2016), http://dx.doi.org/10.1016/j.cattod.2016.11.047

G Model
CATTOD-10482; No. of Pages 9
ARTICLE IN PRESS

and steam using a composite electrolyte based on $CsH_5(PO_4)_2/SiO_2$ and Pt/C-loaded carbon paper as both cathode and anode, but the current efficiency was only around 2%. Ionic liquids or molten salts were also found capable of promoting ammonia formation from low efficiencies to sometimes up to 72% but at relatively high temperatures [17–19]. Although low-pressure ammonia synthesis had been achieved, the aforementioned studies yet suffer from the necessity of relatively high temperatures, which leads to increased risk of product decomposition. The use of complex and expensive electrolytes is another downside that hinders commercialization.

There are also studies that investigated low-temperature ammonia synthesis at ambient pressure with the use of polymer electrolyte membranes (PEM) where the ammonia production can be separated from hydrogen feed gas and thus higher ammonia formation yields is achieved. The highest rate of ammonia formation reported in this fashion is 1.13×10^{-8} mol s^{-1} cm^{-2} with a current efficiency of ~90% obtained at 80 °C where $SmFe_{0.7}Cu_{0.3-x}Ni_xO_3$ (x = 0–0.3) was used as the cathode and wet hydrogen as a feed gas [20]. Replacing the H_2 feed gas with water, Kordali and co-authors synthesized ammonia electro catalytically from N_2 and H_2O at room temperature using Ru cathode in a solid polymer electrolyte cell [21]. Only a low rate of ammonia formation (3.4×10^{-12} mol s^{-1} cm^{-2}) with a low efficiency of around 0.28% was achieved at a relatively high potential (~ −1.3 V vs. SHE) mainly due to competing hydrogen evolution reaction (HER) at the cathode. Using directly air and water as feed gases, the highest rate of ammonia synthesis reported thus far is 1.14×10^{-9} mol s^{-1} cm^{-2}, achieved using a mixed NH_4^+/H^+ Nafion membrane [22]. However, again a low efficiency of around 1% is observed at a relatively high overpotential of −1.6 V. What is obvious here is that while solid-state electrolytes or PEMs offer promise as an electrochemical route to ammonia synthesis, they are still in the early stage of development when compared with production rates nearing that of commercial viability ($4.3–8.7 \times 10^{-7}$ mol s^{-1} cm^{-2}) [23].

The above examples clearly indicate that (electro-) catalytic ammonia synthesis is a particularly feasible method due to the potential of utilizing renewable energy sources and mild operating conditions. But finding (electro-) catalysts that are selective enough towards nitrogen electroreduction reaction (NER) and have a low overpotential is challenging. First-principle calculations have been used to provide more insight about the mechanisms of the reaction and to explore new class of materials with higher activity and selectivity towards NER. Using DFT calculations, a few pure transition metals [24] and transition metal nano-clusters [25] were reported capable of ammonia formation. But for majority of the pure transition metals usually large overpotentials are needed to activate nitrogen to ammonia as well as the surfaces of these materials are covered with H adatoms [24]. Thus, there is lack of available sites for adsorption of nitrogen, which inhibits reduction to ammonia. That mainly causes hydrogen evolution reaction (HER) on most of these surfaces instead of ammonia formation. On the early transition metals, however, it is more likely to cover the surface with nitrogen than hydrogen, but those metals are known to readily form oxides and it remains to be seen if they can be used for N_2 activation. Conversely, transition metal nano-clusters were found capable of enhancing the ammonia activity compared to HER. However, the presence of water in the electrochemical environment will reduce the efficiency of these catalysts by blocking its active site due to preferential adsorption of oxygen rather than nitrogen [26]. A DFT study on cobalt molybdenum nitride enlightens that nitrogen vacancies can contribute to weakening of the strong triple bond of N_2 molecule and thus activate it to ammonia via a Mars-van Krevelen [27] (MvK) mechanism at low temperatures. There, a molybdenum triangular cluster can be a possible activation site for nitrogen along with the surface cavity where N_2 is activated by the inner tetrahedral atom of a cobalt cluster [28,29]. Recently, transition metal nitrides (TMNs) were found promising for ammonia formation electrochemically [30–33] and chemically [28,34] via a MvK mechanism and also as redox materials for solar-driven ammonia synthesis [34,35]. The possibility of experimental growth of the thin films of these transition metal nitrides was already shown by i.e. cathodic arc techniques [36], sputter deposition [37], plasma sputter-type negative ion source [38], and HiPIMS techniques [39]. Theoretical investigations show that earlier TMNs are more stable in the (100) facets of the rocksalt (RS) structure [31]. These are ScN, TiN, VN, CrN, MnN, YN, ZrN, NbN, MoN, HfN, TaN, among which the nitrides of Sc, Ti, Y, Hf, and Ta were found more selective toward HER rather than NER. On the other hand, the later TMNs are more stable in the (110) facets of the zincblende (ZB) structures [31]. These are FeN, CoN, NiN, RuN, RhN, PdN, OsN, and IrN. The surfaces of WN, ReN, PtN, CuN, AgN, and AuN showed significant distortion of the surface atoms during relaxation and thus were considered unstable and eliminated from further analysis in this study. In this paper we also include results of the most promising TMNs (ZrN, NbN, CrN and VN) in their ZB(110) structure.

The purpose of the current work is to determine the most probable reaction mechanism, from the overpotential perspective, for nitrogen activation to ammonia at ambient conditions when TMN surfaces are used to catalyze NER. Thus, we consider the most stable structures and texture orientations of these materials, the (100) facets of the RS as well as the (110) facets of the ZB and exclude those found to be more selective for HER. The NER on these materials could proceed through either one or a combination of the following mechanisms: the MvK mechanism that we already investigated and reported before [31,32], the conventional AM and DM. To compare these two latter mechanisms with the MvK mechanism (where a surface N-atom is reduced to ammonia and the N-vacancy created during the process needs to be regenerated later by N_2 molecule from the solution), we consider conventional AM and DM as processes taking place on the clean surfaces without using a N-atom in the first layer of the surface. We calculate the free energy of the intermediates along the reaction path and construct free energy diagrams (FEDs) to estimate the overpotentials required to form ammonia. In the end, we compare the activity of these TMNs for ammonia formation obtained via these conventional AM and DM with that reported via MvK mechanism. By doing this analysis, we can predict which pathway represents higher likelihood of ammonia formation on the surfaces of these TMNs at ambient conditions.

2. Methodology

2.1. DFT calculations

DFT with the RPBE [40] exchange correlation functional was used to carry out all the calculations. A plane wave basis set with an energy cutoff of 350 eV was utilized to represent the valence electrons with a PAW [41] representation of the core electrons as implemented in the VASP code [42,43]. The self-consistent electron density was determined by the use of iterative diagonalization of the Kohn–Sham Hamiltonian, with the occupation of the Kohn–Sham states being smeared according to a Fermi–Dirac distribution with a smearing parameter of kBT = 0.1 eV. A $4 \times 4 \times 1$ Monkhorst–Pack K-point sampling was used for all the surfaces. We modeled a five-layer nitride slab with four metal atoms and four nitrogen atoms in each layer. The bottom two layers were frozen and the uppermost layers as well as the adsorbed species were allowed to relax. To test convergence with respect to system size, we have carried out some test calculations for i) larger slabs in x and y directions to mimic lower concentration of defects, and ii) increased the number of layers in the slab. Fig. S1 in the supplementary information compares the energy difference of the N-vacancy

Please cite this article in press as: Y. Abghoui, E. Skúlason, Onset potentials for different reaction mechanisms of nitrogen activation to ammonia on transition metal nitride electro-catalysts, Catal. Today (2016), http://dx.doi.org/10.1016/j.cattod.2016.11.047

G Model
CATTOD-10482; No. of Pages 9
ARTICLE IN PRESS

being in the first layer to that being in the second layer, third layer and in the middle of the slab (representing the vacancy being in the bulk) when using 5, 7, 9 or 11 layers in the slab. The energy of the defect in the second layer was found similar to that of the third layer or in the bulk and there is a minor effect of increasing the number of layers from five as used in the remaining of the study. This also shows that calculating the diffusion of the N-vacancy migrating from the surface to the second layer is the key step to determine if the TMN will decompose into the parent metal and ammonia. Fig. S2 shows that the vacancy energy is converged (within 0.1 eV) in the smaller cell (40 atoms in total with 4 metal atoms and 4 nitrogen atoms in a layer and 5 layers in all cases) compared with the big cell (160 atoms in total with 16 metal atoms and 16 nitrogen atoms in a layer and 5 layers in all cases). We conclude that a 40-atom slab is a good approximation for the nitrides and we use that in the remainder of the study. Boundary conditions were periodic in the x and y directions and surfaces were separated by 12 Å of vacuum in the z direction. The structural optimization was considered converged when the forces on all moveable atoms were below 0.01 eV/Å in any direction. Activation energies are calculated as the highest point along the minimum energy path (MEP) calculated using the climbing image nudged elastic band method (CI-NEB) [44]. The (100) facets of the RS structure of the earlier TMNs that make ammonia rather than H_2, and the (110) facets of the ZB structure of later TMNs are chosen for the catalytic investigations via the AM and DM. The RPBE lattice constants for these structures are taken from reference [45].

2.2. Reaction pathways and electrochemical modeling

The cathode reaction of the electrochemical process is:

$$N_2 + 6(H^+ + e^-) \rightleftharpoons 2NH_3 \quad (1)$$

The source of protons is taken to be the anode reaction [46]:

$$H_2 \rightleftharpoons 2(H^+ + e^-) \quad (2)$$

We firstly consider the possibility that the reaction follows via an AM, where the N_2 molecule is adsorbed on the clean surface of TMNs and then its successive hydrogenation by protons results in ammonia formation, as shown in Eqs. (3)–(11) and Fig. 1 (left):

$$N_2 + * \rightleftharpoons *N_2 \quad (3)$$

$$*N_2 + 6(H^+ + e^-) \rightleftharpoons *N_2H + 5(H^+ + e^-) \quad (4)$$

$$*N_2H + 5(H^+ + e^-) \rightleftharpoons *NNH_2 + 4(H^+ + e^-) \quad (5)$$

$$*NNH_2 + 4(H^+ + e^-) \rightleftharpoons *NNH_3 + 3(H^+ + e^-) \quad (6)$$

$$*NNH_3 + 3(H^+ + e^-) \rightleftharpoons *N + NH_3 + 3(H^+ + e^-) \quad (7)$$

$$*N + 3(H^+ + e^-) \rightleftharpoons *NH + 2(H^+ + e^-) \quad (8)$$

$$*NH + 2(H^+ + e^-) \rightleftharpoons *NH_2 + (H^+ + e^-) \quad (9)$$

$$*NH_2 + (H^+ + e^-) \rightleftharpoons *NH_3 \quad (10)$$

$$*NH_3 \rightleftharpoons * + NH_3 \quad (11)$$

Where an asterisk (*) denotes an available site on the surface. We have also considered adsorption of *NNH as the first step in the reaction instead of $*N_2$, and its possibility will be discussed further down in the Result Section. It is noteworthy to mention here that the possibility of formation of *NHNH was also investigated in Eq. (5), but it was found that $*NNH_2$ formation was around 0.5 eV more favourable compared to *NHNH formation. Similar study on pure metals by Skulason et al. also showed that $*NNH_2$ formation is more favourable than *NHNH [24]. Secondly, we explore the possibility of a DM on the clean surface of the TMNs where the nitrogen molecule first splits on the surface according to Eq. (12) and Fig. 1 (right), and then subsequently hydrogenated by direct attachment of protons from the solution as shown in Eqs. (8)–(11).

Table 1
Zero point energy and entropy contributions to the free energy of gas phase and adsorbed species at 300 K for the (100) facets of the RS and the (110) facets of the ZB structures of TMNs.[a] It was assumed that these properties are only structure-dependent and not TMN-dependent. Thus, these calculations were carried out on the (100) surface of VN in its RS structure and the values used for all the other RS (100) TMNs. For the (110) facets of the ZB structure of TMNs, these calculations were conducted on the surface of OsN.

Rocksalt (100)	TS	ZPE	Zincblende (110)	TS	ZPE
NH_3	0.74	0.89	NH_3	0.74	0.89
H_2	0.41	0.27	H_2	0.41	0.27
N_2	0.6	0.15	N_2	0.6	0.15
*N	0.05	0.09	*N	0.05	0.09
$*N_2$	0.17	0.20	$*N_2$	0.14	0.21
*NNH	0.18	0.45	*NNH	0.15	0.49
$*NNH_2$	0.22	0.80	$*NNH_2$	0.13	0.82
$*NNH_3$	0.19	1.12	$*NNH_3$	0.14	0.83
*NH	0.06	0.34	*NH	0.08	0.35
$*NH_2$	0.07	0.69	$*NH_2$	0.10	0.68
$*NH_3$	0.18	0.99	$*NH_3$	0.13	0.92

[a] The values for gas phase molecules are taken from Ref. [52], and the values for the adsorbed species are obtained from DFT calculations of vibrational normal modes.

$$*N_2 \rightleftharpoons *N + *N \quad (12)$$

It was recently shown that H-assisted dissociation of diatomic molecules e.g. CO, NO and O_2 may lower the dissociation barrier and become in favor of the reaction [47]. This has also been explored for the industrial Haber-Bosch process where H-assisted dissociation of N_2 was taken into account by our group [48]. Therefore in addition to direct DM, we also consider the possibility of a mixed AM-DM where hydrogenation of di-nitrogen can take place to form *NNH (Eqs. (13) and (14)) or $*NNH_2$ (Eqs. (15) and (16)) prior to dissociation to *N + *NH and *N + $*NH_2$, respectively.

$$*N_2 + 6(H^+ + e^-) \rightleftharpoons *N_2H + 5(H^+ + e^-) \quad (13)$$

$$*N_2H + 5(H^+ + e^-) \rightleftharpoons *N + *NH + 5(H^+ + e^-) \quad (14)$$

or

$$*N_2H + 5(H^+ + e^-) \rightleftharpoons *NNH_2 + 4(H^+ + e^-) \quad (15)$$

$$*NNH_2 + 4(H^+ + e^-) \rightleftharpoons *N + *NH_2 + 4(H^+ + e^-) \quad (16)$$

For DM and before going through the entire hydrogenation step after dissociation, we analyze the likelihood of dissociation of nitrogen molecule on the surface via NEB calculations. If this initial step is energetically feasible at ambient conditions, then it is worth considering hydrogenation steps for nitrogen reduction and ammonia formation. DFT calculations were used to calculate the minimum energy configuration of each species on the surface and adsorption energies of all intermediates. It is assumed that activation barriers between stable minima can be neglected during the electrochemical reactions [49]. The free energy at T = 300 K of each elementary step is estimated at pH = 0 according to:

$$\Delta G = \Delta E + \Delta E_{ZPE} - T\Delta S \quad (17)$$

ΔE is the reaction energy calculated with DFT. The zero-point energy correction (ΔE_{ZPE}) and entropy differences (ΔS) are calculated within a harmonic approximation and the values of these are given in Table 1. To implicitly account for the bias and estimate the onset potential, the effect of an applied bias, U, is included for all electrochemical reaction steps by shifting the free energy for reactions involving n electrons by −neU: [46]

$$\Delta G = \Delta E + \Delta E_{ZPE} - T\Delta S - neU \quad (18)$$

Please cite this article in press as: Y. Abghoui, E. Skúlason, Onset potentials for different reaction mechanisms of nitrogen activation to ammonia on transition metal nitride electro-catalysts, Catal. Today (2016), http://dx.doi.org/10.1016/j.cattod.2016.11.047

G Model
CATTOD-10482; No. of Pages 9
ARTICLE IN PRESS

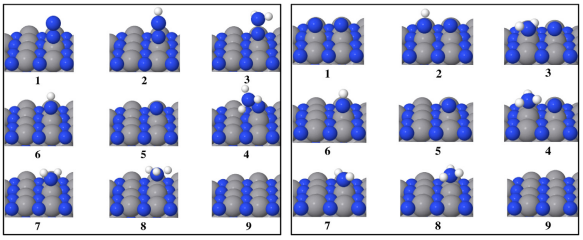

Fig. 1. The metal nitride unit cell and top-tilted views of one of the low index surfaces used in this study (rocksalt (100)), associative (left) and dissociative (right) mechanisms. The surface unit cells have been repeated once in the lateral directions. Metal atoms are represented by grey spheres and nitrogen atoms by dark blue. Hydrogen atoms are shown in white.

The potential-determining step (PDS) is assumed to be a measure of the catalytic activity towards NH_3 formation on each nitride. It is identified as the elementary reaction step with the largest increase in free energy, ΔG. For that reaction step to become thermoneutral or downhill in free energy, an applied potential of at least $U = -\Delta G$ can be applied to get an estimate of the onset potential of the overall reaction [24,46]. Other reaction steps may be rate limiting, such as non-electrochemical steps (e.g. N_2 adsorption or NH_3 desorption) where the applied potential does not have an effect (see Fig. S3). The thermodynamics are considered for both steps as well as kinetic effect for the N_2, N—NH and N—NH_2 dissociation of the N—N bond. However, energy barriers of all the proton-electron transfer electrochemical steps are not considered here but may be important to determine the rate-determining step (RDS), as we have observed recently for CO_2 electroreduction [50,51]. Calculating the proton-electron transfer steps are computational demanding and may be important to predict the right mechanism for N_2 electroreduction to ammonia, and will be a focus of our future studies. However, using this simple gas-phase model is our first step in order to gain insight into the possible mechanism for this reaction.

3. Results and discussion

3.1. Catalytic activity via associative mechanism

We studied the possibility of catalyzing nitrogen activation to ammonia via an AM as given in Eqs. (3)–(11) on the clean surface of the TMNs. With the use of DFT, the free energy of each elementary step was calculated. Figs. 2 and 3 show the FEDs of the TMNs in RS and ZB structures, respectively. The candidates are divided into two groups for clarity, those with ΔG_{PDS} below 1.5 eV and the ones with ΔG_{PDS} above 1.5 eV. As can be seen from Figs. 2 and 3, it is always uphill in free energy to adsorb N_2 on the surface and form N_2 -admolecule for all TMNs, but in most cases this is less than 0.5 eV and should be possible at room temperature. For most of the (100) surfaces of TMNs, first protonation step and formation of *NNH is the PDS. However, for VN and NbN the third protonation step where the first ammonia forms is the PDS. It is also seen that for some of these candidates, desorption of the second ammonia from the surface becomes slightly uphill in free energy. As mentioned earlier, the applied potential does not affect the non-electrochemical steps such as adsorption of N_2 and desorption of NH_3 (see Fig. S3 in ESI). But in reality, in acidic solution, the adsorbed NH3 is likely to get further protonated to NH4+ and then released into the solution, thereby avoiding this increase in free energy. All of these six candidates show activity for electrochemical ammonia formation, among which MoN seems promising with $\Delta G_{PDS} = 0.83$ eV.

The FEDs for nitrogen activation to ammonia on the (110) surface of the ZB structure of TMNs are shown in Fig. 3. On the surface of PdN and NiN, no stable adsorption site was found for adsorption of di-nitrogen, and thus no data is shown for them in the corresponding figures. For CoN, RhN, and IrN this step even becomes the rate-determining step (RDS) of the reaction with largest increase in free energy. That will slow down the reaction at ambient conditions and for those three nitrides it will hinder the reaction to occur at ambient conditions. For ZrN, the PDS is the $*NH_2$ formation after releasing the first ammonia, while for others, *NNH formation on the surface is the PDS. For NbN, desorption of the second ammonia molecule is the PDS. Among these nitrides, OsN and CrN seem promising with $\Delta G_{PDS} = 0.98$ and 0.68 eV, respectively. Thus, it might be possible to form ammonia on these surfaces by applying a bias of less negative than −1.0 V vs. SHE. But still the endothermic adsorption of N_2 on the clean surface might slow down the overall reaction. When we consider *NNH formation as the first step in the reaction instead of $*N_2$, the PDS becomes larger in free energy in most cases compared to when $*N_2$ is the first step. The only exception is the ZB(110) of ZrN where adsorption of NNH becomes so exothermic that both AM and MvK mechanisms might be active and possible on this specific surface.

3.2. Catalytic activity via dissociative mechanism

To investigate the possibility of di-nitrogen dissociation on the clean surface of TMNs, the binding energy of adsorption of two nitrogen atoms was calculated on the surface according to:

$$\Delta E = E_{clean+2*N} - E_{clean} - E_{N2(g)} \quad (19)$$

where $E_{clean+2*N}$ is the total energy of the TMN with two N adatoms adsorbed on the surface, E_{clean} is the total energy of the TMN surface without any adsorbate, and $E_{N2(g)}$ is the total energy of nitrogen molecule in a box. ΔE is, thus, the binding energy of two N adatoms on the clean surface of TMN. The free energy of adsorption of two N adatoms on the surface was obtained with a constant shift of 0.6 eV to account for the loss of entropy of $N_{2(g)}$ [53], ($\Delta G = \Delta E + 0.6$). If this free energy is ≤ 0 eV, it should be exothermic to split nitrogen molecule on the surface. Otherwise, it is endothermic and as it gets more uphill in free energy, it becomes thermodynamically more difficult at ambient conditions. This analysis was done for all the RS and ZB structures of TMNs. For most of these surfaces, it was found that nitrogen dissociation on the surface is endothermic, as presented in Table 2. At these endothermic conditions, nitrogen dissociation should not be feasible at ambi-

Please cite this article in press as: Y. Abghoui, E. Skúlason, Onset potentials for different reaction mechanisms of nitrogen activation to ammonia on transition metal nitride electro-catalysts, Catal. Today (2016), http://dx.doi.org/10.1016/j.cattod.2016.11.047

G Model
CATTOD-10482; No. of Pages 9
ARTICLE IN PRESS
Y. Abghoui, E. Skúlason / Catalysis Today xxx (2016) xxx–xxx

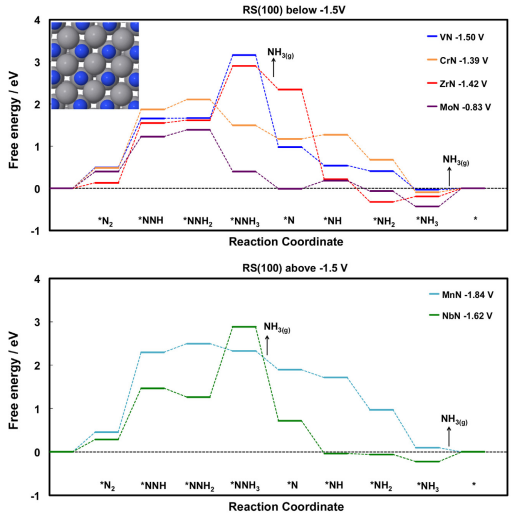

Fig. 2. Free energy diagrams constructed based on the associative mechanism on the (100) facets of the rocksalt structures of earlier transition metal nitrides. The free energy of each intermediate is calculated at room temperature, pH = 0 and an applied potential of 0.0 V vs. the standard hydrogen electrode. The onset potentials for each nitride are indicated in the legend. The potential determining step (PDS) is the first protonation of $*N_2$ to *NNH for all candidates except for VN and NbN for which the formation of $*NNH_3$ is the potential determining step. The inset is a top view of the (100) facets of the rocksalt structure of VN where the surface unit cell is repeated once in the lateral directions.

Table 2
Activation energy (Ea, in eV) and reaction free energy (ΔG, in eV) of N_2 dissociation on the clean surfaces of the (100) facets of the RS and the (110) facets of the ZB structures of TMNs. For almost all nitrides, it is endothermic to bind 2*N on the surface. In addition, the activation barrier for splitting of di-nitrogen on the surface is large for the studied candidates. This endothermicity and the large activation barrier make the DM unlikely to occur at ambient conditions. On the surface of PdN, no stable adsorption sites were found for 2*N and as so marked as "unstable" in the table. Due to endothermic nature of adsorption of 2*N on the surface, we have done activation barrier analyses only for MoN (that has the lowest endothermicity) and the promising nitrides reported before [31,32] and this computationally expensive calculations have not been done for the rest. They are marked with "-".

RS(100)	ΔG_{2*N} (eV)	Ea (eV)	ZB(110)	ΔG_{2*N} (eV)	Ea (eV)
VN	2.97	3.09	FeN	4.61	–
CrN	2.78	3.14	CoN	6.74	–
MnN	4.29	–	NiN	2.54	–
ZrN	0.67	2.35	RuN	4.55	–
NbN	2.48	2.64	RhN	7.17	–
MoN	0.3	2.20	PdN	unstable	–
			OsN	3.17	–
			IrN	5.63	–

ent conditions. However, this step is less endothermic on MoN (0.3 eV). Thus, NEB calculations were conducted on this surface to obtain the activation barriers of nitrogen dissociation. The (100) facets of the RS structure of VN, CrN, ZrN, and NbN were previously reported promising for ammonia formation via MvK mechanism [31,32]. Therefore, the activation barriers of nitrogen dissociation on the clean surface of these promising nitrides were also calculated despite the endothermic nature of this reaction on their clean surface, and those barriers are also presented in Table 2. In all of these cases, large activation barriers of above 2 eV were found for nitrogen dissociation, which should make it unlikely to occur at ambient conditions. These findings are in line with the work of Howalt et al. on MoN nanoclusters where nitrogen dissociation was found unlikely at ambient conditions due to high activation barriers of 1.8 eV at both nitrogen vacancies on a nitrogen covered molybdenum particle and at a clean molybdenum particle [54].

Another possibility for di-nitrogen dissociation might be via a so-called mixed AM-DM where di-nitrogen is firstly hydrogenated to form *NNH or $*NNH_2$ (via AM) and then dissociation takes place on the surface (via DM). The results of this mixed mechanism on dissociation of di-nitrogen on the surface of the nitrides contradicts with what Iglesia and co-workers reported recently on Ru(0001). They showed that H-assisted N_2 activation – unlike the case of O_2, CO and NO – is not significantly more facile than direct N_2 dissociation [47]. But when we considered this pathway on the surface of the most promising nitrides (the (100) facets of the rocksalt structure of VN, NbN, ZrN, and CrN), it was found that dissociation barriers drop going from direct splitting of N_2 to H-assisted splitting (see Fig. 4). This is interesting and shows how initial hydrogenation of $*N_2$ can facilitate its dissociation from kinetic perspective. Therefore, it seems like the most promising reaction mechanism would be hydrogenation to NNH_2 and then N—N dissociation, except for CrN according to Fig. 4. But the downside is that to get to the level where N_2 is protonated to NNH or NNH_2 almost always demand a more negative bias than −1.0 V (see Figs. 2 and 3). While Nitrogen reduction to ammonia occurs at much smaller bias (−0.5 V to −0.8 V) if reaction is considered going through the MvK mechanism [30–33]. That means the MvK mechanism still outweighs this

Please cite this article in press as: Y. Abghoui, E. Skúlason, Onset potentials for different reaction mechanisms of nitrogen activation to ammonia on transition metal nitride electro-catalysts, Catal. Today (2016), http://dx.doi.org/10.1016/j.cattod.2016.11.047

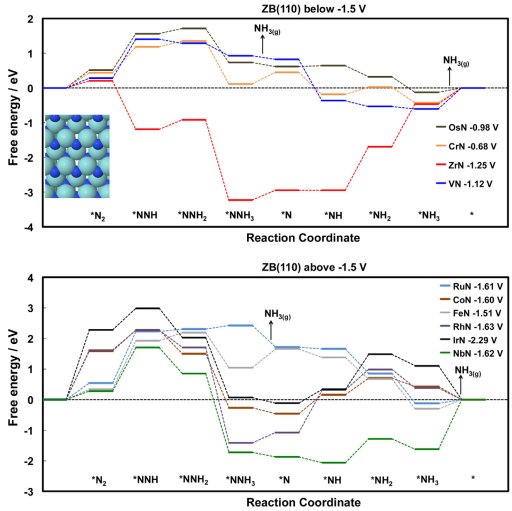

Fig. 3. Free energy diagrams constructed based on the associative mechanism on the (110) facets of the zincblende structures of later transition metal nitrides including VN, NbN, CrN and ZrN. The free energy of each intermediate is calculated at room temperature, pH = 0 and an applied potential of 0.0 V vs. the standard hydrogen electrode. The onset potentials for each nitride are indicated in the legend. The potential determining step is the first protonation step of N_2 to *NNH for most of these candidates. For ZrN, however, the potential determining step is reduction of *NH to form $*NH_2$. For NbN, the potential determining step is desorption of the second NH_3 molecule. This is considered to be a non-electrochemical step here, but in reality an ammonium ion (NH_4^+) would be formed at pH = 0. For CoN, RhN, and IrN, the adsorption of the nitrogen molecule to the surface is highly endothermic. The inset is a top view of the (110) facets of the zincblende structure OsN where the surface unit cell is repeated once in the lateral directions.

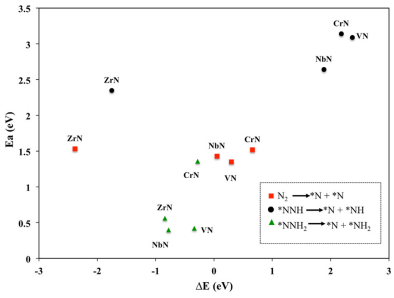

Fig. 4. Activation energy (Ea, in eV) and reaction energy (ΔE, in eV) of N_2 dissociation on the clean surface of the RS(100) facet of the most promising metal nitrides (black circles), *NNH dissociation (red squares), and $*NNH_2$ dissociation (green triangles). (For interpretation of the references to colour in this figure legend, the reader is referred to the web version of this article.)

mixed mechanism. The ZB(110) of ZrN is the only case where *NNH formation is exothermic and $*NNH_2$ formation not that uphill in free energy. Thus, AM and accordingly mixed AM-DM might be feasible as well as the MvK for this nitride. However, smaller onset is yet needed via MvK [13–15] for formation of $2NH_3$ in a catalytic cycle when compared to other pathways shown in this work. So in general AM, DM and mixed AM-DM are unlikely mechanisms for ammonia formation on the surface of these TMNs at ambient conditions when compared with the MvK from the onset potential perspective [13–15]. In the mixed AM-DM, the *NNH or $*NNH_2$ formation needs to be facile via AM (achieved at relatively smaller overpotential, $\Delta G_{(PDS)}$, when compared to MvK) before DM become favourable. Therefore, in the next session we only compare the onset for ammonia formation via MvK with that of mixed AM-DM and then conclude which one of these mechanisms might be more favourable.

3.3. Comparison of mixed AM-DM and MvK mechanism

Up to now, we realized that nitrogen activation and electrochemical ammonia formation on the surface of these TMNs is feasible via mixed AM-DM presented above as well as MvK mechanism elaborated in detail elsewhere [31–33]. But to see which one is more favourable from the overpotential perspective, we will compare in this section the onset potential required for completion of the catalytic cycle and formation of $2NH_3$ via these pathways. Fig. 5 illustrates a comparison between these two possible mechanisms and describes which one might occur at lower onset potentials at ambient conditions.

Fig. 5 shows that nitrogen activation to ammonia is always having a less negative onset potential via MvK mechanism than via

Please cite this article in press as: Y. Abghoui, E. Skúlason, Onset potentials for different reaction mechanisms of nitrogen activation to ammonia on transition metal nitride electro-catalysts, Catal. Today (2016), http://dx.doi.org/10.1016/j.cattod.2016.11.047

G Model
CATTOD-10482; No. of Pages 9
ARTICLE IN PRESS
Y. Abghoui, E. Skúlason / Catalysis Today xxx (2016) xxx–xxx 7

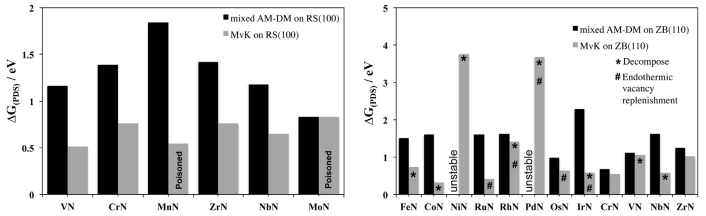

Fig. 5. Free energy change of the PDS of $2NH_3$ formation on both the RS and ZB structures of TMNs. The required onset potential via mixed AM-DM is compared with that of MvK (for which the data is taken from our previous works [31,32] where poisoning, decomposition and regeneration phenomena via MvK were explained in detail). Those TMNs that get poisoned in electrochemical environment when calculated via MvK are distinguished by the term 'Poisoned' inside the bars. Those TMNs that are decomposed at operational conditions due to migration of the N-vacancy into the bulk are determined with '*', and those TMNs having difficulty to regenerate due to endothermicity of the step corresponding to filling the N-vacancy with N_2 are characterized with '#'. Finally, on the ZB TMNs, no stable adsorption site was found for adsorption of di-nitrogen on PdN and NiN via mixed AM-DM, and thus no data is shown and the term "unstable" is inserted in the right figure.

mixed AM-DM on all the TMN surfaces. In the MvK mechanism a surface N is reacted, leaving a surface vacancy at the surface and for the catalytic cycle to complete, this vacancy must be filled with N_2 from the solution. However, there exists the possibility of the vacancy rather being filled with H atoms or O atoms from the aqueous electrolyte, both of which would block this surface site for completion of the catalytic cycle and result in poisoning of the catalyst (for detailed elaboration on poisoning see References [13–15]). There is also a possibility of catalyst decomposition where N from bulk migrates to fill the surface vacancy and reduces to ammonia. This will cause decomposition of the catalyst to its parental metal (for detailed elaboration on catalyst decomposition see References [13–15]). This decomposition was assessed via both thermodynamic (where the difference in total energy of the vacancy being on the surface and in the subsurface layer was investigated) and kinetic (where activation energy barriers of vacancy migration from the surface to the bulk was taken into account). If the AM or mixed AM-DM studied in this work had not led to more negative onset potentials than that of MvK, it would have been possible to avoid these latter issues (decomposition or poisoning) that might occur for some of the nitrides when the reaction goes via MvK mechanism, and then produce ammonia instead with AM or mixed AM-DM at lower onset potentials. But this is not the case and therefore we can conclude that the MvK mechanism is in general the most favourable mechanism for nitrogen activation to ammonia on the surface of these TMNs. The only exception might seem to be the RS (100) facet of MoN for which the onset potential is equal via both mechanisms and to some extend for ZB (110) facets of CrN, VN and ZrN where the MvK mechanism has only a slightly lower onset potential than the mixed AM-DM. When the catalytic investigations were previously carried out for MoN [31], it was reported that the nitrogen vacancy created due to MvK approach might get poisoned in electrochemical environment. That could hinder vacancy replenishment and accordingly cease the catalytic cycle of ammonia formation. According to Fig. 5 here, the free energy of the PDS via mixed AM-MD is found similar to that of MvK mechanism (0.83 eV). But considering endothermic adsorption of di-nitrogen on the surface via AM, still the reaction will most likely proceed via MvK mechanism until the catalytic cycle stops due to poisoning. In the case of VN(110), the nitride will decompose when the MvK mechanism is pursued, and since that starts at a slightly less negative onset potential than for the mixed AM-DM, it is not likely that ammonia can be catalyzed through either mechanisms. However CrN(110) and ZrN(110) seem to be able to produce ammonia via both mechanisms. It is still more likely for the reaction to proceed mainly via MvK mechanism, as adsorbing N_2 on the clean surfaces of these candidates for mixed AM-DM is slightly endothermic (from 0.1 – 0.5 eV). Even for ZrN(110) with exothermic formation of $^*NNH$, the MvK leads to less negative onset potential for ammonia formation. Thus, MvK mechanism is a more likely reaction pathway for nitrogen reduction to ammonia on the surface of these TMNs.

4. Conclusion

With the aid of DFT calculations, we investigated the onset potential required for ammonia formation via the conventional associative mechanism (AM) and dissociative mechanism (DM) (and a combination of these two mechanisms, the so-called mixed AM-DM) on the clean surface of the rocksalt and zincblende structures of transition metal nitrides and compared that with the required onset potential via Mars-van Krevelen mechanism (MvK) to determine which reaction mechanism will have lowest overpotential at ambient conditions. We calculated the free energy of all the stable intermediates along the reaction path. By constructing the free energy diagrams for all the nitrides, we found the free energy change of the potential-determining step. We also considered free energy of adsorption of two N adatoms on the surface and calculated the activation energy of N_2 dissociation both directly and H-assisted. The conclusion is that it might not be favourable to reduce nitrogen to ammonia at ambient conditions via neither DM and AM, nor mixed AM-DM. Due to the endothermic nature of the adsorption of two N adatoms on the surface and large activation barriers of N_2 dissociation, DM is not active for ammonia formation. Via AM, it is usually slightly endothermic to adsorb the N_2 molecule on the clean surface of these nitrides. In addition, quite large bias is usually required to hydrogenate $^*N_2$ to $^*NNH$ in the formation of ammonia via AM. Since the energy barriers to dissociate $^*NNH_2$ to $^*N$ and $^*NH_2$ are low for the studied candidates, there is a possibility of a mixed AM-DM where $^*NNH_2$ would firstly be obtained via the AM and then the N—N bond of the $^*NNH_2$ would dissociate and follow the DM thereafter. However, when we compare the onset potentials of the mixed AM-DM with that of MvK mechanism, we see that MvK mechanism will always result in a smaller overpotential than the mixed AM-DM for all candidates studied here. Therefore, MvK might always be the most favourable mechanism for nitrogen electroreduction to ammonia on these metal mononitride catalysts. However, it should be noted that we have not included any of the electrochemical proton-electron transfer barriers in this study and thus the rates for these different mechanisms have not been estimated yet. In this study, we have used thermodynamics to get an estimate of the onset potentials for these different mechanisms.

Please cite this article in press as: Y. Abghoui, E. Skúlason, Onset potentials for different reaction mechanisms of nitrogen activation to ammonia on transition metal nitride electro-catalysts, Catal. Today (2016), http://dx.doi.org/10.1016/j.cattod.2016.11.047

The highest rate of ammonia synthesis in aqueous solution that has been obtained experimentally thus far is $1.14*10^{-9}$ mol s^{-1} cm^{-2}, with Pt/C as catalyst [22]. There, a low current efficiency of around 1% was obtained when a high voltage of 1.6 V was applied. While based on comprehensive DFT investigations, the most promising nitride candidates shown in Fig. 5 here (VN, NbN, CrN, or ZrN) are expected to reduce nitrogen to ammonia via MvK at smaller overpotentials of around −0.5 to −0.8 V. These findings are also interesting when compared to pure transition metals where higher overpotentials of around −1.0 to −1.5 V were predicted to form ammonia for the most promising candidates [9]. Similar to one of the most active catalysts for the chemical process, the Co_3Mo_3N, where MvK mechanism was explored to be the probable reaction mechanism, for the TMN surfaces studied here, the MvK mechanism is expected to be the most favourable mechanism as well. Although there is not yet any experimental evidence available for electrochemical ammonia formation using these nitride surfaces, these findings might be useful for future research where the possibility of nitrogen activation will be investigated on other surfaces of these active and interesting materials.

Acknowledgments

Financial support is acknowledged from the Icelandic Research Fund and the Research Fund of the University of Iceland. The calculations were in part carried out on the Nordic high performance computer (Gardar).

Appendix A. Supplementary data

Supplementary data associated with this article can be found, in the online version, at http://dx.doi.org/10.1016/j.cattod.2016.11.047.

References

[1] V. Smil, Detonator of the population explosion, Nature 400 (1999) 415, http://dx.doi.org/10.1038/22672.
[2] V. Smil, Global population and the nitrogen cycle, Sci. Am. 277 (1997) 76–81, http://dx.doi.org/10.1038/scientificamerican0797-76.
[3] H. Liu, Ammonia synthesis catalyst 100 years: practice, enlightenment and challenge, Chin. J. Catal. 35 (2014) 1619–1640, http://dx.doi.org/10.1016/S1872-2067(14)60118-2.
[4] M.A. Shipman, M.D. Symes, Recent progress towards the electrosynthesis of ammonia from sustainable resources, Catal. Today (2016), http://dx.doi.org/10.1016/j.cattod.2016.05.008.
[5] V. Kyriakou, I. Garagounis, E. Vasileiou, A. Vourros, M. Stoukides, Progress in the electrochemical synthesis of ammonia, Catal. Today (2016), http://dx.doi.org/10.1016/j.cattod.2016.06.014.
[6] G.N. Schrauzer, T.D. Guth, Photocatalytic reactions. 1. Photolysis of water and photoreduction of nitrogen on titanium dioxide, J. Am. Chem. Soc. 99 (1977) 7189–7193, http://dx.doi.org/10.1021/ja00464a015.
[7] J.Y. Becker, Nitrogen fixation: part II. Electrochemical reduction of hydrazido (-NNH2) Mo and W complexes. Selective formation of NH3 under mild conditions, J. Electroanal. Chem. Interfacial Electrochem. 250 (1988) 385–397, http://dx.doi.org/10.1016/0022-0728(90)870882.
[8] J.Y. Becker, S.A. Tsarfaty, Nitrogen fixation Part III. Electrochemical reduction of hydrazido (-NNH) MO and W complexes. Selective formation of NH under mild conditions, J. Electroanal. Chem. Interfacial Electrochem. 280 (1990) 119–127.
[9] C. Pickett, J. Talarmin, Electrosynthesis of ammonia, Nature 317 (1985) 652–653, http://dx.doi.org/10.1038/317652a0.
[10] A. Sclafani, V. Augugliaro, M. Schiavello, Dinitrogen electrochemical reduction to ammonia over iron cathode in aqueous medium, J. Electrochem. Soc. 130 (1983) 734–736, http://dx.doi.org/10.1149/1.2119794.
[11] D.V. Yandulov, R.R. Schrock, Catalytic reduction of dinitrogen to ammonia at a single molybdenum center, Science 301 (2003) 76–78, http://dx.doi.org/10.1126/science.1085326.
[12] N. Furuya, H. Yoshiba, Electroreduction of nitrogen to ammonia on gas-diffusion electrodes loaded with inorganic catalyst, J. Electroanal. Chem. Interfacial Electrochem. 291 (1990) 269–272, http://dx.doi.org/10.1016/0022-0728(90)87195-P.
[13] G. Marnellos, M. Stoukides, Ammonia synthesis at atmospheric pressure, Science (80) 282 (1998) 98–100 http://www.ncbi.nlm.nih.gov/pubmed/9756486.
[14] G. Marnellos, S. Zisekas, M. Stoukides, Synthesis of ammonia at atmospheric pressure with the use of solid state proton conductors, J. Catal. 193 (2000) 80–87, http://dx.doi.org/10.1006/jcat.2000.2877.
[15] E. Vasileiou, V. Kyriakou, I. Garagounis, A. Vourros, A. Manerbino, W.G. Coors, M. Stoukides, Reaction rate enhancement during the electrocatalytic synthesis of ammonia in a BaZr0.7Ce0.2Y0.1O2.9 solid electrolyte cell, Top. Catal. (2015) 491–499, http://dx.doi.org/10.1007/s11244-015-0491-9.
[16] G. Qing, R. Kikuchi, S. Kishira, A. Takagaki, T. Sugawara, S.T. Oyama, Ammonia synthesis by N2 and steam electrolysis in solid-state cells at 220 °C and atmospheric pressure, J. Electrochem. Soc. 163 (2016) 282–287, http://dx.doi.org/10.1149/2.0161610jes.
[17] T. Murakami, T. Nishikiori, T. Nohira, Y. Ito, Electrolytic synthesis of ammonia in molten salts under atmospheric pressure, J. Am. Chem. Soc. 125 (2003) 334–335, http://dx.doi.org/10.1021/ja028891t.
[18] T. Murakami, T. Nohira, T. Goto, Y.H. Ogata, Y. Ito, Electrolytic ammonia synthesis from water and nitrogen gas in molten salt under atmospheric pressure, Electrochim. Acta. 50 (2005) 5423–5426, http://dx.doi.org/10.1016/j.electacta.2005.03.023.
[19] S. Licht, B. Cui, B. Wang, F.-F. Li, J. Lau, S. Liu, Ammonia synthesis by N_2 and steam electrolysis in molten hydroxide suspensions of nanoscale Fe_2O_3, Science 345 (2014) 637–640, http://dx.doi.org/10.1126/science.1254234.
[20] G. Xu, R. Liu, J. Wang, Electrochemical synthesis of ammonia using a cell with a Nafion membrane and SmFe0.7Cu0.3-x Ni x 03 (x = 0-0.3) cathode at atmospheric pressure and lower temperature, Sci. China Ser. B Chem. 52 (2009) 1171–1175, http://dx.doi.org/10.1007/s11426-009-0135-7.
[21] V. Kordali, G. Kyriacou, C. Lambrou, Electrochemical synthesis of ammonia at atmospheric pressure and low temperature in a solid polymer electrolyte cell, Chem. Commun. (2000) 1673–1674, http://dx.doi.org/10.1039/b004885m.
[22] R. Lan, J.T.S. Irvine, S. Tao, Synthesis of ammonia directly from air and water at ambient temperature and pressure, Sci. Rep. 3 (2013) 1–7, http://dx.doi.org/10.1038/srep01145.
[23] S. Giddey, S.P.S. Badwal, A. Kulkarni, Review of electrochemical ammonia production technologies and materials, Int. J. Hydrogen Energy 38 (2013) 14576–14594, http://dx.doi.org/10.1016/j.ijhydene.2013.09.054.
[24] E. Skúlason, T. Bligaard, S. Gudmundsdóttir, F. Studt, J. Rossmeisl, F. Abild-Pedersen, T. Vegge, H. Jonsson, J.K. Norskov, A theoretical evaluation of possible transition metal electro-catalysts for N2 reduction, Phys. Chem. Chem. Phys. 14 (2012) 1235–1245, http://dx.doi.org/10.1039/c1cp22271f.
[25] J.G. Howalt, T. Bligaard, J. Rossmeisl, T. Vegge, DFT based study of transition metal nano-clusters for electrochemical NH3 production, Phys. Chem. Chem. Phys. 15 (2013) 7785–7795, http://dx.doi.org/10.1039/c3cp44641g.
[26] J. Howalt, T. Vegge, The role of oxygen and water on molybdenum nanoclusters for electro catalytic ammonia production, Beilstein J. Nanotechnol. 5 (2014) 111–120, http://dx.doi.org/10.3762/bjnano.5.11.
[27] P. Mars, D.W. Van, Krevelen, special supplement to Chemical engineering science, Eng. Sci. 3 (1954) 41–45.
[28] C.D. Zeinalipour-Yazdi, J.S.J. Hargreaves, C.R.A. Catlow, Nitrogen activation in a Mars-van krevelen mechanism for ammonia synthesis on Co3Mo3N, J. Phys. Chem. C. (2015) 1–18, http://dx.doi.org/10.1021/acs.jpcc.5b06811.
[29] C.D. Zeinalipour-Yazdi, J.S.J. Hargreaves, C.R.A. Catlow, DFT-D3 study of molecular N2 and H2 activation on Co3Mo3N surfaces, J. Phys. Chem. C. 120 (2016) 21390–21398, http://dx.doi.org/10.1021/acs.jpcc.6b04748.
[30] Y. Abghoui, E. Skúlasson, Transition metal nitride catalysts for electrochemical reduction of nitrogen to ammonia at ambient conditions, Procedia Comput. Sci. 51 (2015) 1897–1906, http://dx.doi.org/10.1016/j.procs.2015.05.433.
[31] Y. Abghoui, A.L. Garden, V.F. Hlynsson, S. Björgvinsdóttir, H. Ólafsdóttir, E. Skúlason, Enabling electrochemical reduction of nitrogen to ammonia at ambient conditions through rational catalyst design, Phys. Chem. Chem. Phys. 17 (2015) 4909–4918, http://dx.doi.org/10.1039/c4cp04838e.
[32] Y. Abghoui, A.L. Garden, J.G. Howalt, T. Vegge, E. Skúlason, Electroreduction of N2 to ammonia at ambient conditions on mononitrides of Zr, Nb, Cr, and V: a DFT guide for experiments, ACS Catal. (2015) 635–646, http://dx.doi.org/10.1021/acscatal.5b01918.
[33] Y. Abghoui, E. Skúlason, Electrochemical synthesis of ammonia via Mars-van Krevelen mechanism on the (111) facets of group III-VII transition metal mononitrides, Catal. Today (2016), http://dx.doi.org/10.1016/j.cattod.2016.06.009.
[34] R. Michalsky, A.M. Avram, B.A. Peterson, P.H. Pfromm, A.A. Peterson, Chemical looping of metal nitride catalysts: low-pressure ammonia synthesis for energy storage, Chem. Sci. 6 (2015) 3965–3974, http://dx.doi.org/10.1039/C5SC00789E.
[35] R. Michalsky, P.H. Pfromm, A. Steinfeld, Rational design of metal nitride redox materials for solar-driven ammonia synthesis, Interface Focus 5 (2015) 20140084, http://dx.doi.org/10.1098/rsfs.2014.0084.
[36] D.F. Arias, Y.C. Arango, A. Devia, Study of TiN and ZrN thin films grown by cathodic arc technique, Appl. Surf. Sci. 253 (2006) 1683–1690, http://dx.doi.org/10.1016/j.apsusc.2006.03.017.
[37] P. Hones, R. Sanjines, F. Levy, Characterization of sputter-deposited chromium nitride thin films for hard coatings, Surf. Coatings Technol. 94 (1997) 398–402, http://dx.doi.org/10.1016/S0257-8972(97)00443-X.
[38] H.J. Ramos, N.B. Valmoria, Thin-film deposition of ZrN using a plasma sputter-type negative ion source, Vacuum 73 (2004) 549–554, http://dx.doi.org/10.1016/j.vacuum.2003.12.158.

Please cite this article in press as: Y. Abghoui, E. Skúlason, Onset potentials for different reaction mechanisms of nitrogen activation to ammonia on transition metal nitride electro-catalysts, Catal. Today (2016), http://dx.doi.org/10.1016/j.cattod.2016.11.047

[39] S. Shayestehaminzadeh, T.K. Tryggvason, F. Magnus, S. Olafsson, J.T. Gudmundsson, Ultra-thin poly-crystalline TiN films grown by HiPIMS on MgO(100) — In-situ resistance study of the initial stage of growth, Thin Solid Films 549 (2013) 199–203, http://dx.doi.org/10.1016/j.tsf.2013.07.074.
[40] B. Hammer, L. Hansen, J. Nørskov, Improved adsorption energetics within density-functional theory using revised Perdew-Burke-Ernzerhof functionals, Phys. Rev. B 59 (1999) 7413–7421, http://dx.doi.org/10.1103/PhysRevB.59.7413.
[41] P. Blöchl, Projector augmented-wave method, Phys. Rev. B. 50 (1994) 17953–17979 (accessed November 01, 2013) http://prb.aps.org/abstract/PRB/v50/i24/p17953_1.
[42] G. Kresse, J. Hafner, Ab. initio molecular dynamics for liquid metals, Phys. Rev. B. 47 (1993) 558–561 (accessed November 01, 2013) http://prb.aps.org/abstract/PRB/v47/i1/p558_1.
[43] G. Kresse, J. Furthmüller, Efficient iterative schemes for ab initio total-energy calculations using a plane-wave basis set, Phys. Rev. B. Condens. Matter 54 (1996) 11169–11186 http://www.ncbi.nlm.nih.gov/pubmed/9984901.
[44] G. Henkelman, B.P. Uberuaga, H. Jónsson, A climbing image nudged elastic band method for finding saddle points and minimum energy paths, J. Chem. Phys. 113 (2000) 9901–9904, http://dx.doi.org/10.1063/1.1329672.
[45] V.F. Hlynsson, E. Skúlason, A.L. Garden, A systematic, first-principles study of the structural preference and magnetic properties of mononitrides of the d-block metals, J. Alloys Compd. 603 (2014) 172–179, http://dx.doi.org/10.1016/j.jallcom.2014.02.153.
[46] J.K. Nørskov, J. Rossmeisl, A. Logadottir, L. Lindqvist, J.R. Kitchin, T. Bligaard, H. Jonsson, Origin of the overpotential for oxygen reduction at a fuel-cell cathode, J. Phys. Chem. B 108 (2004) 17886–17892, http://dx.doi.org/10.1021/jp047349j.
[47] D. Hibbitts, E. Iglesia, Prevalence of bimolecular routes in the activation of diatomic molecules with strong chemical bonds (O2, NO, CO, N2) on catalytic surfaces, Acc. Chem. Res. 48 (2015) 1254–1262, http://dx.doi.org/10.1021/acs.accounts.5b00063.
[48] A.L. Garden, E. Skúlason, The mechanism of industrial ammonia synthesis revisited: calculations of the role of the associative mechanism, J. Phys. Chem. C 119 (2015) 26554–26559, http://dx.doi.org/10.1021/acs.jpcc.5b08508.
[49] E. Skúlason, V. Tripkovic, M.E. Björketun, S. Gudmundsdoíttir, G. Karlberg, J. Rossmeisl, Thomas Bligaard, Hannes Jonsson, Jens K. Nørskov, Modeling the electrochemical hydrogen oxidation and evolution reactions on the basis of density functional theory calculations, J. Phys. Chem. C 114 (2010) 18182–18197, http://dx.doi.org/10.1021/jp1048887.
[50] J. Hussain, E. Skúlason, H. Jónsson, Computational study of electrochemical CO2 reduction at transition metal electrodes, Procedia Comput. Sci. 51 (2015) 1865–1871, http://dx.doi.org/10.1016/j.procs.2015.05.419.
[51] J. Hussain, H. Jonsson, E. Skúlason, Faraday efficiency and mechanism of electrochemical surface reactions: CO2 reduction and H2 formation on Pt(111), Faraday Discuss. (2016), http://dx.doi.org/10.1039/C6FD00114A.
[52] P.W. Atkins, Physical Chemistry, 6th ed., Oxford University Press, 1998, 2016.
[53] D.R. Lide, CRC Handbook of Chemistry and Physic, 78th ed., Florida, 1997.
[54] J. Howalt, T. Vegge, Electrochemical ammonia production on molybdenum nitride nanoclusters, Phys. Chem. Chem. Phys. 15 (2013) 20957–20965, http://dx.doi.org/10.1039/c3cp53160k.

Please cite this article in press as: Y. Abghoui, E. Skúlason, Onset potentials for different reaction mechanisms of nitrogen activation to ammonia on transition metal nitride electro-catalysts, Catal. Today (2016), http://dx.doi.org/10.1016/j.cattod.2016.11.047

V Article 5

Computational Predictions of Catalytic Activity of Zincblende (110) Surfaces of Metal Nitrides for Electrochemical Ammonia Synthesis

Younes Abghoui and Egill Skúlason

J. Phys. Chem. C, in press (2017).

THE JOURNAL OF PHYSICAL CHEMISTRY C

Subscriber access provided by NAT AND UNIV LIB OF ICELAND

Article

Computational Predictions of Catalytic Activity of Zincblende (110) Surfaces of Metal Nitrides for Electrochemical Ammonia Synthesis

Younes Abghoui, and Egill Skulason

J. Phys. Chem. C, **Just Accepted Manuscript** • DOI: 10.1021/acs.jpcc.7b00196 • Publication Date (Web): 22 Feb 2017

Computational Predictions of Catalytic Activity of Zincblende (110) Surfaces of Metal Nitrides for Electrochemical Ammonia Synthesis

*Younes Abghoui and Egill Skúlason**

Science institute and faculty of physical sciences, University of Iceland

*E-mail: egillsk@hi.is

Abstract

Here we present comprehensive results of theoretical analyses conducted with density functional theory on the (110) texture orientations of the zincblende structures of 23 transition metal nitrides to explore new candidates for catalyzing N_2 electroreduction reaction (NER) at ambient conditions. The catalytic activity of these surfaces is investigated by constructing the free energy diagrams via Mars-van Krevelen mechanism. The stability of these materials against poisoning in electrochemical media and decomposition to parental metals under operational conditions is scrutinized. The catalyst regeneration rate is compared with the rate of decomposition in order to explore the sustainability of the catalytic cycle. A relatively good correlation between the onset potential for NER and the binding energy of adsorbed nitrogen on vacancy is obtained. RuN, CrN, and WN are predicted to be stable and active for NER with low onset potentials (from −0.23 V to −0.55 V vs. RHE) among all the nitrides studied here. NiN, RhN, PdN, IrN and PtN were found unable to sustain the catalytic cycle of ammonia at ambient conditions. Instead, they might be interesting as potential reactants for the ammonia reaction.

1. Introduction

Ammonia has received numerous attention as green fuel and hydrogen source for mobile and remote applications[1,2], as a potential indirect hydrogen storage and hydrogen carrier material[3,4], and more importantly as fertilizer[5] where 85% of produced ammonia belongs there. The dominant route to the production of ammonia is the Haber–Bosch process in an industrial scale, which involves the reaction of N_2 and H_2 on a transition metal-based catalyst under high energy consumption conditions.[6] Nitrogen is obtained from air, while hydrogen is taken mostly from steam reforming of natural gas in Europe (42 plants spread over 17 countries), but from coal in China, and from a mix of natural gas and naphtha in India.[7] Following hundred years of improvement, catalytic synthesis of ammonia has made remarkable progress. After discovery of iron catalyst for ammonia production in 1905, cobalt-containing catalyst became an important development for Fe_3O_4-based iron catalyst patented by the British company Imperial Chemical Industries. The amount of cobalt gradually decreased and CeO_2 was added instead in the cobalt-containing catalyst to increase the activity. In 1970s, Ozaki et al.[8] reported high activity for ammonia synthesis when they used Ru as an active component, potassium as a metal promoter, and carbon as a catalyst carrier. In 1992, a new ammonia synthesis process called KAAP (Kellogg Advanced Ammonia Process) was developed that was loading ruthenium carbonyl compounds on graphite carbon carriers to make Ru/C catalysts with around 20 times greater catalytic activity than that of traditional ammonia catalysts and at milder operating conditions.[9] Despite high activity of Ru/C catalysts, the loss of active carbon carrier was found due to the methanation of carbon material of the carriers under ammonia synthesis conditions, and that led to shortening the catalyst life and caused major weakness of the ruthenium catalysts in addition to its scarcity and high expense. So far, the latest improvement in the study of ammonia synthesis catalyst is the discovery of cobalt-molybdenum nitride (Co_3Mo_3N) catalyst.[10–14] Along these improvments in catalyst itself, advancements in technology and engineering also played an

amportant role in development of ammonia synthesis. For example, the daily ammonia production has been increased from the initial 5 tones to the current 3000 tones in modern plants, the reaction pressure has dropped to around 150 atm from the original 986 atm, and the energy consumption has decreased to 28-30 $GJ.t^{-1}$ from the initial 78-80 $GJ.t^{-1}$.[15–17] But ammonia production still consumes 2% of total energy supply in the world and releases around 2.2 tones of CO_2 per tone of ammonia.[17] Still over 90% of this energy that is spent for hydrogen production during ammonia synthesis is provided by fossil fuels, which leads to increased production of various greenhouse gases. Therefore, development of a new process for green and decentralized ammonia synthesis in much milder operating conditions is desired.

Electrocatalytic ammonia synthesis is a particularly attractive alternative method due to the potential of utilizing renewable energy sources and generating new possibilities towards low-temperature and low-pressure ammonia synthesis with low carbon footprint.[18–20] In this approach, instead of a separate H_2(g) production process, the protons could come from a proton-donor containing solution while the electrons would be driven to the electrode surface by an applied electric potential. Numerous efforts have been made towards electrochemical synthesis of ammonia using solid-state electrolytes [21–24], ionic liquids or molten salts [25–27], and polymer electrolyte membranes (PEMs).[28–30] The first two categories are usually used in higher temperature conditions (100 °C < T < 500 °C), but the last one is utilized for milder conditions (T < 100 °C). In the solid-state ammonia synthesis category, Amar et al. recently examined two different cathode catalysts, Fe_3Mo_3N [31] and Co_3Mo_3N [32] under pure nitrogen, with wet hydrogen on the side of the anode. The latter nitride was reported better for which a maximum rate of 3.27×10^{-7} $mol.s^{-1}.cm^{-2}$ was obtained at 0.8 V vs. the counter electrode and at 450 °C in $(Li/Na/K)_2CO_3$ electrolyte that was combined with $LiAlO_2$. But the faradaic efficiency (FE) was very low (~3%). In the category of molten salts, Licht et al. utilized a suspension of iron-oxide nanoparticles in the electrolyte ((molten hydroxide, (NaOH–KOH)) for ammonia synthesis from

air and steam between two Ni electrodes. [27] The rate of ammonia generated by this system was 2.4×10^{-9} mol.s^{-1}.cm^{-2}, which reached the FE of 35% under 1.23 V at ambient pressure. Despite an appreciable rate and FE, relatively high temperatures of around 200 °C were used. For the last category (PEMs), the first observation of low-temperature ammonia synthesis from water and nitrogen was reported on a Ru catalyst in an alkaline solution using a Nafion membrane.[33] Due to the competing hydrogen evolution reaction (HER) at the cathode, only a low rate of 3.4×10^{-12} mol.s^{-1}.cm^{-2} with a low FE of ~0.28% was achieved at a relatively high potential (-1.3 V vs. SHE) at temperatures below 100 °C. However, the highest rate of ammonia synthesis that has been obtained thus far using air and water as feed gases is 1.14×10^{-9} mol.s^{-1}.cm^{-2}, achieved using a mixed NH_4^+/H^+ Nafion membrane.[30] A low FE (~1%) was observed at a relatively high overpotential of -1.6 V.

The above examples indicate that finding active materials that have a low overpotential with enough selectivity towards nitrogen electroreduction reaction (NER) at ambient conditions is challenging in order to reach production rates nearing that of commercial viability ($4.3–8.7 \times 10^{-7}$ mol.s^{-1}.cm^{-2}) with FE's exceeding 50%.[18] First-principle calculations have been employed to provide more insight about the mechanisms of the reaction and to explore new class of materials with higher activity and selectivity towards NER. According to density functional theory (DFT) calculations conducted on a range of pure transition metals, the surface of early transition metals of Sc, Y, Ti, and Zr should bind N-adatoms more strongly than H-adatoms at the operating potentials of around -1.0 to -1.5 V vs. SHE and therefore they should favour NH_3 formation over H_2 evolution.[34] It was also shown that the surface of Fe, Rh, and Ru are mainly covered with H-adatoms under operating conditions. This inhibits nitrogen reduction to ammonia due to lack of available sites for adsorption of nitrogen, which leads to a high rate of HER. These findings might also explain the reason for the generally poor rates of ammonia production compared to hydrogen evolution in much of the existing literature. Conversely, transition metal nano-clusters

as well as MoN nano-clusters were found capable of enhancing the ammonia activity over HER.[35,36] However, the presence of water in the electrochemical environment can reduce the efficiency of these catalysts by blocking its active site due to preferential adsorption of oxygen rather than nitrogen.[37] In the last couple of examples, the studied mechanisms for electrochemical ammonia synthesis was associative and dissociative mechanisms where there are always issues with endothermic adsorption of N_2 molecule on the surface (in the associative mechanism) or high activation barriers for N_2 dissociation (in the dissociative mechanism). However, there exist the possibility of another active mechanism, specifically on the surface of metal nitride materials, where a surface N atom is reduced to NH_3 leaving N-vacancies behind and then the catalyst is regenerated with solvated N_2 in the electrolyte. This is the Mars-van Krevelen mechanism (MvK).[38] We have recently investigated the feasibility of this mechanism on some of the crystallographic structures of TMNs for electrochemical ammonia formation at ambient conditions.[39–41] It was found that the (100) facets of the NaCl-type structures of VN, CrN, ZrN, and NbN are predicted to be stable and active catalyst materials for the NER at ambient conditions via a MvK. Similar difficulties mentioned above regarding the applicability of conventional associative and dissociative mechanisms on transition metal nano-clusters were recently shown on the surface of transition metal nitrides (TMNs) where the MvK was predicted to be the most favorable reaction mechanism offering an easier path and smaller onset potentials for ammonia formation.[42] Indeed, recent DFT analyses indicate that participation of N-vacancies (in large concentrations of $\sim 10^{13}$ cm^{-2}) play an important role for ammonia formation on the surface of Co_3Mo_3N.[43] Also importance of these type of defects was reported in two-step solar-energy driven ammonia formation on metal nitrides.[44,45] Moreover, possible reaction sites on Co_3Mo_3N for adsorption and activation of the reactants of ammonia synthesis were identified via MvK with heterogeneity due to surface nitrogen vacancies.[46] Experimental evidences of the

operation of the MvK mechanism and its influence on enhanced electrocatalytic activity are also reported for example for CO oxidation[47], oxygen evolution reaction[48], and methanol oxidation[49]. In this study, DFT calculations are used to screen for a stable and active material amongst a range of zincblende (ZB) TMN (110) surfaces for catalyzing electrochemical nitrogen reduction to ammonia at ambient conditions. Therefore, catalytic activity of 23 nitrides (ScN, TiN, VN, CrN, FeN, CoN, NiN, YN, ZrN, NbN, MoN, RuN, RhN, PdN, AgN, HfN, TaN, WN, ReN, OsN, IrN, PtN, and AuN) is investigated for reducing N_2 to NH_3 via MvK mechanism. In synthesizing the nitrides, a multifaceted structure is more probable to grow rather than a single-crystal surface.[50–57] Therefore, different texture orientations or facets might be available on the surface with different reactivity towards the reaction. This knowledge about the stability and reactivity of different facets will help better engineering of the catalyst surface and experimental parameters, and thus a better performance in real applications. The generally accepted trends for TMNs is that early TMNs are most stable in rocksalt structure while the later TMNs are usually most stable in zincblende.[58–60] Regarding facet stability, experimental studies with XRD techniques show that usually several texture orientations and surface planes are detectable in manufactured surfaces of these nitrides where (100), (111), and (110) orientations are among the most prevalent orientations in the crystal structures.[52,53,56,57,61] Therefore as we have already investigated the stability and catalytic activity of other surface planes and structures, in this study we only focus on the (110) facets of the zincblende structures. Here, only the mononitrides are investigated and the analyses of other stoichiometry of these nitrides will be the subject of our future work. To investigate the activity, the thermodynamics of the cathode reaction is explored by constructing free energy diagrams (FEDs) for the electrochemical hydrogenation of surface of these mononitride structures. The lowest onset potential required to produce ammonia is estimated for each nitride. Stability of the active sites in electrochemical environment and poisoning of the catalyst under an applied bias are also considered. The likelihood of catalyst

regeneration over decomposition is also taken into account for the most interesting candidates. In addition, the competing hydrogen evolution reaction (HER) on all these nitride surfaces is explicitly investigated within our mechanistic model and the TMN with higher selectivity towards HER were eliminated from the rest of study.

2. Methodology

2.1. Computations

The electronic structure calculations are conducted with density functional theory (DFT) using the RPBE exchange-correlation functional.[62] A plane wave basis set with an energy cutoff of 350 eV is used to represent the valence electrons with a PAW [63] representation of the core electrons as implemented in the VASP code.[64–66] The self-consistent electron density is determined by iterative diagonalization of the Kohn-Sham Hamiltonian, with the occupation of the Kohn-Sham states being smeared according to a Fermi–Dirac distribution with a smearing parameter of K_{BT} = 0.1 eV. A 4×4×1 Monkhorst–Pack k-point sampling is used for all the surfaces. Activation energies are calculated as the highest point along the minimum energy path (MEP) calculated using the climbing image nudged elastic band method (CI-NEB).[67,68]

Each nitride surface is modeled as a five-layer slab with each layer consisting of four metal atoms and four nitrogen atoms. The bottom two layers are fixed whereas the top layers as well as the adsorbed species are allowed to relax. Boundary conditions are periodic in the x and y directions and surfaces are separated by 12 Å of vacuum in the z direction. The structural optimization is considered converged when the forces in any direction on all moveable atoms are less than 0.01 eV $Å^{-1}$. The RPBE lattice constants and are taken from Ref. [69]. These RPBE-calculated lattice constants are 1–2% from the experimental values. VN, CrN and MnN were reported to exhibit strong magnetism at their equilibrium lattice constants, with preferred ordering of ferromagnetic (VN and CrN) and antiferromagnetic (MnN), and as such are treated

as spin-polarized with magnetic moments given in Ref. [69].

2.2. Reaction pathways and electrochemical modeling

The overall cathode reaction of the electrochemical process is:

$$N_{2(g)} + 6(H^+ + e^-) \longrightarrow 2NH_{3(g)} \quad (1)$$

The source of protons could be either water splitting or H_2 oxidation in the anode reaction. But we refer to H_2 here only as a convenient source of protons and electrons to link our absolute potential vs. SHE:[70]

$$H_2 \rightleftharpoons 2(H^+ + e^-) \quad (2)$$

Since we do these analyses at pH = 0, all the predicted onset potentials vs. SHE become equivalent to RHE at zero pH. Doing these analyses at zero pH might bring up the stability concern of these materials at low pH values under operating conditions, however, there are several experimental investigations that prove the high stability of these TMNs in acidic solutions[71–74]. Nonetheless if a specific TMN exhibits insufficient stability at low pH values, the onset potentials predicted in this study can easily be calculated analytically for different pH values according to the Nernst equation.

Hydrogenation of the surface is carried out by adding H atoms one-by-one to the surface to represent a proton from the solution and an electron from the electrode. For hydrogenation, all the possible adsorption sites on the surface are investigated and the most stable site and accordingly the most stable intermediate are taken into account for upcoming hydrogenation steps. In this approach we do the so-called unconstrained [39,75] MvK mechanism where the protons are not constrained to adsorb to a specific atom or a molecule on the surface.

A heterogeneous MvK mechanism with consideration of both single N-vacancy and dimer N-vacancy is investigated. For the former, one ammonia (NH_3) molecule is formed by successive hydrogenation of surface until a surface N atom is reduced to NH_3 and accordingly a N-vacancy

is created. Afterwards, the single N-vacancy is regenerated with dissociation of the solvated N_2 from the electrolyte where one of the two nitrogen atoms of N_2 fills the N-vacancy and the other binds the surface. Reducing this nitrogen at the surface then forms the second NH_3 molecule and completes the catalytic cycle. The hypothetical single N-vacancy MvK reaction mechanism is shown in Eqs. (3)–(11):

$$* + 6(H^+ + e^-) + N_2 \rightleftharpoons *H + 5(H^+ + e^-) + N_2 \quad (3)$$

$$*H + 5(H^+ + e^-) + N_2 \rightleftharpoons *2H + 4(H^+ + e^-) + N_2 \quad (4)$$

$$*2H + 4(H^+ + e^-) + N_2 \rightleftharpoons *3H + 3(H^+ + e^-) + N_2 \quad (5)$$

$$*3H + 3(H^+ + e^-) + N_2 \rightleftharpoons *^{-N} + NH_3 + 3(H^+ + e^-) + N_2 \quad (6)$$

$$*^{-N} + 3(H^+ + e^-) + N_2 \rightleftharpoons * + *N + 3(H^+ + e^-) \quad (7)$$

$$*N + 3(H^+ + e^-) \rightleftharpoons *NH + 2(H^+ + e^-) \quad (8)$$

$$*NH + 2(H^+ + e^-) \rightleftharpoons *NH_2 + (H^+ + e^-) \quad (9)$$

$$*NH_2 + (H^+ + e^-) \rightleftharpoons *NH_3 \quad (10)$$

$$*NH_3 \rightleftharpoons * + NH_3 \quad (11)$$

An asterisk, *, denotes a surface site and "$*^{-N}$" denotes a surface N-vacancy. *N represents one of the nitrogen atoms from N_2 that binds the surface after another nitrogen has replenished the N-vacancy. We also consider the possibility of the dimer N-vacancy MvK mechanism where two NH_3 molecules are formed from two surface N atoms and a dimer N-vacancy is created before regenerating the catalyst with solvated N_2 from the electrolyte. This is given in eqns (3)–(6) when first NH_3 molecule is formed and then eqns (12)-(16) where hydrogenation of the surface is continued to form the second NH_3, the dimer N-vacancy, and eventually replenishment of vacancies.

$$*^{-N} + NH_3 + 3(H^+ + e^-) + N_2 \rightleftharpoons *^{-N} + NH_3 + *H + 2(H^+ + e^-) + N_2 \quad (12)$$

$$*^{-N} + NH_3 + *H + 2(H^+ + e^-) + N_2 \rightleftharpoons *^{-N} + NH_3 + *2H + (H^+ + e^-) + N_2 \quad (13)$$

$$*^{-N} + NH_3 + *2H + (H^+ + e^-) + N_2 \rightleftharpoons *^{-N} + NH_3 + *3H + N_2 \quad (14)$$

$$*^{-N} + NH_3 + *3H + N_2 \rightleftharpoons *^{-2N} + 2NH_3 + N_2 \quad (15)$$

$$*^{-2N} + 2NH_3 + N_2 \rightleftharpoons 2* + 2NH_3 \quad (16)$$

The dimer N-vacancy in the surface layer is denoted as $*^{-2N}$. DFT calculations are used to calculate the minimum energy configuration of each species on the surface and adsorption energies of all intermediates according to reactions (3)-(16). Various surface sites are considered and the optimal binding site is identified. The free energy of each elementary step is estimated at pH = 0 according to:

$$\Delta G(0) = \Delta E + \Delta ZPE - T\Delta S \quad (17)$$

where $\Delta G(0)$ is the free energy change of the reaction at zero potential, and ΔE is the reaction energy calculated with DFT. The differences in zero-point energy correction (ΔZPE) and entropy (ΔS) are calculated within a harmonic approximation and the values of these are given elsewhere.[40] Free energy diagrams were established by using a computational hydrogen electrode (CHE) method, which estimates a chemical potential of proton and electron pair ($\mu(H^+ + e^-)$) equivalent to that of a half of gaseous hydrogen ($0.5\mu(H_2)$) at standard reaction conditions (pH = 0, T = 298.15 K, 1 atm, and U = 0 V vs. SHE).[70] At zero pH, the onset potentials predicted vs. SHE are equivalent to the onset potentials vs. RHE. The chemical potential of the proton and electron pair is shifted by –neU when the external potential U is applied (See Figure S1, VN). Thus $\Delta G(U)$ is the free energy change of the reaction at an applied potential U:

$$\Delta G(U) = \Delta G(0) - neU \quad (18)$$

Explicit inclusion of a water layer [76] has not been considered in the present work due to the large computational effort required. It has been shown that the presence of water may help stabilize some species more than others via hydrogen bonding.[70,77] However, this solvation-induced stabilization of adsorbates in the NER are estimated to be below 0.1 eV.[78] From this we conclude that the onset potentials calculated in the present study are likely to change by a similar magnitude, which is less than 0.1 eV, and we do not include this correction in the data presented here.

3. Result and discussion

3.1. Catalytic activity

The possibility of catalyzing NER to ammonia was studied via MvK mechanism with both single and dimer N-vacancy approaches as given in Eqs. (3)-(16) on the ZB(110) facets of TMNs, where the surface nitrogen atoms are hydrogenated (with consideration of all the possible adsorption sites for H) and reduced to ammonia, and nitrogen vacant sites are created before the catalyst gets replenished by solvated nitrogen from the electrolyte. Two types of elementary steps are assumed in the modeling with regards to the effect of the applied potential in shifting the FEDs. One is an electrochemical step with proton/electron transfer, such as hydrogenation of the nitride surface. In the constructed FEDs shown below, the largest difference between the two adjacent electrochemical steps is termed the potential-determining step (PDS) as it indicates the bias required making all electrochemical steps exergonic. Another type of elementary step is a non-electrochemical step without proton/electron transfer, which are replenishment of the nitride with solvated dinitrogen molecules from the electrolyte and desorption of ammonia molecules from the surface. These types of steps cannot be tuned by applying bias and consequently determines the rate of the reaction (if those steps are endergonic on a particular TMN surfaces) and are labeled rate-determining step (RDS). However in case desorption of ammonia becomes

endergonic, the ammonia molecules formed on the surface are expected to get further protonated in acidic solutions to NH_4^+ and therefore facilitates this step in the reaction.

For the surfaces of ReN, AuN and AgN, significant distortion of the surface atoms is observed during relaxation and thus these nitrides are considered unstable and eliminated from further analyses. For the nitrides of Sc, Ti, Cr, Y, Zr, Nb, Mo, Hf, Ta, Os, and W, it was found that during surface reaction, hydrogenation of both metal atom and surface nitrogen is favorable and before first ammonia formation there are some *MH (H adsorption on the metallic site) and *NH (H adsorption on the surface N) formation steps. But for the nitrides of Fe, Co, Ni, Ru, Rh, Pd, Ir, Pt, and V, the most energetically favorable adsorption site for protons was on surface nitrogen atoms. In all of these surfaces, none of the metallic atoms on the surface bind H stronger than the surface N atoms. This means that when considering 4 nitrogen atoms and 4 metallic atoms on the surface per unit cell, the most thermodynamically favorable intermediate is *NH and not the *MH. Successive hydrogenation of these surfaces resulted in population of all the surface nitrogen atoms with H and formation of either 1^*NH_2 (on the surface of PtN, IrN, RuN, and RhN), 3^*NH_2 (on the surface of VN), or 4^*NH_2 (on the surface of FeN, CoN, NiN, and PdN) prior to formation of the first ammonia molecule and creation of the vacancy (see Figure 1 and Figure S1). On the surfaces of ScN, TiN, YN, HfN and TaN, after formation of *4NH, successive hydrogenation of the surface contributed to formation of $^*4NH_2$ without formation of any $^*NH_3$ intermediate. Thus, 1ML coverage on these five surfaces did not lead to any ammonia formation. Addition of extra protons on the surface caused recombination of surface H-adatoms and evolution of H_2 instead. Therefore, the nitrides of Sc, Ti, Y, Hf, and Ta are excluded from the rest of study, as they cannot be used to activate nitrogen to ammonia.

The free energy of all stable intermediates is calculated according to Eq. (17), with reference to N_2 and H_2 in the gas phase. For all the nitrides studied here it was found that the dimer-vacancy

approach is a more favorable approach for formation of two ammonia molecules. The only exceptions are NbN, CrN, ZrN, NiN, and WN where single-vacancy approach seems more likely (see the provided FEDs in Figures 1 and S1). The FEDs for RuN and CoN (might be good catalysts), NiN and RhN (might be good reactants) are presented in Figure 1 and the remaining FEDs of other nitrides are shown in Figure S1 of the supplementary material, where a pathway towards NH_3 formation via both single and dimer-vacancy MvK mechanism is illustrated and compared. The PDS and the measure of the catalytic activity towards nitrogen reduction to ammonia on each of the nitrides are identified as the elementary reaction step with the largest increase in free energy (ΔG).

As can be seen for RuN, the PDS is the fifth hydrogenation step after formation of the first ammonia with ΔG_{PDS} = 0.23 eV if the reaction proceeds via dimer vacancy approach. Thus, by applying an external bias of −0.23 V vs. RHE, this small increase in free energy can be eliminated and all electrochemical steps will then be downhill in free energy. But if the reaction goes via single vacancy approach, the step to fill the vacancy with nitrogen becomes 1.89 eV endothermic and very difficult at ambient conditions. This step does not involve electron/proton transfer (non-electrochemical step), thus there is no favorable change in its free energy when applying an external bias. So it becomes a RDS and temperature or pressure modification is required to speed up this step. This is seen for CoN as well where filling the vacancy via single vacancy approach becomes 1.31 eV endothermic, while through dimer vacancy approach there is only small endothermicity that needs to be accounted for the reaction to proceed. The ninth hydrogenation step has ΔG_{PDS} = 0.27 eV. Applying a small bias of -0.27 V vs. RHE can shift the FED of CoN in a way that all the steps become downhill in free energy and therefore reaction proceeds at ambient conditions. Both RuN and CoN seem to be very good candidates for catalyzing NER to ammonia when considering the overpotential required for the reaction on these surfaces and comparing it with the equilibrium potential of ammonia formation from H_2(g)

and N_2(g) that is around +0.06 V.[79] However, for both NiN and RhN replenishment of the vacancy was found endothermic via either of the paths. Thus they cannot be good catalysts for this reaction at ambient conditions, as the catalytic cycle cannot be completed due to high endothermic nature of the replenishment step. However, formation of the first ammonia molecule seems exothermic and easy with only small overpotential of around -0.1 V on NiN. On RhN, it seems like there is no overpotential at all and the reaction can proceed spontaneously under operational conditions. Therefore, these latter two nitrides might be interesting reactant materials instead for ammonia synthesis, similar to the case of Mo_2N reported as promising reactant for the solar thermochemical ammonia synthesis.[80] Although from FEDs it is seen that the release of NH_3 is sometimes slightly endergonic, in reality and in acidic conditions the adsorbed NH_3 is likely to get further protonated to NH_4^+ and released into the solution, thereby avoiding this increase in free energy.

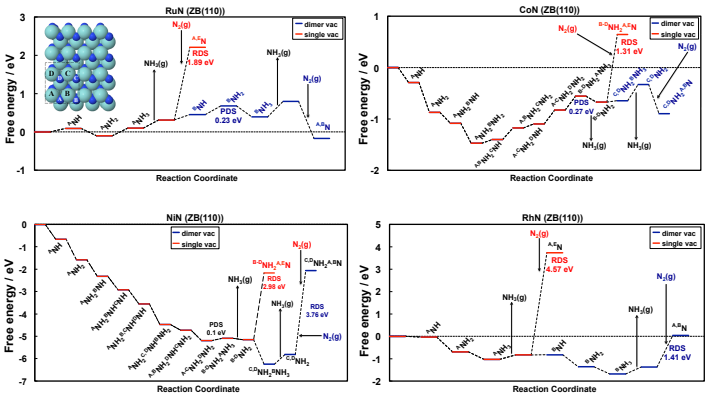

Figure 1. Free energy diagram (FED) for nitrogen electroreduction to ammonia via both a single and a dimer N-vacancy MvK mechanism on RuN, CoN, NiN, and RhN. The red line represents the free energy of all the stable intermediates at zero potential vs. RHE when a single N-vacancy approach is studied. The blue line indicates the

free energy of all the stable intermediates calculated at zero potential vs. RHE when a dimer N-vacancy approach is investigated. For RuN the PDS is the fifth hydrogenation step via dimer N-vacancy with ΔG_{PDS} = 0.23 eV. The rate-determining step (RDS) of 1.89 eV was found when the single N-vacancy is regenerated from solvated nitrogen in the electrolyte, and therefore the dimer N-vacancy pathway is more likely. For CoN the PDS is the ninth hydrogenation step via dimer N-vacancy with ΔG_{PDS} = 0.27 eV. However, via single N-vacancy there is a RDS to fill the single N-vacancy with ΔG_{RDS} = 1.31 eV. As the RDS involves no proton-electron transfer, applying the bias cannot change the free energy landscape in a way surmounting this increase in free energy of this step, but temperature or pressure modification is required. Therefore the dimer N-vacancy pathway is more likely. For NiN and RhN due to existence of a large RDS to replenish both the single and dimer N-vacancy, the catalytic cycle is ceased at ambient conditions. But these last two nitrides might be used as potential reactants for the ammonia synthesis where all the N contents of their material is consumed to ammonia and without possibility of regeneration, a parent metal is remained. The top view of the ZB (110) metal nitride unit cell is shown in the inset where it has been repeated once in the lateral directions. Cyan spheres represent metal atoms and dark blue spheres represent nitrogen atoms. The N atoms of the TMNs are labeled A, B, C and D and the adsorption site at each step of the FEDs are indicating which N atoms are reduced each time. The ^{A,E}N labeling shows that a single N-vacancy has been filled by dissociating N_2 where one N replenishes the vacancy and other N binds the surface. The ^{A,B}N labeling of the final step indicates that a dimer N-vacancy has been filled by dissociating N_2.

In addition, it was found that different number of proton/electron pair is required on each nitride to complete the catalytic cycle of two ammonia formations. In some cases the reaction may look non-stoichiometric, but that is because there more than the minimum proton-electron pairs [6(H^+ + e^-)] are required for formation of two ammonia molecules. The extra hydrogen adatoms remained on the surface after formation of the two ammonia molecules either contribute to hydrogen evolution reaction and consequently reduce the Faradaic efficiency towards ammonia production or in some cases those H adatoms react with other surface nitrogen atoms later on in the process to form ammonia. The nitrides of Ru, Rh, Ir and Pt, need the minimum proton/electron pair [only 6(H^+ + e^-)]. While CrN requires 7(H^+ + e^-), VN, FeN, CoN, NiN, and

PdN each require 10($H^+ + e^-$), NbN 11($H^+ + e^-$), MoN and WN require 12($H^+ + e^-$), and OsN 13($H^+ + e^-$) and ZrN require 16($H^+ + e^-$). Of course, only 6($H^+ + e^-$) are needed to make $2NH_3$, and these "extra" H^+/e^- couples do not indicate that we have a loss of efficiency since they will be converted later on to ammonia since those H^+/e^- couples always reduce surface nitrogen and do not adsorb to the metal ions. Hence the picture is as follows; we start by loading the nitride with H^+/e^- couples until NH and NH_2 species are created on the surface and eventually ammonia is formed.

The free energy change of the PDS, (ΔG_{PDS}), of each nitride is shown in Figure 2. The most interesting nitrides are those with ΔG_{PDS} as small as possible (close to the equilibrium potential that is +0.06 V). But as expected, overpotential is always needed as driving force for the reaction to proceed. From the values of applied potential reported in the literature for this reaction, a material with potential less than 1.0 V would be attractive as a catalyst. Here, we predict that we do not have any H_2 formation which makes this much more promising and efficient than the pure metals that convert most of the electricity to H_2.[34] As seen, some nitrides exhibit endergonic vacancy replenishment with N_2 along the reaction path. This corresponds to a RDS and is demonstrated by white boxes. The height of these boxes corresponds to the value of the free energy change of RDS, (ΔG_{RDS}). These are NiN, RhN, PdN, IrN, and PtN on the surface of which there is either small (in case of NiN and IrN) or no endergonic electrochemical steps (no gray bar is shown) along the reaction path of ammonia formation. Meaning that the ammonia formation reaction can be spontaneous on these 5 surfaces in the operational conditions (see Figure 1 for NiN and RhN, and corresponding FEDs in Figure S1 for the remaining candidates). But when the first ammonia molecule is formed and the nitrogen vacancy created, it becomes difficult to regenerate the catalyst and the catalytic cycle is ceased. Therefore, they would have made a very good catalyst material for ammonia formation if they did not have these relatively large endothermic non-electrochemical steps for filling the vacancy and regeneration. Thus as

mentioned above, the nitrides of Ni, Rh, Pd, Ir, and Pt are not good catalysts at room temperature and pressure, but they could be interesting potential reactants for electrochemical or thermochemical ammonia formation.[80] However, VN, CrN, FeN, CoN, ZrN, NbN, RuN, and WN seem interesting catalyst material with relatively low onset potentials for nitrogen activation and ammonia formation and deserve more analyses and further investigations.

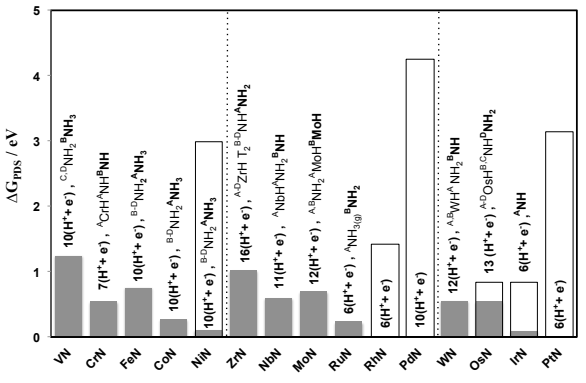

Figure 2. Free energy change of the PDS (ΔG_{PDS}, in eV) of nitrogen activation to ammonia on the (110) facets of the ZB structures of TMN surfaces. Number of proton-electron pairs required for $2NH_3$ formation is added above each bar. The labels above the number of proton-electron pairs indicate the species formed prior to PDS and the bold texts indicate the species formed right at the PDS, the notation of which is explained in Figure 1. The white boxes represent the value of the free energy of the RDS (ΔG_{RDS}, in eV) coming from filling the vacancy and regeneration of the catalyst. The two dashed lines separating the nitrides of different rows is drawn to help the eyes for easier realization of the trend observed from left to the right of the periodic table where the free energy of the PDS is decreasing.

Another interesting observation from the analyses of our data is a trend found in Figure 2 where the free energy of the PDS seems being decreased from left to the right of the periodic table. Therefore, we explored if any correlation could be found between the activity and a material dependent descriptor. The onset potential predicted for ammonia formation was found to

correlate with the dissociation energy of di-nitrogen in the vacancy. This correlation is shown in Figure 3 where the onset potential of these materials becomes less negative as the dissociative energy of di-nitrogen on the vacant sites becomes more positive. However as the dissociative energy becomes more endothermic, the harder it gets to regenerate the vacancies (for example for the NiN and RhN shown in Figure 1, and PdN and PtN shown in Figure S1). It means that the best material is the one that compromises both features; the onset potential and the ability to regenerate the vacant sites.

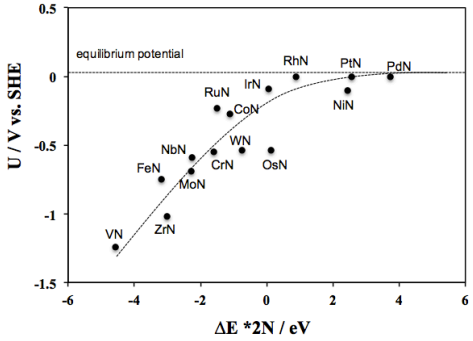

Figure 3. The onset potential of ammonia formation on the (110) facets of the ZB structure of TMNs as a function of the chemisorption energy of two N-adatoms in the N-vacancy.

3.2. Stability against poisoning

The catalytic activity of these nitrides was investigated via MvK mechanism due to the potential benefit these materials offer by the explicit incorporation of nitrogen in their surfaces. However, one important consideration is that after surface Ns have reacted and vacancies created at the surface, these vacancies must be filled with N_2 from the electrolyte for the catalytic cycle to endure. However, the vacancy might rather get filled with a H^+, O^{2-} or OH^- species from the

aqueous electrolyte, all of which could block these active surface sites, avoid filling of the vacancy with nitrogen, and thus poison the catalyst. So the competition between nitrogen with O^{2-}, H^+ and OH^- for filling the surface vacancy is investigated by considering the free energy of filling the vacancy with any of these species relative to nitrogen ($\Delta G_{(*2N-*X)}$), where X = O^{2-}, H^+ or OH^-. The source of these ions is from the water molecules or hydronium ions in the electrolyte that results in formation of O^{2-}, OH^- and H^+ under operating conditions. We calculate the difference in adsorption energy of these species compared to adsorbing nitrogen at the onset potential of ammonia formation. These free energies are referenced to N_2, H_2O and H_2 in the gas phase. A negative value of $\Delta G_{(*2N-*X)}$ indicates that it is thermodynamically favorable to fill the vacancy with nitrogen, rather than other three species. These values are shown in Figure 4 for all the nitrides studied here (whether catalytically active or not), and the onset potential (V vs. RHE) of each nitride at which these values are calculated also provided in this Figure.

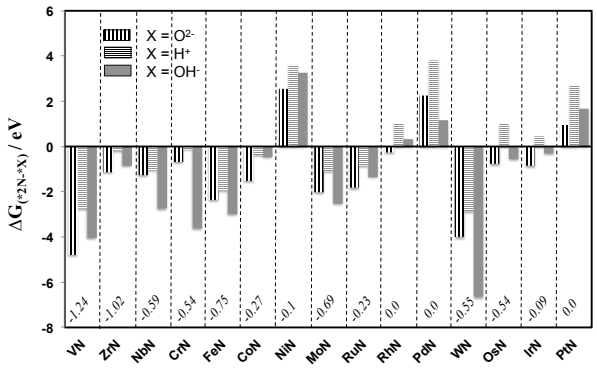

Figure 4. Free energy of adsorption of O^{2-}, H^+ or OH^- relative to free energy of adsorption of nitrogen on the surface vacancy of the nitrides. Free energies are calculated relative to N_2(g), H_2(g) and H_2O(g). All free energies are evaluated at the calculated onset potential (V vs. RHE) for each nitride given at the bottom of this Figure.

It can be seen that for most of the nitrides, nitrogen atoms bind more strongly to the surface vacancy compared with other three species. Thus the surface vacancies are unlikely to get poisoned, and by replenishment of the vacancy with nitrogen the catalytic cycle can complete and sustain. The exceptions are NiN, RhN, PdN, OsN, IrN and PtN. For NiN, PdN, and PtN where adsorption of nitrogen is the weakest and thus the vacant site is most likely to get poisoned mainly with H^+ or OH^-. Therefore the catalytic cycle cannot be completed by replenishment of the vacant sites with nitrogen and the catalytic activity will cease. For IrN and OsN only protons from the electrolyte might occupy the vacancy, while for RhN both protons and hydroxyls bind stronger.

Overall, when considering both the activity (Figure 2) and the stability of the nitrides against poisoning (Figure 4) the most promising candidates are CoN and RuN with very small overpotentials of around -0.2 to -0.3 V. Second most promising nitrides are CrN, NbN and WN that need a slightly higher overpotential for the reaction and the third promising nitrides are VN, FeN, ZrN and MoN with even higher overpotentials for ammonia formation. Therefore, more detailed stability assessment of vacancy is carried out for these nine nitrides in the following section where vacancy migration into the bulk (the fist step towards decomposition) and stability of the nitrides against decomposition is taken into account.

3.3. Stability against decomposition

As explained earlier, in the MvK mechanism a surface nitrogen atom is reduced to form NH_3 after which the resulting vacancy is replenished by an N_2 molecule solvated in the electrolyte. For this replenishment to occur, the vacancy needs to be stable at the surface. If this is not the case, the vacancy may migrate to the bulk of the catalyst, meaning that the N-vacancy in the first surface layer is replaced with more nitrogen from the catalyst itself, rather than with N_2. This

process can, in principle, continue until all the nitrogen atoms of the metal nitride have been reacted and reduced to NH_3, leaving only the pure metal.

The stability of the vacancy at the surface and thus stability of the nitrides against decomposition is estimated by comparing the difference in energy of a nitride slab with a single N-vacancy in the surface layer ($E_{vac,i}$) and to that of a single N-vacancy in the first subsurface layer ($E_{vac,f}$). The minimum energy configuration of each of these slabs is found and the energy difference ($\Delta E_{vac} = E_{vac,f} - E_{vac,i}$) used as an estimation of the thermodynamic stability of the vacancy at the surface of the nitride. Activation barriers for vacancy migration ($E_{a,vac}$) are also calculated with NEB calculations. Figure 5 shows the kinetics of the vacancy migration into the bulk as a function of thermodynamics. It is found that, for almost all the nitrides (except for CrN), it is thermodynamically favorable for the vacancy to migrate into the bulk, with $\Delta E_{vac} \leq 0.0$ eV. However, it is clear that some of the nitrides exhibit a high activation barrier of above 1.0 eV for vacancy migration and are thus likely to demonstrate a stable surface vacancy at room temperature.

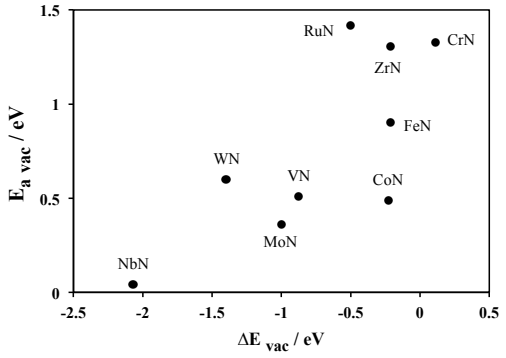

Figure 5. Energy difference (ΔE_{vac}) of a vacancy in the surface layer and in the first subsurface layer of a nitride and the associated activation barrier of vacancy migration ($E_{a,vac}$).

3.4. Regeneration of the active site on the surface

For a more detailed assessment of the stability of the nitrogen vacancy and feasibility of regeneration of the catalyst, the competition between migration of the vacancy from the surface into the bulk (decomposition) after formation of ammonia molecule and replenishment of the vacancy with nitrogen is inspected. The activation free energy (G_a) for both processes are calculated, where $G_a = E_a$ for the vacancy migration process, but $G_a = E_a + 0.6$ eV for the process of replenishing the vacancy with nitrogen. When molecular nitrogen splits and binds to the vacancy, it looses 0.6 eV of entropy at room temperature going from gas phase to the adsorbed state on the surface. The entropy loss of molecular nitrogen is taken from Ref. [81]. Therefore, even if the activation free energy of vacancy replenishment is calculated to be 0.0 eV, the activation free energy of migration should be higher than 0.6 eV so that replenishment can occur faster. If the vacancy is likely to replenish faster than it migrates into the bulk, the catalyst is likely to be able to regenerate itself and endure the catalytic cycle. These activation barriers are plotted and compared in Figure 6.

Although nitride of V and specially nitrides of Fe, Co, Nb and Mo show relatively good activity (according to Figure 2) and low probability of being poisoned from the electrolyte (according to Figure 4), there are lower activation barriers found for migration of the vacancy into the bulk of these nitrides (first step of decomposition) compared to regeneration of the vacancy with nitrogen. That implies that the rate of decomposition should be faster than the rate of regeneration and accordingly these five nitrides should decompose to ammonia and their parental metal under operating conditions. Although these latter nitrides cannot be used as catalyst for ammonia synthesis, they might be potential reactant materials for this process. For WN, however, the activation free energy of decomposition seems to be slightly smaller (around 0.06 eV) than regeneration. Therefore decomposition might not happen that fast before appreciable

amount of ammonia is produced, and this nitride might yet be worthwhile tested experimentally. On the other hand, nitrides of Cr, Zr, and Ru seem very interesting in the sense that they should be able to regenerate them and thus sustain the catalytic cycle of ammonia formation on their surface, since the activation free energy for replenishment is smaller than that of decomposition, and that contributes to higher rate of regeneration.

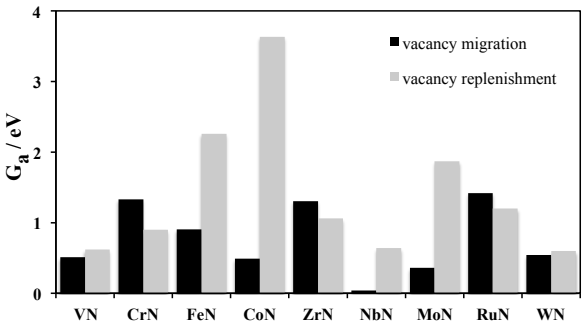

Figure 6. Calculated activation free energies (G_a) of the catalyst replenishment by N_2 dissociation for refilling the N-vacancy compared with activation free energies of vacancy migration into the bulk (migration of nitrogen atoms from the bulk toward the surface).

4. Conclusions

A theoretical analysis of the possibility of nitrogen electroreduction to ammonia at ambient conditions was presented on the (110) facets of the zincblende structures of ScN, TiN, VN, CrN, FeN, CoN, NiN, YN, ZrN, NbN, MoN, RuN, RhN, PdN, AgN, HfN, TaN, WN, ReN, OsN, IrN, PtN, and AuN. Except for ScN, YN, HfN, and TaN that were found inactive for ammonia formation, and AgN, ReN, and AuN that were found unstable, other (110) nitride surfaces were predicted more selective towards nitrogen electroreduction reaction under electrochemical

environment. Despite small overpotentials found for ammonia formation on NiN, RhN, PdN, OsN, IrN, and PtN, they were shown susceptible to poisoning under operating conditions in electrochemical media. In addition, replenishment of the vacancy was shown very endergonic on these latter surfaces hindering the endurance of the catalytic cycle. Thus, they cannot be good catalyst materials but instead might be good potential reactants for this reaction. For the remaining nitrides, VN, CrN, FeN, CoN, ZrN, NbN, MoN, RuN, and WN, kinetics were also taken into account in order to conclude whether the nitrogen vacancy created during the catalytic cycle will be regenerated with N_2 molecules or will be unstable and migrate into the bulk of the nitride. When calculating the activation free energy of both these processes, we showed that only CrN, ZrN, RuN, and WN are predicted to be promising candidates that can be regenerated and sustain the catalytic cycle of nitrogen activation and ammonia formation under ambient conditions. Especially RuN, CrN, and WN were predicted to require small overpotentials (from −0.23 V to −0.55 V vs. RHE) among all the nitrides studied here to catalyze ammonia formation at ambient conditions.

ASSOCIATED CONTENT

Supporting Information. Free energy diagrams for all the transition metal nitrides investigated here are provided in the Supporting Information.

AUTHOR INFORMATION

Corresponding Author

*egillsk@hi.is

Author Contributions

The manuscript was written through contributions of both authors. Both authors have given approval to the final version of the manuscript.

5. Acknowledgments

Financial support is acknowledged from the Icelandic Research Fund and the Research Fund of the University of Iceland. The calculations were in part carried out on the Nordic high performance computer (Gardar).

6. References

(1) Zamfirescu, C.; Dincer, I. Using Ammonia as a Sustainable Fuel. *J. Power Sources* **2008**, *185*, 459–465.

(2) Zamfirescu, C.; Dincer, I. Ammonia as a Green Fuel and Hydrogen Source for Vehicular Applications. *Fuel Process. Technol.* **2009**, *90*, 729–737.

(3) Klerke, A.; Christensen, C. H.; Nørskov, J. K.; Vegge, T. Ammonia for Hydrogen Storage: Challenges and Opportunities. *J. Mater. Chem.* **2008**, *18*, 2304–2310.

(4) Lan, R.; Irvine, J. T. S.; Tao, S. Ammonia and Related Chemicals as Potential Indirect Hydrogen Storage Materials. *Int. J. Hydrogen Energy* **2012**, *37*, 1482–1494.

(5) Markey study : Ammonia. Cerasena Market Intelligence Consulting. http://www.ceresana.com/en/market-studies/agriculture/ammonia/ammonia-market-study-analysis-trends.html (accessed Feb 19, 2017).

(6) Schlögl, R. Catalytic Synthesis of Ammonia-A "Never-Ending Story"? *Angew. Chem. Int. Ed. Engl.* **2003**, *42*, 2004–2008.

(7) Agency, I. E. Chemical and Petrochemical Sector. Potential of Best Practice Technology and other Measures for Improving Energy Efficiency. https://www.iea.org/publications/freepublications/publication/chemical_petrochemical_sector.pdf (access Feb 19, 2017).

(8) Ozaki, A. Development of Alkali-Promoted Ruthenium as a Novel Catalyst for

Ammonia Synthesis. *Acc. Chem. Res.* **1981**, *14*, 16–21.

(9) Rhodes, A. K. New Ammonia Process, Catalyst Proven in Canadian Plant. *Oil Gas J.* **1996**, *94*, 37–41.

(10) Jacobsen, C. J. H.; Dahl, S.; Clausen, B. S.; Bahn, S.; Logadottir, A.; Nørskov, J. K. Catalyst Design by Interpolation in the Periodic Table: Bimetallic Ammonia Synthesis Catalysts. *J. Am. Chem. Soc.* **2001**, *123*, 8404–8405.

(11) Kojima, R.; Aika, K. Cobalt Molybdenum Bimetallic Nitride Catalysts for Ammonia Synthesis Part 1 . Preparation and Characterization. *Appl. Catal. A Gen.* **2001**, *215*, 149–160.

(12) Kojima, R.; Aika, K. Cobalt Molybdenum Bimetallic Nitride Catalysts for Ammonia Synthesis Part 2 . Kinetic Study. *Appl. Catal. A Gen.* **2001**, *218*, 121–128.

(13) Kojima, R.; Aika, K. Cobalt Molybdenum Bimetallic Nitride Catalysts for Ammonia Synthesis Part 3 . Reactant Gas Treatment. *Appl. Catal. A Gen.* **2001**, *219*, 157–170.

(14) Hargreaves, J. S. J. Nitrides as Ammonia Synthesis Catalysts and as Potential Nitrogen Transfer Reagents. *Appl. Petrochemical Res.* **2014**, *4*, 3–10.

(15) Appl, M. *Ammonia: Principles and Industrial Practice*, 1st ed.; Wiley-VCH, 1999.

(16) Agarwal, P. Ammonia: the next step. Chemical and Process Engineering Resources. http://www.cheresources.com/content/articles/processes/ammonia-the-next-step (accessed Feb 19, 2017).

(17) Rafiqul, I.; Weber, C.; Lehmann, B.; Voss, A. Energy Efficiency Improvements in Ammonia Production - Perspectives and Uncertainties. *Energy* **2005**, *30*, 2487–2504.

(18) Giddey, S.; Badwal, S. P. S.; Kulkarni, A. Review of Electrochemical Ammonia Production Technologies and Materials. *Int. J. Hydrogen Energy* **2013**, *38*, 14576–14594.

(19) Kyriakou, V.; Garagounis, I.; Vasileiou, E.; Vourros, A.; Stoukides, M. Progress in the Electrochemical Synthesis of Ammonia. *Catal. Today* **2016**, "in press", doi: 10.1016/j.cattod.2016.06.014.

(20) Shipman, M. A.; Symes, M. D. Recent Progress towards the Electrosynthesis of Ammonia from Sustainable Resources. *Catal. Today* **2016**, "in press", doi: 10.1016/j.cattod.2016.05.008.

(21) Amar, I. A.; Lan, R.; Petit, C. T. G.; Tao, S. Solid-State Electrochemical Synthesis of Ammonia: A Review. *J. Solid State Electrochem.* **2011**, *15*, 1845–1860.

(22) Garagounis, I.; Kyriakou, V.; Skodra, A.; Vasileiou, E.; Stoukides, M. Electrochemical Synthesis of Ammonia in Solid Electrolyte Cells. *Front. Energy Res.* **2014**, *2*, 1–10.

(23) Vasileiou, E.; Kyriakou, V.; Garagounis, I.; Vourros, A.; Manerbino, A.; Coors, W. G.; Stoukides, M. Reaction Rate Enhancement During the Electrocatalytic Synthesis of Ammonia in a $BaZr_{0.7}Ce_{0.2}Y_{0.1}O_{2.9}$ Solid Electrolyte Cell. *Top. Catal.* **2015**, *58*, 1193–1201.

(24) Qing, G.; Kikuchi, R.; Kishira, S.; Takagaki, A.; Sugawara, T.; Oyama, S. T. Ammonia Synthesis by N_2 and Steam Electrolysis in Solid-State Cells at 220°C and Atmospheric Pressure. *J. Electrochem. Soc.* **2016**, *163*, 282–287.

(25) Murakami, T.; Nishikiori, T.; Nohira, T.; Ito, Y. Electrolytic Synthesis of Ammonia in Molten Salts under Atmospheric Pressure. *J. Am. Chem. Soc.* **2003**, *125*, 334–335.

(26) Murakami, T.; Nohira, T.; Goto, T.; Ogata, Y. H.; Ito, Y. Electrolytic Ammonia Synthesis from Water and Nitrogen Gas in Molten Salt under Atmospheric Pressure. *Electrochim. Acta* **2005**, *50*, 5423–5426.

(27) Licht, S.; Cui, B.; Wang, B.; Li, F.-F.; Lau, J.; Liu, S. Ammonia Synthesis by N_2 and Steam Electrolysis in Molten Hydroxide Suspensions of Nanoscale Fe_2O_3. *Science* **2014**, *345*, 637–640.

(28) Xu, G.; Liu, R.; Wang, J. Electrochemical Synthesis of Ammonia Using a Cell with a Nafion Membrane and $SmFe_{0.7}Cu_{0.3-x}Ni_XO_3$ (X = 0−0.3) Cathode at Atmospheric Pressure and Lower Temperature. *Sci. China Ser. B Chem.* **2009**, *52*, 1171–1175.

(29) Zhang, Z.; Zhong, Z.; Liu, R. Cathode Catalysis Performance of $SmBaCuMO_{5+\delta}$ (M=Fe, Co, Ni) in Ammonia Synthesis. *J. Rare Earths* **2010**, *28*, 556–559.

(30) Lan, R.; Irvine, J. T. S.; Tao, S. Synthesis of Ammonia Directly from Air and Water at Ambient Temperature and Pressure. *Sci. Rep.* **2013**, *3*, 1–7.

(31) Amar, I. A.; Lan, R.; Petit, C. T. G.; Tao, S. Electrochemical Synthesis of Ammonia Using Fe_3Mo_3N Catalyst and Carbonate-Oxide Composite Electrolyte. *Int. J. Electrochem. Sci.* **2015**, *10*, 3757–3766.

(32) Amar, I. A.; Lan, R.; Petit, C. T. G.; Tao, S. Electrochemical Synthesis of Ammonia Based on Co_3Mo_3N Catalyst and $LiAlO_2$–$(Li,Na,K)_2CO_3$ Composite Electrolyte. *Int. J. Electrochem. Sci.* **2015**, *6*, 286–294.

(33) Kordali, V.; Kyriacou, G.; Lambrou, C. Electrochemical Synthesis of Ammonia at Atmospheric Pressure and Low Temperature in a Solid Polymer Electrolyte Cell. *Chem. Commun.* **2000**, *17*, 1673–1674.

(34) Skúlason, E.; Bligaard, T.; Gudmundsdóttir, S.; Studt, F.; Rossmeisl, J.; Abild-

Pedersen, F.; Vegge, T.; Jónsson, H.; Nørskov, J. K. A Theoretical Evaluation of Possible Transition Metal Electro-Catalysts for N_2 Reduction. *Phys. Chem. Chem. Phys.* **2012**, *14*, 1235–1245.

(35) Howalt, J. G.; Bligaard, T.; Rossmeisl, J.; Vegge, T. DFT Based Study of Transition Metal Nano-Clusters for Electrochemical NH_3 Production. *Phys. Chem. Chem. Phys.* **2013**, *15*, 7785–7795.

(36) Howalt, J. G.; Vegge, T. Electrochemical Ammonia Production on Molybdenum Nitride Nanoclusters. *Phys. Chem. Chem. Phys.* **2013**, *15*, 20957–20965.

(37) Howalt, J.; Vegge, T. The Role of Oxygen and Water on Molybdenum Nanoclusters for Electro Catalytic Ammonia Production. *Beilstein J. Nanotechnol.* **2014**, *5*, 111–120.

(38) Mars, P.; Van Krevelen, D. W. Special Supplement to Chemical Engineering Science. *Eng. Sci* **1954**, *3*, 41–45.

(39) Abghoui, Y.; Garden, A. L.; Hlynsson, V. F.; Björgvinsdóttir, S.; Ólafsdóttir, H.; Skúlason, E. Enabling Electrochemical Reduction of Nitrogen to Ammonia at Ambient Conditions through Rational Catalyst Design. *Phys. Chem. Chem. Phys.* **2015**, *17*, 4909–4918.

(40) Abghoui, Y.; Garden, A. L.; Howalt, J. G.; Vegge, T.; Skúlason, E. Electroreduction of N_2 to Ammonia at Ambient Conditions on Mononitrides of Zr, Nb, Cr, and V: A DFT Guide for Experiments. *ACS Catal.* **2016**, *6*, 635–646.

(41) Abghoui, Y.; Skúlason, E. Electrochemical Synthesis of Ammonia via Mars-van Krevelen Mechanism on the (111) Facets of Group III–VII Transition Metal Mononitrides. *Catal. Today* **2016**, "in press", doi:

10.1016/j.cattod.2016.06.009.

(42) Abghoui, Y.; Skúlason, E. Onset Potentials for Different Reaction Mechanisms of Nitrogen Activation to Ammonia on Transition Metal Nitride Electro-Catalysts. *Catal. Today* **2016**, "in press", doi: 10.1016/j.cattod.2016.11.047.

(43) Zeinalipour-Yazdi, C. D.; Hargreaves, J. S. J.; Catlow, C. R. A. DFT-D3 Study of Molecular N_2 and H_2 Activation on Co_3Mo_3N Surfaces. *J. Phys. Chem. C* **2016**, *120*, 21390–21398.

(44) Michalsky, R.; Pfromm, P. H.; Steinfeld, A. Rational Design of Metal Nitride Redox Materials for Solar-Driven Ammonia Synthesis. *Interface Focus* **2015**, *5*, 20140084.

(45) Michalsky, R.; Avram, A. M.; Peterson, B. A.; Pfromm, P. H.; Peterson, A. A. Chemical Looping of Metal Nitride Catalysts: Low-Pressure Ammonia Synthesis for Energy Storage. *Chem. Sci.* **2015**, *6*, 3965–3974.

(46) Zeinalipour-Yazdi, C. D.; Hargreaves, J. S. J.; Catlow, C. R. A. Nitrogen Activation in a Mars–van Krevelen Mechanism for Ammonia Synthesis on Co_3Mo_3N. *J. Phys. Chem. C* **2015**, *119*, 28368–28376.

(47) Katsaounis, A.; Nikopoulou, Z.; Verykios, X. E.; Vayenas, C. G. Comparative Isotope-Aided Investigation of Electrochemical Promotion and Metal-Support Interactions: 2. CO Oxidation by $^{18}O_2$ on Electropromoted Pt Films Deposited on YSZ and on Nanodispersed Pt/YSZ Catalysts. *J. Catal.* **2004**, *226*, 197–209.

(48) Macounova, K.; Makarova, M.; Krtil, P. Oxygen Evolution on Nanocrystalline RuO_2 and $Ru_{0.9}Ni_{0.1}O_{2-\delta}$ Electrodes - DEMS Approach to Reaction Mechanism Determination. *Electrochem. commun.* **2009**, *11*, 1865–1868.

(49) Rebello, J. S.; Samant, P. V.; Figueiredo, J. L.; Fernandes, J. B. Enhanced Electrocatalytic Activity of Carbon-Supported MnO_x/Ru Catalysts for

Methanol Oxidation in Fuel Cells. *J. Power Sources* **2006**, *153*, 36–40.

(50) Hones, P.; Sanjines, R.; Levy, F. Characterization of Sputter-Deposited Chromium Nitride Thin Films for Hard Coatings. *Surf. Coatings Technol.* **1997**, *94*, 398–402.

(51) Gillan, E.; Kaner, R. Rapid Solid-State Synthesis of Refractory Nitrides. *Inorg. Chem.* **1994**, *768*, 5693–5700.

(52) Ramos, H. J.; Valmoria, N. B. Thin-Film Deposition of ZrN Using a Plasma Sputter-Type Negative Ion Source. *Vacuum* **2004**, *73*, 549–554.

(53) Arias, D. F.; Arango, Y. C.; Devia, A. Study of TiN and ZrN Thin Films Grown by Cathodic Arc Technique. *Appl. Surf. Sci.* **2006**, *253*, 1683–1690.

(54) Shayestehaminzadeh, S.; Tryggvason, T. K.; Magnus, F.; Olafsson, S.; Gudmundsson, J. T. Ultra-Thin Poly-Crystalline TiN Films Grown by HiPIMS on MgO(100) — In-Situ Resistance Study of the Initial Stage of Growth. *Thin Solid Films* **2013**, *549*, 199–203.

(55) Shayestehaminzadeh, S.; Thorsteinsson, E. B.; Primetzhofer, D.; Magnus, F.; Olafsson, S. Epitaxial and Textured TiN Thin Films Grown on MgO(100) by Reactive HiPIMS: The Impact of Charging on Epitaxial to Textured Growth Crossover. *J. Phys. D. Appl. Phys.* **2016**, *49*, 455301–455314.

(56) Choi, D.; Kumta, P. N. Chemically Synthesized Nanostructured VN for Pseudocapacitor Application. *Electrochem. Solid-State Lett.* **2005**, *8*, 418–422.

(57) Song, J.; Li, G. R.; Xiong, F. Y.; Gao, X. P. Synergistic Effect of Molybdenum Nitride and Carbon Nanotubes on Electrocatalysis for Dye-Sensitized Solar Cells. *J. Mater. Chem.* **2012**, *22*, 20580–20585.

(58) Eck, B.; Dronskowski, R.; Takahashi, M.; Kikkawa, S. Theoretical Calculations on the Structures, Electronic and Magnetic Properties of Binary

3d Transition Metal Nitrides. *J. Mater. Chem.* **1999**, *9*, 1527–1537.

(59) Stampfl, C.; Mannstadt, W.; Asahi, R.; Freeman, A. Electronic Structure and Physical Properties of Early Transition Metal Mononitrides: Density-Functional Theory LDA, GGA, and Screened-Exchange LDA FLAPW Calculations. *Phys. Rev. B* **2001**, *63*, 155106(1)-155106(11).

(60) Patil, S. K. R.; Mangale, N. S.; Khare, S. V.; Marsillac, S. Super Hard Cubic Phases of Period VI Transition Metal Nitrides: First Principles Investigation. *Thin Solid Films* **2008**, *517*, 824–827.

(61) Zhou, X.; Chen, H.; Shu, D.; He, C.; Nan, J. Study on the Electrochemical Behavior of Vanadium Nitride as a Promising Supercapacitor Material. *J. Phys. Chem. Solids* **2009**, *70*, 495–500.

(62) Hammer, B.; Hansen, L.; Nørskov, J. Improved Adsorption Energetics within Density-Functional Theory Using Revised Perdew-Burke-Ernzerhof Functionals. *Phys. Rev. B* **1999**, *59*, 7413–7421.

(63) Blöchl, P. Projector Augmented-Wave Method. *Phys. Rev. B* **1994**, *50*, 17953–17979.

(64) Kresse, G.; Hafner, J. Ab Initio Molecular-Dynamics Simulation of the Liquid-Metal–amorphous-Semiconductor Transition in Germanium. *Phys. Rev. B* **1994**, *49*, 14251–14269.

(65) Kresse, G.; Furthmüller, J. Efficient Iterative Schemes for Ab Initio Total-Energy Calculations Using a Plane-Wave Basis Set. *Phys. Rev. B. Condens. Matter* **1996**, *54*, 11169–11186.

(66) Kresse, G.; Furthmüller, J. Efficiency of Ab-Initio Total Energy Calculations for Metals and Semiconductors Using a Plane-Wave Basis Set. *Comput. Mater. Sci.* **1996**, *6*, 15–50.

VI Article 6

On the Possibility of Catalysing the Hydrogen Evolution Reaction with Transition Metal Nitrides as Cathode Material

Younes Abghoui and Egill Skúlason

submitted to J. Mat. Chem. A, March , (2017).

Journal of Materials Chemistry A

ARTICLE

On the possibility of catalysing the hydrogen evolution reaction with transition metal nitrides as cathode material

Received 00th January 20xx,
Accepted 00th January 20xx

DOI: 10.1039/x0xx00000x
www.rsc.org/

Younes Abghoui [a] and Egill Skúlason [a,†]

Density functional theory (DFT) calculations are used in this study to screen for highly stable and active catalyst material amongst transition metal nitrides (TMN) for the hydrogen evolution reaction (HER). Previously we have predicted with DFT calculations that some TMNs form ammonia under electrochemical conditions, while others get poisoned or they react to ammonia and its parental metal. The TMNs of Sc, Ti, Y, Hf, Ta, and Mo, however, get fully covered with H adatoms without forming any ammonia. These TMNs are investigated further here, where we focus on the (100) facet of the rocksalt structure. We calculate the H coverage as a function of applied potential. Activation energies of H2 formation via the Tafel reaction are also calculated at varying applied potentials. The results nominate a few nitrides (TaN, HfN, MoN and ScN) capable of catalyzing HER at low overpotentials of -0.09 to -0.34 V vs. RHE with the activation energies of the Tafel reaction relatively similar to that reported on Pt(111).

Introduction

The world vulnerability to the energy being almost only supplied from natural gases and fossil fuels is constantly increasing with the increased population of our planet and environmentally harmful energy production patterns. To achieve viable development and persist human society with high quality, environmentally sounds and secured renewable energy services that are evenly distributed throughout the world is vital. Efficient deployment of wind, water or solar renewables will undoubtedly lead to a reduced vulnerability. But, the challenge of energy storage and energy transportation have hampered the implementation of these renewable energies and slowed down reduction of the overall dependency on unendurable resources [1,2].

Hydrogen appears to be a promising fuel offering safe and versatile renewable source of energy with a possibility of high-efficient conversion into water, electricity and heat when used in fuel cells [3,4]. The energy produced per unit mass of hydrogen is much more than that generated from gasoline and coal [5]. As a prospective sustainable source of hydrogen for energy storage applications without evolution of CO_2, electrochemical water splitting is a promising approach [6]. It facilitates conversion of electrical energy to chemical energy and its storage in form of hydrogen that can be converted back to electric energy when needed. In a water splitting cell, the overall water splitting reaction is:

$$H_2O \rightarrow H_2 + 1/2O_2 \quad (1)$$

The anodic half reaction is the oxygen evolution reaction (OER):

$$H_2O \rightarrow 1/2O_2 + 2H^+ + 2e^- \quad (2)$$

and the cathodic counter reaction is the hydrogen evolution reaction (HER):

$$2H^+ + 2e^- \rightarrow H_2(g) \quad (3)$$

Most water-splitting processes usually start with hydrogen adsorption on the surface of catalyst by a charge transfer or Volmer reaction (eqn. 4) and rely on electrochemical hydrogen evolution ($2H^+ + 2e^- \rightarrow H_2$) in the final step where either two adsorbed hydrogen on the surface combine and evolve molecular hydrogen via a Tafel (atom-atom recombination) reaction (eqn. 5) or a proton from the solution reacts with an electron and a H-adatom on the surface and forms H_2 via Heyrovsky (ion-atom recombination) reaction (eqn. 6):

$$H^+ + e^- + * \rightarrow H^* \quad (4)$$

$$H^* + H^* \rightarrow H_2 + 2^* \quad (5)$$

$$H^+ + e^- + H^* \rightarrow H_2 + * \quad (6)$$

The HER is one of the most important electrochemical reactions where protons produced via OER in electrolyte combine with electrons at the cathode electrode surface and are reduced to hydrogen gas. The most stable and active catalysts in acid environments for HER are currently precious metals, specially Pt-based materials [7]. But as Pt is rare and expensive, there is a need to explore a new class of materials that are free of Pt, cheaper and more abundant but yet stable, active and with as small overpotential for HER as possible. Regarding the mechanism of the reaction, a previous study on metal electrodes showed that the predominant reaction mechanism for HER is the Tafel reaction being the rate-determining step (RDS), which is a potential-independent

Science Institute and Faculty of Physical Sciences, VR-III, University of Iceland, IS-107 Reykjavik, Iceland.
† Corresponding author: egillsk@hi.is

mechanism but the rate as a function of potential is influenced indirectly by the hydrogen coverage on the surface [8]. Therefore, by calculating the free energy of atomic hydrogen when it binds to the surface can give a comparison of the activity among different catalysts. According to the Sabatier principle [9]; too strong hydrogen bond to the surface of a catalyst results in hydrogen poisoning and no free sites for adsorption. On the other hand, if hydrogen bond to the surface is too weak, high overpotentials will be needed for proton adsorption. Hence, the ideal catalyst should be the one with binding free energies close to 0.0 eV with a compromise between these two extremes [10]. So if a new class of material is found with such hydrogen binding properties, it might be a potential replacement catalyst for Pt in the HER.

Over the years, numerous theoretical and experimental studies have explored the possibility of HER on different classes of non-precious materials as an alternative for Pt-based systems. Electrode materials made by Ni and its alloys, for example, exhibited promising HER activity through water electrolysis in alkaline solutions [11,12]. However, high-energy consumption and low efficiency gained in those systems are known as their major disadvantage [13]. Afterwards, electrocatalytic activity of Ni-based alloy films was investigated for HER in acidic electrolytes by studying Ni-P, Ni-W-P, and Ni-Mo-P. It was found that the activity of these alloys decreases with increasing P content, whereas increases with increasing W or Mo content due to specific electronic structure of these different alloys [14]. Nonetheless, their corrosion in acid solutions is of important concern. The results of a theoretical screening on binary-surface-alloy transition metals showed promising HER system based on Cu and W (W-Cu) with improvements over both pure W and Cu electrodes [15]. The edges of the MoS_2 nano-particle (NP) were also shown promising non-precious HER catalyst material, first with DFT calculations [16] and then with experiments [17–19]. The experiments showed that MoS_2 is around 2-3 orders of magnitude less active than Pt. The HER activity was also investigated on cobalt promoted and unpromoted nano-particulates of MoS_2 and WS_2 structures by Bonde and co-authors, and cobalt was found capable of promoting the HER in both cases with WS_2 being the least and Co-W-S being the highest active material [20].

Very recently, synthesis, characterization, and properties of transition metal phosphides (TMPs) were reviewed on highly active and Earth-abundant phosphides of Ni, Co, Fe, Mo and W [21]. The first Ni_2P materials studied experimentally as HER catalysts were nanoparticles on Ti foil substrates where 1.0 $mg.cm^{-2}$ of these nanoparticles produced the exchange current density of -10 $mA.cm^{-2}$ only at overpotential of around 116 mV in a strongly acidic electrolyte (0.5 M H_2SO_4), with good stability and quantitative Faradaic efficiencies over 2 hours of sustained hydrogen production [22]. Under similar conditions, carbon-encapsulated Ni_2P nanocomposites (Ni_2P/C) were shown capable of enhancing the HER performance with only an overpotential of around 87 mV [23]. The high activity of these peapoded Ni_2P nanoparticles was explained to be due to enriched nanoporosity and more efficient use of the available active sites. Ni_2P nanoparticles supported on a Ti plate also showed high catalytic activity for HER at overpotentials of around 140 to 190 mV obtaining current densities of up to 100 $mA.cm^{-2}$ [24]. A recent DFT study on these nanoparticles shows that Ni_2P has many active sites for HER and that is an explanation for its good performance in experiments [25]. The most active Ni-based phosphide material with consideration of the current density of 10 $mA.cm^{-2}$ was found to be Ni_5P_4 micron-sized particles with exceptional efficiency in both alkaline (overpotential of 49 mV vs. RHE) and acidic (overpotential of 23 mV vs. RHE) environments [26]. These pellet materials showed HER electrocatalytic geometric activity on par with bulk Pt catalysts and with minimal loss in activity after 16 hours of H_2 evolution in both 1 M H_2SO_4 and 1 M NaOH. Following these promising studies on Ni_2P as an Earth-abundant HER catalyst, uniform and multi-faceted cobalt phosphide (CoP) nanoparticles on a Ti support were also identified as an active and acid-stable HER catalyst [27]. Overpotential of 85 mV was enough for 2 $mg.cm^{-2}$ of these nanoparticles to produce a cathodic current density of 20 $mA.cm^{-2}$ for over 24 hours of sustained hydrogen production in 0.5 M H_2SO_4. Very recently, a series of cobalt phosphide-based electrocatalysts, including Co_2P, CoP, Co_2P/CNTs, CoP/CNTs, Co_2P/nitrogen-doped carbon nanotubes (NCNTs), and CoP/NCNTs were synthesized and investigated by Pan and co-authors in order to explore the influence of phase, structure, and support effects on the HER activity [28]. Their results indicated that catalytic activity follows the order of CoP/NCNTs > Co_2P/NCNTs > CoP/CNTs > Co2P/CNTs > CoP > Co_2P, which was attributed to the different atomic ratio of cobalt to phosphorous with the more phosphorus-rich phase performing better than the corresponding Co_2P counterparts in each case. On iron-based phosphide systems, the best HER activity so far belongs to the FeP fabricated on carbon cloth [29]. The high-surface area morphology of these rugae-like FeP nanocrystals enhance the HER activity in a way that the required overpotential to reach 10 $mA.cm^{-2}$ is only 34 mV with the loading density of 4.9 $mg.cm^{-2}$. In addition to these examples, there are several studies on Mo-based, W-based, and Cu-based phosphides in literature as well. However, based on the best results obtained so far in each case; amorphous MoP [30], amorphous WP [31], and Cu_3P nanocubes [32], these systems are overall not as active and stable as Ni-based systems. With combination of theory and experiment, Kibsgaard and co-authors investigated TMP catalysts for the HER where they tested a combined experimental-DFT model by designing new mixed metal TMPs [33]. They demonstrated that the (101) surface of $Fe_{0.5}Co_{0.5}P$ is the most thermo-neutral in ΔG_H (0.004 eV) of the systems considered and exhibits the highest activity of all the other TMP catalysts examined, including pure FeP and CoP.

Transition metal nitrides have also appeared as efficient HER electrocatalysts for hydrogen production [34,35]. For the nitride-based HER electrocatalysts, ternary transition metal nitrides including bimetallic nitrides and transition metal carbonitrides have received considerable attention due to their high HER activity. A novel heterogeneous HER catalyst based on a nickel molybdenum nitride (NiMoNx) nanosheet grown on a carbon support was reported to exhibit a very small onset potential of -78 mV (vs. RHE) to drive the HER in 0.1 M $HClO_4$ [36]. The exchange current density for this catalyst is around 0.24 $mA.cm^{-2}$, in the same order to that of the Pt/C catalyst (0.78 $mA.cm^{-2}$)[35]. In the same electrolyte, the $Co_{0.6}Mo_{1.4}N_2$ material was reported to be stable and active at low catalyst loadings of

0.24 mg.cm^{-2} in rotating disk experiments with ability to catalyze the HER at -200 mV (vs. RHE) contributing to 10 mA.cm^{-2} catalytic current [37]. On binary nitrides, a systematic investigation of the HER was recently done on atomically-thin (1.3 nm) molybdenum nitride (MoN) nanosheets [38]. At 100 mV overpotential, the exchange current density reaches 8.375 × 10^{-2} mA.cm^{-2}. According to DFT calculations, the atomically-thin MoN nanosheets display metallic characteristics, and therefore ensure fast electron transportation during the HER catalytic process. Very recently, the electrocatalytic HER activity of the TiN nanowires (NWs) was investigated by depositing it on a glassy carbon (GC) electrode with an optimal catalyst loading of 0.51 mg cm^{-2} [39]. For the TiN NWs, the catalytic current of 1 mA.cm^{-2} was obtained at a low onset potential of around -92 mV vs. RHE, above which the current density increases rapidly at more negative potentials with a substantial current density of around 40 mA.cm^{-2} at an overpotential of 270 mV. Such electrocatalytic activity is one of the best reported for transition metal nitride catalysts to date and comparable to some of the best non-noble catalysts reported in recent years [37,40–43]. The commercial bulk TiN electrode, however, needed overpotential of around 405 mV vs. RHE to only produce 1 mA.cm^{-2} [39], 313 mV higher than that of the TiN NWs. This different activity is presumably due to alternate reactive sites (e.g. edges) that the TiN NWs provide but are not as common on a bulk TiN electrode. To investigate the stability of these materials under operating conditions, the TiN NWs catalyst was continuously cycled for a total of more than 20000 cycles in 1 M $HClO_4$. The current density of TiN NWs remained nearly unchanged after 10000 cycles, and slightly decreased to about 90% after 20000 cycles, indicating excellent electrochemical stability. This exceptional durability shows promise for practical applications of the TiN NWs catalysts over the long-term operations.

In addition to above-mentioned examples, several studies have been conducted on nitride-based electrocatalysts either as cathode material or as a support for different pathways of energy conversion, including HER, oxygen evolution reaction (OER), oxygen reduction reaction (ORR), as well as methanol oxidation reaction (MOR) [35]. Although great efforts have been made to enhance the electrocatalytic activity, the state-of-the-art synthesis and performance of the current catalysts still cannot meet the expectation for replacing noble metal-based catalysts. Therefore, developing more efficient catalysts and more straightforward synthesis approaches will remain a challenge for scientists in this field.

In pursuit of new catalyst materials for nitrogen electroreduction reaction (NER) to ammonia, we have previously reported that amongst the mono-nitrides of most of the d-block metals, the early transition metal nitrides of Sc, Ti, Y, Hf, Mo, and Ta were most stable in the (100) facet of the NaCl-type structure and with no catalytic activity toward NER [44–46]. The surface of these nitrides were found to be mainly populated and covered with H up to 1 monolayer (ML) with no *NH_3 formation. The only exception was MoN where *NH_3 was formed at -0.83 V vs. RHE, but the catalytic cycle did not sustain due to poisoning with H^*, OH^* or O^* species from the aqueous electrolyte. Therefore, we hypothesized that they might catalyse the HER instead, which are a competing reaction to NER. In the present study, these six nitrides are fully investigated for electrochemical HER. Density functional theory (DFT) calculations are used to study the thermodynamics of the cathode reaction. Differential binding free energy is calculated for the electrochemical hydrogenation of the metal nitride surfaces. For H_2 formation, the Tafel mechanism is investigated here as it was found that the Tafel barrier is the predominant and rate-limiting step for HER on all metal electrodes [8].

Methodology

The results presented in this work are calculated by density functional theory (DFT) using the RPBE exchange-correlation functional [47]. A plane wave basis set with an energy cutoff of 350 eV is used to represent the valence electrons with a PAW [48] representation of the core electrons as implemented in the VASP code [49,50]. Activation energies are obtained as the highest point along the minimum energy path (MEP) calculated using the climbing image nudged elastic band method (CI-NEB)[51,52]. The self-consistent electron density is determined by iterative diagonalization of the Kohn– Sham Hamiltonian, with the occupation of the Kohn–Sham states being smeared according to a Fermi–Dirac distribution with a smearing parameter of k_BT = 0.1 eV. A 4 × 4 × 1 Monkhorst–Pack k-point sampling is used for all the surfaces.

The nitride slabs are modeled with 40 atoms in five layers, each layer consisting of four metal atoms and four nitrogen atoms. The bottom two layers are fixed whereas the top layers as well as the adsorbed species are allowed to relax. Boundary conditions are periodic in the x and y directions and surfaces are separated by 12 Å of vacuum in the z direction. The structural optimization is considered converged when the forces in any direction on all moveable atoms are less than 0.01 eV Å^{-1}. The RPBE lattice constants used in this study were: ScN: 4.56 Å, TiN: 4.29 Å, YN: 4.95 Å, HfN: 4.57 Å, TaN: 4.44 Å, MoN: 4.40 Å. Hydrogen adsorption was allowed on all the metal and nitrogen atoms as well as any other possible configurations on the slab (a so-called unconstrained mechanism) [45].

The total hydrogen evolution reaction is:

$$H^+ + e^- \rightarrow 1/2H_2 \qquad (7)$$

It takes place at an electrode supplying the electrons, which provides an intermediate state of the process [see eqns. 4 (Volmer reaction) and 5 (Tafel reaction)]. For recombination of H-adatoms contributing to H_2 formation, the Tafel mechanism is considered in this study, which is equivalent to the traditional Langmuir-Hinshelwood type reaction for H_2 desorption from a metal surface into a vacuum. A good agreement throughout the metal series indicated that the Tafel reaction is the predominant H_2 formation step on all metal electrodes [8]. Also, the Volmer reaction can be treated as being in equilibrium at room temperature during HER/HOR [8]. This means that close to the equilibrium potential, the barrier for this process is small, a finding that is in good agreement with conclusions from experiments [53]. Thus, the coverage of hydrogen on the surface is given by the chemical potential of hydrogen, which at standard conditions (298 K, pH = 0, 1 bar)

is determined by the potential, (U, μ_H = -eU), relative to the standard hydrogen electrode. Besides, the energetics of adsorbed H as well as for the Tafel reaction barrier have been shown to be not affected by including water, electric fields and potentials in the calculations [54–56]. The reason is that there is insignificant electron transfer involved in Tafel reaction and the dipole of the adsorbed H is small in the direction perpendicular to the surface. As we focus here on energetics of elementary reaction steps occurring directly at the electrode surface where solvation effects from the liquid should not play such direct role, it is not crucial to explicitly include the effect of water, ions, electric potentials, or electric fields due to the large computational effort required [54]. Hence, these effects can be neglected and only a surface slab and adsorbed hydrogen need to be included in the atomic model. This makes the computational cost much less demanding. However, as the activation energy of the Tafel reaction is affected by the H coverage, different coverage needs to be taken into account. Including water and calculation of the barrier for proton transfer (Volmer or Heyrovsky step) is out of the scope of this paper, since it requires very precise information on the interfacial structure and is computationally expensive [57,58]. On the other hand, transition metal catalysts have binding energies that are coverage dependent. It means that electrochemical potential can indirectly affect the Tafel reaction by changing the coverage, as it is a function of the potential. So coverage effect needs to be considered in the modelling and as so we have treated it in this work. The free energy of the steps associated with adsorption of H is estimated at pH = 0 according to:

$$\Delta G\,(0) = \Delta E + \Delta E_{ZPE} + T\Delta S \qquad (8)$$

where ΔE is the reaction energy calculated using DFT. The zero-point energy corrections (ΔE_{ZPE}) and entropy differences (ΔS) are calculated within a harmonic approximation for adsorbed species but taken from a handbook for H_2 in a gas phase and the values of these are reported elsewhere [45,59]. The effect of an applied bias, U, can be included for all electrochemical reaction steps by shifting the free energy for reactions involving n electrons by -neU:[60]

$$\Delta G\,(U) = \Delta G\,(0) - neU \qquad (9)$$

The theoretical current densities of the Tafel reaction is estimated as a function of applied potential on the surfaces of these metal nitride catalysts and compared with that of Pt(111) in Figure 5B. The rate constant for the Tafel reaction of HER is given by:

$$k = \nu \exp(-E_a/k_B T) \qquad (10)$$

We use the normal attempt frequency, ν = 10^{13} site^{-1}.s^{-1}, for the prefactor, which was found to agree well with the measured absolute rate for HER when used together with the calculated activation energies [8], E_a is the activation energy (eV) for the Tafel reaction, k_B is the Boltzmann constant and T is the temperature. A typical value of the exchange current density, i_0, on Pt(111) is 4.6 × 10^{-4} A.cm^{-2},[61] and the surface area per Pt atom, A/N, is 6.64 × 10^{-16} cm^2. To obtain the theoretical current densities, we apply:

$$i = ke\,(N/A) \qquad (11)$$

and get i for each nitride. The N/A values calculated for each nitride are: TaN: 1.36 × 10^{15} cm^{-2}; HfN: 1.32 × 10^{15} cm^{-2}; MoN: 1.38 × 10^{15} cm^{-2}; TiN: 1.41 × 10^{15} cm^{-2}; ScN: 1.33 × 10^{15} cm^{-2}; YN: 1.22 × 10^{15} cm^{-2}.

Results and discussion

Free energy diagram

The trends in hydrogen evolution activity over various transition metals, metal alloys and non-metal catalysts have been investigated using DFT with the use of descriptors [10,15,62]. ΔG_{H^*} which is indicative of the adsorption free energy of hydrogen has become a conventional descriptor to use when new class of materials are being screened for HER. According to this descriptor and as explained by Sabatier principle, the best catalyst should possess binding free energies of H close to 0.0 eV. Therefore, calculating the adsorption free energy of H for different materials is expected to be a suitable approach for quick comparison of their catalytic activity towards HER.

In Figure 1A, the free energy diagrams for hydrogen evolution over the studied nitrides are shown for a single H adatom. Their catalytic activity is also compared with the most efficient catalyst already known for this reaction, the Pt(111). For HER to take place close to the equilibrium potential (zero Voltage), no reaction step can be associated with large changes in the free energy. This instantaneously eliminates Mo(110) as good catalyst, because it forms strong bonds to atomic hydrogen that the hydrogen release step will be slow. The same holds true for one of the nitrides studied in this work, the ScN. On the other hand, hydrogen binds weakly to the Au(111) surface and therefore it is not a good catalyst because the Volmer step is thermodynamically uphill in free energy and relatively high overpotential is needed to surpass it and get the proton to bind to the surface. The same holds true for TiN studied here.

As can be seen, YN and MoN with adsorption free energy of +0.004 and -0.008 eV, respectively, bind the first H adatom moderately (around 0.0 eV) and that should make them as good HER catalyst as Pt(111). They also look more promising than W-Cu catalyst with ΔG_{H^*} of 0.07 eV [15] and MoS_2 edges with ΔG_{H^*} = 0.08 eV [16]. HfN and TaN are also predicted to be active within this analysis with ΔG_{H^*} = -0.059 and -0.092 eV, respectively. They all even look more promising when compared with Ni_2P with the free energy of adsorption of H to be 0.19 eV [24]. The binding free energy of H to the surface of ScN and TiN are -0.35 and 0.60 eV, respectively. The former binds H stronger and that makes evolution of H_2 difficult compared to Pt; whereas the latter binds H so weakly that it is difficult to add the proton on the surface without applying a more negative bias. The activity of ScN might be on par with that of Mo(111), and TiN seem to be the least active candidate from the perspective of this common descriptor. From these FEDs, it appears that some of the nitrides shown in Figure 1A adsorb H relatively moderately (not too weak nor too strong), and therefore, it could be anticipated that hydrogen evolution

Journal of Materials Chemistry A

ARTICLE

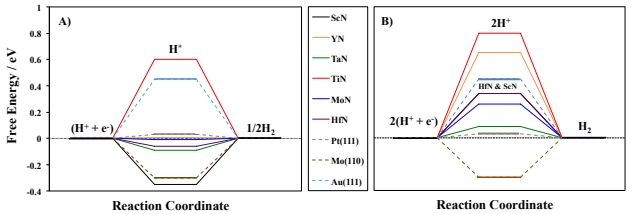

Figure 1. *H-descriptor based (A) and 2*Hs-descriptor based (B) free energy diagrams for HER. In order for the H_2 to evolve, there should be at least 2*Hs on the surface to recombine via a Tafel mechanism. The *H-descriptor based FED is the conventional approach for comparison of the catalytic activity of various materials. However, as can be seen by comparing (A) and (B), the 2*H-descriptor based FED provides completely different picture and would give different predictions of the catalytic activities of these materials than the *H-descriptor would predict. The energies for the adsorbed intermediate are calculated with DFT for the coverage of 1/8 (A) and 2/8 (B) at standard conditions (pH = 0, 1 bar of H_2, U = 0, and 298 K). The values for pure metals are taken from ref [8] and shown with dashed lines for comparison. There is an insignificant difference in the binding free energy of *H on the pure metals at this low coverage and therefore the values for ¼ H coverage is used in both (A) and (B). The nitrides are shown with solid lines. The values corresponding to HfN & ScN are 0.34 eV overlaying each other in Figure 1B.

become facilitated on the surface of these materials. It is a necessary but not sufficient criterion for a material to be a good catalyst where the free energy of adsorbed H is close to that of the reactant and product (i.e., $\Delta G_{H^*} = 0$).

Differential free energy of H adsorption

In the modelling, every possible adsorption site is investigated for each H addition step. DFT is used to evaluate the most stable adsorption site at each step and construct the free energy landscape until a full monolayer of hydrogen (1ML = 8H*) is built on the surface of the nitrides. These free energy landscapes provide more mechanistic details of the process and are shown in Figure 2. For some of the metal nitrides we have considered earlier, H adsorption is found mostly limited to the surface N atoms and therefore N atom in the surface layer is reduced to NH_3 [45,59,63]. However, earlier transition metal nitrides of Sc, Ti, Y, Hf, and Ta investigated here reach an even distribution of H on the slab where both metal and nitrogen atoms on the surface are entirely protonated without formation of any $*NH_2$ or $*NH_3$ species. So hydrogen coverage on these surfaces builds up by adsorption of H on each and every exposed atom on the surface until 1 ML hydrogen coverage is reached (1ML = 8H*, 8 hydrogen atoms for 4 surface N atoms and 4 surface metal atoms). Addition of the ninth hydrogen atom to the surface of these studied nitrides causes H_2 to be formed, as there is a lack of available sites for *H adsorption on the surface. Neither $*NH_2$ nor $*NH_3$ is found to be an energetically favourable intermediate along the path. Therefore, no ammonia formation should be produced on the nitrides considered in this work. The only exception is MoN that, in addition to HER at lower coverage; results in reduction of surface nitrogen to NH_3 at more than 6/8 H coverage on the surface corresponding to onset potential of around -0.83 V vs. RHE. But below this onset potential and H coverage, no ammonia should be produced but adsorbed Hs, especially those bound the Mo metal atoms, can evolve and form H_2. For TaN, MoN, and HfN the protons adsorb and bind rather to the metal atoms than to the surface nitrogen atoms up to 4/8 ML for TaN and MoN and 3/8 ML for HfN. Afterwards, surface N atoms are populated each by one hydrogen (to reach 1ML). But on ScN, YN and TiN, H adsorption does not follow a specific trend regarding adsorption occurring first on metal sites (*MH) or on N sites (*NH).

As can be seen, adsorption of the first H to the surface is very moderate for mononitrides of Y, Mo, Hf and Ta but very weak on Ti and rather strong on Sc (same as shown by figure 1A). When estimating the catalytic activity of these different material only based on the free energy of adsorption of first hydrogen atom (ΔG_{H^*} descriptor), YN seems to be the most active candidate with ΔG_{H^*} around zero. But for HER to occur, either the H-adatom should react with a coming proton from electrolyte via Heyrovsky mechanism (eqn. 6) (which has been concluded to have a high activation energy [8]) or a second proton needs to be adsorbed on the surface and then

recombine with the first H-adatom to evolve hydrogen via Tafel mechanism (eqn. 5).

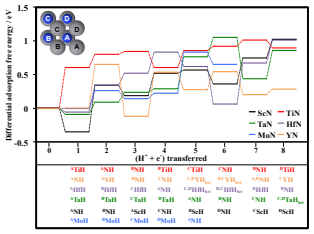

Figure 2. Differential free energy of H adsorption. The labels present the most stable species formed at each hydrogenation step; *NH or *MH. The inset shows the top-view structure of the surface where the labelling from A to D indicates where the H-adatoms prefer to adsorb.

Therefore, using the differential H adsorption free energy of 2H* rather than 1H* is more realistic descriptor for the activity on these metal nitrides. In Figure 1B we use the 2H* descriptor in the FED, and as can be seen, these two descriptors give rather different trends.

Considering hydrogen recombination via the Tafel mechanism, a potential of -0.65 V vs. RHE is needed to be applied on YN in order to reach a coverage of 2/8 so that the second hydrogen atom is adsorbed and then the two *Hs can recombine to desorb H_2. For TaN on the other hand, only a small potential of -87 mV is required (similar to the Ni_2P nanocomposites) to build up such coverage on the surface and evolve H_2. Therefore in reality, TaN should be by far a better candidate compared to YN. For MoN, HfN, ScN, and TiN, potentials of -0.26, -0.34, -0.34, and -0.8 V are needed to apply to reach 2/8 ML, respectively. Apparently, a FED only based on the free energy of 1*H as descriptor did not identify these at all. The 1H* descriptor works reasonably well on the flat metal surfaces [64], whereas it does not at all for the flat metal nitride (100) surfaces, as shown in this paper. This difference comes from the more complicated electronic structure of the ionic metal nitrides compared to pure metals.

Figure 3 shows the hydrogen coverage on the surface as a function of the applied potential for the metal nitrides. For TiN and YN, a rather negative potential is required to reach 0.25 ML (where there is a possibility to have two Hs next to each other) but as soon as that potential is reached, the surfaces get fully covered with H-adatoms. The onset potential for TiN and YN is thus large. All the other nitrides build up the H coverage gradually as the potential becomes more negative. All these nitrides show different trend from Pt(111). There, almost a full ML is reached at only slightly negative potential whereas it suddenly requires a rather negative potential to go beyond a ML.

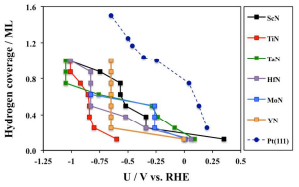

Figure 3. Hydrogen coverage on the surface of the transition metal nitrides as a function of applied potential (U/V vs. RHE). 1 ML coverage corresponds to 8H* on the surface in our model system (consisting of 4 surface metal atoms and 4 surface nitrogen atoms). The values for Pt(111) are adapted from ref. [8]

Activation barrier for Tafel reaction and rate of the HER

In Figure 4 the activation energy (E_a/eV) is plotted as a function of hydrogen coverage until 1 ML H coverage is reached. This is compared with Pt(111) data reported elsewhere [8]. As expected, the activation barriers for HER gets lower with increasing H coverage. The activation barrier drops down gradually for all the nitrides except again; TiN and YN. There the barriers are rather constant at any H coverage. This is due to the weak binding of H on TiN and YN where a potential of around -0.8 V is needed to get the minimum H coverage for HER (Fig 2).

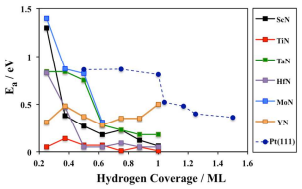

Figure 4. Activation energy (E_a/eV) for the Tafel reaction in HER on several transition metal nitrides as a function of hydrogen coverage. 1ML coverage corresponds to 8H* on the surface in our model system (consisting of 4 surface metal atoms and 4 surface nitrogen atoms). The values for Pt(111) are adapted from ref. 8.

Figure 5A shows the activation energy for the Tafel reaction on the metal nitrides studied here as a function of the electrode potential. Usually the trend is that the more negative potential applied, the higher H coverage builds on the surface (Figure 3). That causes the activation energy of the 2H* ⟶ H_2 reaction to decrease. As already

mentioned, TaN needs only a small overpotential of -0.087 V vs. RHE to reach 2/8 coverage (which is the coverage needed for HER to start in our model system). The barrier of this Tafel reaction is calculated to be 0.84 eV that is surprisingly very similar to that of Pt(111) reported to be 0.85 eV [8]. Therefore, it is expected that TaN catalyses HER in relatively similar manner as Pt(111) does. Comparing the activation energies of hydrogen evolution from the surface of ScN, HfN and MoN, the Tafel reaction barrier drops significantly when coverage changes from 2/8 to 3/8. The lowest activation energy found for the Tafel reaction is for TiN (less than 0.14 eV). But a relatively high overpotential of -0.8 V is required to adsorb 2Hs on its surface before H_2 evolution starts. This makes TiN the least active candidate here and should reduce its attractiveness for experimental analyses. The same holds true for YN where -0.65 V is needed to reach 2/8 ML where the activation energy of 2*Hs recombination is calculated to be rather low, or 0.31 eV.

In figure 5B, the rates (current densities) are estimated based on the activation energy of the Tafel reaction and calculated for different coverage of H on the surface up to -1.1 V. As can be seen, at around equilibrium potential, TaN and Pt(111) have a similar rate and as the coverage increases, the rate of HER increases gradually. Similar trends are seen for HfN, MoN, and ScN as well, where the rate of HER increases as the coverage increases. However, the trends are quite different on the surfaces of YN and TiN. First of all, as has been discussed earlier, a much more negative potential is required to start HER on YN and TiN than all the other nitrides studied here. However, when the onset potential is reached, the rate of the Tafel reaction is rather high and it does not change much depending on the H coverage on the surface.

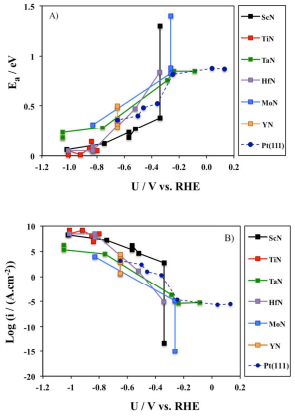

Figure 5. Activation energy of Tafel reaction (E_a/eV) (A) and theoretical current densities of the Tafel reaction of the HER (B) as a function of the electrode potential, U, vs. RHE on several transition metal nitride catalysts obtained according to eqns. 10 and 11 and compared with Pt(111) adapted from ref. [8]. Applying a potential of -0.65 V vs. RHE to get minimum H coverage (2/8) on YN will spontaneously result in a full H coverage as shown in Figure 2, and that is why all the points are lying vertically at -0.65 V for YN.

Volcano plot

Volcano plots became common approach for comparison of the catalytic activity of different materials. Therefore, the theoretical current density of the Tafel reaction for the lowest possible coverage for HER (2/8 ML) is used to get the location of the best candidate of this study, TaN, on the experimental volcano plot made for the metals (adapted from ref.[8]). In Figure 6, the theoretical current density on the surface of TaN is obtained from the activation energy calculations when adsorbed Hs on the surface recombine and evolve H_2, and that is plotted against the free energy of 2H* adsorbed on the surface. The results are compared with the experimentally measured exchange current density on pure metals where the ΔG_{H^*} descriptor is calculated with DFT and 1 ML is used for the left leg of the volcano and the top of the volcano whereas 0.25 ML are used for the right leg of the volcano.

As can be seen, TaN with ΔG_{H^*} close to zero (0.087 eV) is comparable with the hydrogen descriptor for Pt(111) (0.03 eV), and TaN shows relatively high rate for HER. Interestingly, the H binding free energy on TaN is the same as for the MoS_2 and the theoretical current density for TaN is the same as the experimental current density for MoS_2.

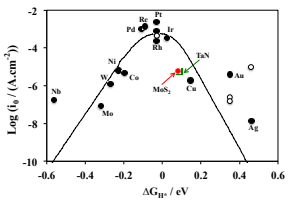

Figure 6. A volcano plot of the HER for various pure metals, MoS_2, and the most promising transition metal nitride surface, TaN. The ΔG_{H^*} value for TaN is calculated for 2/8 ML H coverage at 1 bar of H_2 and 298 K. Experimental data are adapted from reference [8] where the circular data points are the measured exchange current density (open data points for (111) facets but filled data points for polycrystalline) plotted versus the calculated free energy of H adsorption. The metals on the left side of the volcano have high H coverage (1 ML) and the metals on the right side low H coverage (0.25 ML). The experimental data for MoS_2 is taken from ref. [17].

Conclusions

Possibility of catalysing the hydrogen evolution reaction (HER) was investigated by DFT calculations on the (100) facet of the

NaCl-type structure of mononitrides of Sc, Ti, Y, Hf, Ta, and Mo at pH = 0. On the basis of the calculated differential adsorption free energy of H up to a full monolayer and activation energy of the Tafel reaction for forming H_2, we estimated the current densities of HER as a function of applied potential on all the nitrides. It was found that the most promising nitride catalyst is TaN, which should catalyse HER at potential of around -0.09 V with respect to RHE. In addition, the activation energy and rate of the Tafel reaction on TaN was found very similar to that previously reported on Pt(111) at around the equilibrium potential.

Acknowledgements

Financial support is acknowledged from the Icelandic Research Fund and the Research Fund of the University of Iceland. The calculations were in part carried out on the Nordic high performance computer (Gardar).

References

1 K. L. Lim, H. Kazemian, Z. Yaakob and W. R. W. Daud, *Chem. Eng. Technol.*, 2010, **33**, 213–226.
2 N. L. Panwar, S. C. Kaushik and S. Kothari, *Renew. Sustain. Energy Rev.*, 2011, **15**, 1513–1524.
3 E. Fontes, E., & Nilsson, *Ind. Phys.*, 2001, **7**, 14–17.
4 E. Fakiolu, *Int. J. Hydrogen Energy*, 2004, **29**, 1371–1376.
5 M. Dresselhaus and I. Thomas, *Nature*, 2001, **414**.
6 A. Züttel, A. Borgschulte and L. Schlapbach, *Hydrogen as a Future Energy Carrier*, Wiley-VCH Verlag GmbH & Co. KGaA, Weinheim, Germany, 2008.
7 S. Trasatti, *J. Electroanal. Chem.*, 1971, **39**, 163–184.
8 E. Skúlason, V. Tripkovic, M. E. Björketun, S. Gudmundsdóttir, G. Karlberg, J. Rossmeisl, T. Bligaard, H. Jónsson and J. K. Nørskov, *J. Phys. Chem. C*, 2010, **114**, 18182–18197.
9 R. Parsons, *Trans. Faraday Soc.*, 1958, **54**, 1053.
10 J. K. Nørskov, T. Bligaard, A. Logadottir, J. R. Kitchin, J. G. Chen, S. Pandelov and U. Stimming, *J. Electrochem. Soc.*, 2005, **152**, J23.
11 J. Divisek, H. Schmitz and B. Steffen, *Electrochim. Acta*, 1994, **39**, 1723–1731.
12 W. Hu and J. Lee, *Int. J. Hydrogen Energy*, 1998, **23**, 253–257.
13 B. Børresen, G. Hagen and R. Tunold, *Electrochim. Acta*, 2002, **47**, 1819–1827.
14 G. Lu, P. Evans and G. Zangari, *J. Electrochem. Soc.*, 2003, **150**, A551–A557.
15 M. E. Björketun, A. S. Bondarenko, B. L. Abrams, I. Chorkendorff and J. Rossmeisl, *Phys. Chem. Chem. Phys.*, 2010, **12**, 10536–41.
16 B. Hinnemann, P. G. Moses, J. Bonde, K. P. Jørgensen, J. H. Nielsen, S. Horch, I. Chorkendorff and J. K. Nørskov, *J. Am. Chem. Soc.*, 2005, **127**, 5308–9.
17 T. F. Jaramillo, K. P. Jørgensen, J. Bonde, J. H. Nielsen, S. Horch and I. Chorkendorff, *Science*, 2007, **317**, 100–102.
18 J. Kibsgaard, Z. Chen, B. N. Reinecke and T. F. Jaramillo, *Nat. Mater.*, 2012, **11**, 963–9.
19 J. D. Benck, T. R. Hellstern, J. Kibsgaard, P. Chakthranont and T. F. Jaramillo, *ACS Catal.*, 2014, **4**, 3957–3971.
20 J. Bonde, P. G. Moses, T. F. Jaramillo, J. K. Nørskov and I. Chorkendorff, *Faraday Discuss.*, 2009, **140**, 219.
21 J. F. Callejas, C. G. Read, C. W. Roske, N. S. Lewis and R. E. Schaak, *Chem. Mater.*, 2016, **28**, 6017–6044.
22 E. J. Popczun, J. R. McKone, C. G. Read, A. J. Biacchi, A. M. Wiltrout, N. S. Lewis and R. E. Schaak, *J. Am. Chem. Soc.*, 2013, **135**, 9267–9270.
23 Y. Bai, H. Zhang, X. Li, L. Liu, H. Xu, H. Qiu and Y. Wang, *Nanoscale*, 2015, **7**, 1446–1453.
24 Z. Pu, Q. Liu, C. Tang, A. M. Asiri and X. Sun, *Nanoscale*, 2014, **6**, 11031–4.
25 M. H. Hansen, L.-A. Stern, L. Feng, J. Rossmeisl and X. Hu, *Phys. Chem. Chem. Phys.*, 2015, **17**, 10823–9.
26 A. B. Laursen, K. R. Patraju, M. J. Whitaker, M. Retuerto, T. Sarkar, N. Yao, K. V. Ramanujachary, M. Greenblatt and G. C. Dismukes, *Energy Environ. Sci.*, 2015, **8**, 1027–1034.
27 E. J. Popczun, C. G. Read, C. W. Roske, N. S. Lewis and R. E. Schaak, *Angew. Chemie - Int. Ed.*, 2014, **53**, 5427–5430.
28 Y. Pan, Y. Lin, Y. Chen, Y. Liu and C. Liu, *J. Mater. Chem. A*, 2016, **4**, 4745–4754.
29 X. Yang, A.-Y. Lu, Y. Zhu, S. Min, M. N. Hedhili, Y. Han, K.-W. Huang and L.-J. Li, *Nanoscale*, 2015, **7**, 10974–10981.
30 J. M. McEnaney, J. Chance Crompton, J. F. Callejas, E. J. Popczun, A. J. Biacchi, N. S. Lewis and R. E. Schaak, *Chem. Mater.*, 2014, **26**, 4826–4831.
31 J. M. McEnaney, J. Chance Crompton, J. F. Callejas, E. J. Popczun, C. G. Read, N. S. Lewis and R. E. Schaak, *Chem. Commun.*, 2014, **50**, 11026–11028.
32 L. Ma, X. Shen, H. Zhou, J. Zhu, C. Xi, Z. Ji and L. Kong, *RSC Adv.*, 2016, **6**, 9672–9677.
33 J. Kibsgaard, C. Tsai, K. Chan, J. D. Benck, J. K. Nørskov, F. Abild-Pedersen and T. F. Jaramillo, *Energy Environ. Sci.*, 2015, **8**, 3022–3029.
34 W.-F. Chen, J. T. Muckerman and E. Fujita, *Chem. Commun.*, 2013, **49**, 8896–8911.
35 J. Xie and Y. Xie, *Chem. - A Eur. J.*, 2016, **22**, 3588–3598.
36 W.-F. Chen, K. Sasaki, C. Ma, A. I. Frenkel, N. Marinkovic, J. T. Muckerman, Y. Zhu and R. R. Adzic, *Angew. Chemie Int. Ed.*, 2012, **51**, 6131–6135.
37 B. Cao, G. M. Veith, J. C. Neuefeind, R. R. Adzic and P. G. Khalifah, *J. Am. Chem. Soc.*, 2013, **135**, 19186–19192.
38 J. Xie, S. Li, X. Zhang, J. Zhang, R. Wang, H. Zhang, B. Pan and Y. Xie, *Chem. Sci.*, 2014, **5**, 4615–4620.
39 Y. Han, X. Yue, Y. Jin, X. Huang and P. K. Shen, *J. Mater. Chem. A*, 2016, **4**, 3673–3677.
40 D. Kong, H. Wang, Z. Lu and Y. Cui, *J. Am. Chem. Soc.*, 2014, **136**, 4897–4900.
41 M. A. Lukowski, A. S. Daniel, F. Meng, A. Forticaux, L. Li and S. Jin, *J. Am. Chem. Soc.*, 2013, **135**, 10274.
42 H. Wang, D. Kong, P. Johanes, J. J. Cha, G. Zheng, K. Yan and N. Liu, *Nano Lett.*, 2013, **13**, 3426–3433.
43 J. Yang, D. Voiry, S. J. Ahn, D. Kang, A. Y. Kim, M. Chhowalla and H. S. Shin, *Angew. Chemie - Int. Ed.*, 2013, **52**, 13751–13754.
44 Y. Abghoui and E. Skúlasson, *Procedia Comput. Sci.*, 2015, **51**, 1897–1906.
45 Y. Abghoui, A. L. Garden, V. F. Hlynsson, S. Björgvinsdóttir, H. Ólafsdóttir and E. Skúlason, *Phys. Chem. Chem. Phys.*, 2015, **17**, 4909–4918.

46 Y. Abghoui and E. Skúlason, *Catal. Today*, 2016, doi:10.1016/j.cattod.2016.11.047.
47 B. Hammer, L. Hansen and J. Nørskov, *Phys. Rev. B*, 1999, **59**, 7413–7421.
48 P. Blöchl, *Phys. Rev. B*, 1994, **50**, 17953–17979.
49 G. Kresse and J. Furthmüller, *Comput. Mater. Sci.*, 1996, **6**, 15–50.
50 G. Kresse and J. Furthmüller, *Phys. Rev. B. Condens. Matter*, 1996, **54**, 11169–11186.
51 G. Henkelman and H. Jónsson, *J. Chem. Phys.*, 2000, **113**, 9978–9985.
52 G. Henkelman, B. P. Uberuaga and H. Jónsson, *J. Chem. Phys.*, 2000, **113**, 9901–9904.
53 N. Markovic, *Surf. Sci. Rep.*, 2002, **45**, 117–229.
54 E. Skúlason, G. S. Karlberg, J. Rossmeisl, T. Bligaard, J. Greeley, H. Jónsson and J. K. Nørskov, *Phys. Chem. Chem. Phys.*, 2007, **9**, 3241–3250.
55 G. S. Karlberg, T. F. Jaramillo, E. Skúlason, J. Rossmeisl, T. Bligaard and J. K. Nørskov, *Phys. Rev. Lett.*, 2007, **99**, 126101.
56 Y. Gohda, S. Schnur and A. Groß, *Faraday Discuss.*, 2009, **140**, 233–244.
57 J. Rossmeisl, E. Skúlason, M. E. Björketun, V. Tripkovic and J. K. Nørskov, *Chem. Phys. Lett.*, 2008, **466**, 68–71.
58 J. Rossmeisl, K. Chan, R. Ahmed, V. Tripković and M. E. Björketun, *Phys. Chem. Chem. Phys.*, 2013, **15**, 10321–5.
59 Y. Abghoui, A. L. Garden, J. G. Howalt, T. Vegge and E. Skúlason, *ACS Catal.*, 2016, **6**, 635–646.
60 J. K. Nørskov, J. Rossmeisl, A. Logadottir, L. Lindqvist, J. R. Kitchin, T. Bligaard and H. Jónsson, *J. Phys. Chem. B*, 2004, **108**, 17886–17892.
61 A. Wieckowski, *Interfacial electrochemistry: theory: experiment, and applications.*, 1999.
62 Y. Zheng, Y. Jiao, Y. Zhu, L. H. Li, Y. Han, Y. Chen, A. Du, M. Jaroniec and S. Z. Qiao, *Nat. Commun.*, 2014, **5**, 1–8.
63 Y. Abghoui and E. Skúlason, *Catal. Today*, 2016, doi:10.1016/j.cattod.2016.06.009
64 J. K. Nørskov, T. Bligaard, A. Logadottir, J. R. Kitchin, J. G. Chen, S. Pandelov and U. Stimming, *J. Electrochem. Soc.*, 2005, **152**, J23–J26.

VII Article 7

Applications of Nitrides as Electrocatalysts

Anna L. Garden, Younes Abghoui, and Egill Skúlason

Book chapter submitted to Royal Society of Chemistry Book Series entitled Novel Catalytic Materials, edited by Justin Hargreaves, Andrew McFarlane and Said Laassiri , February (2017).

content/publications/publication7.pdf not found...

VIII Article 8

Transition Metal Nitride Catalysts for Electrochemical Reduction of Nitrogen to Ammonia at Ambient Conditions

Younes Abghoui and Egill Skúlason

Procedia Computer Science ***51****, 1897–1906 (2015).*

Procedia Computer Science

Volume 51, 2015, Pages 1897–1906

ICCS 2015 International Conference On Computational Science

Transition Metal Nitride Catalysts for Electrochemical Reduction of Nitrogen to Ammonia at Ambient Conditions

Younes Abghoui and Egill Skúlasson

Science Institute and Faculty of Physical Sciences, VR-III, University of Iceland, IS-107 Reykjavík, Iceland

yoa2@hi.is and egillsk@hi.is

Abstract

Computational screening for catalysts that are stable, active and selective towards electrochemical reduction of nitrogen to ammonia at room temperature and ambient pressure is presented from a range of transition metal nitride surfaces. Density functional theory (DFT) calculations are used to study the thermochemistry of cathode reaction so as to construct the free energy profile and to predict the required onset potential via the Mars-van Krevelen mechanism. Stability of the surface vacancy as well as the poisoning possibility of these catalysts under operating conditions are also investigated towards catalyst engineering for sustainable ammonia formation. The most promising candidates turned out to be the (100) facets of rocksalt structure of VN, CrN, NbN and ZrN that should be able to form ammonia at -0.51 V, -0.76 V, -0.65 V and -0.76 V vs. SHE, respectively. Another interesting result of the current work is that for the introduced nitride candidates, hydrogen evolution is no longer the competing reaction; thus, high formation yield of ammonia is expected at low onset potentials.

Keywords: DFT calculations, Electrochemical synthesis of ammonia, Electrochemical reduction of N_2 to NH_3, Transition metal nitride catalysts

1 Introduction

Ammonia is one of the highly produced chemicals in the globe, which is primarily used in production of fertilizer [1, 2]. Since hundred years ago, ammonia has been synthesized mainly through the Haber-Bosch process where gaseous nitrogen and hydrogen are passed over a Ru- or Fe-based catalyst at high pressure and high temperature to form NH_3 as: [3]

$$N_2(g) + 3H_2(g) \rightarrow 2NH_3(g) \quad (1)$$

Selection and peer-review under responsibility of the Scientific Programme Committee of ICCS 2015

doi:10.1016/j.procs.2015.05.433

The required hydrogen gas for this process is often provided by natural gas, which leads to increased production of various greenhouse gases. The alternative is to produce hydrogen from water splitting, which is a cleaner but very energy intensive process. The Haber-Bosch process is in stark contrast to the function of the enzyme nitrogenase in bacteria in which ammonia is produced from solvated protons, electrons and atmospheric nitrogen at ambient conditions. The active site of the enzyme is a $MoFe_7S_9N$ cluster that catalyzes the electrochemical reaction:

$$N_2 + 8H^+ + 8e^- \rightarrow 2NH_3 + H_2 \quad (2)$$

The source of energy for this reaction is at least 16 adenosine triphosphate (ATP) molecules [4], which are used to increase the chemical potential of the electrons and the protons. Therefore, it is possible that this natural process could be emulated in a man-made and commercial installation. Instead of a separate hydrogen production process, the protons could come from an acidic solution while the electrons would be driven to the electrode surface by an applied electric potential. Various potential routes for ammonia synthesis at ambient conditions are currently being explored (see Refs. 1,2 and 8 for recent reviews). To increase the yields of ammonia, solid-state proton conductors have been employed; resulting in up to 78% conversion of cathodic supplied nitrogen to ammonia [5, 6]. Ionic liquids or molten salts also promote ammonia formation from low current efficiencies up to 72% at high temperatures [7, 8, 9]. While having achieved low-pressure ammonia synthesis, the abovementioned studies still suffer from the requirement of relatively high temperatures, which leads to increased product decomposition. Another drawback is the use of complex and expensive electrolytes that hinder commercialization. To the best of the authors' knowledge, the first observations of ammonia synthesis at milder conditions were reported with homogeneous catalysts with tungsten [10] and zirconium [11] as the central atoms. However, for the sake of distributed use of ammonia, simpler methods are needed, ideally using heterogeneous catalysis, which allows for facile isolation of product.

With advancements in the field of computations and modeling, theoretical investigations have provided deeper insight into catalysis [12, 13, 14, 15, 16, 17, 18, 19, 20, 21, 22, 23, 24, 25, 26]. The use of computations can thus facilitate rational catalyst design, by enabling whole classes of material to be assessed for their suitability as catalysts. The simplest catalyst for electrochemical ammonia formation is a pure transition metal catalyst. In a recent theoretical study, electrochemical formation of ammonia on a range of flat and stepped transition metal surfaces was studied [27]. It was found that many metals require a relatively small overpotential of -0.5 to -1 V vs. SHE to form ammonia in 1 M aqueous electrolyte (pH = 0) at room temperature. However, the hydrogen evolution reaction (HER) can be very fast and severely hinder the production of ammonia unless the surface is covered with N-adatoms, rather than H-adatoms. It was found that the majority of metals are likely covered with H-adatoms at the onset potential of ammonia formation. This is less likely for the early transition metals, however these are known to readily form oxides. Another study used a similar approach on transition metal Nano-clusters [28] to enhance the ammonia activity compared to HER. However, the presence of water in the electrochemical environment will reduce the efficiency of catalyst by blocking its active site due to preferential adsorption of oxygen rather than nitrogen [29].

In the present study, transition metal nitride catalysts are investigated for electrochemical formation of ammonia at ambient conditions. These materials offer the potential advantage of being able to form ammonia by way of a Mars-van Krevelen mechanism [30], in which a surface N atom is reduced to NH_3 and the catalyst later regenerated with gaseous N_2, rather than adsorbing N_2 to the catalyst surface in the first step. Density functional theory (DFT) calculations are used to study the thermodynamics of the cathode reaction. Free energy diagrams are constructed for the electrochemical protonation of surface nitrogen or metal atoms to obtain onset potentials required for the ammonia synthesis on rocksalt and zincblende transition metal mononitride structures. The effect of an external

potential is included using the computational standard hydrogen electrode [12] and the lowest onset potential required to reduce N_2 to ammonia is estimated for each nitride.

2 Methodology

Mononitrides of the naturally occurring d-block metals are considered in the present study, in both the rocksalt (RS) and zincblende (ZB) structures. The low index facets are considered for each crystal structure, the (100) facets of the RS structure and the (110) facets of the ZB structure. Each nitride surface is modeled by 40 atoms in five layers, with each layer consisting of four metal atoms and four nitrogen atoms. The bottom two layers are fixed whereas the top layers as well as the adsorbed species are allowed to relax. Boundary conditions are periodic in the x and y directions and surfaces are separated by 12 Å of vacuum in the z direction. The structural optimization is considered converged when the forces in any direction on all moveable atoms are less than 0.01 eV/Å. A previous study showed several of the 3d mononitrides to be either antiferromagnetic (RS structure of VN, CrN, MnN, FeN and ZB structure of MnN) or ferromagnetic (ZB structure of VN, CrN) at their equilibrium lattice constants and as such are treated as spin-polarized [31]. The RPBE lattice constants are also taken from that study. The calculations are conducted with density functional theory (DFT) using the RPBE exchanges correlation functional [32]. A plane wave basis set with an energy cutoff of 350 eV is used to represent the valence electrons with a PAW [33] representation of the core electrons as implemented in the VASP code [34]. Activation energies are calculated as the highest point along the minimum energy path (MEP) calculated using the climbing image nudged elastic band method (CI-NEB) [35]. The self-consistent electron density is determined by iterative diagonalization of the Kohn-Sham Hamiltonian, with the occupation of the Kohn-Sham states being smeared according to a Fermi-Dirac distribution with a smearing parameter of kBT = 0.1 eV. A 4 × 4 × 1 Monkhorst-Pack k-point sampling is used for all the surfaces.

3 Results and Discussion

3.1 Stability of the surface nitrogen vacancy

In the Mars-van Krevelen mechanism considered in the present work, a surface nitrogen atom is reduced to form NH_3 after which the resulting vacancy is replenished by a gaseous N_2 molecule. For this replenishment to occur, the N-vacancy needs to be stable at the surface. If this is not the case, the N-vacancy may migrate to the bulk of the catalyst, that is, the reacted nitrogen on the surface is replaced with more nitrogen from the catalyst itself, rather than with gaseous N_2. This process can, in principle, continue until all the nitrogen atoms of the metal nitride have reacted and formed NH_3, leaving only the pure metal. The stability of the N-vacancy at the surface of the catalyst is estimated by comparing the difference in energy of a nitride slab with a single N-vacancy in the surface layer (E_{vac},1) and to that of a single N-vacancy in the first subsurface layer (E_{vac},2). The minimum energy configuration of each of these slabs is found and the energy difference (ΔE_{vac} = (E_{vac},2) - (E_{vac},1)) used as an estimation of the thermodynamic stability of the vacancy at the surface of the nitride. Activation barriers for vacancy migration ($E_{a,vac}$) are also calculated and both ΔE_{vac} and $E_{a,vac}$ are presented in Fig. 1. It is found that, for most of the nitrides, it is thermodynamically favorable for the vacancy to migrate to the bulk, with ΔE_{vac} less than or close to zero. However, it is clear that many of the nitrides exhibit a high activation barrier for vacancy migration and are thus likely to demonstrate a stable surface vacancy. All nitrides with an activation barrier for a vacancy migration of > 1 eV is retained

for further screening, since a barrier of such magnitude is unlikely to be overcome at room temperature.

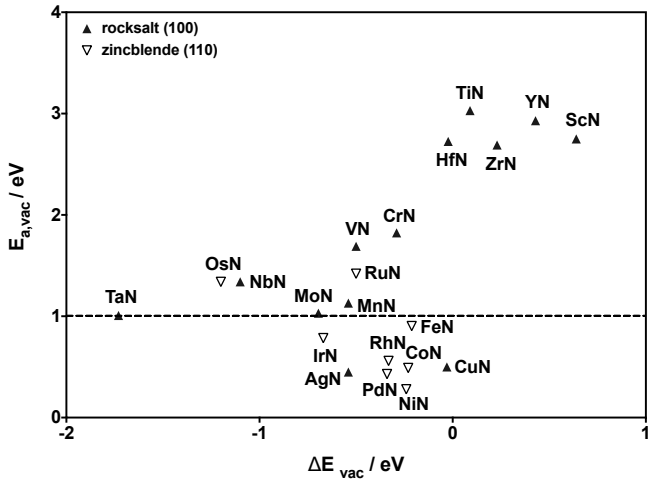

Figure 1: Energy differences (ΔE_{vac}) of a vacancy at the surface layer and in the first subsurface layer of a nitride and the associated activation barrier of vacancy migration ($E_{a,vac}$). The dashed line at $E_{a,vac}$ = 1 eV represents the cutoff above which metal nitrides are considered sufficiently stable for further study.

3.2 Catalytic activity

The rate-determining step (RDS) and our measure of the catalytic activity towards NH_3 formation on each nitride is identified as the elementary reaction step with the largest increase in free energy. When this elementary step can be eliminated by applying a bias, it is referred to as the onset potential, which is the bias that needs to be applied in order to shift the free energy landscape in such a way that all reaction steps become downhill in free energy. The catalytic activity is studied for the nitrides that exhibit stable vacancy on the surface (with $E_{a,vac}$ > 1 eV, Fig.1) where at each H addition step every possible adsorption site is investigated, including other N atoms, metal atoms and bridging sites.

For VN and RuN (shown in Fig. 2) as well as for CrN, each added H adds to the same N atom, forming one NH_3, then the second, with only 6($H^+ + e^-$) required to form 2NH_3. For ZrN, allowing the H to bind to any surface site results in firstly a surface Zr atom being protonated, and then an N atom. The protonation of N is the RDS in NH_3 formation. A similar case is seen for NbN, where two neighboring Nb atoms are protonated before the RDS, which is protonation of the first surface N. For MnN, 3(*NH_2) and 1(*NH) form before the first ammonia is released and 9($H^+ + e^-$) are needed to form 2NH_3. In this case, no metal atoms are protonated. In contrast, for MoN and OsN, H atoms cover all the metal atoms on the surface as well as surface N atoms and 12($H^+ + e^-$) and 13($H^+ + e^-$) are

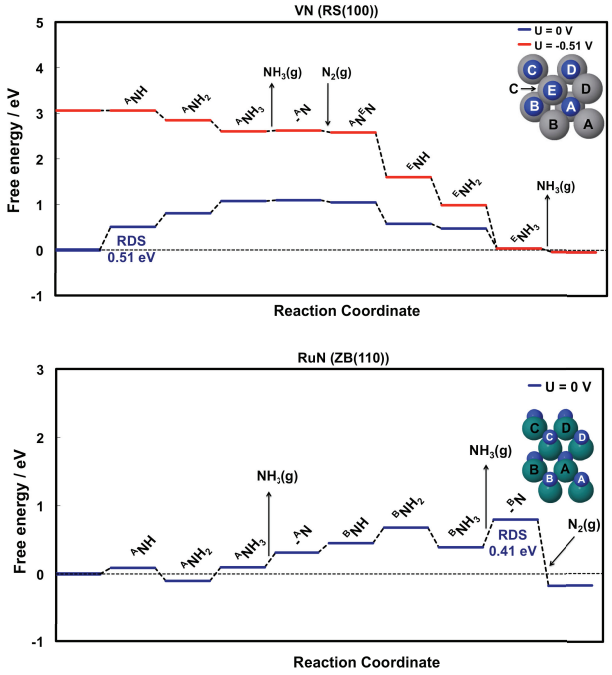

Figure 2: Free energy diagram for NH_3 formation via Mars-van Krevelen mechanism on the (100) facet of RS structure of VN and the (110) facet of ZB structure of RuN. For VN the rate-determining step is the first protonation step with ΔG = 0.51 eV. The blue line indicates the free energy of all the stable intermediates calculated at zero potential. The red line represents the free energy of all the stable intermediates at the onset potential. For RuN the RDS is to release the ammonia with ΔG = 0.41 eV. As the RDS involves no proton-electron transfer, no bias is applied and the free energy landscape of RuN is depicted only at zero potential.

needed to form $2NH_3$. For MoN, to form NH is the RDS. For OsN addition of N_2(g) to fill the N-vacancy is endothermic, which corresponds to an increase in free energy that cannot be surpassed by an external applied bias as no proton-electron transfer is involved at this step. For such cases that require more than the minimum $6(H^+ + e^-)$ to form $2NH_3$, a lower faradaic efficiency is likely to be observed. For TiN, YN, ScN, HfN and TaN an unconstrained mechanism yields a full H coverage on the surface with no NH_3 formation. The catalytic activity of these nitrides are thus instead being considered as potential hydrogen evolution catalysts, the results of which are beyond the scope of the present study. After exclusion of those nitrides that do not form NH_3 (TiN, TaN, ScN, YN and HfN),

eight metal nitride catalysts are considered potentially active towards NH_3 formation and presented in Fig. 3. The RuN from ZB as well as the six RS nitrides shown in Fig.3 should make ammonia electrochemically under ambient conditions whereas ZB OsN likely requires high pressure to fill the N-vacancy in order to complete the catalytic cycle of ammonia formation.

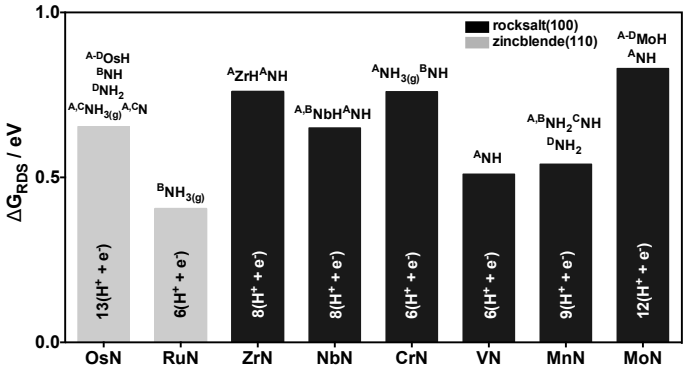

Figure 3: Free energy change (ΔG_{RDS}, in eV) of the rate-determining step of NH_3 formation on transition metal nitride catalysts. At each H addition step every possible adsorption site is investigated including other N atoms, metal atoms and bridging sites and at least $6(H^+ + e^-)$ are needed to form $2NH_3$. The labels above each bar indicate the species formed in the rate-determining step, the notation of which is explained in Fig. 2. The labels in each bar indicate the number of protons and electrons required to make $2NH_3$.

3.3 Poisoning of the surface vacancy

As previously discussed, in the Mars-van Krevelen mechanism considered in this work a surface N is reacted, leaving a surface vacancy at the surface and for the catalytic cycle to complete, this vacancy must be filled with N_2(g). However, there exists the possibility of the vacancy rather being filled with H atoms or O atoms from the aqueous electrolyte, both of which would block this surface site for completion of the catalytic cycle. In the present section the competition between N, O and H for filling the surface vacancy is investigated by considering the free energy of filling the vacancy with O or H relative to N ($\Delta G_{(*N-*X)}$, where X = O or H). These free energies are referenced to N_2, H_2O and H_2 in the gas phase and are calculated at the onset potential for each nitride. A negative value of $\Delta G_{(*N-*X)}$ indicates that it is thermodynamically favorable to fill the vacancy with N, rather than O or H. The values of $\Delta G_{(*N-*X)}$ are shown in Fig. 4 for all the catalytically active nitrides. It can be observed that N atoms bind more strongly to the surface vacancy than O atoms by over 1 eV for most nitrides. Hence, it is not likely for the surface vacancy to be poisoned by O atoms. For poisoning by H, though, the surface vacancy in MnN, MoN and RuN is likely to be filled by H, rather than N. For the remaining nitrides, ZrN, NbN, CrN and VN, the vacancy is likely refilled by N and thus the catalytic cycle may continue to form the second NH_3. These results are as expected as when the bias is tuned

towards more negative values, the electropositive O species bind weaker on the surface compared to H_2O in the gas phase, as they would rather form bonds with the surface when the bias is more positive:

$$H_2O + * \rightarrow *O + 2H^+ + 2e^- \quad (3)$$

Conversely, the H adsorption free energy becomes more negative when the bias is lowered:

$$H^+ + e^- \rightarrow * H \quad (4)$$

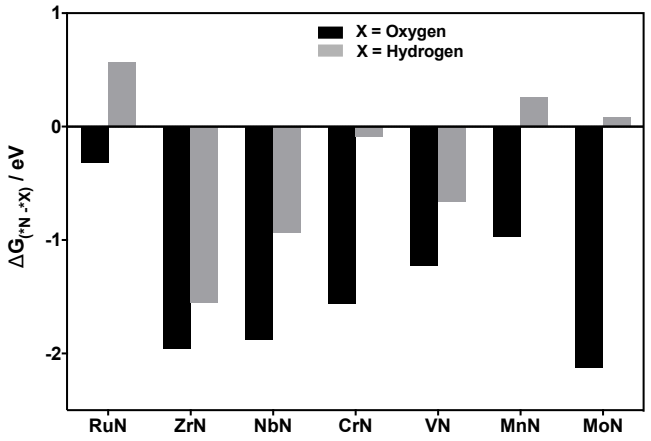

Figure 4: Free energy of adsorption of O or H (relative to N) to the surface vacancy of catalytically active nitrides ($\Delta G_{(*N-*X)}$ in eV). Free energies are calculated relative to N_2(g), H_2(g) and H_2O(g). All free energies are evaluated at the calculated onset potential for each nitrides: ZrN, -0.76 V; NbN, -0.65 V; CrN, -0.76 V; VN, -0.51 V; MnN, -0.54 V; MoN, -0.83 V; and RuN, -0.41 V.

4 Summary and Conclusions

In this paper, first principles calculations are used to screen for nitrogen reduction electrocatalysts that efficiently form ammonia at ambient conditions and in aqueous electrolyte. The most promising nitride catalysts are the (100) facets of rocksalt structure of ZrN, NbN, CrN and VN. The suggested catalysts should have stable N-vacancy at the surface and not be poisoned by oxygen or hydrogen from the aqueous electrolyte. In contrast to previous studies where relatively high onset potentials are required for ammonia formation, and hydrogen evolution is a competing reaction, the most promising RS candidates presented in this paper only need a low applied bias to form ammonia and the competing HER is suppressed. Therefore, a significant amount of ammonia compared with hydrogen gas can be expected. Furthermore, at the onset potential, the N-vacancy is stable towards both

protonation and oxidation from water and it should get easily repaired with atmospheric nitrogen injected to the system at ambient conditions. Other crystal facets and other mechanisms of ammonia formation on these nitride catalysts are currently being studied to further investigate the catalytic capability of this class of catalyst.

5 Acknowledgements

Financial support is acknowledged from the Icelandic Research Fund, Nordic Energy Research by way of the Nordic Initiative for Solar Fuel Development, the Icelandic Student Innovation Fund, and the Research Fund of the University of Iceland. The calculations were in part carried out on the Nordic high performance computer (Gardar).

References

[1] S. Giddey, S. P. S. Badwal, and A. Kulkarni. Review of electrochemical ammonia production technologies and materials. *Int. J. Hydrogen Energy,* **38** (2013) 14576−14594.

[2] I. A. Amar, R. Lan, C. T. G. Petit, and S. Tao. Solid-state electrochemical synthesis of ammonia: a review. *J. Solid State Electrochem.,* **15** (2011) 1845−1860.

[3] V. Smil. Global Population and the Nitrogen Cycle. *Sci. Am.,* **277** (1997) 76−81.

[4] J. M. Berg, J. L. Tymoczko, and L. Stryer. *Biochemistry*, W. H. Freeman, New York (2002) 988−990.

[5] G. Marnellos and M. Stoukides. Ammonia synthesis at atmospheric pressure. *Science,* **282** (1998) 98−100.

[6] G. Marnellos, S. Zisekas, and M. Stoukides. Synthesis of Ammonia at Atmospheric Pressure with the Use of Solid State Proton Conductors. *J. Catal.,* **193** (2000) 80−87.

[7] T. Murakami, T. Nishikiori, T. Nohira, and Y. Ito. Electrolytic synthesis of ammonia in molten salts under atmospheric pressure. *J. Am. Chem. Soc.,* **125** (2003) 334−335.

[8] T. Murakami, T. Nohira, T. Goto, Y. H. Ogata, and Y. Ito. Electrolytic ammonia synthesis from water and nitrogen gas in molten salt under atmospheric pressure. *Electrochim. Acta.,* **50** (2005) 5423−5426.

[9] T. Murakami, T. Nohira, Y. Araki, T. Goto, R. Hagiwara, and Y. H. Ogata. Electrolytic Synthesis of Ammonia from Water and Nitrogen under Atmospheric Pressure Using a Boron-Doped Diamond Electrode as a Nonconsumable Anode. *Electrochem. Solid-State Lett.,* **10** (2007) E4−E6.

[10] J. Catt, A. J. Pearman, and R. L. Richards. The reduction of mono-coordinated molecular nitrogen to ammonia in a protic environment. *Nature,* **253** (1975) 39−40.

[11] J. Pool, E. Lobkovsky, and P. Chirik. Hydrogenation and cleavage of dinitrogen to ammonia with a zirconium complex. *Nature,* **427** (2004) 527−530.

[12] J. K. Nørskov, J. Rossmeisl, A. Logadottir, L. Lindqvist, J. R. Kitchin, T. Bligaard, and H. Jnsson. Origin of the overpotential for oxygen reduction at a fuel-cell cathode. *J. Phys. Chem. B,* **108** (2004) 17886−17892.

[13] J. Greeley and M. Mavrikakis. Alloy catalysts designed from first principles. *Nat. Mater.,* **3** (2004) 810−815.

[14] K. Honkala, A. Hellman, I. N. Remediakis, A. Logadottir, A. Carlsson, S. Dahl, C. H. Christensen, and J. K. Nørskov. Ammonia synthesis from first-principles calculations. *Science,* **307** (2005) 555−558.

[15] J. Hafner and C. Wolverton. Toward Computational Materials Design : The Impact of Density Functional. *MRS Bull,* **31** (2006) 659−668.

[16] F. Abild-Pedersen, J. Greeley, F. Studt, J. Rossmeisl, T. Munter, P. Moses, E. Skúlason, T. Bligaard, and J. Nørskov. Scaling Properties of Adsorption Energies for Hydrogen-Containing Molecules on Transition-Metal Surfaces. *Phys. Rev. Lett.,* **99** (2007) 0161051−0161054.

[17] F. Studt, F. Abild-Pedersen, T. Bligaard, R. Z. Srensen, C. H. Christensen, and J. K. Nørskov. Identification of non-precious metal alloy catalysts for selective hydrogenation of acetylene. *Science,* **30** (2008) 1320−1322.

[18] H. J. Freund and G. Pacchioni. Oxide ultra-thin films on metals: new materials for the design of supported metal catalysts. *Chem. Soc. Rev.,* **37** (2008) 2224−2242.

[19] J. Greeley, I. E. L. Stephens, A. S. Bondarenko, T. P. Johansson, H. A. Hansen, T. F. Jaramillo, J. Rossmeisl, I. Chorkendorff, and J. K. Nørskov. Alloys of platinum and early transition metals as oxygen reduction electrocatalysts. *Nat. Chem.,* **1** (2009) 552−556.

[20] J. K. Nørskov, T. Bligaard, J. Rossmeisl, and C. H. Christensen. Towards the computational design of solid catalysts. *Nat. Chem.,* **1** (2009) 37−46.

[21] J. K. Nørskov, F. Abild-Pedersen, F. Studt, and T. Bligaard. Density functional theory in surface chemistry and catalysis. *Proc. Natl. Acad. Sci. U. S. A.,* **108** (2011) 937−943.

[22] J. G. Howalt, T. Bligaard, J. Rossmeisl, and T. Vegge. DFT based study of transition metal nano-clusters for electrochemical NH3 production. *Phys. Chem. Chem. Phys.,* **15** (2013) 7785−7795.

[23] V. Tripkovic, M. Vanin, M. Karamad, M. E. Bjrketun, K. W. Jacobsen, K. S. Thygesen, and J. Rossmeisl. Electrochemical CO2 and CO Reduction on Metal-Functionalized Porphyrin-like Graphene. *J. Phys. Chem. C,* **117** (2013) 9187−9195.

[24] A. Verdaguer-Casadevall, D. Deiana, M. Karamad, S. Siahrostami, P. Malacrida, T. W. Hansen, J. Rossmeisl, I. Chorkendorff, and I. E. L. Stephens. Trends in the electrochemical synthesis of H2O2: enhancing activity and selectivity by electrocatalytic site engineering. *Nano Lett.,* **14** (2014) 1603−1608.

[25] A. A. Peterson, F. Abild-Pedersen, F. Studt, J. Rossmeisl, and J. K. Nørskov. How copper catalyzes the electroreduction of carbon dioxide into hydrocarbon fuels. *Energy Environ. Sci.,* **3** (2010) 11311−1315.

[26] Y. Abghoui, A. L. Garden, V. F. Hlynsson, S. Björgvinsdóttir, H. Ólafsdóttir, and E. Skúlason. Enabling electrochemical reduction of nitrogen to ammonia at ambient conditions through rational catalyst design. *Phys. Chem. Chem. Phys.,* **17** (2015) 4909-4918.

[27] E. Skúlason, T. Bligaard, S. Gudmundsdóttir, F. Studt, J. Rossmeisl, F. Abild-Pedersen, T. Vegge, H. Jónsson, and J. K. Nørskov. A theoretical evaluation of possible transition metal electro-catalysts for N2 reduction. *Phys. Chem. Chem. Phys.,* **14** (2012) 1235−1245.

[28] J. Howalt, T. Bligaard, J. Rossmeisl and T. Vegge. DFT based study of transition metal nano-clusters for electrochemical NH3 production. *Phys. Chem. Chem. Phys.,* **15** (2013) 7785−7795.

[29] J. Howalt and T. Vegge. The role of oxygen and water on molybdenum nanoclusters for electro catalytic ammonia production. *Beilstein J. Nanotechnol.,* **5** (2014) 111−120.

[30] P. Mars and D. W. Van Krevelen. Special supplement to chemical engineering science. *Eng. Sci.,* **3** (1954) 41−45.

[31] V. F. Hlynsson, E. Skúlason, and A. L. Garden. A systematic, first-principles study of the structural preference and magnetic properties of mononitrides of the d-block metals. *J. Alloys Compd.,* **603** (2014) 172−179.

[32] B. Hammer, L. Hansen, and J. Nørskov. Improved adsorption energetics within density-functional theory using revised Perdew-Burke-Ernzerhof functionals. *Phys. Rev. B,* **59** (1999) 7413−7421.

[33] P. Blchl. Projector augmented-wave method. *Phys. Rev. B,* **50** (1994) 17953−17979.

[34] G. Kresse and J. Hafner. Ab. initio molecular dynamics for liquid metals. *Phys. Rev. B,* **47** (1993) 558−561.

[35] G. Henkelman, B. P. Uberuaga, and H. Jonsson. A climbing image nudged elastic band method for finding saddle points and minimum energy paths. *J. Chem. Phys.,* **113** (2000) 9901−9904.

IX Article 9

Nitrogen Activation to Ammonia via a Mars-van Krevelen Mechanism on Nitride Electro-Catalysts

Younes Abghoui and Egill Skúlason

*American Institute of Chemical Engineers **(AIChE)**, ISBN: 978-0-8169-1094-6 (2015).*

Nitrogen Activation to Ammonia via a Mars-van Krevelen Mechanism on Nitride Electro-Catalysts

Younes Abghoui and Egill Skulason
University of Iceland, Reykjavik, Iceland

Abstract

Viable design of a green route for production of ammonia represents a cost-effective and environmental solution. One of promising alternatives to the centralized Haber-Bosch process is electroreduction of nitrogen to ammonia renewably where proton is provided by water splitting in anode and both nitrogen and electron are provided in the cathode. For the sake of decentralization, small-scale N_2 reduction devices are necessary that are equipped with selective and active catalyst running well at ambient conditions without the sophistications of the Haber-Bosch process. Here, we present the results of density functional theory (DFT) calculations conducted on different facets of transition metal mononitrides of Zr and V for possibility of catalytic conversion of nitrogen to ammonia under ambient conditions. The Mars-van Krevelen mechanism was studied on (100/111) facets of rocksalt and (100/110) facets of zincblende structures. We studied the catalytic activity, calculated free energy of all intermediates along the reaction path for nitrogen reduction to ammonia and constructed free energy diagrams to estimate onset potential necessary for the reaction on each different facet. Ammonia formation was found more energetically favorable on the (100) facets of rocksalt with less numbers of proton/electron pairs and with smaller potential-determining step (PDS) compared to other facets. Therefore, less negative potentials should be required to apply for electrochemical ammonia formation if single crystal (the (100) facet) of the rocksalt structure is utilized.

Introduction

The use of ammonia as an energy carrier and specially fertilizer has triggered increased interest in developing alternative methods in pursuit of a more decentralized and environmentally friendly approach for ammonia synthesis. Without ammonia and thus deprived of inorganic fertilizer, almost half the world´s population would be at risk of starvation[1]. Human survival has been thus depending a great deal on the Haber–Bosch process[2], which is the most pivotal industrial installation for catalytic cleavage of N_2 and hydrogenating nitrogen to ammonia heterogeneously over promoted transition metal-based catalysts. Although Ru and Fe within the Haber-Bosch process show good activity for this catalytic conversion, the expense and scarcity of these catalysts as well as the harsh operational conditions and sophisticated industrial setup of the Haber-Bosch process are all prohibitive to decentralization of ammonia synthesis. This complicates ammonia production in regions with relatively undeveloped infrastructure such as developing countries. Besides, the reliance of this process on natural gases for supplying its necessary hydrogen feedstock not only promotes severe CO_2 emission to the environment but it also makes the production of ammonia and accordingly food susceptible to natural gas price fluctuations and political conflicts in the oil-rich regions. Most importantly, a sustainable process needs to be developed for ammonia production to maintain food supply since at some point natural gas will be depleted.

Electro-catalytic ammonia synthesis is a particularly feasible method due to the potential of utilizing renewable energy sources and mild operating conditions[3–8]. But finding a (electro-) catalyst that is selective enough towards nitrogen electroreduction reaction (NER) and has a low over-potential is challenging for distributed and decentralized high-efficient ammonia production at ambient conditions. As hydrogen evolution reaction (HER) is known the most competitive side reaction in ammonia synthesis decreasing the current efficiency and yield of NER, first-principle calculations were used to provide more insight about the mechanism of the reaction and to explore new class of material with higher activity and selectivity towards NER. Using DFT calculations, a few pure transition metals[9] and transition metal nano-clusters[10] were reported capable of ammonia formation. Recently, transition metal nitrides were found extremely promising for electrochemical ammonia formation at ambient conditions where the rocksalt (100) of VN and ZrN found to be very stable and active catalyst materials[11,12].

In this work, we considered the rocksalt (111) and zincblende (100/110) structures of VN and ZrN, calculated and compared their catalytic activity to the (100) of the rocksalt. The main reason is that in manufacturing of thin films of these materials, it is very common to fabricate a catalyst with more than one crystallographic texture orientation (a polycrystalline structure). Therefore, the fabricated catalysts benefit multifaceted structure and catalytic activity of each facet might not be necessarily the same as the (100) facet. Also, the instability or inactivity of one facet might jeopardize the proper functionality of the other active facets and therefore decrease the yield of the reaction or even cease the catalytic cycle.

Methodology

We used DFT with the RPBE[13] exchange correlation functional to carry out all the calculations. We also used a plane wave basis set with an energy cutoff of 350 eV to represent the valence electrons with a PAW[14] representation of the core electrons as implemented in the VASP code[15,16]. We used iterative diagonalization of the Kohn– Sham Hamiltonian to determine the self-consistent electron density, with the occupation of the Kohn–Sham states being smeared according to a Fermi–Dirac distribution with a smearing parameter of kBT = 0.1 eV. We used a 4×4×1 Monkhorst–Pack K-point sampling for all the surfaces. We modeled a five-layer nitride slab with four metal atoms and four nitrogen atoms in each layer. We fixed the bottom two layers and allowed the top layers as well as the adsorbed species fully relax. Boundary conditions were periodic in the x and y directions and surfaces were separated by 12 Å of vacuum in the z direction. We considered the structural optimization converged when the forces in any direction on all moveable atoms were below 0.01 eV $Å^{-1}$.

Results and discussion

The stability of four different faces of mononitrides of V and Zr was investigated by calculating the total energy of each slab. The surface with most negative total energy was assumed to be the most energetically favorable. These values are given in table 1. The (100) facet of zincblende of ZrN transformed to the (100) of rocksalt upon geometry optimizations and therefore not analyzed further and not shown in the results.

Table 1. Comparison of total energy of the relaxed surfaces of VN and ZrN

	Total energy of the relaxed surface (eV)	
	VN	**ZrN**
Rocksalt (100)	-377.03	-391.87
Rocksalt (111)	-371.70	-388.22
Zincblende (100)	-358.28	-
Zincblende (110)	-363.72	-371.20

To study the catalytic activity of these surfaces, we calculated the binding energy of H on different surfaces of these two nitrides by the use of DFT to construct the free energy diagrams (FED) and estimate the onset potential required for reduction of surface nitrogen to ammonia. We considered all the possible adsorption sites for each H on the surface and at each protonation step we selected energetically favorable configuration and therefore the most stable intermediates along the reaction path. Figure 1 illustrates and compares the FEDs of different facets of both VN and ZrN towards formation of two ammonia molecules. As can be seen, the reaction path towards ammonia formation is very different from one facet to the other on both nitrides. It usually takes less intermediates to form ammonia molecule on the (100) facet of rocksalt but much more intermediates on the (100/110) facets of zincblende. On both VN and ZrN, the (100) facet of rocksalt is the only structure on which ammonia formation proceeds via single nitrogen vacancy (N-vacancy) formation. For all the other facets, addition of $N_2(g)$ to fill the N-vacancy is endothermic corresponding to an increase in free energy that cannot be surpassed by an external applied bias, as it is not an electrochemical step with proton/electron transfer. Therefore, a mechanism of forming a dimer N-vacancy is considered instead for these nitrides[17]. The result is that the free energy landscape changes significantly in such a way that the addition of $N_2(g)$ becomes downhill in free energy in all cases. In addition, for the rocksalt structures of VN the PDS is in the first catalytic cycle and before formation of the first ammonia molecule, while for the zincblende structures of VN the PDS is in the second part of the cycle and after formation of the first ammonia molecule. However, for ZrN this seems a bit different where the PDS is prior to formation of the first ammonia molecule only on the (100) facet of rocksalt. But on the (111) facet of rocksalt and (110) of zincblende the PDS is after formation of the first ammonia molecule. For VN, the less active surfaces are the zincblende surfaces with free energy of the PDS being 1.22 and 1.24 eV. For ZrN, the less active surface is the (111) facet of rocksalt with the free energy of the PDS being 1.56 eV.

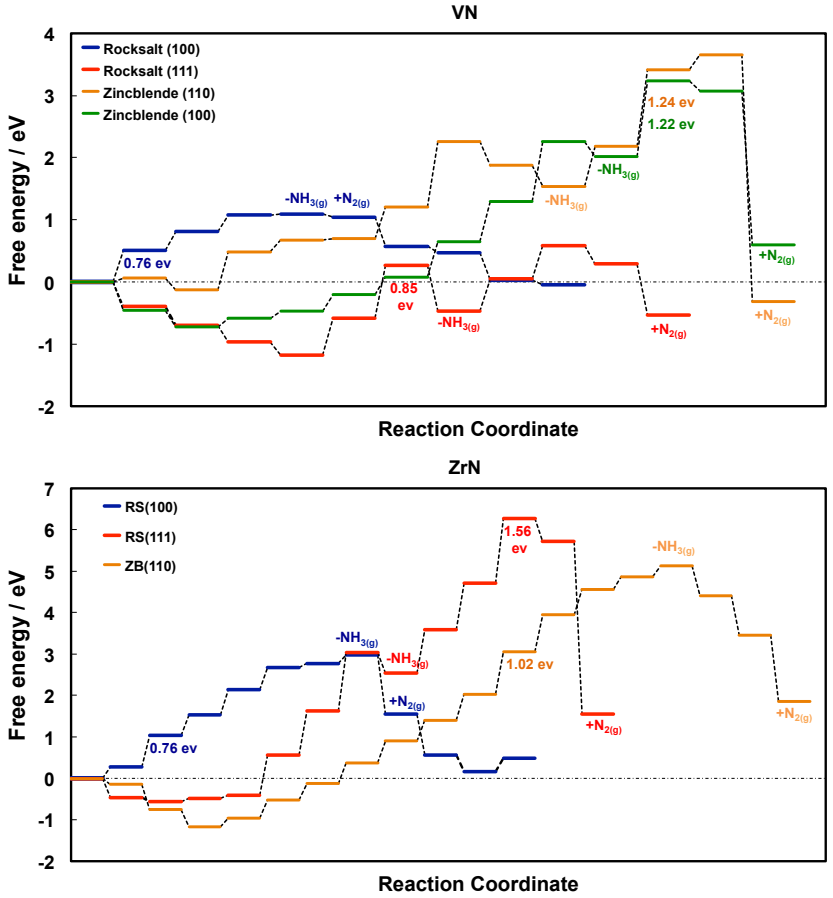

Figure 1. Free energy diagrams for different facets of VN and ZrN. The free energy of the potential-determining step is estimated and mentioned for all different facets. Steps corresponding to release of ammonia and addition of nitrogen is also shown ($-NH_{3(g)}$ and $+N_{2(g)}$, respectively).

Conclusion

We conducted DFT to calculate the binding energy of H on the surface of ZrN and VN in four different crystallographic features namely as (100/111) of rocksalt and (100/110) of zincblende. We

investigated the catalytic activity of these 8 surfaces for reduction of nitrogen to ammonia. We found that the (100) of rocksalt structure is the most active surface in both mononitrides of Zr and V. Besides, less number of proton/electron pairs are required for formation of two ammonia molecules on these surfaces. Whereas, other facets require having the neighboring metal atoms or nitrogen atoms populated by more protons before reducing surface nitrogen to ammonia. In addition, the nature of the PDS was found very different on various facets of these mononitrides. All in all, in case of fabrication of multifaceted films of these catalysts, electrochemical activation of nitrogen to ammonia should be feasible on both VN and ZrN but at different overpotentials.

References

1. Smil, V (1999), "Detonator of the population explosion," *Nature* **400,** pp. 415.
2. Smil, V (1997), "Global Population and the Nitrogen Cycle," *Sci. Am.* **277,** pp. 76–81.
3. Kordali, V., Kyriacou, G. and Lambrou, C (2000), "Electrochemical synthesis of ammonia at atmospheric pressure and low temperature in a solid polymer electrolyte cell," *Chem. Commun.* pp. 1673–1674.
4. Murakami, T., Nishikiori, T., Nohira, T. and Ito, Y (2003), "Electrolytic synthesis of ammonia in molten salts under atmospheric pressure," *J. Am. Chem. Soc.* **125,** pp. 334–335.
5. Lan, R., Irvine, J. T. S. and Tao, S (2013), "Synthesis of ammonia directly from air and water at ambient temperature and pressure," *Sci. Rep.* **3,** pp. 1–7.
6. Giddey, S., Badwal, S. P. S. and Kulkarni, A (2013), "Review of electrochemical ammonia production technologies and materials," *Int. J. Hydrogen Energy* **38,** pp. 14576–14594.
7. Amar, I. A., Lan, R., Petit, C. T. G. and Tao, S (2011), "Solid-state electrochemical synthesis of ammonia: a review," *J. Solid State Electrochem.* **15,** pp. 1845–1860.
8. Garagounis, I., Kyriakou, V., Skodra, A., Vasileiou, E. and Stoukides, M (2014), "Electrochemical Synthesis of Ammonia in Solid Electrolyte Cells," *Front. Energy Res.* **2,** pp. 1–10.
9. Skulason, E., Bligaard, T., Gudmundsdottir, S., Studt, F., Rossmeisl, J., Abild-Pedersen, F., Vegge, T., Jonsson, H. and Nørskov, J. K (2012), "A theoretical evaluation of possible transition metal electro-catalysts for N2 reduction," *Phys. Chem. Chem. Phys.* **14,** pp. 1235–1245.
10. Howalt, J. G., Bligaard, T., Rossmeisl, J. and Vegge, T (2013), "DFT based study of transition metal nano-clusters for electrochemical NH3 production," *Phys. Chem. Chem. Phys.* **15,** pp. 7785–7795.
11. Abghoui, Y. Garden, A. Hlynsson, V. Bjorgvinsdottir, S. Olafsdottir, H. and Skulason, E (2015), "Enabling electrochemical reduction of nitrogen to ammonia at ambient conditions through rational catalyst design," *Phys. Chem. Chem. Phys.* **17,** pp. 4909–4918.

12. Abghoui, Y. and Skúlasson, E (2015), "Transition Metal Nitride Catalysts for Electrochemical Reduction of Nitrogen to Ammonia at Ambient Conditions," *Procedia Comput. Sci.* **51,** pp. 1897–1906.

13. Hammer, B., Hansen, L. and Nørskov, J (1999), "Improved adsorption energetics within density-functional theory using revised Perdew-Burke-Ernzerhof functionals," *Phys. Rev. B* **59,** pp. 7413–7421.

14. Blöchl, P (1994), "Projector augmented-wave method," *Phys. Rev. B* **50,** pp. 17953–17979.

15. Kresse, G. and Hafner, J (1993), "Ab. initio molecular dynamics for liquid metals," *Phys. Rev. B* **47,** pp. 558–561.

16. Kresse, G. and Furthmüller, J (1996), "Efficient iterative schemes for ab initio total-energy calculations using a plane-wave basis set," *Phys. Rev. B. Condens. Matter* **54,** pp. 11169–11186.

17. Abghoui, Y., Garden, A. L., Howalt, J. G., Vegge, T. and Skúlason, E (2015), "Electroreduction of N2 to ammonia at ambient conditions on mononitrides of Zr, Nb, Cr, and V – A DFT guide for experiments," submitted to ACS-Catalysis.

X Article 10

Transition Metal Nitrides As Promising Electro-Catalysts for Either Reduction of Nitrogen to Ammonia or Hydrogen Evolution Reaction

Younes Abghoui and Egill Skúlason

American Institute of Chemical Engineers ***(AIChE)****, ISBN: 978-0-8169-1094-6 (2015).*

Transition Metal Nitrides As Promising Electro-Catalysts for Either Reduction of Nitrogen to Ammonia or Hydrogen Evolution Reaction

Younes Abghoui and Egill Skulason
University of Iceland, Reykjavik, Iceland

Abstract

Here we report the discovery of a new class of electro-catalyst material that enables nitrogen electroreduction reaction (NER) to ammonia at ambient conditions under small overpotentials. The most promising electro-catalysts are identified among a range of transition metal nitride surfaces with the use of comprehensive Density Functional Theory (DFT) calculations. In addition to very promising nitride candidates explored for NER, a few nitrides were found to be interesting for Hydrogen Evolution Reaction (HER) that could potentially evolve H_2 with potentials nearing that of Pt. Thus, it might be possible to replace the expensive Pt catalysts with cheaper nitride compounds. After screening out these promising nitride candidates for both NER and HER with DFT, we are now testing them experimentally to see their suitability for real-life applications.

Introduction

Conversion and storage of energy via an electrochemical approach is promising for development of green power resources for electric transportation and renewable energy production/storage. Both NER and HER are considered important electrochemical reactions in this regard. NER is mainly interesting for electrochemical reduction of nitrogen to ammonia, which is extremely important for decentralized and evenly distributed production of fertilizers throughout the world. If that were realized, the sophisticated infrastructures and economical-intensive operational conditions needed for the Haber-Bosch process would be surmounted. Ammonia is also becoming attractive as an energy carrier and a transportation fuel owing to its high energy density and lack of CO_2 emissions[1]. Therefore, successful NER can help develop environmentally and economically friendly methodologies for growing a new energy economy. In addition to NER, HER is another important electrochemical reaction that is critical in fuel cells/electrolyzers where protons produced via water splitting in electrolyte combine with electrons at surface of the electrode, form H-adatoms and then get reduced to hydrogen gas. This is central for storage of clean energy via H_2 production and accordingly for energy transportation.

One of the largest cost and efficiency limitations of these electrochemical technologies lies in either the slow kinetics of the electrochemical reactions (regarding NER) or scarce and high-cost electrode material (concerning HER). To tackle both of these challenges and to increase the reaction kinetics and accordingly lessen the cost and inefficiency, it is necessary to explore for new class of materials that facilitate and catalyze the electrochemical processes, yet are abundant and cheap to prepare.

In this study, we used GGA-DFT calculations to screen for a stable and active catalyst amongst a range of transition metal nitride surfaces for catalyzing either NER or HER. We studied the (100) facet of the rocksalt structure of the mononitrides of Sc, Ti, V, Cr, Mn,Y, Zr, Nb, Hf, Ta and Mo, as it

turned out that this crystallographic structure is the most stable texture orientations of these materials[2,3]. We constructed the free energy diagrams for the electrochemical protonation of surface atoms to obtain onset potentials required for catalyzing NER or HER on the surface of these mononitride structures.

Methodology

All calculations were conducted with DFT using the RPBE exchange correlation functional[4]. A plane wave basis set with an energy cutoff of 350 eV was used to represent the valence electrons with a PAW[5] representation of the core electrons as implemented in the VASP code[6,7]. Iterative diagonalization of the Kohn– Sham Hamiltonian was used to determine the self-consistent electron density, with the occupation of the Kohn–Sham states being smeared according to a Fermi–Dirac distribution with a smearing parameter of kBT = 0.1 eV. The k-point sampling used for all the surfaces was a 4×4×1 Monkhorst–Pack sampling with maximum symmetry to reduce the number of k-points in the calculations.

A five-layer slab with four metal atoms and four nitrogen atoms in each layer was used to model each nitride. The bottom two layers were fixed whereas the top layers as well as the adsorbed species were allowed to fully relax. Boundary conditions were periodic in the x and y directions and surfaces were separated by 12 Å of vacuum in the z direction. The structural optimization was considered converged when the forces in any direction on all moveable atoms were below 0.01 eV $Å^{-1}$. The RPBE lattice constants used in this study were: ScN: 4.56, TiN: 4.29, VN: 4.17, CrN: 4.19, MnN: 4.21, YN: 4.95, ZrN: 4.65, NbN: 4.48, HfN: 4.57, TaN: 4.44, MoN: 4.40.

Results and discussion

Firstly, we studied the possibility of catalyzing NER on the surface of mononitrides via a Mars-van Krevelen mechanism where upon freely protonation of the surface (with consideration of all the feasible adsorption sites for H) a nitrogen atom was reduced to ammonia and a nitrogen vacant site created. Secondly, we investigated the feasibility of HER on the surface of the nitrides that got totally covered by protons and could not produce ammonia at all.

We used DFT to study the binding energy of H adsorption on the surface of the mononitrides. Initially, we limited H addition to only a single surface nitrogen atom. We considered all the intermediates along the path (*NH, *NH_2 and *NH_3) and constructed the free energy diagrams (FED) to be able to determine the most endothermic step known as the potential-determining step (PDS). Figure 1 shows that all of the studied mononitrides exhibited catalytic activity for NER and reduced the surface nitrogen to NH_3. However, few of these mononitrides (ScN, TiN, YN, HfN and TaN) showed very less activity towards NER due to huge PDS along the reaction path with the free energy above 1.0 eV. To surmount this endergonic step, a huge negative bias of -1.0 to -2.0 V versus SHE is needed to shift the free energy diagram in a way that all the steps become downhill in free energy and therefore NER proceed. That is a huge overpotential making these mononitrides less interesting.

In a second consideration, we removed the limitation of H adsorption on a single nitrogen site of the surface. Instead, we considered all the possible adsorption sites for each proton addition and found the most energetically favorable configuration for making each intermediates along the path. Therefore, we allowed the possibility of coverage to build up on the surface with more H added and

accordingly included the coverage effect on the proposed onset potential for ammonia formation. The result of this consideration is shown in the inset of figure 1. We can see different behavior in catalytic activity of the mononitrides due to inclusion of the coverage effect, exploration of all the possible adsorption sites and selection of the most energetically favorable configuration along the reaction path. As can be seen from figures 1 and its inset, those nitrides with ΔG_{PDS} greater than 1.0 eV that assumed being inactive/less active towards NER when H adsorption was limited to one specific site are no longer capable of catalyzing NER when coverage effect is taken into account. However, the full free energy diagram of these five mononitrides shows that protonation of their surface continues until all the surface atoms (both the surface N atoms and the surface metal atoms) are occupied by proton and a full monolayer of hydrogen (1ML= $8H^+$) is formed on the surface (see figure 2, right). After that, addition of any extra proton to the surface results in either recombination of 2 H adatoms (Tafel mechanism) or binding of H adatom with a new proton coming towards the surface (Heyrovsky mechanism) to evolve hydrogen gas. Therefore, the red mononitrides shown in figure 1 might have a great potential for HER instead.

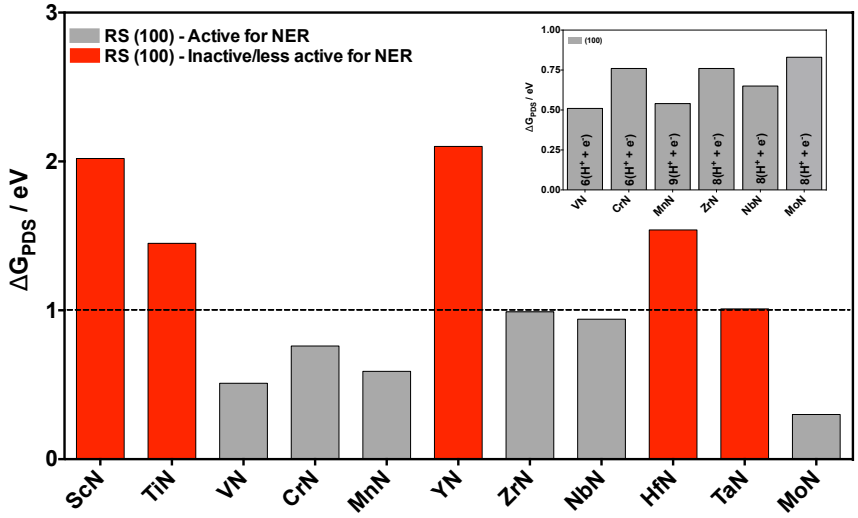

Figure 1. Free energy change of the PDS for NER on transition metal mononitride catalysts. H addition is restricted to a single nitrogen surface site and the minimum $6(H^+ + e^-)$ are used for formation of $2NH_3$. All mononitrides with free energy below 1.0 eV are interesting candidates for catalyzing NER. However, the ones marked red should be inactive/less active and thus less interesting due to huge overpotentials needed to apply. Inset shows the free energy change of the PDS for NER on transition metal mononitride catalysts. Considering all the possible adsorption sites of H on the surface and including the coverage effect, most of the nitrides require more than 6 proton/electron pairs for formation of two ammonia molecules. The labels in each bar indicate the number of protons and electrons required to make two ammonia molecules.

ΔG_{H^*} which is indicative of the adsorption free energy of hydrogen has become a conventional

descriptor to use when new class of materials are being screened for HER[8,9]. In Figure 2 (left), the free energy diagrams for hydrogen evolution over the nitride catalysts of Sc, Ti and Y are shown at the equilibrium potential. Their catalytic activity towards HER is also compared with the most efficient catalyst already known for this reaction, the Pt(111)[10]. The binding free energy of H to the surface of ScN and TiN is -0.35 and 0.60 eV, respectively. The former binds H stronger and that makes evolution of H_2 difficult compared to Pt; whereas the latter binds H so weakly that it is difficult to add the proton on the surface which can be circumvented by applying a greater negative bias. However, YN seems to bind H very moderately (around 0.0 eV) and that should make it as good HER catalyst as Pt. It even looks better in activity compared with Ni_2P with 0.19 eV being the free energy of adsorption of H[11].

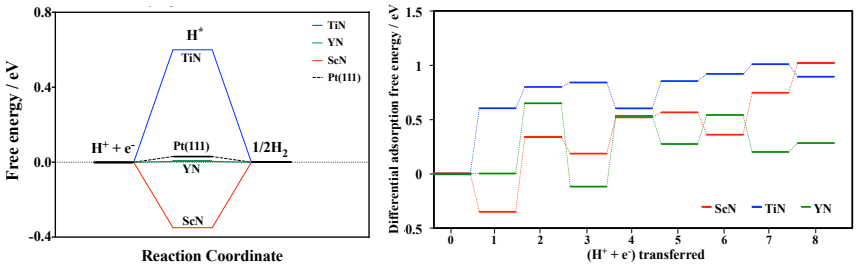

Figure 2. (Left) Free energy diagrams for HER at zero potential. The energies for the adsorbed intermediate are calculated with DFT for 1/8 ML coverage at standard conditions (zero pH, 1 bar of H_2 and at room temperature). The value for Pt(111) is taken from reference [10] and shown for comparison. (Right) Differential free energy of adsorption of H on the surface of ScN, TiN and YN where all the possible adsorption sites for H are explored and the most energetically favorable one is adapted along the path. A full monolayer of H (1ML= 8 *H) is formed on the surface without any possible activity for NER.

Protonation of the surface of Ti, Y and Sc mononitrides have been done thoroughly until a full monolayer of H (1ML = 8 *H) was formed on the surface. Neither $*NH_2$ nor $*NH_3$ was found being an energetically favorable intermediate along the path. Therefore, no ammonia formation was observed. After a full coverage of H, there was no longer an adsorption site available for H and therefore H_2 formation was observed upon addition of the 9th proton. The differential free energy of adsorption of H on these surfaces were constructed and shown in figure 2 (right), and Hf and Ta mononitrides are still under consideration. As can be seen and similar to what shown in figure 2 (left), it is only YN that has a moderate binding of first H on the surface. TiN binds it very weakly whereas ScN binds it very strongly. Figure 2 (left) is constructed based on a conventional descriptor for screening for HER catalysts and proposes that YN should be an extremely promising candidate for HER. But for HER to occur, either this H-adatom should react with a coming proton from electrolyte via Heyrovsky mechanism or a second proton needs to be adsorbed on the surface and then recombine with the first H-adatom to evolve hydrogen via Tafel mechanism. On TiN, according to figure 2 (right), both the Heyrovsky and Tafel mechanisms seem difficult, as the free energy of adsorption of first proton is relatively high. However on the surface of YN, only Tafel mechanism seems difficult due to relatively weak free energy of adsorption of the second proton (0.65 eV) where a 2/8 ML coverage is reached. Nonetheless, the Heyrovsky mechanism might be fast and easy especially on YN as adsorption of the first proton should happen at U=0 V vs. SHE. ScN starts to adsorb the 2nd proton at around -0.30 V

where HER can start via the Tafel mechanism. This deserves a detailed analysis that is beyond the scope of this paper, but is currently being investigated.

Conclusion

We used DFT calculations to investigate the possibility of using transition metal mononitrides for catalyzing NER or HER. Complete mechanistic analysis of these mononitrides showed that VN, CrN, MnN, ZrN, NbN and MoN can catalyze reduction of surface nitrogen and form *NH, $*NH_2$ and $*NH_3$ intermediates necessary for ammonia formation. VN and CrN specifically should produce ammonia with higher current efficiency, as they only need the minimum number of proton/electron pairs to form 2 ammonia molecules. In addition, we explored that a full monolayer of H (1ML = 8 *H) covers the surface of ScN, TiN, YN without any possibility of formation of $*NH_2$ and $*NH_3$ intermediates and accordingly no ammonia molecule. The free energy diagram of these nitrides together with the differential free energy of adsorption of H plot suggest that YN might be a promising material for catalyzing HER via a Heyrovsky mechanism and ScN via the Tafel mechanism and therefore deserves more detailed kinetic analysis for efficient HER activity.

References

1. Klerke, A., Christensen, C. H., Nørskov, J. K. and Vegge, T (2008), "Ammonia for hydrogen storage: challenges and opportunities," *J. Mater. Chem.* **18,** pp. 2304–2310.

2. Abghoui, Y. Garden, A. Hlynsson, V. Bjorgvinsdottir, S. Olafsdottir, H. and Skulason, E (2015), "Enabling electrochemical reduction of nitrogen to ammonia at ambient conditions through rational catalyst design," *Phys. Chem. Chem. Phys.* **17,** pp. 4909–4918.

3. Abghoui, Y. and Skulasson, E (2015), "Transition Metal Nitride Catalysts for Electrochemical Reduction of Nitrogen to Ammonia at Ambient Conditions," *Procedia Comput. Sci.* **51,** pp. 1897–1906.

4. Hammer, B., Hansen, L. and Nørskov, J (1999) "Improved adsorption energetics within density-functional theory using revised Perdew-Burke-Ernzerhof functionals," *Phys. Rev. B* **59,** pp. 7413–7421.

5. Blöchl, P (1994), "Projector augmented-wave method," *Phys. Rev. B* **50,** pp. 17953–17979.

6. Kresse, G. and Hafner, J (1993), "Ab. initio molecular dynamics for liquid metals," *Phys. Rev. B* **47,** pp. 558–561.

7. Kresse, G. and Furthmüller, J (1996), "Efficient iterative schemes for ab initio total-energy calculations using a plane-wave basis set," *Phys. Rev. B. Condens. Matter* **54,** pp. 11169–11186.

8. Nørskov, J. K., Bligaard, T., Logadottir, A., Kitchin, J. R., Chen, J. G., Pandelov, S. and Stimming, U (2005), "Trends in the Exchange Current for Hydrogen Evolution," *J. Electrochem. Soc.* **152,** pp. J23–J26.

9. Björketun, M. E., Bondarenko, A. S., Abrams, B. L., Chorkendorff, I. & Rossmeisl, J (2010), "Screening of electrocatalytic materials for hydrogen evolution," *Phys. Chem. Chem. Phys.* **12,** pp. 10536–10541.

10. Skúlason, E., Tripkovic, V., Björketun, E. M., Gudmundsdóttir, S., Karlberg, G., Rossmeisl, J., Bligaard, T., Jónsson, H. and Nørskov, K. J (2010), "Modeling the Electrochemical Hydrogen Oxidation and Evolution Reactions on the Basis of Density functional theory calculations," *J. Phys. Chem. C* **114,** pp. 18182–18197.

11. Pu, Z., Liu, Q., Tang, C., Asiri, A. M. and Sun, X (2014), "Ni2P nanoparticle films supported on a Ti plate as an efficient hydrogen evolution cathode," *Nanoscale* **6,** pp. 11031–11034.